UNDERSTANDING POWDER BEHAVIOR IN PHARMACEUTICAL MANUFACTURING TO ENHANCE DRUG PRODUCTIVITY AND THERAPEUTIC PERFORMANCE

By

ZHANJIE LIU

A dissertation submitted to the

School of Graduate Studies

Rutgers, The State University of New Jersey

In partial fulfillment of the requirements

For the degree of

Doctor of Philosophy

Graduate Program in Chemical and Biochemical Engineering

Written under the direction of

Fernando J. Muzzio and Gerardo Callegari

And approved by

_____

_____

_____

_____

New Brunswick, New Jersey

October 2020

ABSTRACT OF THE DISSERTATION

Understanding Powder Behavior in Pharmaceutical Manufacturing to Enhance Drug Productivity and Therapeutic Performance

By ZHANJIE LIU

Dissertation Directors:

Fernando J. Muzzio and Gerardo Callegari

In the pharmaceutical industry, processing granular materials is inevitable when manufacturing solid dosage forms, such as tablets, capsules, dry powder inhalants, vascular stent, or injectable solid compositions. As pharmaceutical industries make products that necessitate a significant (albeit controllable) risk to human health, a systematic, proactive, scientific, and risk-based approach has been adopted by health authorities (e.g., Food and Drug Administrative) for drug safety: Quality-by-Design (QbD). The QbD-based pharmaceutical development emphasizes the mechanistic understanding of input material properties and process dynamics to recognize how the formulation and process factors affect the final product. Once we have comprehensive material and process understanding, the manufacturing process is stable and predictable, the performance and safety of the final product can be predicted and ensured, the entire drug product development can run faster with less waste and cost.

In the last decade, the pharmaceutical industries have grasped a world-wide transformation to continuous manufacturing technologies due to its capability of fast development, enhanced risk management, and improved quality control. The deep understanding of

material behavior and process dynamics on the continuous manufacturing platform will be one of the primary focuses for the entire pharmaceutical industry in the next decades.

By considering all of the above regulatory requirements and state-of-the-art pharmaceutical techniques, this dissertation is constructed toward unraveling the possible correlation between material properties, process parameters, and product performance, based on continuous manufacturing platform for solid dosage development. In each chapter, attempts have been made to investigate a) how the certain properties of an input material impact its process behavior and performance of output material or final product, b) how the certain process parameters alter process dynamics which further impact the performance of output material or final product, and c) how to design formulation and production methodology to enhance drug productivity or therapeutic performance.

Four specific investigations are implemented:

(1) The effect of twin-screw feeders on material properties is investigated to understand whether the post-feeder powder has the same properties as the pre-feeder one. The flowing behavior of fourteen pharmaceutical powders is characterized before and after feeder. it has been found that powder may behave more cohesively after passing through a twin-screw feeder due to electrostatic charge acquisition. Such behavior can only be discerned by performing the appropriate characterization method, which can be correlated with the tendency of powder electrostatic charging and its particle size,

(2) API agglomeration behavior during the continuous process is investigated. A novel method for quantifying material agglomeration tendency is developed based on image analysis. It enables us to assess the risk of non-uniform products caused by ingredient

agglomeration. In this work, it has been found that the powder is densified in the twin-screw feeder and then introduced as lumps to the downstream process, which generates difficulty for uniform mixing. Twenty-two pharmaceutical powders are examined and the capability is developed to assess ingredient agglomeration risk based on proper raw material characterization.

(3) The existence of API agglomerates reduces content uniformity of the final product. we also explore how to design blending processes to diminish or even eliminate API agglomerates, which are generated due to feeder passage. A case study is performed in a continuous powder blending system, which consists of two feeders, a conical mill, and a tubular blender. Multiple blending protocols are implemented, involving different impeller rotational speed of blender, multiple levels of powder holdup in blender, with/without using the conical mill at multiple impeller speeds and screen size. It has been found that the API agglomerates can be significantly reduced when powder passes through an extensive number of blades (NOB) in a blender, or a conical mill is assembled

(4) Improving the dissolution of poorly soluble drug products is a key challenge in drug product development. In this dissertation, a novel approach is invented to enhance the dissolution of poorly soluble drugs by applying the concept of the surface coating. A simple process, twin-screw extrusion at low process temperature, is performed that enables the melt-coating of API particles with a small amount of surfactant. Four case studies are conducted to evidence the practicality of the melt-coating methodology, in which the combinations of three BCS class II drugs and three surfactants are examined. Remarkably, the results support that the melt-coating technique significantly improves the dissolution of poorly soluble drugs.

Acknowledgements

As approaching the destination of the long but life-changing journey in pursuing the doctoral degree at Rutgers, I am contructing this document as the cumulation and summary of my effort in several years. I have been fortunate to have the support and encouragement from everyone who have been an integral part of this journey. I would like to acknowledge all individurals who have helped me reach this far.

Foremost, I would like to express my deepest gratitude to my dissertation advisiors, Dr. Fernando J. Muzzio and Dr. Gerardo Callegari, for their continuous mentorship, guidance and trust. I would especially like to thank Fernando for his tremendous, perspicacious, and enthusiastic inspiration thoughtout my journey in Rutgers. Fernando, thank you for providing me this wonderful opportunities to challenge myself and helping me improve my communication and decision making skills. I would also especially like to thank Gerardo for his dedication to improving my scientific thinking, writing and presenting skills. Gerardo, thank you for being with me and helping me overcome many challenges in this journey. I would also like to extend my appreciation to my committee members, Dr. Rohit Ramachandran and Dr. Thomas Bieringer for providing valuable inputs and suggestions to the dissertation.

I am grateful for being involved in the Engineering Research Center for Structured Organic Particular Systems (ERC-SOPS). The opportunities to interact with industrial and academic collaborators have helped me to exchange ideas and understand the industry needs in the pharmaceutical field. My experience in the ERC-SOPS have shaped my personality and helped me develop the confidence in my future career.

This dissertation is also the result of contribution from many talented colleagues at Rutgers. It has been my privilege to work with them who have made this journey full of friendship and enjoyment. I would like to thank former and current ERC-SOPS members, Dr. Alberto Cuitino, Dr. James Scicolone, Dr. Sonia M. Razavi, Dr. Ravendra Singh, Dr. Andres Roman-Ospino, Dr. Xue Liu, Dr. Wei Meng, Dr. Yifan Wang, Dr. Sarang Oka, Dr. Pallavi Pawar, Dr. Jun Zhang, Dr. Zhonghui Huang, Dr. Douglas Hausner, Dr. Thamer Omer, Dr. Bereket Yohannes, Dr. Tianyi Li, Dr. Hao Chen, Dr. Savitha Panikar, Dr. Sejal Shah, Dr. Sebastian Escotet, Golshid Keyvan, Shashwat Gupta, Jingzhe Li, Qiushi Zhou.

This endeavor would have been impossible without the support from my family. I would like to thanks my parents, Rongqing Liu and Jingyan Xu for raising and supporting me in all walks of life selflessly. You are always there for me. I wouldn't complete this journey without you. I particularly would like to express my most heartfelt appreciation to my beloved wife, Yi Tao, for your understanding, accompany, patience and endless love. You are the source of tremendous motivation for this journey.

Table of Content

List of Tables

List of Figures

1 Chapter 1 Introduction

1.1 Background

Powders and granular materials are ubiquitous. Many industries, such as chemicals, food, agriculture, pharmaceuticals, cosmetics, pigments, cement, mining, petroleum, and ceramics, engage in powder processing or design their products in powder-related forms[1-4]. It has been documented that more than 60% of chemical products are in granular form as the product, raw or intermediate material[5]. The manufacturing of powder-related products typically requires several unit operations. Some very common powder-related processes are the feeding of granular material during the continuous process[6-8], the particle size reduction to improve particle functionality[9, 10], the granulation to increment flowability[11, 12], the blending of several components[2, 13], and the compaction of granular material as tablet or pellet[14]. Due to the prevalent applications of granular forms, the understanding of powder properties and its behavior in industrial processes is critical for maximizing the manufacturability and reducing risks that directly or indirectly lead to a lesser quality product.

In the pharmaceutical industry, processing granular materials is inevitable when manufacturing solid dosage forms, such as tablets, capsules, dry powder inhalers, vascular stents, or injectable solid compositions. Among them, solid oral dosage forms, like tablets and capsules, play a critical role in the dispensing of medicine. Tablets or capsules are the most convenient way to take medication, and more than 70% of total medicines are dispensed in those forms[15]. The manufacturing of these products involves processing one or more than one ingredient, either separately or simultaneously. These ingredients can

be divided into two classes, namely, active pharmaceutical ingredients(APIs) and excipients. The APIs are the biologically active components in a drug product that deliver the intent and therapeutic effect. In contrast, the excipients are the inactive components that are used to be as a medium to (1) provide the volume of dosage form and convey APIs as a vehicle, (2)confer therapeutic enhancement, such as enhancing solubility, promoting absorption, and (3) aid in the manufacturing of drug product[16-19]. According to different functions, excipients can serve as fillers, disintegrants, binders, release modifiers, lubricants, glidants, antiadherents, surfactants, flavors, sweeteners, coatings, stabilizers, pH modifiers, etc. The processing of these ingredients comprises of a series of unit operations, such as milling, drying, handling, mixing, granulation, extrusion, drying, compaction/capsules filling, coating[20]. ***Figure 1-1*** depicts a representative operation sequence for manufacturing tablets/capsules in the traditional pharmaceutical industry.

It has been widely accepted that most APIs are toxic. When people take any medications, they are consuming a potentially hazardous substance, which is designed to intendedly affect human physiology. As the pharmaceutical industries make products that necessitate a significant (albeit controllable) risk to human health, every manufacturing procedure must be closely regulated for drug safety by health authorities, such as Food and Drug Administration (FDA) in US, European Medicines Agency (EMA) in Europe. A poor drug product possibly exposes the patient to unexpected and uncontrolled allergic reactions. As shown in ***Figure 1-1***, pharmaceutical manufacturing is a complex process requiring high reliability and uniformity in each unit operations. In fact, its complexity also kept growing in past decades due to that the complicated formulations and novel production techniques. The industry has been innovating and updating to maximize compound therapeutic

performance and product reliability, such as the solid dispersion techniques for bioavailability enhancement[21], Cyclodextrin complexation for bioavailability enhancement[22], and continuous manufacturing techniques for its improved risk assessment and fast development[23-25]. Therefore, the regulatory requirements for the understanding of raw and intermediate materials, understanding and controlling processes, product risk assessment, product quality characterization and monitoring, are increasingly demanding.

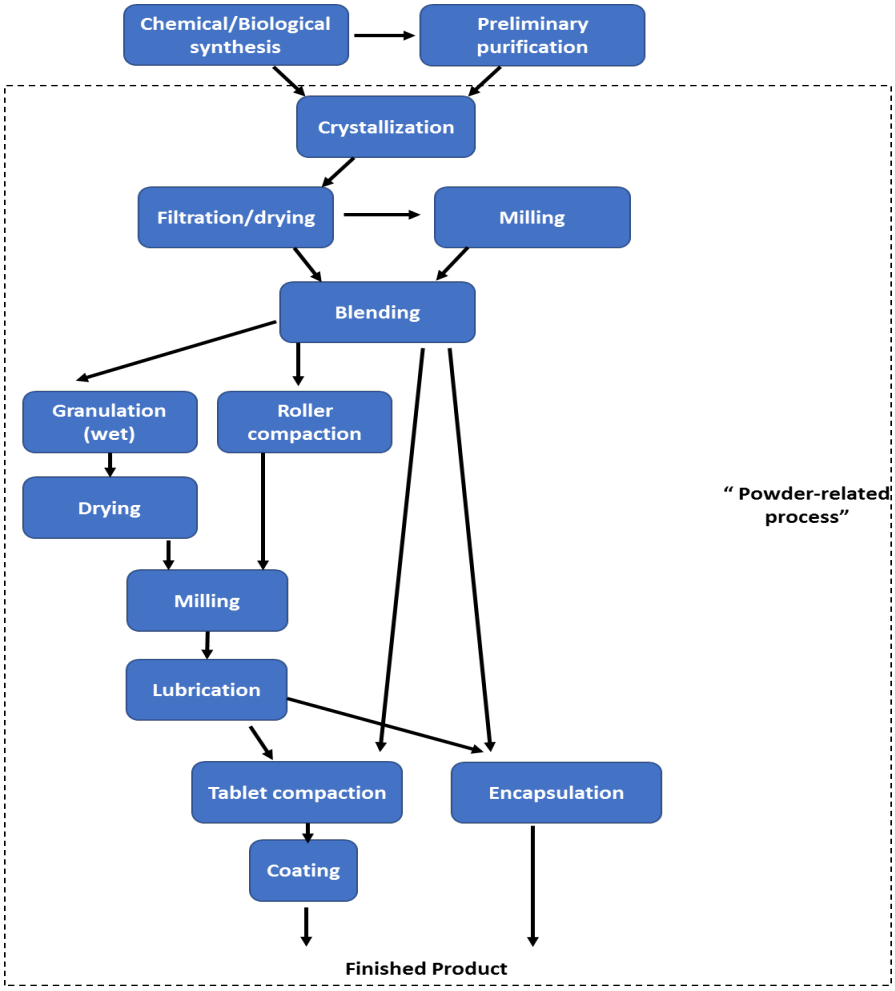

Figure 1-1 Representative operation sequence of solid dose forms drug product manufacturing.

Quality by design (QbD), initiated by Joseph M. Juran and adopted by the Food and Drug Administrative (FDA) as a main tool for process development, requires a systematic approach for the design and development of pharmaceutical products, which is based on sound science and quality risk management[26, 27]. In this approach, the quality and performance of the final product are ensured through the design of an effective and efficient manufacturing process rather than the testing of the product alone. QbD-based pharmaceutical development begins with predefined objectives, then emphasizes the mechanistic understanding of input material properties and process dynamics to recognize how the formulation and process factors affect the final process. Such development should be accomplished via multivariate experimental design and advanced process monitoring and controlling[28, 29]. Once a comprehensive material and process understanding is achieved, and the manufacturing process is stable and predictable, further drug product development can run faster with less waste and less cost, product performance can be predicted, and product safety is ensured.

One of the most important QbD elements is to identify critical material attributes (CMAs), critical process parameters (CPPs), and critical quality attributes (CQAs). The CMAs include chemical, physical, biological, or microbiological attributes of an input material that can be defined, quantified, continually monitored to ensure that the output material remains in acceptable quality limits. The CPPs are demonstrated as the key variables that potentially impact production and product performance. In practice, the CPPs should be first fully understood, then monitored, and controlled to ensure that the process is within a predefined range (the design space) and produces the desired qualities. The CQAs are identified as a chemical, physical, biological, or microbiological characteristic that should

be within an appropriate range to ensure the desired quality of the finished product. The relationship between CMAs, CPPs, and CQAs can be simply diagramed as shown in ***Figure 1-2***. Given all of the above regulatory requirements and guidance, this dissertation attempts to unravel the possible correlation between material properties, process parameters, and product performance for specific case studies. In each chapter, we attempt to investigate how the certain properties of an input material impact its process behavior and the performance of the output material or the final product, how the certain process parameters alter process dynamics, which further impact the performance of output material or final product, or how to design a formulation and production methodology to enhance drug productivity or therapeutic performance.

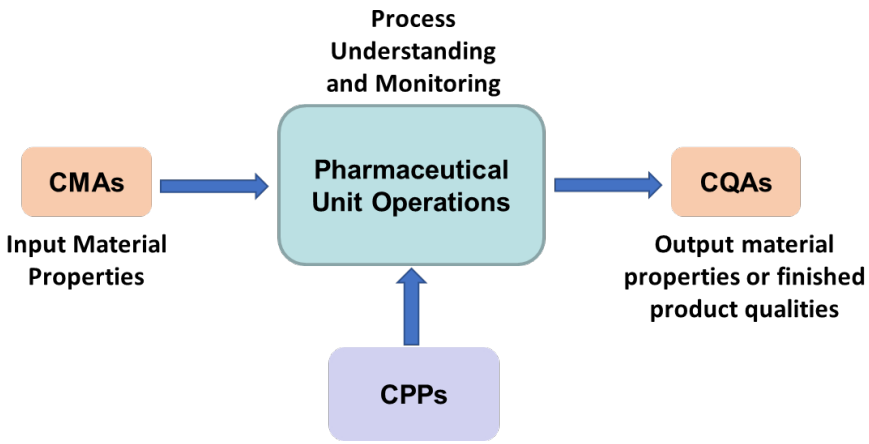

Figure 1-2 Relationship between CMAs, CPPs and CQAs

1.2 Flowing behavior of granular material

As the aforementioned, powder is a prevalent material form that exists in many chemical industries. The full understanding of powder properties and its behavior (mostly flowing behavior) is one of the critical steps towards the successful development of powder-related manufacturing. The poor flowability of powder during a process would lead to many

problems, such as powder jamming, clumping, building-up, arching in hopper, agglomeration, segregation, inconsistent flow etc. Although these cohesive phenomena can be simply interpreted as that the particle-particle cohesive forces are higher than its weight, the quantitative measurement, prediction, and optimization of handling are always challenges that need to be fully understood in modern pharmaceutical manufacturing.

First of all, it is important to clarify that a powder is a unique material state consisting of three phases: the solid as the form of particles, air between the particles as long as they are assembling as a bulk powder, and liquids on the surface or within porous particles. When we attempt to interpret powder behaviors, it is necessary to consider the possible contribution of all of these phases. In fact, the powder also behaves as three phases (solid, liquid, and gas) during processes[30]. Powder acts as a liquid when flowing. Most of the powder process is developed based on its flowability. However, it does not obey the same stress-strain relations as the liquid. In this aspect, powder is solid-like as it can withstand external normal and shear stresses in equilibrium. Powder can also behave like gas because it can be compressed to a certain degree. Additionally, the volume of bulk powder can expand when the air is blown through it, which causes it to be fluidized. Due to this ternary behavior, powder can not be treated as a single continuum. Namely, there is no set of universally accepted constitutive equations that describe powder flowing behavior. Therefore, powder-related characterizations and process developments are nearly always semi-empirical[31].

Powder flowability is a multi-dimensional property. Its complexity is the result of several mechanisms acting together at different length scales[31, 32]. First, the intrinsic physical properties determine the surface interaction between particles, such as particle size, density,

particle shape, surface roughness, surface area, Van der Waals force, conductivity, and triboelectric charging potential. Second, the collective properties of particles (i.e., bulk powder properties), such as particle size distributions, hygroscopicity, bulk density, frictional interactions, powder bed packing, the force transmitting during flow, and particle-particle mechanical interlocks, are also able to change flowing behavior. The macroscopic flow properties are affected by powder bulk structure which is the cumulative behaviors of millions of particles. Third, powder flowing behavior depends on the processing environment, such as handling stress, flow rate, humidity, temperature, surface charging intensity.

Considering the flowing behavior of powder is the function of particle intrinsic physical characteristics, bulk powder structure, and environmental or processing factors, it is far from being adequate to use the only single index to represent powder flow in any scenario. The full characterization of powder flowability must be done by using multiple techniques that encompass different consolidation conditions during processing, including dynamic flowing state, loosely packed state, and densely packed state. In general, powder flow is more of a functional or performance test than a physical measurement. Previously, many characterization techniques have been developed, such as the avalanche test, the angle of repose test, compressibility test, dynamic flow test, fluidization test, hopper flowing test, etc. From these tests, numerous flow indexes have been defined, such as avalanche size, dilution index, angle of repose, flow function coefficient, Carr index/Hausner ratio, fluidization index, etc. In chapter 2, several widely used powder characterization techniques are detailed, and the different flow indexes are reviewed and interpreted.

In order to numerically model powder flowing behavior during the process, several simulation-based attempts have also been made by describing powder flowing behavior based on how force is transmitted between particles and through the bulk powder structure. For example, modeling the powder system using the discrete element method (DEM) is one of the prevalent approaches which simulates particle movement and interactions between particles. The key aspect of DEM is that each particle is treated individually. Particle movement is described by Newton's motion equation, and their interactions are described by several contact models (e.g., Hertz-Mindlin model, Johnson-Kendall-Roberts model, adhesive elasto-plastic model) with non-contact forces (e.g., gravitational force) as extra inputs[33-35]. The DEM simulation has been applied to many pharmaceutical processes, such as die filling[36], particle compaction[37], powder mixing[38], and powder feeding[39].

Alternatively, the bulk powder can be treated as a continuum when it flows. Thus, continuum mechanics can be applied to describe powder flowing behavior by modeling the stress transmission within the powder structure. This simulation approach begins with the Quasi-static flow theory, which addresses slowly moving powder flows[40]. This theory is established by using the Mohr-Coulomb failure criterion (Mohr circle analysis), which models behavior as a friction-like response. When densely packed powder structure yields and shears, forces are concentrated on the particles within the shearing plane (called the shear band) and form a force chain. The friction-like response is the result of the internal structure of the force chain. On the other end of the spectrum, rapid-flow (i.e., inertial flow) theory can be established based on the assumption that all of the particle contacts occur instantaneously[41]. Kinetic theory, for example, Navier-Stokes equations, can be used to

model powder flow at this regime. Campbell has invested in substantial efforts to advance our understanding of powder flow by considering force transmission across interparticle contacts and further fills in the gap between the quasi-static and rapid-flow range[42-45]. He draws the complete flowmaps for granular material by introducing two more elastic granular flow regimes: elastic-quasi-static and elastic inertial. There is some inertial effect through these elastic flow regimes in comparison to the pure quasi-static regime. However, the formation and deformation of the force chains still occur during shearing flow, and the rate of chain production is proportional to the shear rate. At a relatively low shear rate, the elastic-quasi-static theory is applied, where the interparticle force is independent of the shear rate. But at a high shear rate, the interparticle force is linearly dependent on the shear rate, where the elastic-inertial theory is established. In this regime, the inertial force becomes of the same magnitude as the interparticle elastic force so that the modeling must reflect the inertia of particles.

1.3 Continuous manufacturing of solid oral dosage forms

The pharmaceutical industry is a global business that develops performance-based products to fulfill the requirement of healthcare for billions of people. This industry is strongly motivated to invest in more efficient and robust manufacturing technologies. Especially, in 2020, a history of global and rapid evolving of the COVID-19 pandemics highlights the requirement for rapid product and process development to respond to emergencies. Such development is not only essential for a new therapeutic but also necessary for a product that needs to be re-developed due to shortages of previous manufacturing protocols. Moreover, the growth of the market for generic drug products constantly requires a cost-effective, highly reliable, and scale-flexible drug product development. It has been reported

that more than 90 percent of prescriptions in the U.S were dispensed using generic drugs (in 2017)[46]. Unfortunately, for decades, the batch-wise pharmaceutical manufacturing technology has been near-stagnation.

In the last decade, pharmaceutical manufacturing is experiencing an unprecedented modernization. The pharmaceutical industries, including brand manufacturers, genetic manufacturers, ingredients suppliers, and facilities manufacturers, have joined a world-wide transformation to continuous manufacturing technologies. In fact, prior to pharmaceutical manufacturing, the positive experience of continuous manufacturing techniques has been gained in many other industries for a long time, such as food, consumer product, diary, and petrochemical industries[47-49]. Continuous manufacturing is an integrated system consisting of a series of unit operations, such as feeding, milling, mixing, granulation, and compaction. During such manufacturing, each ingredient (including APIs and excipients) is fed into process continuously at a controlled flow rate. Then, these ingredients travel non-stop from one manufacturing unit to the next. At each unit operation, the ingredients are also processed continuously under controlled process parameters. Finally, the finished products are continuously removed from the system.

Compared with traditional batch manufacturing methods, continuous manufacturing enables smaller equipment being used to fulfill the requirement of a large number of products. Only a small amount of material is resident in each equipment at any time, and the intermediate storage of material is eliminated. Throughout the entire manufacturing timeline, the quality attributes of intermediate materials and final products can be monitored continuously as small as unit dose size. Moreover, an effective control system

can be assembled, which enables online and real-time adjustment of process parameters to assure that the final products have pre-defined quality attributes.

Typically, the continuous manufacturing of solid oral dosage forms has been implemented in three main systems, as shown in ***Figure 1-3***: the continuous direct compaction line, the continuous wet granulation line, and the continuous dry granulation line[50]. Certain unit operations including feeding, blending, and tableting are the most common process through all manufacturing routes. They are the inevitable units in continuous manufacturing which have been considerably investigated[6, 13, 51, 52].

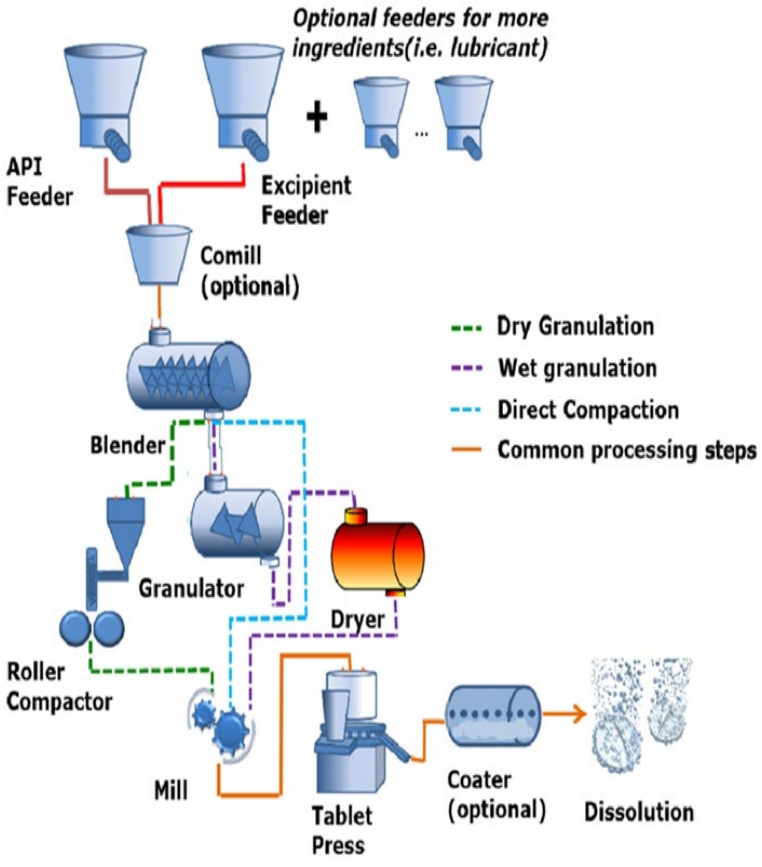

Figure 1-3 Typical continuous manufacturing of solid dosage forms by direct compaction, dry granulation, and wet granulation[50].

The adoption of continuous manufacturing techniques enables several considerable improvements in the pharmaceutical industry, such as lowering drug product prices, shortening product development timeline, enhanced risk management, improved quality control, and correspondingly enhanced product reliability. Remarkedly, the two key advantages of continuous manufacturing over batch-type are its fast product and process development and fast response to product shortage or process failure. First of all, the product and process development for such techniques are implemented on the same equipment and level of scale that will be subsequently used for pilot-plant and full-scale manufacturing. No scale-up studies are needed during a continuous process development, which is one of the most time-consuming and problematic steps in batch-type development. Secondly, a typical continuous manufacturing system of solid dosage forms (can be seen in ***Figure 1-3***) can reach a steady-state and operational state of control just in a matter of minutes. Thus, a process can be developed by using a small amount of material. Also, extensive trials for multiple process designs and formulation candidates can be performed just in few days. If there is any process failure, the system can rapidly detect it with a real-time monitoring and control system assembled, and process adjustment can be done within a short time. If the developed product has any shortage, the re-development can also be completed within a short period. Moreover, continuous manufacturing techniques allow unit-dose-size monitoring and rapid process feedback, which intrinsically enhance product reliability. This capacity enables easier approval from regulatory authorities, which further accelerates the total production timeline.

Due to these pronounced advantages, the pharmaceutical manufactures, ingredients suppliers, and facilities suppliers have actively engaged in this renovation of the

pharmaceutical manufacturing platform. Since 2015, six brand drug products have already been produced by using continuous manufacturing techniques: Orkambi (lumacaftor/ivacaftor, 2015), Prezista (darunavir, 2016), Symdeko (tezacaftor/ivacaftor, 2018), Verzenio (abemaciclib, 2018), Daurismo (glasdegib, 2018), Trikafta (elexacaftor/ivacaftor/tezacaftor, 2019). Dozens of pharmaceutical manufactures, such as Johnson&Johnson, Vertex, Eli Lilly, Pfizer, Glaxo SmithKline, Merck, Bayer, and Novartis, have also made the plan to either transfer a large fraction of developed product to continuous manufacturing platform or newly develop drug product based on continuous manufacturing techniques in next few years. Furthermore, in order to facilitate the implementation of continuous manufacturing, FDA released a draft guidance, "Quality considerations for continuous manufacturing," for the industry in 2019[53].

Therefore, the deep understanding of material behavior and process dynamics on the continuous manufacturing platform will be one of the key focuses for the entire pharmaceutical industry in the next decades.

1.4 Overview of the dissertation

This dissertation is motivated by the regulatory requirement or aspiration, for a given pharmaceutical ingredient, to maximize the manufacturability, productivity, therapeutic performance, and minimize the risks that directly or indirectly lead to a lesser-quality product. Efforts have been invested in understanding the possible correlation between the material properties and a certain process behavior, and between process parameters and process performance of an intermediate material or a final product. Although all of the investigations in this dissertation are experimentally implemented on a continuous manufacturing platform for pharmaceutical solid dosage development, the experimental

methodologies, discussions, and conclusions are also significant to be applied for batch-type pharmaceutical development.

The rest of the dissertation consists of six chapters. In chapter 2, widely used powder characterization techniques are reviewed and detailed. These powder characterization methodologies include flowing performance measurement, wettability measurement, surface properties measurement, electrostatic properties measurement.

Next, from chapter 3 to chapter 6, each chapter discusses a very common issue that is experienced during pharmaceutical development or manufacturing. A series of experiments are performed to reveal the possible correlations between material properties and such behavior in the unit operation. By fully understanding this powder behavior during manufacturing, we are able to gain the capability of assessing the manufacturability of an ingredient based on its raw material characteristics. Then, the possible process designs are further investigated for minimizing the occurrence of these issues. Furthermore, the quantity attributes of output material or final product are experimentally measured to reveal the correlation between process parameters and product performance. The effectivity and efficiency of such process design are also illustrated by characterizing the performance of the final product. Specifically, the research scope of each chapter is briefly described below.

- **Chapter 3: Powder property change after passing through a twin-screw feeder: the effect of electrostatics on powder flow.**

  In continuous pharmaceutical manufacturing, feeders are required to deliver ingredients in the downstream process precisely. Typically, the twin-screw feeder is widely used. This chapter is established to demonstrate how the feeder passage

alters powder flowing behavior. Additionally, there are three more deliverables in this chapter: (1) If the powder flowing behavior is indeed changed due to material passing through the feeder, which characterization method is able to discern the difference. (2) This study set out to further investigate the correlation between the behavior of flowability change after feeder and material properties (or indexes extracted from characterization methods). (3) This study seeks to generally interpret the effect of the powder tribo-electrostatic charge on its flowing behavior. To that end, the flowability of fourteen pharmaceutical materials is characterized both before feeder and immediately after feeder by using multiple techniques: shear cell test, compressibility test, and dynamic flow energy test. The charge-to-mass ratio is measured to examine material electrostatic behavior. In this chapter, it has been found that powder may behave more cohesively after passing through a twin-screw feeder due to electrostatic charge acquisition. This behavior can be correlated with the tendency of powder electrostatic charging and its particle size. Also, if powder acquired significant electrostatic charges, the substantial powder buildup is immediately observed at the exit of the feeder.

- **Chapter 4: Measuring powder agglomeration after the twin-screw feeder.**

  Ingredient agglomeration is a common issues when blending micronized and cohesive API for both continuous process and batch processes, which leads to product failure in content uniformity. In this chapter, relying on the continuous manufacturing platform, we seek to understand API agglomeration tendency as a function of the values of flow properties. We have found that the formation of agglomerates in most cases is the result of cohesive powder being densified locally.

In continuous manufacturing, as powder passes through a twin-screw feeder, it is consolidated at the pocket of screws which leads to powder being fed as lumps instead of as primary particles. Introducing powder lumps to the downstream process would result in the existence of agglomerates in the final product. To quantify the tendency of powder agglomeration at feeding, a novel method is developed which measures powder agglomerates size post-feeding by using image analysis. The endurance of the agglomerates can also be quantified by performing this measurement after a conical mill (i.e., feeder + conical mill). Twenty-two pharmaceutical materials are examined in this chapter. Ultimately, the conclusion is drawn that powder agglomeration tendency can be assessed by characterizing its particle size, compressibility, and cohesion value (shear cell test).

- **Chapter 5: Agglomeration reduction of cohesive powder in continuous powder blending system**

  If we knew a specific ingredient would have the high tendency of forming agglomerates during the manufacturing process, the challenges are how to directly find the agglomerates in blends and how to design the process to mitigate or eliminate agglomeration. In this chapter, a methodology is developed by using NIR spectrometric techniques to detect ingredient agglomerates in a powder mixture. Then, this methodology is applied to investigate the API agglomeration during a continuous powder blending process, which consists of two feeders, a conical mill, and a tubular blender. A case study is performed for a simple binary formulation (a cohesive API + a free-flowing excipient) of relatively low drug loading. The agglomeration of the cohesive API at each process condition is quantified and

compared. Additionally, the effect of API agglomeration on tablet content uniformity and dissolution profile is examined. Conclusively, the API agglomerates can be significantly reduced when the powder passes through an extensive number of blades (NOB) in a blender, or a conical mill is assembled between feeder and blender.

- **Chapter 6: Melt-coating of APIs with surfactants for drug dissolution enhancement**

  Approximately 40% of approved drugs and 90% of drugs under development are categorized as low water-solubility and low bioavailability molecules. Improving the dissolution of poorly soluble drug products is a key challenge in drug product development. This chapter provides a novel approach to enhance the dissolution of poorly soluble drugs by applying the concept of the surface coating. A simple process, twin-screw extrusion at low process temperature, is used that enables the melt-coating of API particles with a small amount of surfactant. This chapter lists four case studies to evidence the practicality of the melt-coating methodology, which encompasses three poorly soluble drugs and three surfactants. Dissolution of both unformulated powder and the finished product is inspected. Remarkably, the results support that the melt-coating technique significantly improves the dissolution of poorly soluble drugs.

In the last chapter (chapter 7), the key conclusions of each investigation are summarized. The direction of further work is suggested for other researchers.

2 Chapter 2 Overview of Powder Characterization Techniques

2.1 Introduction

As introduced in chapter1, the powder material is the combination of three phases: solid, liquid, and gas. Also, the powder can behave as any of these three phases during the process. When flowing, the powder acts as a liquid. Its flowability directly dictates powder performance in the process and further impact the qualities of output material. The powder can also behave like gas since the bulk powder can be compressed to a certain degree. Its air-related properties such as compressibility, air permeability, and fluidization behavior are important criteria in certain processes, such as tableting and fluidized drying. These properties are also considered as critical indexes to indicate powder flowing behavior. As a solid, powder withstands both normal and shear stress. Its solid component, the particles, exhibit surface properties and complies with certain surface principles. The general surface-related properties are electrostatic properties, wettability, and surface energy. These properties not only affect powder behavior during certain unit operations, for example, wettability determines the particle-particle liquid bridge formtion and the subsequent growth of granules, but also, they relate to powder flowing behavior. Therefore, the deep understanding of a powder material should engage in the characterization of flowing behavior, surface properties, and air-related performance.

In this chapter, severall powder characterization techniques, covering flowability and surface properties, are detailed. Owing to that the powder air-related performance (compressibility, aerated density, permeability, and fluidization) is typically considered as flowing performance, these characterization techniques are presented in the flowability section. Several listed characterization techniques are utilized in later chapters, aiming to

reveal the correlation between powder characterization results with its process performance. Although several listed characterization techniques are not deeply investigated in this work, given their application in the pharmaceutical industry is worthwhile to devote more effort to understanding them in the future.

2.2 Characterization of powder flowability

The flowability of granular materials is one of the critical material attributes since the performance of powder processing and the quality of its product are directly dependent on material flowing behavior[54, 55]. Poor flowability leads to multiple issues during the manufacturing process, such as powder jamming, clumping[6], arching in hopper[56], agglomeration or segregation in mixing[57], content variability[54], tablet weight variability[58]. As far as we currently know, flowability is a complex and multi-dimensional property[31, 56, 59, 60]. Multiple characterization methods have been developed under specific conditions, such as avalanche test, angle of repose test, shear cell test, compressibility test, tapped density test, dynamic flow test, fluidization, etc., and numerous flowability indexes have been defined, such as avalanche size, angle of repose, flow function coefficient, compressibility index, Carr index/Hausner ratio, and fluidization index[32, 59, 61]. According to the testing condition, these tests can be classified as static test, quasi-static test, and dynamic test. However, it is difficult to only use a single index to fully describe how well the powder flows in various situations. For a long time, in powder industries, inconsistency has also been reported that using different characterization techniques may obtain opposite results[62]. In this situation, the confusion makes it difficult to decide which test should be trusted and which powder behavior is true. More recent literature pays particular attention to comparing different powder

characterization techniques to reveal the relationship between them[63]. They suggested that powder flow properties are dependent upon the stress state and that the results from static and dynamic tests do not necessarily agree with each other. Thereby, to fully understand powder flowing behavior, powder characterization must be done by applying multiple techniques that cover static, quasi-static, and dynamic tests[60, 64]. In fact, flowability is characterized routinely before process design. Based on flowability characterizations, materials can be classified and mapped into different flowing behavior regime[32, 65], which is helpful to design an appropriate manufacturing procedure using the optimal process setting and tooling. Due to the complex nature of powder properties, large quantities of data are collected. In recent years, there has been an increasing amount of literature that proposed utilizing multivariate statistics to address powder multi-dimensional properties[56, 60, 64, 66]. For the modern pharmaceutical industry, this approach not only comprehensively represent powder behavior but also unravel similarity and dissimilarity between powders. In addition, It helps to fulfill the requirement that material process performance should be predicted[60], process failure should be warned, based on raw material properties, especially in the early stage drug product development. In order to maximize the ability of prediction with minimal testing effort, practicers are motivated to select the most relevant properties to predict the performance of interest[56]. It requires the product developer has a full understanding of powder properties and its possible correlation with specific behavior within a particular process.

In this work, a commercially available powder flow tester, FT4 powder rheometer (Freeman Technology Inc., Worcestershire, UK) is used to perform shear cell test, compressibility test, permeability test, and dynamic flow energy test.

2.2.1 Shear cell test

The shear cell methodology was initially developed by A.W. Jenike for developing hoppers and silos based on the principles of stress condition with a powder bed. Currently, the shear cell test is prevalently and internationally used for ranking powder flowability according to the dimensionless flow function coefficient.

Typically, shear cell indicates the flowing behavior of previously consolidated and at rest powder, which is considered as "incipient failure". Therefore, the shear cell is considered as static test which represents powder flowing behavior at a high-stress condition. In certain processes or storage environments, the powder is subjected to external consolidation stress resulting in a densified powder bed, in which particle-particle contact is maximized and interparticle forces play a critical role to maintain the powder bed matrix. For the flow to occur, the yield point of the powder bed must be overcome. The shear cell test measures a series of yield points as a function of certain normal stress. FT4 powder rheometer is designed to implement shear cell under four optional consolidation stresses: 3kpa, 6kpa, 9kpa, and 15kpa. The procedure consists of four steps: conditioning, consolidation, pre-shearing, and shearing. The powder is first fed into a standard 25mm×10ml split vessel. The powder bed was then conditioned by a helical blade moving downward and upward for one cycle, as shown in **Figure *2-1a***. FT4 has been designed to apply this conditioning cycle before performing all tests, in order to (1) aerate the powder bed; (2) avoid macro void in the powder bed, and (3) remove historical effects to create a uniform and reproducible initial packing. In the consolidation step, a vented piston proceeds to induce precise consolidation stress on the sample. After splitting the vessel, the volume of the sample that is subjected to further test is fixed. Then, the shear cell head is assembled to

apply the pre-shearing step. In the pre-shearing step, the shear cell head vertically applies normal stress and horizontal shear stress at the same time, as shown in **Figure *2-1b***, until the shear stress reaches a steady state. The shear stress and normal stress were recorded which were denoted as the pre-shear point. When the pre-shear point is achieved, the normal stress decreases serially, and the sample is further sheared to reach a yield point, where the layer of particles at interface is not able to withstand the shear stress and exhibits a relative displacement. The process of pre-shearing and shearing are repeated for all the normal stress to obtain 5 yield point. A linearized yield locus which goes through 5 yield points (best-fit) is plotted as $\tau - \sigma$ diagram **Figure *2-1c***. The angle between the yield locus and x-axis is defined as the angle of internal friction (AIF). The shear stress where the yield locus intercepts the y-axis (zero normal stress) it defined as the cohesion value (τ_0). Moreover, the Mohr-circle analysis is performed on the yield locus, which geometrically represents the transformation law of particle coordination for Cauchy stress tensor. From the Mohr-circle analysis, the principal stress of the powder bed can be identified. Two circles are drawn. The smaller Mohr-circle goes through the original point and is tangent with yield locus. It intercepts the x-axis which is defined as unconfined yield stress (UYS), i.e., the yield stress of the powder bed in the free surface condition. The larger Mohr-circle is tangent with yield locus and goes through the pre-shear point. It also intercepts the x-axis which is defined as major principal stress (MPS), i.e., the compacting stress in the powder bed. Then, the flow function coefficient (ffc) can be calculated as the ratio of UYS to MPS.

$$ffc = {}^{MPS}/_{UYS} \tag{2-1}$$

Previously, materials can be classified based on its dimensionless flow function coefficient, as shown in

Table 2-1.

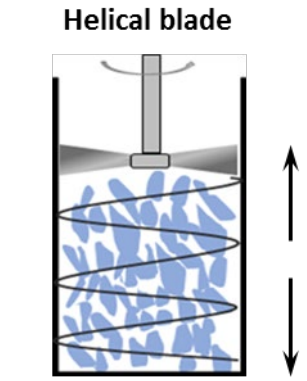

a

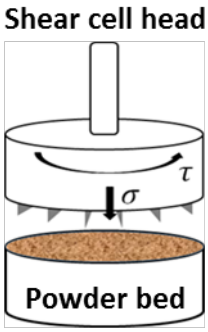

b

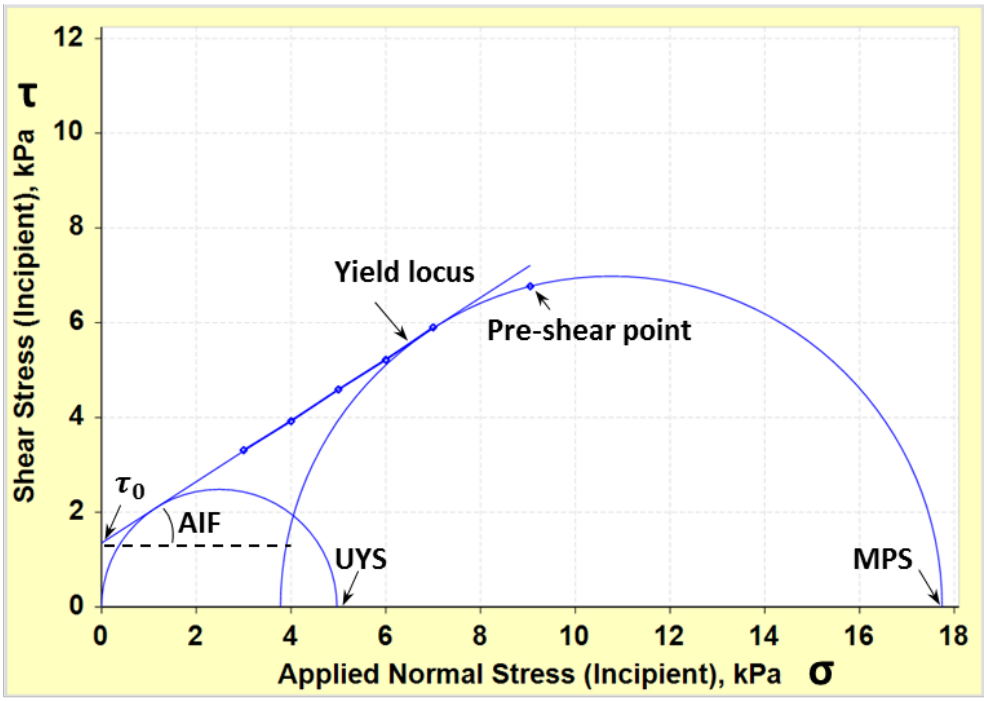

c

Figure 2-1 Shear cell test: a) The schematic of conditioning cycle. b) The schematic of shear cell testing. c) $\tau - \sigma$ diagram and Mohr-circle analysis.

Table 2-1 Category of powder flowability by flow function coefficient (ffc)

ffc	Category of flowability
$ffc < 1$	Not flowing
$1 < ffc < 2$	Very cohesive
$2 < ffc < 4$	Cohesive
$4 < ffc < 10$	Easy flowing
$10 < ffc$	Free flowing

Wang et. al. reported a linear correlation between UYS and cohesion value and a reciprocal correlation between FFC and cohesion value [67]. Therefore, cohesion value can also be considered as a critical index in this test. Generally, cohesion value is used as a flowability index to describe how easily a previously consolidated and rest powder begins to flow. Cohesive powder generally reflects a higher cohesion value and a smaller flow function coefficient. It is important to note that the term “cohesion value” is only used as a mechanical index when discussing shear cell test a high normal stress contidion, indicating the yield point to shear one plane against another in a pre-consolidated powder bed. It should not be regarded as an equivalent term to “cohesive”. A powder is called “cohesive” in this document are used to generally describe the powder has a poor flowability, which represent the cohesive behavior of powder rather than a specific index.

2.2.2 Compressibility test

As a bulk property, compressibility is the measurement of how the density of a sample changes as a function of applied normal stress. The standard measurement consists of two steps: conditioning and compressing. The powder bed was firstly conditioned by a helical blade moving downward and upward three times. After splitting the vessel, the conditioned bulk density (CBD) of powder is reported. In the compressing step, controlled normal stress, which is serially increasing from 0.5 kPa to 15 kPa, is slowly applied to the sample by a vented piston, holding each stress for 60s to allow the powder to reach equilibrium, as shown in ***Figure 2-2a***. At each normal stress, the compressibility of powder is automatically calculated as the percentage change in volume comparing to the initial volume after conditioning and vessel splitting, as shown in ***Figure 2-2b***. Specifically, the volume change at 15 kPa normal stress is documented as the compressibility index (CPS), whose physical meaning is analogous to Carr index (equation 2-8)) but at the different testing conditions. Moreover, the compressed density under each normal stress is reported.

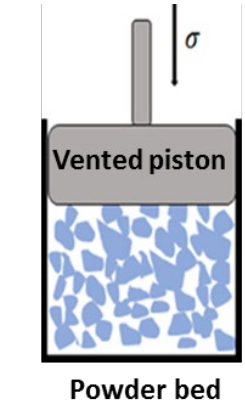

a

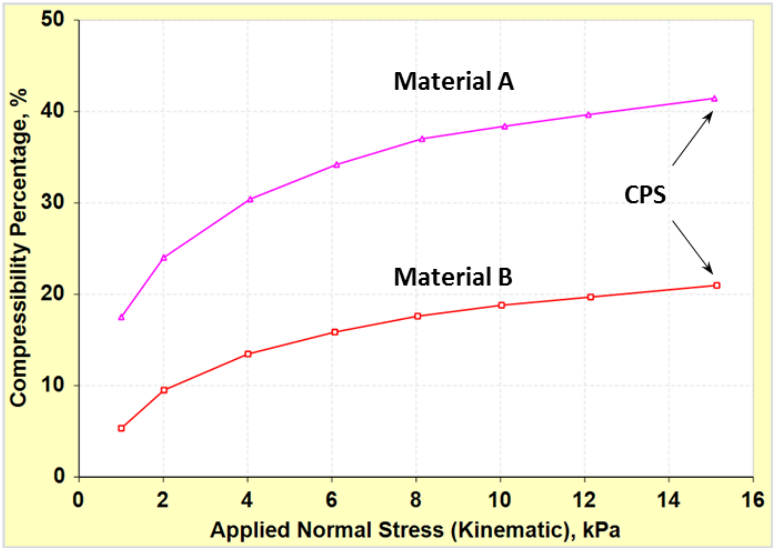

b

Figure 2-2 Compressibility test: a) The schematic of compressibility testing. b) The percentage of volume change as function of normal stress.

This methodology is not a direct measurement of flowability, but it can be correlated with many process conditions, such as powder storage in hopper, handling in feeder, and behavior during a compression process (e.g. roller compaction, tableting). In general, cohesive powder exhibits larger compressibility attributed to initially loose packing state and being sensitive to external stress. Such a powder bed typically contains a relatively high volume of entrained air which results in a large volume change before the powder bed is able to withstand the applied normal stress and reach an equilibrium. In contrast, a free-flowing powder creates a tightly packed powder bed which can withstand the applied normal stress with a small amount of particle re-accommodation. This index is highly dependent on the powder flowing behavior during the conditioning step, which represents a low-stress condition. In addition, the consolidation of powder at a low compression rate is a quasi-static process so compressibility is considered as a quasi-static test.

2.2.3 Dynamic flow energy test

The dynamic flow measurement generally represents powder flowing behavior at low-stress condition. In the FT4, the dynamic flow energy test was programmed as stability & variable flow rate method to measure the energy required to move a helical shape blade through a powder bed as a function of time and blade tip speed, as shown in ***Figure 2-3a***. This test is able to represent the friability and force transmitting between particles when exposed to the very low-stress condition. Similar to other methods, the test consists of two steps globally: conditioning and testing. In the testing step, the conditioning cycle followed the testing cycle repeats seven times where a helical blade moves downward and upward

through a powder bed with a constant tip speed of 100mm/s. The system measures the energy consumed to elicit the particle to flow, as shown in ***Figure 2-3b***. The following indexes will be extracted: Basic flow energy (BFE), which is the measurement of the seventh downward energy consumption; Specific energy (SE), which is the measurement of the average of the sixth and seventh upward energy consumption normalized by mass; Stability index (SI), which reflects the stability of flow energy with time:

$$BFE = the\ energy\ of\ seventh\ downward\ (E_7) \tag{2-2}$$

$$SE = \frac{(sixth\ upward\ energy + seventh\ upward\ energy)/2}{mass} \tag{2-3}$$

$$SI = \frac{E_7}{E_1} \tag{2-4}$$

Where E7 is the flow energy on the seventh downward, and E1 is the flow energy on the first downward. After that, four additional testing cycles are fulfilled with different shear rates (blade tip speed from 100mm/s to 10mm/s). The flow rate index (FRI) can be calculated to describe the flow energy change over the shear rate:

$$FRI = \frac{E_{11}}{E_8} \tag{2-5}$$

Where, E11 is the flow energy at the tip speed of 10mm/s, E8 is the flow energy at the tip speed of 100mm/s. Also, conditioned bulk density (CBD), derived after the conditioning step, is reported.

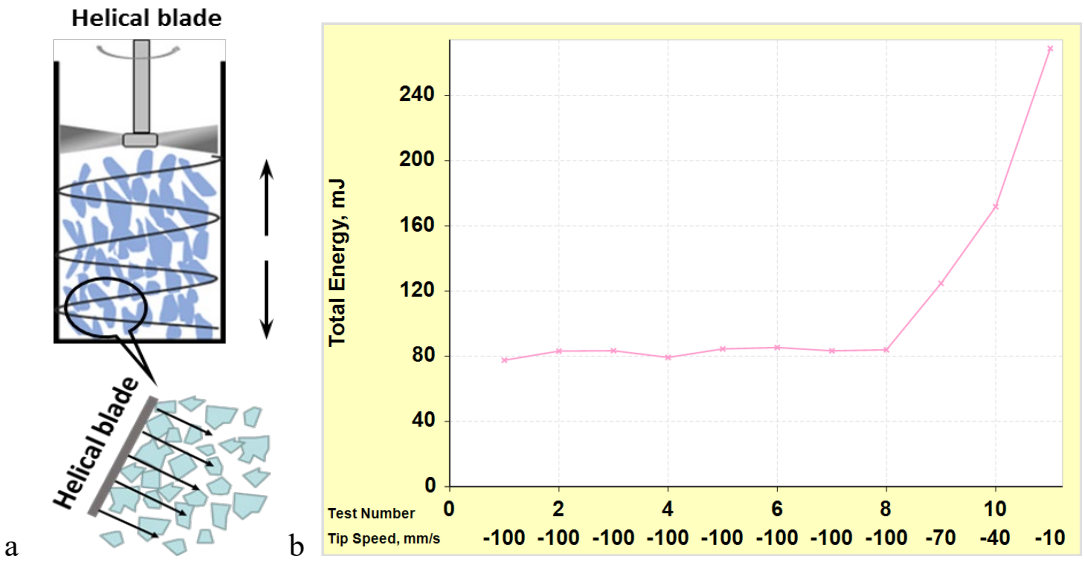

Figure 2-3 Dynamic flow energy test: a) The schematic of flow energy testing. b) The flow energy as function of time and tip speed.

In general, a robust material that is not affected by being made to flow exhibits $SI \approx 1$. In contrast, a friable powder shows a significant change in the flow energy over time (i.e., $SI > 1$ or $SI < 1$)and shear rate due to agglomeration, caking, segregation, aeration, de-aeration, electrostatic charging, granules attrition, moisture uptake, etc.

It is important to note that the results of the dynamic flow test don't necessarily directly relate to how cohesive the powder is. This test is designed to quantifying the flow pattern transmitting or the force transmitting within the powder bed when the blade moving around. Figure 2-3a shows how the flow pattern is transmitted. BFE data can be complicated to interpret as it is dependent on many powder physical properties, such as particle size distribution, density, moisture content, electrostatic charge, surface additive, texture, friability, etc. The way in which these physical properties affect flowing behavior will vary from powder to powder. In practice, the BFE is very useful to quantify the effect of a certain variable on powder flowing, such as the amount of flow additive, moisture, milling, etc.

and possibly to measure how the material properties change after feeder in our case. It is the fact that BFE data significantly relates to powder bulk density. For a low-density powder bed, the helical blade faces a flow zone with a small mass of powder which results in low energy needed. Vice versa, larger BFE data is expected for a high-density powder bed. In order to understand the particle-particle interaction force, normalized BFE with the mass of powder bed can be calculated, named NBFE:

$$NBFE = \frac{BFE}{(CBD \times volume)} \tag{2-6}$$

More discussion of this methodology and its correlation with material behavior is detailed in section 3.4.1 in chapter3

2.2.4 Permeability test

The permeability test is designed to measure how easily air passes through a consolidated powder bed. In many powder processes, such as storage in and flow out of hoppers, vial filling or die filling, compaction in a tablet die, pneumatic transfer, and dry dosage inhalation, air must effortlessly travel through powder bed. Otherwise, a vacuum is created or a large volume of air is entrapped within powder bed which further lead to process failure, such as inconsistent flow, inconsistent amount of filling, tablets capping or laminating, rat hole in the powder bed, insufficient fluidization, spouting. Powder bed permeability is greatly influenced by many physical properties of bulk powder such as particle size and distribution, cohesiveness, particle shape, surface texture, and bulk density.

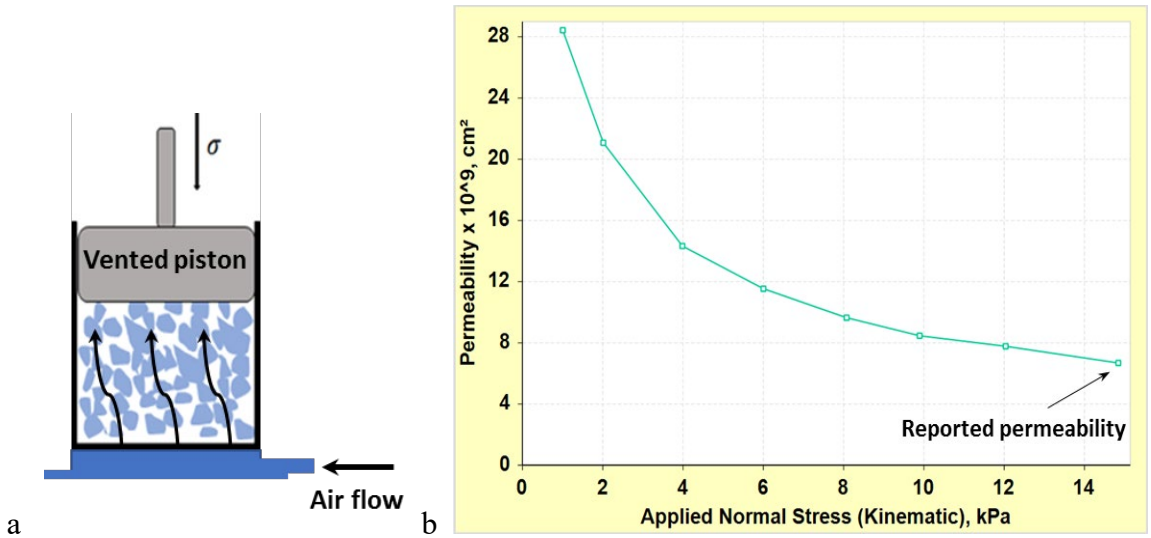

Figure 2-4 Permeability test: a) The schematic of permeability testing. b) The permeability as function of normal stress.

The procedure of the permeability test in FT4 is similar to the compressibility test, it consists of conditioning and compressing steps. The normal stress is applied to the powder bed, rising from 0.5 to 15 kPa serially. Meantime, an upward airflow was introduced at the velocity of 2mm/s, as shown in ***Figure 2-4a***. The pressure drop (ΔP) throughout the powder bed is recorded under each normal stress. Then, the permeability (k) can be calculated dividing and rearranging Darcy's law:

$$k = \frac{q\mu L}{\Delta P} \tag{2-7}$$

Where q is the airflow rate, μ is air viscosity, L is the length of the powder bed.

Specifically, the permeability value at 15kPa normal stress is documented as the index, as shown in ***Figure 2-4b***.

2.2.5 Aerated density, Tapped density, Carr index and Hausner ratio.

The bulk density of powder is a critical material attribute, which defined as the ratio of mass to the volume of the powder bed. The bulk density is the result of both the particle density (i.e., true density) and the packing state of the powder bed. Namely, the measurement of bulk density highly depends on the packing of the powder bed which is the function of powder flowability and the way of preparing such a powder bed. Therefore, according to the packing of the powder bed, two different bulk density indexes are defined: aerated density (ρ_0) and tapped density (ρ_T). Aerated density can be calculated when immediately read the volume (V_0) after gently pouring a known mass of powder into a graduated cylinder without any mechanical energy input. On the other end of the spectrum, the tapped density is usually calculated when the same cylinder, which is prepared for measuring aerated density, is subjected to a series of mechanical tapping. The mechanical tapping is performed by using an Autotaps tapped density analyzer (Quantachrome Instruments, Boynton Beach, FL) with 260/min in tapping rate and 3mm in tapping height. The number of tapping is gradually increased as 10, 500, and 1250 taps and the corresponding volume (V_{10} , V_{500}, V_{1250}) is read. If the difference between V_{1250} and V_{500} is less than 2ml, the V_{1250} is considered as tapped volume (V_T). Otherwise, the tapping is repeated with 1250 taps as interval until the difference between succeeding measurement is less than 2ml, and the corresponding volume is considered as tapped volume. As discussed above, the interactions between particles affect powder packing state and these interactions dictate powder flowability. Thus, the comparison between tapped density and aerated density reveals powder flowing behavior, which is defined as Carr index and Hausner ratio (HR).

$$Carr\ index = \frac{V_0 - V_T}{V_0} \times 100\% \quad (2\text{-}8)$$

$$HR = \frac{\rho_T}{\rho_0} = \frac{V_0}{V_T} \quad (2\text{-}9)$$

The Carr index is mathematically analogous to the compressibility index (CPS) from FT4, but they are obtained at the testing conditions with different mechanical input (tapping for Carr index but compressing for CPS).

2.2.6 Angle of repose

When pouring a bulk powder on a flat surface, it forms a pile. As long as an equilibrium structure forms, the subsequently fresh material slides erratically along the slope of the pile. The angle of repose refers to the steepest angle between the slope of the pile and horizontal plane, which can be measured geometrically after the system reaching the equilibrium structure, as shown in ***Figure 2-5a***. For this equilibrium structure, particles on the slope is at the verge of sliding. Therefore, this measurement is considered as a static test for quantifying powder flowability which indicating powder flowing behavior at free surface (i.e., low stress) condition[63]. In general, a cohesive powder exhibits yield a large angle of repose.

2.2.7 Avalanching method in a rotating drum

A rotating drum is used in a characterization technique that quantifies powder flowing behavior in a cylindrical container which rotates around its axis at a controlled angular speed. During this process, the powder is first carried up on the side with the rotating of the drum until the structure cannot support the weight of the powder bed anymore. Then,

the powder structure collapses resulting in an avalanche. Such a drum is equipped with transparent walls that allows a CCD camera to record this process and capture the largest angle of the interface before the formation of an avalanche in each revolution, as shown in ***Figure 2-5b***. After a certain number of revolutions, the average value of the angle is documented and named as avalanche angle which is used as an index to represent powder flowability. In general, a free-flowing powder exhibits a smaller avalanche angle. Additionally, in some versions of rotating drum tester, a loading cell is equipped beneath the drum. During the measurement, the loading cell captures the variation of weight in the moment of powder inertia as the avalanche fall, which is defined as avalanche size or avalanche energy. For a more cohesive powder, the larger avalanche forms, which lead to the larger standard deviation of the force signal measured by the loading cell. The rotating drum measurement is usually performed at multiple rotational speeds. It is worthwhile to note that the rotating drum methodology is a dynamic test and measures powder flowing behavior in a free surface (i.e., low stress) condition[32, 63].

The prevalent rotating drum testers are Granudrum developed by GranuTools^{TM} (Awans, Belgium), Revolution Powder Analyzer developed by Mercury Scientific Inc (Mount Pleasant, SC), and Gravitational Displacement Rheometer (GDR) developed in Rutgers university[68, 69].

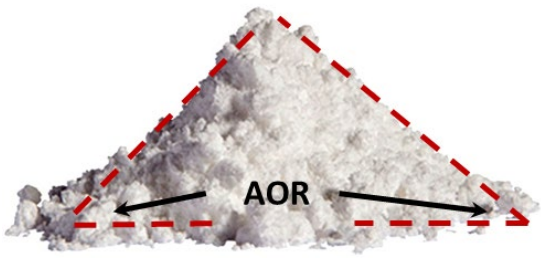

a

b 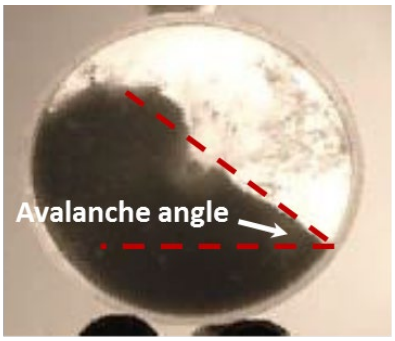

Figure 2-5 a) Angle of repose (AOR) and b) avalanche angle.

2.3 Characterization of powder electrostatic properties

Most pharmaceutical materials are electrically insulating material. Hence, electrostatic charge generates during powder handling. Electrostatic charging plays a critical role in powder handling and powder processing. Many issues in pharmaceutical manufacturing, such as inconsistent flow, insufficient mixing, sticking on instrument, and jamming, are attributed to electrostatic charging. Typically, when particles contact, roll, and slide against each other or equipment surface, electrons transfer from one surface to the other. Particularly, when the surface is electrically non-conductive the acquired charges cannot dissipate instantaneously resulting in unbalanced electrostatic forces acting between particles, which further cause aforementioned electrostatic behavior. In chapter 3, the effect of electrostatics on powder flow and the phenomenon of powder buildup on equipment surface is discussed. To capture these risks fast, appropriate methodologies are required in modern pharmaceutical development, which can be used to quantify powder electrostatic properties with sufficient consistency and reproducibility. Unfortunately, electrostatic charging during a process is a complex phenomenon, which is the function of both material intrinsic properties and environmental conditions. For example, material

properties, like particle size, particle shape, conductivity, surface area, bulk powder density, crystal form, moisture content, and surface chemistry, affect electrostatic charging. Also, electrostatic behavior is dependent on environment humidity and external stress. Although a growing number of literature works attempted to reveal the fundamental causes of this phenomenon, the complete theory of powder electrostatic charging and prediction of electrostatic behavior is missing. In this section, four electrostatic characterization techniques are introduced: charge-to-mass ratio measurement, resistivity measurement, impedance measurement, and dielectrophoresis measurement. In later technical chapters, the charge-to-mass ratio is used as an index to indicate powder electrostatic charging tendency. Moreover, in chapter 7, the future direction of investigation to fully understand powder electrostatic behavior by using multiple characterization techniques is recommended.

2.3.1 Charge-to-mass ratio

The Charge-to-mass ratio is a direct measurement that determines the polarity and quantifies the net amount of electrostatic charge acquired per unit mass in a controlled process. Powder electrostatic potential is traditionally assessed by using this methodology in the pharmaceutical industry and other powder-related fields. There are multiple versions of the setup to measures charge-to-mass ratio based on the way of charging particles, such as particles freely moving through a chute or an incline, particle moving through a vibratory surface or pipeline, particle passing through a screw feeder at a constant speed, and particles processed in a closed container. To compare the electrostatic tendency of materials, they must be measured at the exact same process condition.

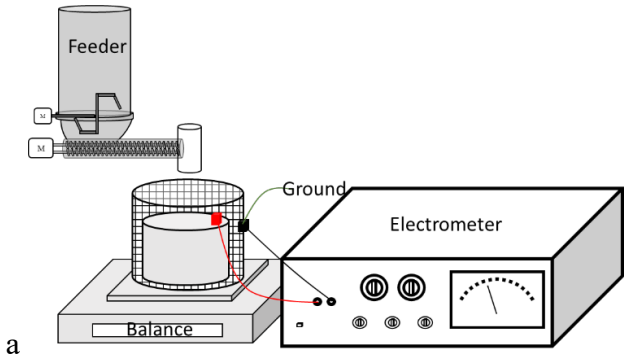

a

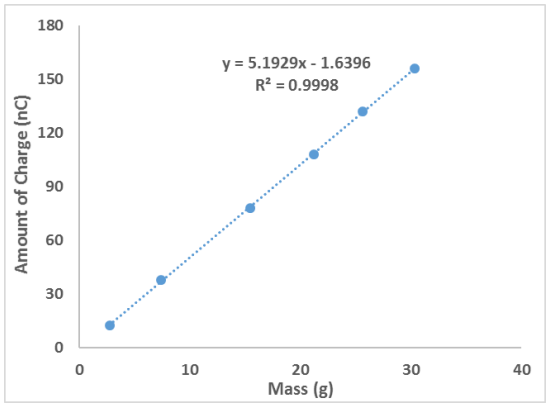

b

Figure 2-6 Charge-to mass ratio: a) Experimental setup. b) Calculating charge-to-mass ratio

In this work, a twin-screw feeder is used to be the controlled charging process. The set-up for measuring charge-to-mass ratio is displayed in ***Figure 2-6a***. A powder sample is discharged in an aluminum cup via a twin-screw feeder with fine concave screw assembled. The aluminum cup is placed in a grounded Faraday cage to eliminate the effect of spurious charge from the environment and connected with an electrometer. Then, the polarity of the net charge is determined. Also, the amount of charge and mass of the sample are recorded. We repeatedly discharge powder in the cup further until 6~8 data points are achieved. By plotting mass value on the X-axis and the absolute value of net charge on the Y-axis, linear

fitting net charge value versus mass, the charge-to-mass ratio is determined as the slope of the fitted line, as shown in ***Figure 2-6b***.

2.3.2 Powder resistivity

This test is to directly measure powder resistivity by applying the direct current (DC) voltage on the powder bed, as shown in ***Figure 2-7***. The sample of interest is placed into a cylindrical vessel, which has Teflon walls and a conductive top and bottom. The volume of the test cup has been specified. Both conductive lid and bottom acted as electrodes. A DC voltage is then applied between the lid and the bottom, and the current flows through the sample bed is measured using an electrometer. Then, the resistance (R), defined as the ratio of the voltage (V) and current (I), can be calculated. When considering the geometry of the cup (i.e., inner diameter (D) and height (H)), the resistivity (ρ_R) of material can be calculated as:

$$R = \frac{V}{I} \tag{2-10}$$

$$\rho_R = R\frac{\pi(D/2)^2}{H} \tag{2-11}$$

It is very important to note that the powder bed packing (i.e., solid fraction) within the cup significantly influences its apparent resistance owing to that the packing dictates the connectivity between particles. To ensure the powder bed packing for different materials is comparable, the volume of the cup should remain constant and the mass of the sample should be specified according to its compressibility (CPS), which can be easily obtained from compressibility test.

$$Sample\ mass = volume\ of\ cup \times \frac{CBD}{1 - CPS} \tag{2-12}$$

where CBD is conditioned bulk density of powder.

The resistivity of powder plays a critical role in tribo-electrostatic charging since it indicates how easy the static charge dissipates once it is generated[70]. For a material with low resistivity, electrostatic charge flow and dissipate rapidly, which can extremely reduce electrostatic effects[71].

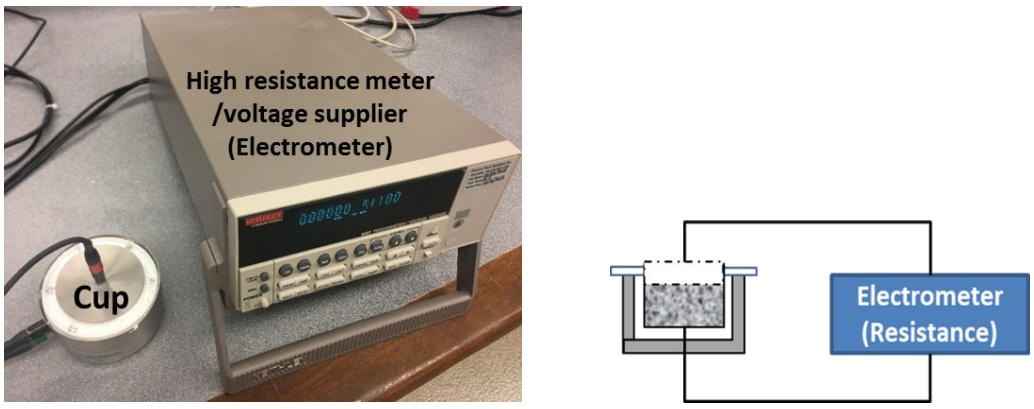

Figure 2-7 Experimental setup of powder resistivity measurement.

2.3.3 Powder impedance measurement

In an alternative current (AC) circuit, the impedance is the apparent opposition of a system to current when a voltage is applied. For a circuit consists of a resistor and a capacitor in parallel, the current of the circuit represented as a complex quantity (I), where the real part is the result of conductivity or resistance (I_R) of the system and the imaginary part is the result of reactance (I_X).

$$I = I_R + jI_X \tag{2-13}$$

To measure the impedance of powder material, the experiment can be set up as shown in ***Figure 2-8a***.

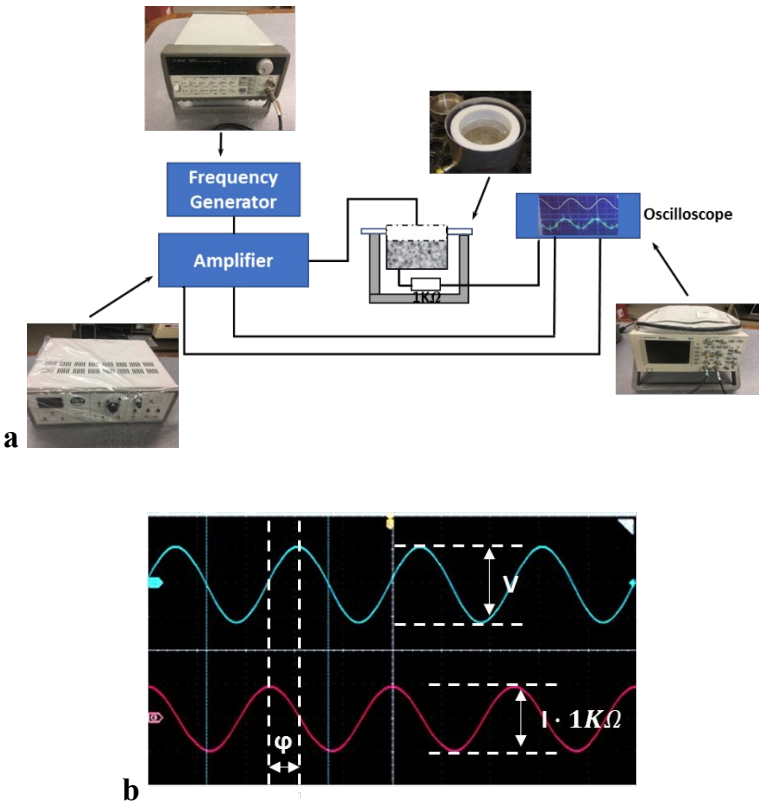

Figure 2-8 Powder Impedance measurement: a) Experimental setup, b) Data acquisition.

The sample of interest is loaded into a cylindrical container, acting as a Faraday cup, which has Teflon walls and a conductive top and bottom. This cup is also internally equipped with a 1000Ω known resistor in series with powder bed. In each measurement, the volume of the cup (both the diameter (D) and height (H)) remains constant. The top lid is heavy so that the powder within the container will be consolidated and also achieve efficient contact with the top and bottom metal electrodes. An AC sinusoidal voltage is generated by a function generator, where the frequency (f) and amplitude of voltage can be adjusted, and

amplified at a constant magnitude (1000X) using an amplifier. Then, the amplified voltage (V) is applied between the lid and the bottom, and the current of the system is subsequently presented using an oscilloscope. The entire circuit can be simplified as a resistor and capacitor in parallel, where the electrically conductive behavior of powder is regarded as a resistor and the powder polarization at an electrical field is considered as a capacitor. The impedance is calculated as the modulus of the current intensity (I) divided by the amplitude of the voltage signal (V). The phase angle (φ) between the voltage signal and the current signal is also reported, as shown in ***Figure 2-8b***, which is used to calculate the resistive (i.e., resistance) and capacitive (i.e., reactance) components of the system. For pharmaceutical powder, its non-conductive nature causes the current of the circuit to be mainly the results of capacitive components and only a minuscule amount of current pass through powder bed, which results in the phase angle close to 90°. Therefore, the calculation of powder resistivity (or conductivity) from this methodology is not practical. However, this measurement can be used to accurately calculate dielectric permittivity of powder. For measuring powder resistivity, the DC methodology described in section 2.3.2 is recommended. Simply put, the Impedance (Z), the resistance of powder bed (R), the capacitance of the cup with powder bed loaded (C), and the dielectric permittivity (ε) of powder can be calculated as:

$$Z = \frac{V}{I} \tag{2-14}$$

$$R = \frac{V}{I \cdot \cos(\varphi)} \tag{2-15}$$

$$C = \frac{1}{\frac{V}{I \cdot \sin\varphi} \cdot 2\pi f} \tag{2-16}$$

$$\varepsilon = \frac{C \cdot H}{\pi\left({}^{D}/_{2}\right)^{2}} \tag{2-17}$$

Typically, the dielectric permittivity of a material is presented as a ratio relative to the vacuum permittivity ($\varepsilon_0 \approx 8.85 \times 10^{-12}\ F \cdot m^{-1}$), which is named as relative permittivity or dielectric constant (ε_r).

$$\varepsilon_r = {}^{\varepsilon}/_{\varepsilon_0} \tag{2-18}$$

Once again, the powder bed packing (i.e., solid fraction) within the cup significantly influences its apparent impedance owing to that the packing dictates the connectivity between particles and determines the total number of particles in a constant volume. To ensure the powder bed packing for different materials is comparable, the mass of the sample should be specified based on the equation 2-12. After loading the specified mass of powder in the cup, external stress may be required to compress the powder bed to the predetermined height so that the volume of the sample is also specified.

By varying the input frequency, the impedance at multiple frequency conditions can be recorded. The impedance and dielectric permittivity imply how the powder is polarized when subjected to an alternating electric field as occurring during contact charging. *Pingali et al* has correlated this measurement to powder flowing behavior and observed that powder flow properties were directly proportional to impedance[69, 72].

2.3.4 Powder dielectrophoresis measurement

This is a technique that assesses the tendency for a powder to develop a dipolar moment in the presence of a DC electrical field. The powder is placed in a non-conductive container (either Teflon or acrylic) and consolidated slightly to create a flat surface. To ensure the powder in the container is not significantly charged when preparing the sample, an ionizer gun is frequently used to neutralize the accumulated electrostatic charge. Then, this container is subjected to a controlled DC voltage relative to the ground, which is generated using a Van der Graff generator (VDG). As shown in ***Figure 2-9a***, the voltage of the VDG is controlled by constructing a voltage divider, which is a grounded metal wire. By adjusting the distance between the tip of the grounded wire and the top surface of VDG, a specific amount of charge is drained from the VDG, which promises an accurate control over the voltage of the VDG. During the experiment, the voltage of the VDG is monitored by measuring the current passing through a known large resistor ($R = 50\ G\Omega$) using an electrometer. The voltage of VDG is controlled and maintained to be at least 20KV. A grounded metal rod is attached to a movable jog which was placed above the VDG on the center of the powder container. Firstly, the VDG is activated and its voltage reaches the steady-state. Then, the metal rod is moved down and immersed in the powder bed to a depth of 6mm. Contact is allowed for 10 seconds before the metal rod is smoothly retracted. In this process, the electric field exhibits a maximum gradient in a small area around the metal rod, when it contacts the powder bed. The powder then becomes polarized and the electrostatic charge on each particle experience rearrangement, causing the powder to stick on the metal rod (as shown in ***Figure 2-9b***). Material that is attached to the rod is collected and weighted. The amount of attached powder can be used to quantify the intensity of the

electrical dipoles of powder particles. Previous investigations have correlated this measurement with the tendency of powder sticks on the equipment surface[73, 74].

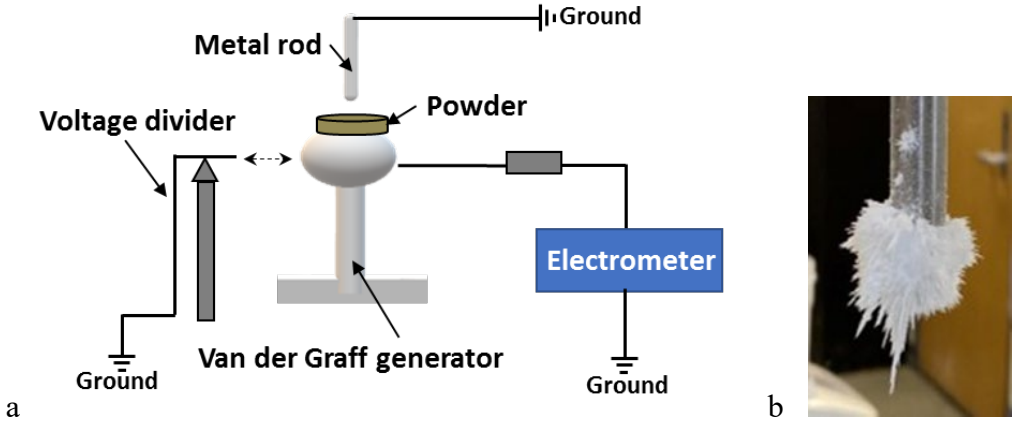

Figure 2-9 Powder dielectrophoresis measurement: a) Experimental setup. b) Powder sticking on the metal rod.

2.4 Powder wettability measurement

Wetting is the phenomenon of a liquid spreading and maintaining contact with a solid surface. The degree of wetting, so-called wettability, is defined geometrically by the contact angle between the liquid and solid at equilibrium, as shown in ***Figure 2-10a***, given by Young's equation:

$$\gamma_{lv}cos\theta = \gamma_{sv} - \gamma_{sl} \tag{2-19}$$

Where θ is the contact angle, γ_{lv}, γ_{sv} and γ_{sl} are the surface free energy of liquid-vapor, solid-vapor, and solid-liquid. In general, a smaller contact angle indicates a higher tendency for the liquid to spread over a solid surface, known as better wettability. Based on the contact angle, materials can be categorized as: complete wetting ($\theta = 0°$), high wettability or hydrophilic ($0° < \theta < 90°$), low wettability or hydrophobic ($90° < \theta < 180°$), and non-wetting ($\theta = 0°$)[75].

For pharmaceutical solid dose form, knowing the wettability of API, excipient and intermediate or final mixtures is crucial for a number of processes ranging from formulation development to manufacturing the final product. For example, a successful wet granulation process requires a liquid binder to penetrate into powder bed instantaneously and spread over the particle surface in order to obtain uniform granules in both size distribution and composition. Additionally, a number of processes potentially change the surface properties of material which affect material wettability. For example, an uncontrolled shearing process would result in a decrease of wettability of mixture when it contains magnesium stearate as lubricant, called over-lubrication. Furthermore, the dissolution rate of the final product, especially for fast release formulation, depends significantly on the wettability of blend since the first stage of dissolution is the medium penetrating into tablets matrix and adequately wet API particles.

As a result, numerous techniques for measuring powder wettability has been developed. For a hydrophilic porous structure like the powder system, it is difficult to directly measure the contact angle from the three-phase geometry (***Figure 2-10a***) since the test liquid soaks into pores. The prevalent strategy for quantifying the wettability of such materials is to analyze the liquid penetration process to estimate the dynamic contact angle. One of the traditional methods, Washburn column, was developed based on measuring the mass of water uptake when immersing a tightly packed powder column into a liquid bath[76]. Here, an alternative technique, drop penetration method, is detailed. This method exhibits advantage over the Washburn column when only a small amount of powder and a small amount of liquid is available for characterization.

In this technique, the process of drop penetrating into a powder bed is captured and analyzed. The powder bed is prepared by using the FT4 powder rheometer to partially go through the procedure of shear cell test. The powder is conditioned and then consolidated at 15kpa normal stress. Next, the vessel is split so that the compressed powder is scraped to produce a relatively flat surface. The experimental setup is shown in ***Figure 2-10b***. The powder bed is placed on a lifting platform. A syringe of liquid is placed, in the focus of a digital camera, on the top of the powder bed held by a height-adjustable platform. Droplets were delivered from a controlled height close to the powder bed surface, with a gap of approximately 5mm between the needle tip and powder bed surface. Such distance should be predetermined aiming to minimize any effect of droplet momentum. Also, the gap should be large enough to avoid the case of droplet touching the powder bed surface before leaving the needle. The digital camera is assembled to be perpendicular to the droplet. The drop penetration is recorded using the StreamPix video recorder at a controlled frame rate, as shown in ***Figure 2-10c***. The videos are then analyzed using ImageJ, removing the background, and converting pictures into binarized images, as shown in ***Figure 2-10d***. The volume of droplet in each frame is calculated by plugging in a JAVA code assuming that the shape of the droplets is axisymmetric. Then, the drop volume as a function of time can be plotted. To calculate the contact angle of powder with water, a reference liquid that completely wets the powder (assuming contact angle with powder $\theta = 0°$) is needed. Specifically, silicone oil is used as the reference liquid.

A detailed discussion and validation of the drop penetration method used to measure the wettability of powder were reported in our previously published work[77]. Below, I briefly summarize the main calculation procedure. The calculation is based on non-

dimensionalizing penetration process and then combining both water and reference liquid penetration. The contact angle of reference liquid can be considered as zero degree. Firstly, it is assumed that the contact radius of a droplet remains constant during the penetration process when deposited on a powder bed. Then, this contact radius r_c is defined as the characteristic length of the problem. Using Darcy's law, we can obtain the characteristic velocity $u_c = (kp_c)/(\mu r_c)$, where k is the permeability of the powder bed, p_c is the capillary pressure inside the powder bed. μ is the viscosity of liquid. Therefore, the characteristic time for drop penetration, when considering powder bed porosity ε, is:

$$t_c = \frac{\varepsilon r_c}{u_c} = \frac{\mu r_c^2}{k p_c} \tag{2-20}$$

Where capillary pressure can be written as p_c=$2\gamma_{lv}cos\theta/r_{eff}$, γ_{lv} is the surface tension of liquid and r_{eff} is the effective pore size of the powder bed. Note that, the non-dimensional penetration process, that is $\widehat{V_p}(\hat{t})$, is a universal curve, which is independent with liquid properties, contact angle, capillary pressure, drop size etc. This universal curve is equal for both reference liquid and water. That means, for a give non-dimensional penetration volume α, the non-dimensional penetration time for both liquids are the same. Hence, the contact angle of powder with water can be derived as:

$$\cos\theta = \frac{t_{\alpha/R}}{t_{\alpha/T}} \cdot \frac{\mu_T}{\mu_R} \cdot \left(\frac{r_{c/T}}{r_{c/R}}\right)^2 \cdot \frac{\gamma_R}{\gamma_T} \tag{2-21}$$

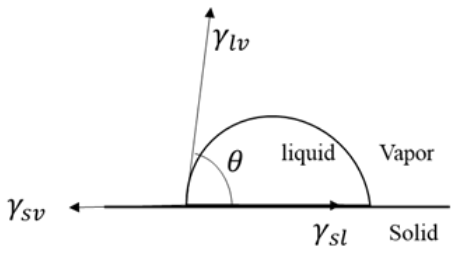

a

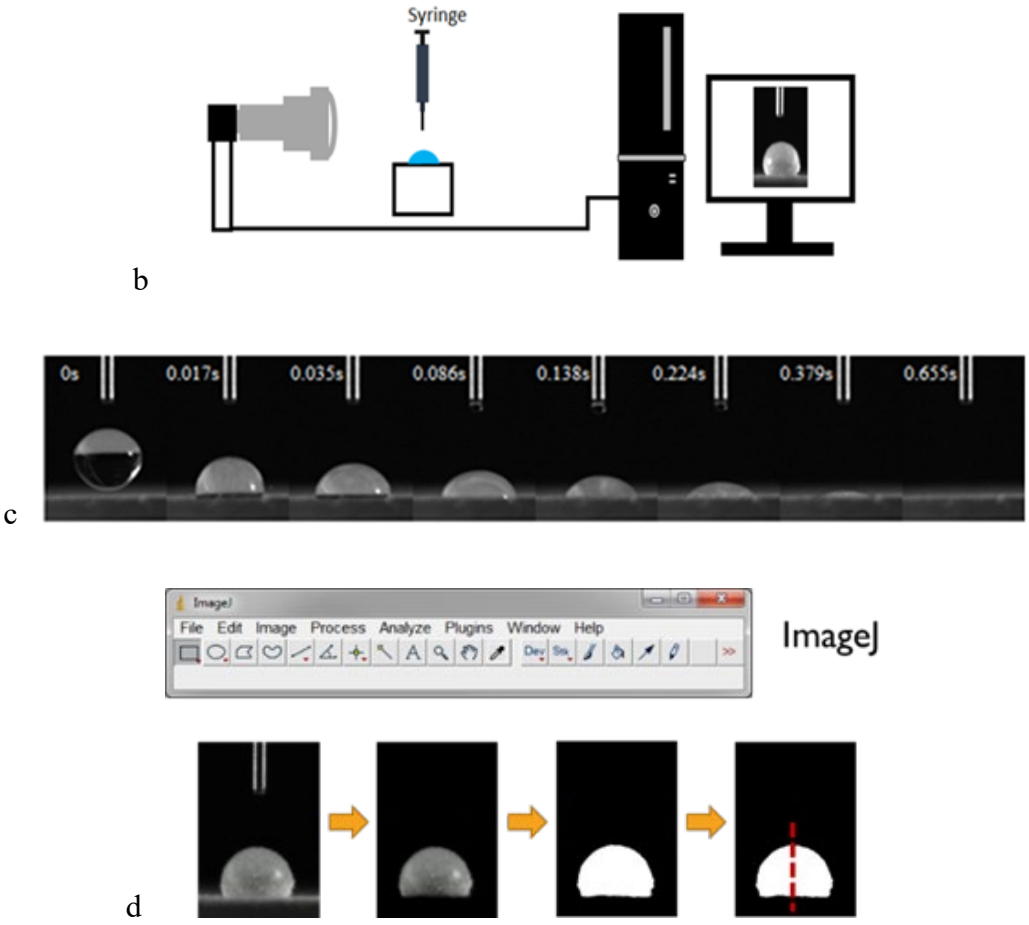

Figure 2-10 Powder wettability measurement: a) Definition of contact angle. b) Experimental setup of drop penetration. c) Drop penetration into a porous powder bed. d) Analyzing drop penetration video.

2.5 Powder surface energy by inverse gas chromatography

The surface energy or surface free energy refers to the energy required to disrupt intermolecular bonds and produce a unit surface of the material. This energy greatly influences the interaction between surfaces, including solid-solid, solid-liquid, and solid-gas interactions. In the pharmaceutical field, for example, the interaction can be the formation of liquid bridge in wet granulation[78, 79], particle-particle interaction during powder handling[80-82], the interaction between the guest particle and host particle in dry-

mixing coating[83, 84], the formation of bonding during compaction[85], the formation of solid suspension in a solvent[86], liquid wetting, dissolution[87], film coating[88], moisture uptake, etc. Moreover, surface energy characterization is beneficial in quantifying material variation between different batches [89, 90], understanding powder surface properties change during milling and its effect on the subsequent unit operations[90, 91], understanding powder tribo-electrostatic behavior[92, 93], detecting the difference of crystal morphology[94], monitoring the lubrication of pharmaceutical blends[95], and detecting the change in the degree of amorphous form or crystallinity[96, 97].

The surface energy of powder material can be measured primarily by two method: (1) estimating contact angle between powder and multiple liquids including both polar and non-polar liquids, then calculating surface energy based on Young's equation (equation (2-19)[98, 99], and (2) inversed gas chromatography (IGC). This section overviews the operating principle of IGC.

To measure surface energy by IGC, the powder material of interest is first packed into a glass column and fixed with glass wool at both the top and bottom of the column. Then, the sample is usually conditioned by employing a carrier gas (e.g. dry Nitrogen or Helium) to continuously pass through the column at a controlled flow rate and controlled column temperature. Next, the surface energy is determined by injecting a series of non-polar and polar vapor probe of known properties in the column, which results in an approximately gaussian peak in the IGC chromatogram. The retention time (t_r), determined from the maximum of the peak of each probe, is extracted, which represents the interaction between the organic molecule and the surface of particles. In addition, the dead time (t_0) of the

column can be determined from the injection of an inert probe (methane). Hence, the net retention volume (V_n) of the probe can be expressed as:

$$V_n = \frac{j}{m} \cdot F \cdot (t_r - t_0) \cdot \frac{T}{273.15} \tag{2-22}$$

where F is the flow rate of the carrier gas, m is the mass of sample in the column, T is the temperature of the column in degrees centigrade, j is a correction factor considering the pressure gradient between inlet (P_{in}) and outlet (P_{out}) of the column, given by the following equation:

$$j = \frac{3}{2} \frac{\left({P_{in}}/{P_{out}}\right)^2 - 1}{\left({P_{in}}/{P_{out}}\right)^3 - 1} \tag{2-23}$$

The Gibbs free energy (ΔG_a) of the interaction between probe and particles can be further determined according to the net retention volume, given by:

$$\Delta G_a = R \cdot T \cdot \ln V_n + C \tag{2-24}$$

where R is the gas constant and T is the temperature of the column.

It is important to note that the total surface energy (γ_s) consists of two components: (1) non-polar energy (i.e., dispersive energy, γ_s^d), and (2) polar energy (i.e., specific energy, γ_s^{sp}), such as hydrogen bonding or acid-base interactions. Therefore, the total free energy of probe adsorption (ΔG_a) also splits into the dispersive component (ΔG_a^d) and the specific component (ΔG_a^{sp}), given by:

$$\gamma_s = \gamma_s^d + \gamma_s^{sp} \tag{2-25}$$

$$\Delta G_a = \Delta G_a^d + \Delta G_a^{sp} \quad (2\text{-}26)$$

Dispersive energy

The dispersive surface energy is determined based on the injection of non-polar probes, like n-alkanes (Hexane, Heptane, …, Decane). The interaction between non-polar probe and particles is only driven by dispersive forces. Therefore, the free energy of non-polar adsorption can be defined as:

$$-\Delta G_a = N \cdot a \cdot W_{adh} \quad (2\text{-}27)$$

where N is the Avogadro's number, a is the cross-sectional area of the probe, and W_{adh} is the work of adhesion. According to Fowkes's equation, the work of adhesion is determined by the dispersive surface energy of probe and particles:

$$W_{adh} = 2\sqrt{\gamma_l^d \cdot \gamma_s^d} \quad (2\text{-}28)$$

Combining the previous equations, the relationship between dispersive energy and net retention volume can be express as:

$$R \cdot T \cdot \ln \quad _n = 2N \cdot a \cdot \sqrt{\gamma_l^d \cdot \gamma_s^d} + C \quad (2\text{-}29)$$

By plotting $R \cdot T \cdot \ln V_n$ as a function of $a \cdot \sqrt{\gamma_l^d}$ for n-alkanes, a best-fit straight line can be obtained, as shown in ***Figure 2-11a***. The dispersive surface energy of powder material (γ_s^d) can be calculated from the slope of the line.

Specific energy

According to Van Oss model[100], the specific energy of material can be further split into two components, named as Lewis base (electron donor, γ_s^-) and Lewis acid (electron acceptor, γ_s^+). Both components contribute to the specific free energy during the interaction with polar probes, given by:

$$\Delta G^{sp} = 2N \cdot a(\sqrt{\gamma_l^+ \gamma_s^-} + \sqrt{\gamma_l^- \gamma_s^+}) \quad (2\text{-}30)$$

Both components can be determined from the injection of two monopolar probes. Ethyl Acetate is usually used as a pure basic probe ($\gamma_l^+ = 0$) and Dichloromethane is usually used as a pure acidic probe ($\gamma_l^- = 0$). The interaction of these two probes with particles is driven by both dispersive force and specific acid-base force. The dispersive contribution can be derived from the previous best-fit line, so that the specific component (ΔG_a^{sp}) can be calculated by subtracting the dispersive contribution from the total adsorption free energy. Geometrically, it is the vertical distance between the data point ($R \cdot T \cdot \ln V_n$) of the polar probe to the vertical projection of this point on the best-fit line, as shown in ***Figure 2-11a***. Then, the specific surface energy of powder (γ_s^{sp}) can be calculated from the Lewis acidic (γ_s^+) and Lewis basic (γ_s^-) energy, given by:

$$\gamma_s^s = 2\sqrt{\gamma_s^+ \gamma_s^-} \quad (2\text{-}31)$$

Acid-Base properties

On the other hand, the acid-base properties of powder can be represented by the electron donor (K_b) and an electron acceptor (K_a) parameters. The related theories are developed previously by Gutmann and Drago et al[101, 102]. To calculate these parameters, multiple polar probes are injected into the column, such as Ethyl Acetate, Acetone, Acetonitrile,

Ethanol, and Dichloromethane. The retention volume of each probe is determined according to equation 2-22. In Gutmann's theory, for each polar probe, the electron donor number (DN) and electron acceptor number (AN) represent its Lewis acidity and Lewis basicity, respectively. Therefore, the specific interaction of these polar probes with the particles can be described as:

$$\Delta G^{sp} = DN \cdot K_a + AN \cdot K_b \tag{2-32}$$

The equation can be rearranged as:

$$\frac{\Delta G^{sp}}{AN} = \frac{DN}{AN} \cdot K_a + K_b \tag{2-33}$$

By plotting ${\Delta G^{sp}}/{AN}$ as function of ${DN}/{AN}$ for all of the polar probes, a best-fit line can be obtained, as shown in ***Figure 2-11b***. The slope and intercept with y-axis represent the electron donor (K_b) and the electron acceptor (K_a) parameters, respectively.

Typically, the characterization of powder surface energy is performed at multiple surface coverage of particles by injecting different amounts of vapor for each probe. In such a manner, not only the surface energy but also the distribution of surface energy can be quantified, which is defined as the heterogeneity of surface energy.

a

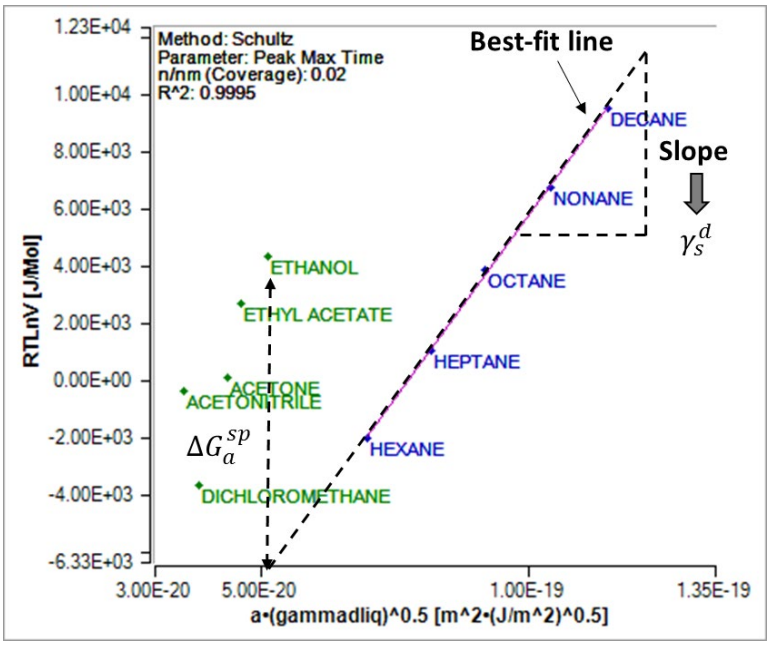

b

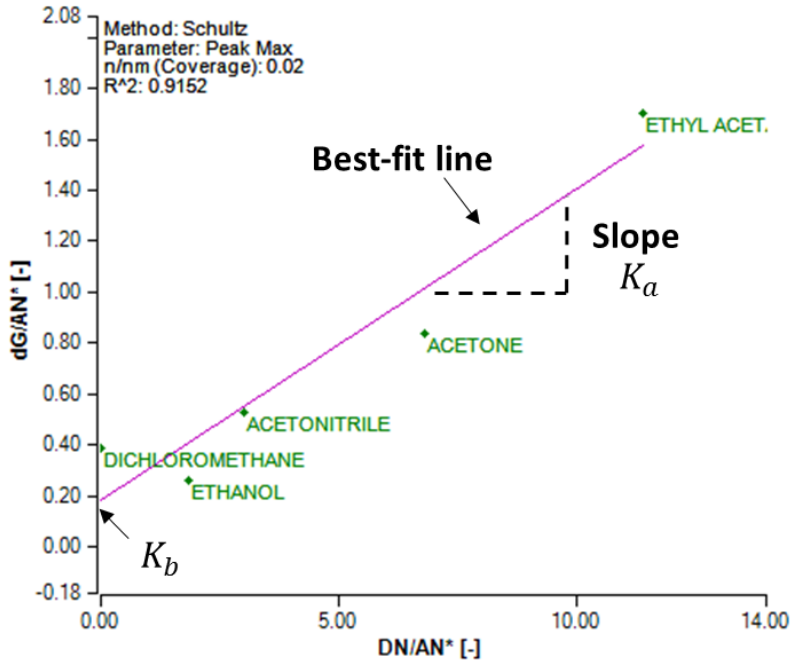

Figure 2-11 Powder surface energy by inversed gas chromatography: a) Dispersive energy and specific energy. b) Acid-base properties.

3 Chapter 3 Powder Property Change after Passing Through a Feeder: the Effect of Electrostatics on Powder Flow

3.1 Introduction

Recently, the powder industries are shifting from the traditional batch process to continuous process, especially in pharmaceutical manufacturing, which requires the process to have high robustness, improved risk assessment, and easier transfer from process development at the pilot scale to commercial manufacturing[103]. When assessing process risk and analyzing failure modes, it is essential not only for traditional powder processing issues to be considered, but also to note new factors that can potentially lead to product failure[104]. As an example, in continuous or semi-continuous drug product manufacturing, powder feeding is regarded as one of the most critical processes, which is rarely used in the traditional batch process. Successful manufacturing requires feeders discharging material with high reliability, stability and minimal disturbance. In general, material feeder performance is pre-defined by performing feeder characterization. A large and growing body of literature has investigated the effect of feeder critical process parameters on powder feeding stability[6, 105]. Many works have also been performed to reveal the correlation between feeder performance and powder flowing properties[60, 106]. However, how feeder impacts powder flowability has not been investigated. As mentioned above, raw materials are usually characterized as the first step. Then, the formulation and all the downstream processes are developed according to the raw material properties. Unexpected flowability change during manufacturing can result in improper process design, which can further lead to unexpected product failure. This raises challenging questions, such as: Is the material after the feeder still the same as what we have characterized before the feeder?

Which material flow index should be characterized to discern material properties change? Which raw material properties drive this behavior? Is it possible to assess this risk in advance?

It is accepted as a generality that the process may alter the properties of powders as it traverses multiple unit operations which generate mechanical action on particles. These changes in properties either beneficially or adversely affect powder performance in next unit operation. If the adverse effect is poorly understood, hardly monitored and poorly controlled, eventually, it may impact the quality of the final product. Work has been performed to explore the effect of the specific process on powder properties. A prevalent topic is that the uncontrolled lubrication process would cause “over-lubricated” blends, which significantly increase particles hydrophobicity[107]. In the pharmaceutical industry, poor blends wettability further causes low tablet dissolution. In addition, over-lubrication causes soft tablets as it weakens particle-particle bonding[108]. Applying high shear mixing, Rajesh Dave and his group reported the enhancement of powder flowability, when adding a slight amount of nanosized SiO_2 as a cohesive ingredient[54]. For the single-ingredient powder system, passing particle through a milling instrument is widely used as an operation to enlarge API bioavailability[9, 10]. However, the size-reduced powder may become more cohesive and easier to form agglomerates. Even powder handling may also alter its properties. When the powder is moved from one environment to another, flow properties can be easily affected due to factors such as the change in humidity and/or temperature, particles segregation, electrostatic charging, etc. Numerous studies have attempted to explain that humidity varyiations and electrostatic charging can significantly alter powder flow behavior[109-111]. Both of them impact inter-particle cohesive force,

where air humidity induces inter-particle capillary interaction, and electrostatic force makes particles either repel or attract each other. Consequently, to develop a robust process, it is critical to understand powder properties as they evolve throughout the manufacturing process. Powder characterization is indispensable not only for raw materials but also for intermediate pure materials and blends.

With regard to powder electrostatic charging, there is a large volume of published studies describing the role of electrostatics on powder handling and process. Unfortunately, the electrostatic charging results in many issues in powders handling and processing, including powder jamming, dusting, adhering to equipment, inconsistent flowing[112, 113], and even sparking and explosion hazards[114]. In practice, when two dissimilar surfaces are brought together and then separate, the electrons transfer from one surface to another. In the case of powder handling, the charge transferring could be more complex as particles roll, slide, rub against each other. This is defined as tribo-electrification[115]. Further investigation has been attempted to allow us to understand the generation of electrostatics as the function of particle size, resistivity, particle shape, crystal form, surface chemistry, moisture content, etc.[116-118]. In the pharmaceutical field, electrostatic charging of powder has been assessed in measuring the amount and polarity of net charges carried by a specified mass of powder, as particles freely moving in a chute or an incline. Applying a similar experimental approach, Ireland previously reported that triboelectrification also highly depends on the way that particles contact with each other[119, 120], then, conclusively demonstrated that greater contact area, longer contact time and higher contact normal stress generate more charge accumulation. It is later confirmed by Naik *et al.*, and

further generalized that electrostatic charging increases with rising of the intensity of particles interaction[121].

There are four objectives of this research: (1) We are aiming to demonstrate whether or not the feeder passage alters powder flowing behavior in the continuous powder process. (2) If the powder flowing behavior is indeed changed due to the feeder passage, we need to determine a method to monitor the change of the flowability. Namely, by performing which characterization method, we will be able to discern the difference. (3) This study set out to further investigate the correlation between the behavior of flowability change after feeder and material properties (or indexes extracted from characterization methods). (4) This study seeks to interpret the effect of powder tribo-electrostatic charge on its flowing behavior.

In total, fourteen pharmaceutical powders were characterized both before and after being fed using a commercialized powder flow tester (FT4 Powder Rheometer). As aforementioned, it has been seen that electrostatic charging may affect the behavior of dry particulate system. We hereby hypothesize that it is possible that material passing through a feeder may change its flowability due to electrostatic charges being accumulated on particles. Moreover, we sought to explore which flow characterization techniques can be used to discern powder flowability changing when material get charged. Our results further suggest a possible correlation between the properties changing and particle size and charging acquisition. In the section of discussion, we suggest a possible explanation on how the electrostatic charging affects powder flowability in the condition of low external stress. Then, a multivariate statistical analysis was performed to strengthen our hypothesis further that electrostatic charging and particle size, maybe bulk density as well, act as

critical factors to alter powder properties when passing through a feeder. In addition, the phenomenon of powder sticking on a feeder pipeline was also illustrated.

3.2 Materials.

This study focuses on the raw materials of frequently considered particle size range in the pharmaceutical industry, which is from about 10μm to 150 μm. Fourteen pharmaceutical powders in this range were investigated. Among them, eight materials are commercially available. They are Ibuprofen USP, Semi-fine Acetaminophen, Powder Acetaminophen, Caffeine, Avicel 105, Maize Starch, Avicel 102, and Solka Floc. Two pharmaceutical active ingredients were supplied by Janssen Pharmaceutical Inc, called API1 and API2. The last three materials were modified in-house by micronizing commercially available materials using an Air Jet mill. They are named as Micronized Ibuprofen, Milled Acetaminophen (S), and Milled Acetaminophen (M), where (S) and (M) represent the difference in particle size grade. Materials and their suppliers are listed in ***Table 3-1***.

Table 3-1 Materials and their suppliers for chapter 3

Materials	Suppliers
Micronized Ibuprofen	Air jet milled
Ibuprofen USP	RIA International LLC
Milled Acetaminophen (S)	Air jet milled
Milled Acetaminophen (M)	Air jet milled
Semi-fine Acetaminophen	Mallinckrodt Pharmaceuticals
Powder Acetaminophen	Mallinckrodt Pharmaceuticals
Caffeine	CSPC Innovation Pharmaceutical
API1	Janssen Pharmaceutical Inc.
API2	Janssen Pharmaceutical Inc.
Solka Floc	International Fiber Corporation
Microcrystalline cellulose (Avicel 105)	FMC Corporation
Microcrystalline cellulose (Avicel 102)	FMC Corporation
Maize Starch	Everest Starch
Micronized Lactose	Air jet milled

3.3 Methods

3.3.1 Powder feeding.

In this study, we use a commercialized twin screw loss-in-weight feeder: K-Tron20 (Coperion K-Tron Pitman, Inc. Sewell, NJ, USA.). As shown in ***Figure 3-1***, it consists of three parts: a volumetric feeder, a weighing platform (load cell), and a gravimetric controller. The volumetric feeder contains a horizontal agitator inside the hopper, which is designed to provide powder circular movement and facilitate powder to fill the pocket created by screw flights. The type C gearbox controls the speed of screws with a maximum rate of 154rpm. Fine concave screws with 20mm in diameter were selected. For Milled Acetaminophen (S), the coarse concave screw was used, because it hardly flowed through the fine concave screws. The coarse concave screw has a similar flight shape as the fine concave screw but gives a larger screw pitch. The hopper and screws of the feeder are electrically grounded throughout experiments. Note that our main goal in this study is to investigate the changes in material properties as the material exits the feeder. Therefore, we use the feeder in the volumetric mode to maintain the screw speed constant. Two speed levels are used: 20% drive command (20%DC) (20%×154rpm= 31rpm), 80% drive command (80%DC) (80%×154rpm=123rpm).

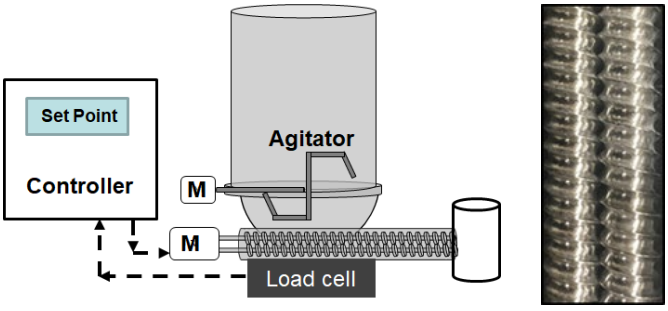

Figure 3-1 A schematic illustration of a loss-in-weight feeder and fine concave screws.

3.3.2 Powder characterization.

Powders were characterized in terms of their flowability, particle size distribution and electrostatic charge-to-mass ratio. FT4 powder rheometer (Freeman Technology Inc., Worcestershire, UK) was used to identify powder flowability. The following tests were performed: compressibility test, shear cell test, and dynamic flow test. Electrostatic characterization was done by measuring charge-to-mass ratio within a controlled process. Particle size distribution were measured using a laser diffraction analyzer. Both pre-feeder and post-feeder material were characterized in same day. All of the experiments was performed at the 40% relative environment humidity. Additionally, feeder directly discharged powder in the FT4 sample vessel as post-feeder material and preformed characterization immediately. For each test, at least three replicates were implemented.

3.3.2.1 Shear cell test

Shear cell test is detailed in section 2.2.1. In this chapter, the initial consolidation stress of 9kPa is selected. It is important to note that the term “cohesion value” is only used as a mechanical index when discussing shear cell test a high normal stress contidion, indicating the yield point to shear one plane against another in a pre-consolidated powder bed. It should not be regarded as an equivalent term to “cohesive”. A powder is called “cohesive” in this document are used to generally describe the powder has a poor flowability, which represent the cohesive behavior of powder rather than a specific index.

3.3.2.2 Compressibility test

Compressibility test is detailed in section 2.2.2.

3.3.2.3 Dynamic flow energy test

Dynamic flow energy test is detailed in section 2.2.3.

3.3.2.4 Charge-to-mass ratio

Charge-to-mass ratio measurement is detailed in section 2.3.1. The scheme of the experimental setup and data analysis are shown in ***Figure 2-6***. When characterizing post-feeder material, the powder is directly delivered in the cup using the screw feeder running at both 80%DC and 20%DC. While characterizing the pre-feeder material, powder is gently placed in the cup using an aluminum spoon. A large difference in charge-to-mass ratio before and after feeding the material is expected as material becomed charged when processed.

3.3.2.5 Particle size distribution

Material particle size distribution is determined using a multi-wavelength laser diffraction particle size analyzer (LS 13320) with tornado dry module (Beckman Coulter, Indiana, USA). This instrument conducts Polarization Intensity Differential Scattering (PIDS) technology so that particle size ranging from 0.017μm to 2000μm can be measured. The dry module creates a vacuum in the system with the pressure of 1990.7Pa (8 inch of water) for the entire sample. In this way, approximately 20 ml of the sample is subject to analyzing and particle size is calculated using Fraunhofer method. Particle size information of D10, D50, D90 are documented.

3.4 Results

3.4.1 Screening varying material properties.

Firstly, to understand which material properties changed when powders pass through a feeder, five pharmaceutical APIs: Micronized Ibuprofen, Milled Acetaminophen (S), Milled Acetaminophen(M), Caffeine and Ibuprofen USP were characterized by applying material characterization techniques described in section 3.3.2. These APIs were chosen as

preliminary study on account of the fact that some of them had displayed remarkable change in flow while others did not. The flow properties of pre-feeder materials and charge-to-mass measurement are reported in ***Table 3-2***.

Table 3-2 Flow properties and charge-to-mass ratio of selected materials for screening study.

	Micronized Ibuprofen	Milled Acetaminophen (M)	Milled Acetaminophen (S)	Caffeine	Ibuprofen USP
Compressibility, %	38.1±1.4	50.1±2.0	52.3±1.5	23.2±1.9	22.2±0.8
CBD, g/ml	0.26±0.01	0.30±0.02	0.16±0.01	0.51±0.01	0.46±0.01
BFE, mJ	63±5	150±20	104±9	101±14	151±7
SE, mJ/g	6±1	10±1	17±1	6.2±0.7	5.16
SI	0.82±0.04	1.1±0.1	0.9±0.2	1.02±0.06	1.01±0.04
FRI	1.4±0.2	1.2±0.1	1.0±0.1	1.9±0.4	0.92±0.02
NBFE, mJ/g	9.5±0.5	20±2	26±2	7.6±0.9	13.4±0.4
Cohesion value, kPa	1.5±0.1	1.6±0.2	2.2±0.2	1.4±0.1	0.81±0.07
UYS, kPa	5.0±0.3	5.5±0.7	8.7±0.8	4.4±0.6	2.7±0.2
FF	3.1±0.2	3.4±0.4	2.4±0.3	3.5±0.2	5.5±0.4
MPS, kPa	15.3±0.1	18.6±0.3	20±1	15±1	15.0±0.3
AIF, °	27.7±0.7	33±1	37±2	24±4	28.6±0.2
Charge-to-mass ratio, nC/g (pre-feeder)	1.2±0.1	1.0±0.3	4±1	0.88±0.08	0.16±0.01
Charge-to-mass ratio, nC/g (80% FC post-feeder)	24±2	11.6±0.4	23±1	4.0±0.7	3.1±0.1
Charge-to-mass ratio, nC/g (20% FC post-feeder)	22±2	12.0±0.5	30±10	4.4±0.6	4.2±0.3
D10, µm	7.10	3.83	3.30	9.32	17.69
D50, µm	16.71	23.32	12.10	32.48	59.45
D90, µm	32.39	53.98	27.90	77.13	111.20

First, as shown in ***Table 3-2***, a remarkable observation can be made that the charge-to-mass ratio for all of them increased dramatically when passing through a feeder. The relative charge-to-mass ratio change is above 500%. This means that the accumulation of electrostatic charge occurred in the feeding process. Moreover, for micronized Ibuprofen, Milled Acetaminophen(M) and Milled Acetaminophen(S), their charge-to-mass ratio after

feeder becomes extremely high, above 20nc/g for Micronized Ibuprofen and Micronized Acetaminophen(S), above10nc/g for Milled Acetaminophen(M). It indicates that these materials acquired a very large amount of electrostatic charge during the feeding process. When comparing different feeding speeds, no considerable difference of charge-to-mass ratio is obtained. The charge acquisition is shown less dependence on the feeding process speed. For this behavior, more discussion will be made in the next section.

Figure 3-2 to ***Figure 3-6*** display the relative change in properties when powder passes through a feeder, comparing 80% DC feeding with pre-feeder and 20% DC feeding with pre-feeder. The indexes described in method section are presented. The positive change represents the increase of this index and the negative change describes the index decreases after feeding. The numbers listed in the graph indicate P-value when performing 2-sample t-test, where the null hypothesis is that the mean value is the same for each sample. A p-value smaller than 0.05 rejects the null hypothesis, confirming that the difference is statistically significant. A P-value larger than 0.05 indicates the difference between the mean values is uncertain and the property likely remains the same. As shown in ***Figure 3-2*** to ***Figure 3-6***, it is apparent that the change in material properties after feeder marginally depends on feeding speed.

Figure 3-2 to ***Figure 3-6*** have also shown that the cohesion value from shear cell test does not change significantly. The comparison of other indexes (UYS, MPS, AIF) from shear cell has also been made (not shown in graphs), but noticeable variation is not suggested.

However, other flow indexes do change. For Micronized Ibuprofen (***Figure 3-2***), Milled Acetaminophen(S) (***Figure 3-3***), Milled Acetaminophen(M) (***Figure 3-4***), some properties are significantly altered. Among them, the compressibility index increased significantly.

In general, the increment of compressibility indicates that powder becomes more "cohesive", so that the initial packing of powder bed is more compressible. In other words, the packing is looser and the density of the initial powder bed becomes smaller. This is also suggested by the decrease of CBD from dynamic flow energy test. A decrease in bulk density indicates particles or powder lumps are farther from each other, probably due to increase of particle-particle repulsion or cohesivity of bulk powder, resulting a looser powder bed packing. As aforementioned, it is well documented that the electric force plays a role in powder flow. Hence, it is reasonable that we first hypothesize the change in material properties is associated with the triboelectric charging. A detailed discussion about how electrostatic charging impacts flowing behavior will be clarified later.

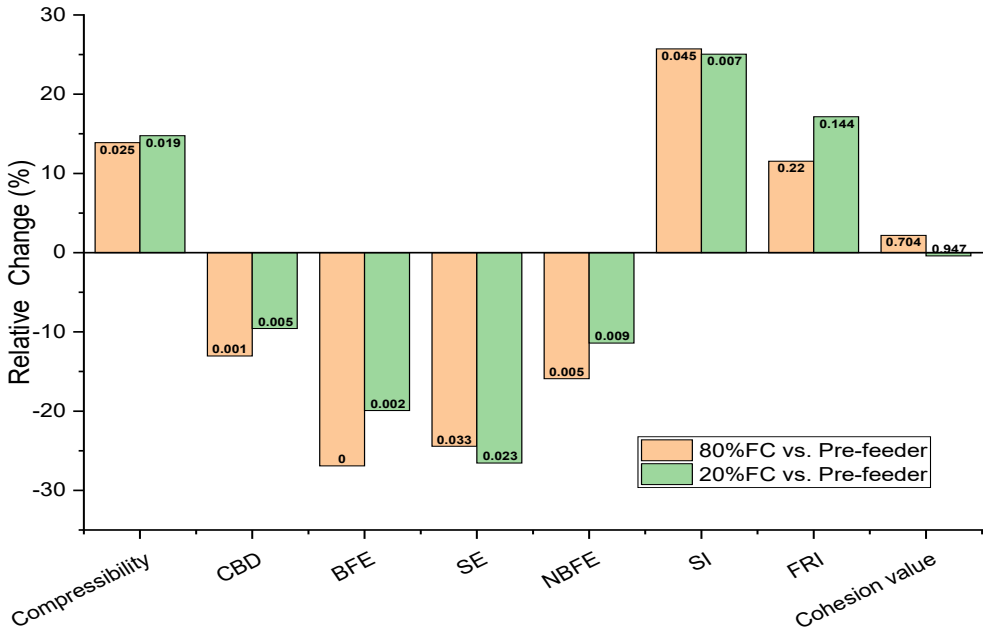

Figure 3-2 Micronized Ibuprofen properties change after feeder.

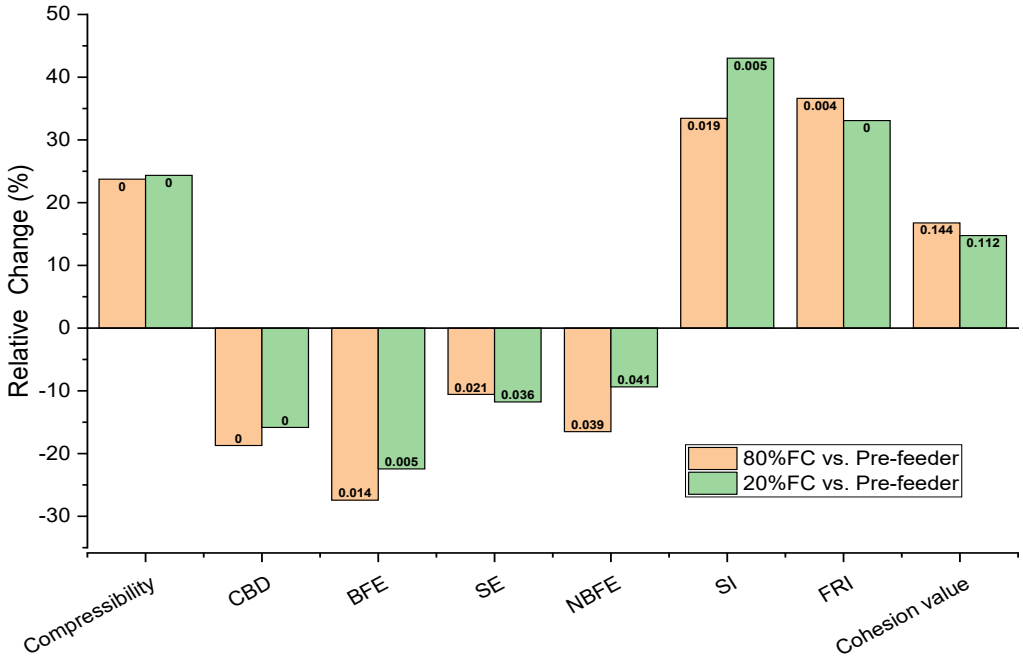

Figure 3-3 Milled Acetaminophen (S) properties change after feeder.

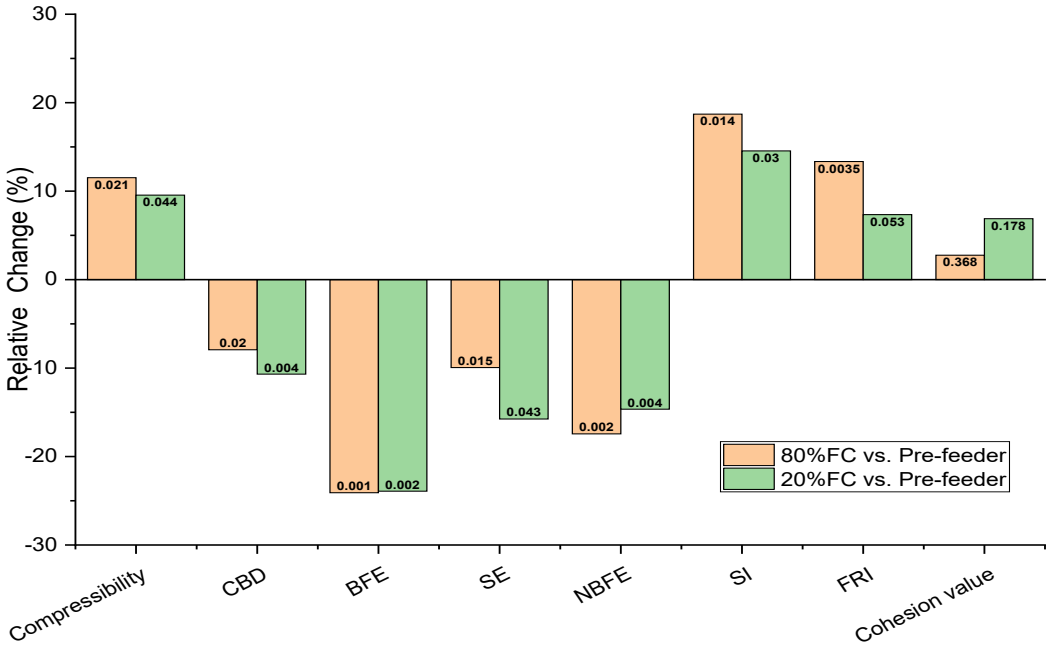

Figure 3-4 Milled Acetaminophen (M) properties change after feeder.

Furthermore, These graphes is showing that dynamic flow energy, including BFE, SE and NBFE, decreased. As discussed above, the decrease of BFE can be explained as that either

a lower density of powder bed or a decrease in particle-particle force transmitting which facilitate the movement of the helical blade when pushing bulk powders. Since the calculation of SE and NBFE have removed the effect of powder bed density, the decrease of these two indexes specifically indicates that particle-particle force transmitting decreases after the feeding process. One of the possible explaination is that particle-particle repulsion increases due to acquiring electrostatics of same polarity. With respect to SI and FRI, significant increase has also been described althrough few p-values are slightly above 0.05. The large measurement error possibly makes some p-values larger than 0.05. The raising of SI can be attributed to the effect of powder bed de-aeration during test. As the acquisition of electrostatics, the looser packing is more fragile that is being broken by the passage of the blade and the powder bed acquire a more consolidated state. Thus. the de-aeration become higher. FRI refers to the sensitivity of a powder to shear rate. The possible interpretation for the increase of FRI (the ratio of flow energy at low shear rate to high shear rate), similar to the interpretation of SI, can be that the powder bed after feeding process contains higher volume of air. At high shear rate, more air is entrained resulting in lower energy consumption, while at low shear rates, more air is excluded resulting in higher energy.

Next, for Caffeine (***Figure 3-5***) and Ibuprofen USP (***Figure 3-6***), all the FT4 powder tests suggest marginal changes of flow indexes. It is worthwhile to note that the charge-to-mass ratio of post-feeder Caffeine (~4nc/g) and Ibuprofen USP (3nc/g~4nc/g) are much less than the previous three materials. Based on our hypothesis, the case is acceptable that small triboelectric charging didn’t impact powder flowing behavior.

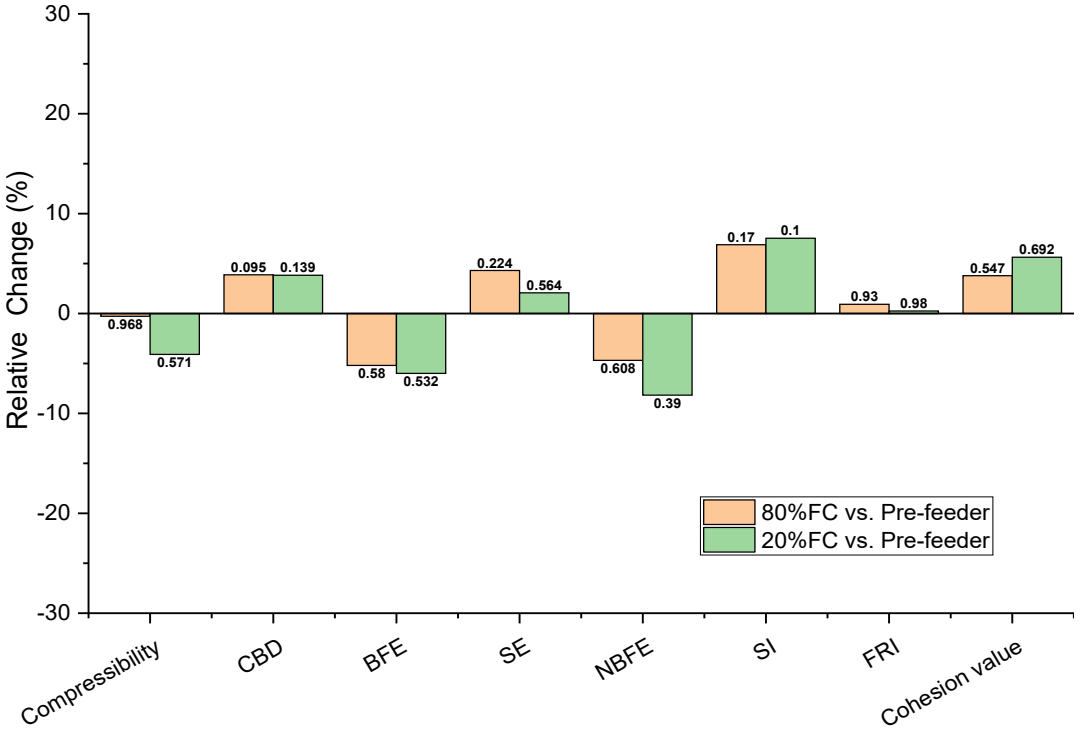

Figure 3-5 Caffeine properties change after feeder.

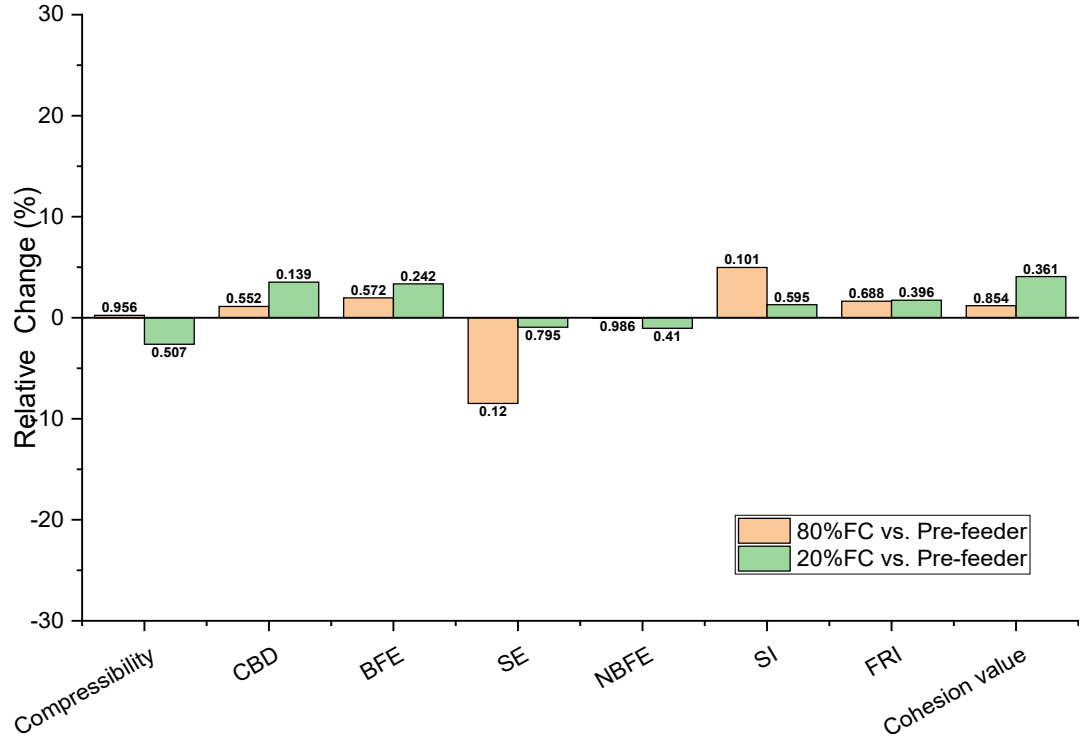

Figure 3-6 Ibuprofen USP properties change after feeder.

For all of these materials above, particle size distribution was also measured after feeding. This is no change in particle size when powder passes through feeder, which could have been one cause of the change in flow observed . We are not presenting particle size data of post-feeder material in this document.

To summarize, powder feeding possibly alters its flowing behavior, which seemed dependent on raw powder electrostatic properties rather than the feeding speed. When passing through a screw feeder, the increment of charge-to-mass ratio indicated there is a stronger particle-particle electrostatic interaction involved. If the electrostatic interaction is sufficiently dominant, powder experiences the increase of compressibility, decrease of bulk density and dynamic flow energy. All of these behavior changes can be attributed to the looser initial powder bed packing. By comparing these properties for pre- and post-feeder materials, we can assess manufacturing risk related to powder flow behavior change. Compressibility test is a more general characterization method than dynamic energy test and a more reproducible method than directly measuring density, according to the error shown in ***Table 3-2***. Additionally, it is widely available in other commercially available instruments or easy to be made in-house. Therefore, we select the compressibility test to identify whether material properties change or not for a larger study, taking into account that other properties also should vary as was shown in this section .

3.4.2 The correlation of powder behavior with raw material properties and electrostatics

As we discussed before, some materials show property changes and others do not when a powder passes through a twin screw feeder. In order to correlate this behavior with raw material characteristics, we further examined nine more pharmaceutical materials in the

conditions of both high-speed feeding and low-speed feeding. The two conditions were again chosen to confirm the outcome of the screening study suggesting that the screw speed has no effect on the change in the material properties. Previously, we have clarified measuring material compressibility as a feasible approach to identify powder property changes after feeding. Hence, the compressibility test was performed for all of these materials. We present all of the data in ***Table 3-3***, including particle size (D50), compressibility of pre-feeder powder (CPS), relative increase in compressibility of 80% DC vs. pre-feeder (Rev. increase 80% vs. pre-), 20% DC vs. pre-feeder (Rev. increase 20% vs. pre-), 80% DC vs. 20% DC (Rev. increase 80% vs. 20%), and charge-to-mass ratio under two feeding speeds. The statistical significance of compressibility variation is demonstrated performing 2-sample t-test and presented as p-value.

First, we confirmed the finding of whether the change in powder flow is independent of feeding speed. Either the p-values are above 0.05 suggesting lack of significance under present test conditions, or the variations are small when comparing different feeding speeds. In addition, the charge-to-mass ratio measured at two feeding speeds are comparable and with no particular trend, which implies that the feeding speed does not provide a significant difference in terms of charge accumulation for the type of feeder tested. A similar amount of electrostatic charges accumulated in this process regardless of how fast powder passed throughout the feeder. This observation seems contradictory with previous documentation, as mentioned in the introduction, which reported that the contact time played an important role in electrostatic charging when powder flowed in a chute[121]. However, note that, when powder flowed into the feeder screw pocket, powder was consolidated and forced to move forward due to the rotating of twin screws, where particles sustained rubbing, sliding

and rolling. It is unlike the reported free-falling condition. In general, particle rolling makes the entire surface available for charge transfer. With consolidation stress, particles are compressed together and makes continuous contact with each other. Thus, the particle contact area is enhanced, which facilitate charge tranfer. Especially for a cohesive (compressible) material, the particle-particle contact area is substantially enhanced at a consolidated state comparing to free-surface state. This behavior was also confirmed by previous studies, also described in the introduction[119, 120]. All of these factors enable considerable electrostatic charge generation, even within a comparatively short time. Therefore, in our case, this is a possible explanation that the charge-to-mass ratio was independent on feeding speed.

Relative compressibility change in the condition of 80%DC is highlighted in ***Figure 3-7***. It is evident that the compressibility of some materials increased remarkably. They are API2, Milled Acetaminophen(S), Micronized Ibuprofen, Avicel 105, Milled Acetaminophen (M) and Semi-fine Acetaminophen. These powders either have very small particle size or acquire a substantial amount of electrostatic charges (as seen in the next figure). Materials are mapped in the diagram of particle size (D50) vs. charge-to-mass ratio of 80%DC (nC/g), as shown in ***Figure 3-8***. This graph suggests that materials that display property changes depend primarily on both particle size and electrostatic charging. A charge-to-mass ratio of 7nC/g is large enough to produce changes in Avicel 105 with a 20microns D50, but not enough for powder Acetaminophen particles (doubling Avicel's 105 size). Also, changes are seen for materials presenting D50 in the range of 11-13 microns and charge-to-mass ratio larger than 3nC/g as in API2, but not for materials that acquire less electrostatic charges as micronize lactose or Maize starch. Similar behavior is

seen at the D50 level of 30 microns with a threshold of charge-to-mass ratio in the range of 6nC/gr. Finally, we did not find any material with a D50 above 30 microns that changes its flowing behavior after passing through the feeder.

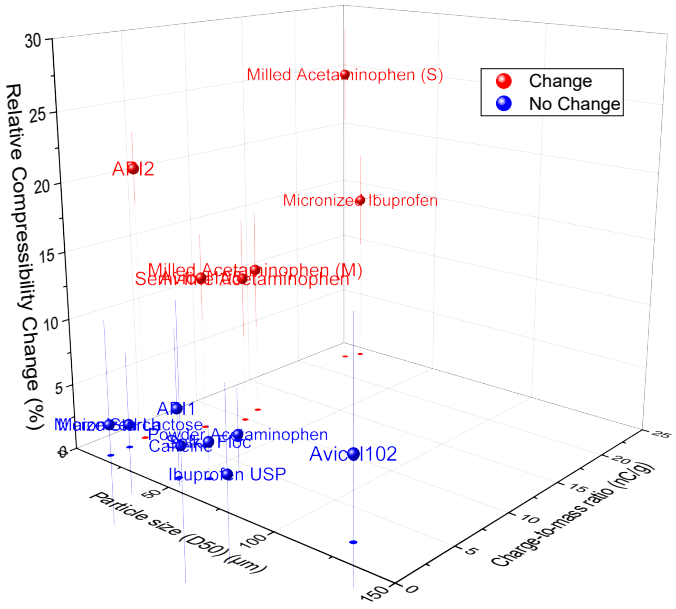

Figure 3-7 Relative compressibility changes after feeding vs. particle size and charge-to-mass ratio

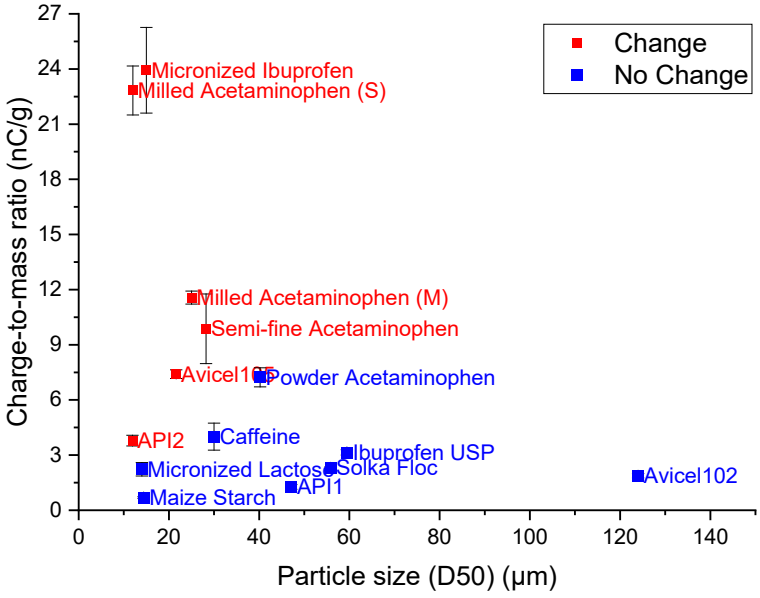

Figure 3-8 Mapping material with charge-to-mass ratio vs particle size.

Table 3-3 Material relative compressibility change and charge-to-mass ratio after feeder.

Material	D50 (um)	CPS, %	Rev. increase (80% vs. pre-) (p-value)	Rev. increase (20% vs. pre-) (p-value)	Rev. increase (80% vs. 20%) (p-value)	Charge-to-mass ratio	
						80% DC (nC/g)	20%DC (nC/g)
Micronized Ibuprofen	**16.71**	**38.1**	**13.9% (0.025)**	**14.8% (0.019)**	**0.8% (0.430)**	**24±2**	**22±2**
Milled Acetaminophen (S)	**12.10**	**52.3**	**23.7% (0.000)**	**24.4% (0.000)**	**0.5% (0.544)**	**23±1**	**30 ±10**
Avicel 105	**18.61**	**21.4**	**11.9% (0.004)**	**14.7% (0.001)**	**2.5% (0.119)**	**7.4±0.2**	**5.2±0.1**
Semi-fine Acetaminophen	**28.22**	**50.0**	**11.4% (0.009)**	**13.0% (0.001)**	**1.4% (0.548)**	**10±2**	**9±3**
API2	**11.90**	**39.7**	**20.7% (0.000)**	**17.7% (0.000)**	**-2.5% (0.111)**	**3.8±0.3**	**2.7±0.3**
Milled Acetaminophen (M)	**23.32**	**50.1**	**11.5% (0.021)**	**9.6% (0.044)**	**-1.8% (0.256)**	**11.6±0.4**	**12.0±0.5**
Caffeine	32.48	23.2	-0.3% (0.968)	-4.1% (0.571)	-3.8% (0.593)	4.0±0.7	4.4±0.6
API1	47.10	16.8	5.6% (0.137)	8.9% (0.149)	3.1% (0.515)	1±0.1	2±0.2
Solka Floc	55.80	40.3	2.8% (0.038)	0.8% (0.357)	-1.9% (0.010)	2.31±0.04	1.6±0.1
Avicel 102	124.7	10.0	6.1% (0.366)	5.1% (0.446)	1.0% (0.897)	1.9±0.1	1.3±0.1
Maize Starch	14.40	16.3	2.4% (0.576)	2.0% (0.603)	-0.3% (0.945)	0.69±0.05	0.22±0.01
Powder Acetaminophen	40.20	43.4	-0.5% (0.783)	0.5% (0.843)	1.0% (0.651)	7.2±0.5	8.0±0.3
Ibuprofen USP	59.45	22.2	0.2% (0.956)	-2.6% (0.507)	-2.9% (0.452)	3.1±0.1	4.2±0.3
Micronized Lactose	13.99	32.6	1.8% (0.534)	-0.1% (0.958)	-1.9% (0.434)	2.2±0.4	2.5±0.3

Another observation arising from our study is that powders of the same nature increase their acquired charge through the feeder process as the particle size decreases, which then causes instability of flow during the process. In our material list, the particle size of Acetaminophen decreases in the order of Powder Acetaminophen, Semi-fine Acetaminophen, Milled Acetaminophen(M) and Milled Acetaminophen(S). Correspondingly, the total amount of acquired electrostatic charges increases following this rank order. The charge-to-mass ratio(q) of these Acetaminophen materials versus their particle size($r = D50$) are shown in ***Figure 3-9***, where the charge-to-mass ratio is proportional to the reciprocal of particle size ($q \propto 1/r$). Since the surface area-to-mass ratio is also proportional to the reciprocal of particle size, for particles of similar shape, this observation indicates that the charge per unit area remains constant with particle size. In other words, when powder passes through the screw feeder, the charge density per unit area (charge-to-surface area ratio) is independent with particle size and depends on the nature of the chemical entity. This result agrees with our previous interpretation that when powder is in the screw feeder, particles are compressed and continuously contact with each other, and particle rolling and rubbing then enable its entire surface to be available for charge acquisition, especially for cohesive or micronized powder. As the material with the largest particle size, Powder Acetaminophen is in the no-change regime (shown in ***Figure 3-8***). With the reduction of particle size, its flowing behavior also becomes more sensitive to electrostatic charging and exhibits deterioration during the feeding process, reflected in a change in tis compressibility. Moreover, the relative value of compressibility change also increases along with the particles size reduction. The other example is Ibuprofen. We previously micronized Ibuprofen USP using an air jet mill, named Micronized Ibuprofen

(S). Charge acquisition is enhanced by a factor of about 10 times, which also caused a change in compressibility following feeder passage. As a summary, powders experience variation in their flowing properties after passing through a feeder when the mean particle size is below a certain threshold that depends on the acquired charge per mass or per surface area. However, while the charge per mass depends on the particle size, the value of the charge per surface area seems not to.

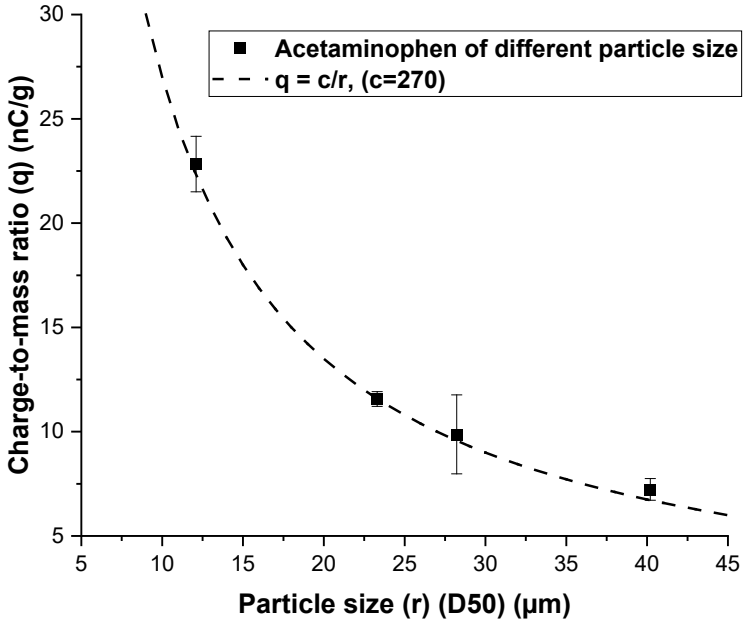

Figure 3-9 Correlation between charge-to-mass ratio and particle size of Acetaminophen.

3.4.3 Powder buildup on feeder surface

In continuous manufacturing, a successful process first requires that each ingredient can be discharged with sufficient accuracy, reliability and robustness. To achieve this objective, feeders have been designed to achieve a controlled process which is able to maintain a set point, within acceptable deviation, throughout the manufacturing timeline. Any powder

jamming, sticking, building up and clogging affect final product performance adversely. For example, in pharmaceutical solid dose manufacturing, the powder feeding directly impact product content uniformity. It is also possible that the product either contains no active ingredient or contains too much, causing superpotent tablets, which can be toxic and harmful to people. In this work, the behavior of powder sticking on feeder tools was also investigated, as shown in ***Figure 3-10a***. These photographs were captured after a feeding time of about 15min. Evidently, in some cases, powder built up significantly on the surface of the feeder pipeline and formed "snow cover" layers. If this material build-up grows large enough, a powder avalanche may suddenly fall into the downstream process, causing an increment of the ingredient concentration. This can possibly lead to superpotent tablets. In our case, a similar observation was made for all of the materials with a charge-to-mass ratio above 6nC/g (shown in ***Figure 3-10b***). Note that although it seems that the sticking phenomenon corresponds to the altering of the flowability, it is not necessary to consider them as equivalent behavior. For example, based on the data above, the compressibility of post-feeder Powder Acetaminophen remains the same as the pre-feeder one, whereas powder sticking was observed due to its high charge accumulation. For API2, there was no powder appearing on the feeder pipeline even though change in powder flow indeed occured after the feeder. This is perhaps due to its moderate electrostatic charging. In this study, as long as charge-to-mass ratio below 6nC/g, no sticking or only negligible sticking was observed.

a i.   ii. 

iii. 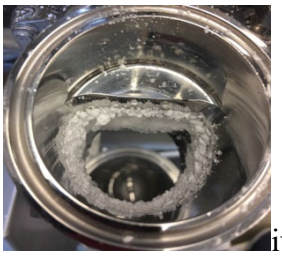 iv.  v. 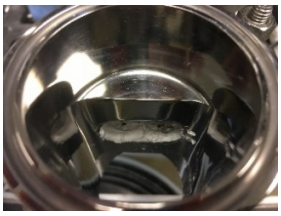

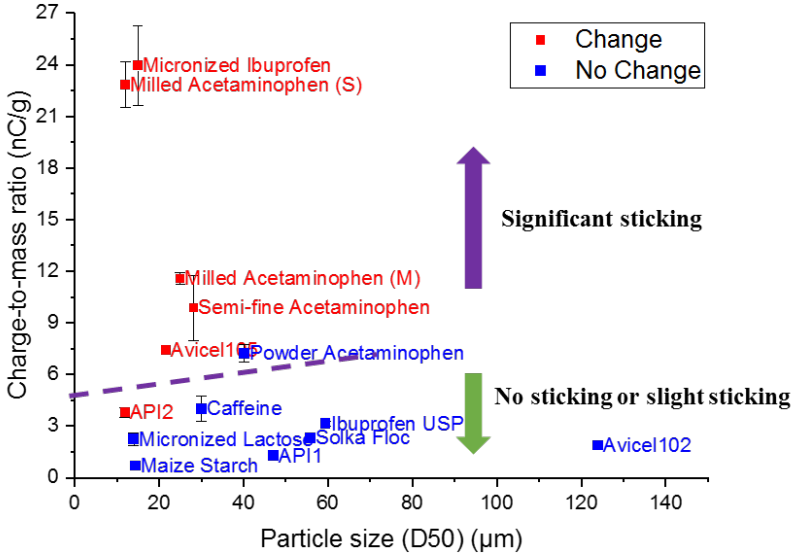

b

Figure 3-10 The phenomenon of powder sticking on feeder: a) Powder sticking on feeder: i. Milled Acetaminophen (S), ii. Micronized Ibuprofen, iii. Semi-fine Acetaminophen. No-sticking or very slight sticking on feeder: iv. API1, v. API2. b) Correlation with charge acquisition.

3.5 Discussion

3.5.1 Interpretation of observed changes in flow behavior

In this document, powder flowability was found to be possibly altered when materials, with a small particle size and a large tendency of electrostatic charging, passed through a twin-

screw feeder. Specifically, the altered flowing indexes were obtained from the test in low external stress condition, including compressibility, conditioned bulk density and dynamic flow energy, rather than the indexes from the high-stress condition as shear cell test. Ideally, when powder is in a low-external-stress environment, for example, in the case of flowing on an inclined plane, gravity is the main driving force for powder flow. In this situation, particle-particle cohesive forces (Van der Waals, capillary, particle interlock etc.), including electrostatic force, prevent powder from freely flowing. It can be regarded as intrinsic-driven flow at the free-surface condition, where the bulk powder flow performance is determined by the competition between inter-particles cohesive interaction and particle gravity. Thus, this is a force balance problem between the surface cohesive component ($F_{surface}$) and particle gravity (W_g). A term of the bond number (Bo_g) was previously defined as the ratio of surface cohesive force and particle weight, describing this flowing mechanism[122, 123].

$$Bo_g = \frac{F_{surface}}{W_g} \tag{3-1}$$

With the accumulation of electrostatic charge, the surface cohesive component is generally enhanced. Net charge-to-mass ratio is easy to be measured. Both the amount of charge and polarity can be determined using the method described in section 3.3.2. Unfortunately, electrostatic charging is more complicated than it appears. In fact, both charge polarities are present during powder handling. If particles come together, which carry electric charges of the same polarity, they will repel each other, causing poor packing of the powder bed, as shown in ***Figure 3-11***. This behavior can be used to interpret our observation of the decrease in density, increase in compressibility and decrease in dynamic flow energy.

Figure 3-11 Decreasing of powder packing as the effect of charge acquisition.

Althrough it seems counterintuitive to consider the repulsive interaction as a surface cohesive component, the particle-particle repulsion leads to powder packing poorly which is also one of the results of particle-particle cohesive interaction. On the other hand, if powder particles carry electric charges of opposite polarity, they will form clumps and stick on equipment surface or on each other. However, in a high external stress condition, like a shear cell test, the powder bed is consolidated, then, the shearing tool force an upper layer of powder to move against the adjacent lower layer. In this situation, it can be regarded as extrinsic-driven flowing at the packed bed condition, where the particles flow as being consolidated and pushed by a tool. The electrostatic charge impacts powder flow only marginally, since particle repulsion has been overcome by external normal stress. Moreover, the forced contacts due to compression will probably lead to increased conductivity, charge dissipation, and charge neutralization. Therefore, material property changes due to electrostatic charge development are best discerned in the low-stress test: compressibility and dynamic energy, instead of shear cell test. Our observations offered strong evidence of the significance of selecting a proper powder characterization method in order to characterize post-feeder material. As mentioned, powder flow is a complex and multi-dimensional phenomenon. Single flowability index is, in general, not sufficient to fully represent powder flow performance. Different flowing measurements describe

powder behavior in various conditions. Characterizations must be done by associating with specific powder handling conditions and considering the actual scenarios around particles. Otherwise, selecting improper methods would cause the characterizations lack of distinguishability, which can mislead the understanding of powder behavior. In our case, according to the effect of electrostatic charging on powder flowability, besides these indexes we have used, any other low-stress characterization should also be appropriate to be applid, such as Carr index, avalanche angle, avalanche size, angle of repose etc.

This behavior seems to be the result of to electrostatic charging and particle size interacting together. As discussed above, observed changes in flow material properties under dilated conditions are driven by a balance between cohesive force, affected by electrostatic force, and particle gravity. The contribution of particle size to changes in powder flow properties can be interpreted as following: (1) The weight of particles or particle agglomerates decreases significantly with particle size, which means the bond number is potentially changes along with moderate rising of electrostatic force. For example, when the material has a very small particle size, as API2 (D50=11.9um), powder flow is sensitively altered by electrostatic charging, even if charge acquisition is moderate. (2) Particle surface area increases substantially with particle size reduction. If there is larger and more surface exposed to contacting and rubbing, the chance of charge transfer is highly increased, improving total charge acquisition. For the material to pick up a large amount of charge, the electrostatic force is so predominant that powder flow is impacted. In summary, The surface forces increases with the surface area of the particles (as the square of the particle radius), and the bulk forces decreases with the decrease of volume (as the cube of the

particle radius). As a result, the bond number is expected to decrese with particle size as 1/R.

It is also worthwhile to note that all of the characterizations should be performed immediately after the feeder. Otherwise, electrostatic charge decay may occur. Thus, a misleading conclusion may be drawn that the flow performance of this powder remains the same when passing through a screw feeder, when it is actually due to an improper characterization protocol. In our previous experience, if the post-feeder material is first collected and stored for some time and then characterized, the change of its flowability is mitigated or even eliminated. Therefore, in order to precisely understand powder flowing behavior, it is essential to have material characterization completed right after the powder passing through feeder without any storage time.

3.5.2 Statistical analysis of correlation between the change in powder flow and material characterization

As explained earlier, we have correlated powder properties change in process with particle size and charge-to-mass ratio. This empirical conclusion is made based on our observations, seeking to achieve a fundamental understanding of powder flowing phenomenon. In this section, we aim to understand which material potentially experience the change in flow when passes through feeder by applying a multivariate statistical analysis (partial least squares regression (PLS)). In such manner, multiple material property indexes can be involved and examined. PLS models both X-variables (or variables) and Y-variables (or responses) simultaneously to find latent X-variables that can be best linked to the responses either positively or negatively. The PLS analysis is performed here using the software The Unscrambler X 10.4 (Camo, Oslo, Norway). The X-variables are selected to include

particle size, charge-to-mass ratio and all the indexes extracted from material characterization. Compressibility changes are defined as Y-variables, including the relative increase in compressibility, the numerical increase in compressibility and the classification of "change or not (C/N)", which is determined based on p-value (<0.05).

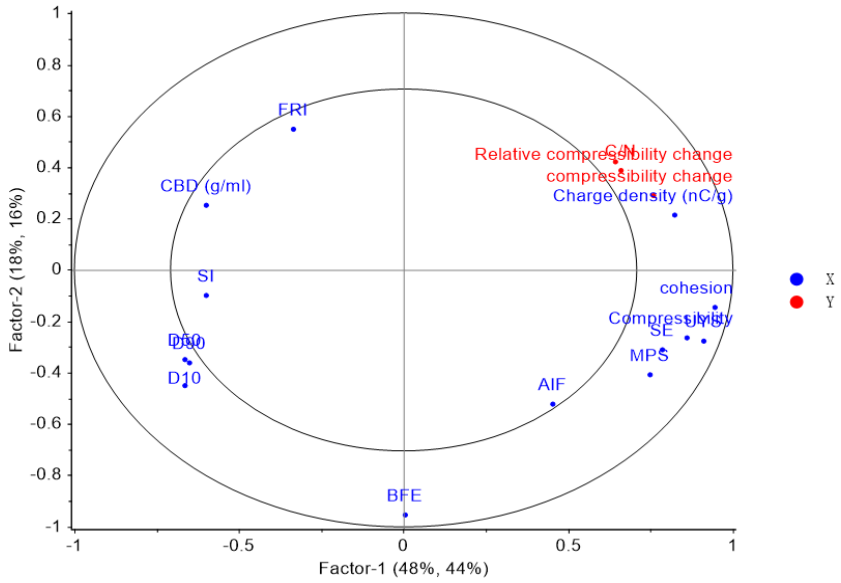

a

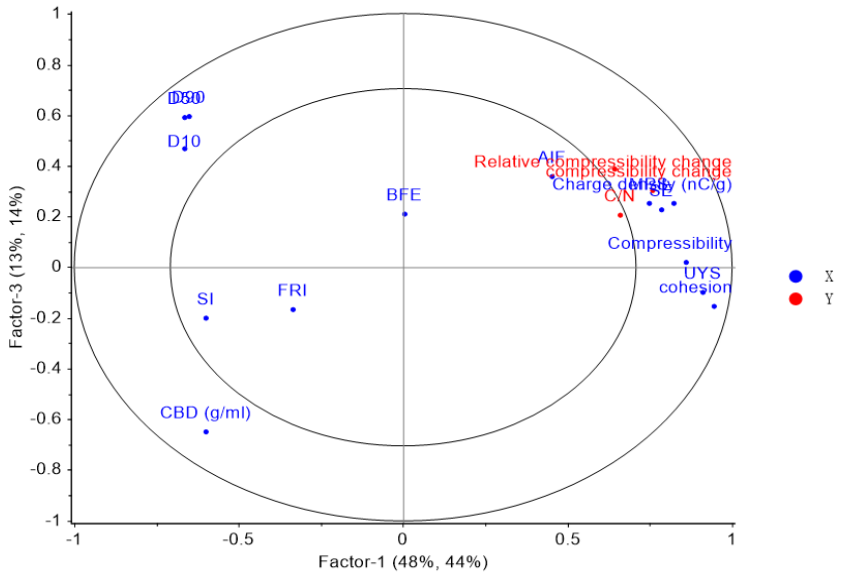

b

Figure 3-12 Partial least squares regression analysis correlation loading plots: a) factor 1 vs. factor 2. b) factor 1 vs. factor 2.

The loading plots are shown in ***Figure 3-12***, where red dots mark Y-variables and blue dots mark X-variables. Simply put, these two plots are displaying the spaces which is defined by three PLS factors: factor 1 vs. factor 2 and factor 1 vs. factor 3. Overall, these spaces can explaint 73% of the variation of Y-variables and 81% of the variation of X-variables. The plots represent the largest variations in the X-data that can explain the largest variation in the Y-data. Respectively, factor 1 explains the most variation in our data set with 46% in Y-variables and 46% in X-variables, which can be considered as the most critical component. Any property that contributes considerably to this factor should be examined particularly. Next two significant factors are labeled as factor 2 and factor 3, coupling with factor 1 to interpretate the correlation between response and X-variables with more variation included. Since our primary purpose is to discern the most critical properties associated with the powder behavior, we first seek insight into the responses. Property indexes that are projected in the same direction from the origin as a response are positively linked to that response. Indexes projected in the opposite direction have a negative correlation. If an index is projected near the center, it means the correlation is not well represented. Remarkably, a strong correlation can be demonstrated between charge-to-mass ratio and compressibility change, as charge-to-mass ratio is located very close to all Y-variables along with all three factors. It is also apparent that cohesion value, UYS and compressibility are positively linked with the response on factor 1, which means, in most cases, materials that displays compressibility increases after the feeder are compressible and cohesive material. Moreover, particle size displays strong negative correlation with the responses on both factor 1 and factor 2. This observation is aligned with our previous hypothesis. Smaller particle size possibly causes compressibility changes. On the other

hand, conditioned bulk density also are also worthwhile to be discussed. It oppositely correlated with responses on both factor 1 and factor 3. This can be easily explained. According to the discussion of bond number, gravity force, acting as a driving force for powder flow, is directly dependent on its bulk density. Therefore, powder with low bulk density generally exhibits poor flow behavior. In our case, lower bulk density indicates the powder is fluffier. Its flowing behavior is easier to be altered when acquiring electrostatic charge.

Figure 3-13 presents the PLS scores plots. This plot displays the projection of each material in the space of factor 1 vs. factor 2 and factor 1 vs. factor 3, in which the red color marks materials experiencing compressibility increment. Obviously, all of these powders are projected towards the direction in which charge-to-mass ratio is large, the particle size is small, and conditioned bulk density is also small

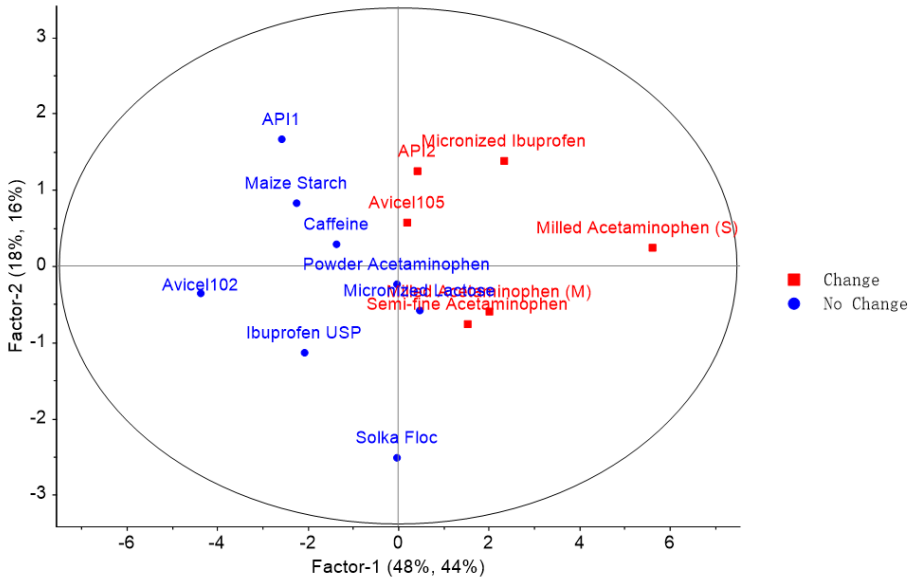

a

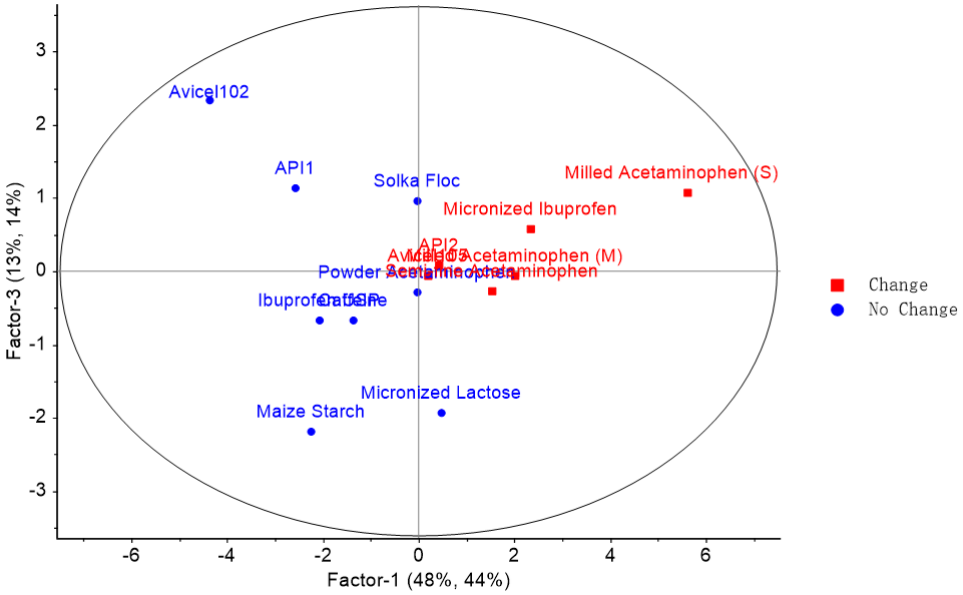

b

Figure 3-13 Partial least squares regression analysis score plots: a) factor 1 vs. factor 2. b) factor 1 vs. factor 2.

3.6 Conclusions

In this study, we attempt to identify how material properties are altered when passing through a screw feeder. In the first step, five pharmaceutical APIs were fully characterized immediately after feeder, using multiple techniques of FT4 powder rheometer. One of the observations is that charge-to-mass ratio tends to increase for all the materials, suggesting that electrostatic charges accumulate during the powder feeding as particles contact, roll, slide, rub against each other as well as feeder tools. For some materials, the flowability of post-feeding powder seems to vary when compared to pre-feeding powder. As conditioned bulk density decreases, compressibility increases, dynamic flow energy decreases, indicating that the powder become more cohesive. We also find that these flowing-altered powders obtain an extremely high amount of electrostatic charges. However, indexes from the shear cell test, such as cohesion value, FFC and UYS, don't show noticeable change.

In addition, particle size distribution remains the same. According to these observations, we first hypothesized that powder electrostatic charging leads to the flowability change. Then, the compressibility test was selected as the technique to discern whether the powder changed or not for later investigation, due to that the compressibility test is a widespread method to characterize powder, which can be easily performed either using other commercialized equipment or making in-house setup. In the next step, nine more pharmaceutical powders were characterized both before and immediately after feeding. Results demonstrate that when the powder has a very small particle size, generally less than 30μm, and exhibit a high electrostatic charging tendency, its flow performance would be altered by feeder passage, showing an increment of compressibility.

Secondly, This study has also shown that, when passing through a screw feeder, both the charge acquisition and changes in flow performance are independent of feeding speed. It is further interpreted that the rolling and rubbing of particles can enable the entire surface to be available for charging. With powder being compressed in screws, particles continuously contact with each other to have complete (saturated) charge acquisition. Thus, the particle charging capacity has been reached at a lower feeding speed.

Thirdly, when powder picked up a large amount of electrostatic charge, above 6nC/g in our case, it build up significantly on the feeder surface in a relatively short time, which may cause adverse effects on product content uniformity.

Forthly, This study provided an important opportunity to advance the understanding of how electrostatic charging affects powder flowing behavior. We have explained how the electrostatic charging affects flowability of small particles more than large particles, due

to its low bulk forces (or particle weight). Powder flowability is altered since particles either repel or attract with each other depending on charge polarity.

Fifthly, selecting the proper characterization techniques is very critical to discern the change in powder flow during a process. Since the effect of electrostatic charging is more dominant on intrinsic-driven flowing at free surface condition, using low-stress characterization techniques is more appropriate to identify the flowing behavior related with electrostatic charging, such as compressibility, dynamic flow test, avalanche test, angle of repose and Carr index, rather than high-stress characterization such as the shear cell test.

Another deliverable rising from this study is a way to characterize post-feeder material or a way to investigate the influence of electrostatic charging on powder flowing behavior. The materials should be characterized immediately after feeder without any storage time in order to avoid the decay of electrostatic charge with time.

4 Chapter 4 Powder Agglomeration after Twin Screw Feeder and Powder Agglomeration Tendency Assessment

4.1 Introduction

In the pharmaceutical industry, the mixing of dry granular materials can be regarded as one of the most critical steps, since mixing performance of active pharmaceutical ingredient (API) with excipients directly affects the homogeneity of mixture and the performance of the final product [13, 51, 107, 124-126]. In a powder mixture, any ingredient would generally be present as two conditions: primary particles (i.e., discrete particles) and particles assemblages in the form of agglomerates or/and aggregates. Since there was widespread confusion on using the term agglomerates and aggregates, Nichols *et al.* reviewed the definitions in multiple industries and proposed that the term *agglomerate* should be used exclusively to describe an assemblage of particles in powder[127]. In contrast, *aggregate* should be confined to pre-nucleation structures. The author further distinguished agglomerates as soft and hard agglomerates. Soft agglomerates are readily eliminated and dispersed as primary particles when applying mechanical or sonication stresses, whereas hard agglomerates are non-friable and may remain as lumps even after the shear. In this chapter, we discuss powder agglomeration according to this definitions. However, nomenclature of ‘unenduring’ and ‘enduring’ is applied to replace the term of ‘soft’ and ‘hard’. They are referred here irrespectively of the intrinsic mechanism that produces their endurance in the system.

Generally, fine or cohesive powder has a strong tendency to form agglomerates during dry powder processing. Formation of ingredient agglomerates is due to particle-particle

cohesive interactions that are strong enough that enables of individual particles group together. The cohesive interaction can be van der Waals force, electrostatic force and capillary force [128-132]. Moreover, Orr and Sallam found that agglomerates form when the powder is subjected to forces that cause powder compression in certain local areas[133]. Therefore, the agglomeration tendency of dry granular material can be correlated with its physico-chemical properties, such as particle size, particle shape, surface energy, surface roughness, moisture content, and electrostatics. As these physico-chemical properties deeply impact powder flowability, the agglomeration tendency thus is possibly correlated with a powder's flow performance characterization, such as shear cell test, consolidation test, Carr index, etc. In our study, we attempt to exanimate the possible correlation between powder agglomeration and flow characterization.

The presence of API agglomerates (i.e. enduring agglomerates) is one common issue during dry powder mixing. It has been considerably documented that API agglomerates adversely impact product quality. In particular, the API agglomeration is a challenge during low-dose drug product manufacturing. First of all, API agglomeration increases the inhomogeneity of blends and adversely affects the content uniformity of the final product [51, 124, 125]. Cases have been observed where product units contained no active ingredient or where they were formulated as a large dosage tablet, which is harmful to people[134, 135]. Additionally, If the API is agglomerated, the dissolution of the drug product can be delayed, which reduces the bioavailability of the drug, especially for a low solubility drug[136-138]. For a poorly wettable powder, the dissolution of agglomerates is much slower than the dissolution of discrete particles, in particular for hydrophobic materials that create additional difficulty for water to penetrate into the capillary spaces

within agglomerates, so that the surface wetting time is much longer than for discrete particles[77].

Given these issues, measuring API agglomeration is an area of interest in pharmaceutical manufacturing. There is a large volume of literature describing methods to examine agglomeration and de-agglomeration quantitatively. Traditionally, because agglomeration directly impacts homogeneity of blends, powder agglomeration is assessed by measuring blend homogeneity or content uniformity [51, 139]. Alternatively, agglomeration has been quantified by passing blends through sieves to screen agglomerates, where other free-flowing ingredients pass but agglomerates remain on the mesh[57, 140, 141]. In particular, this method is widely used when exploring API de-agglomeration during powder blending. More recently, it has becomes more common to utilize chemical imaging to visualize API agglomeration and micro-mixing with excipients in blends or tablets [53, 142, 143]. However, all of these methodologies depend on the mixing behavior of the API with other ingredients in a controlled blending process, which may not represent its general agglomeration tendency. In addition, they are either time- and material-consuming or an indirect quantitative method. In the early stage of pharmaceutical development, it is required to enhance the understanding of the API, and then build a material property database to assess its process performance[64]. On the other hand, only a limited amount of API is available for characterization considering its costs. Therefore, it is necessary to develop a methodology that is able to directly quantify the agglomeration tendency of API with modest material consumption or the possibility of material recycling. Unfortunately, it is difficult to measure the agglomeration tendency of powder directly. One of the challenges is to efficiently sample real agglomerates in ways that are representative of the

powder natural agglomeration tendency in the process. In this study, a novel method is developed that enables us to measure powder agglomeration without mixing with other ingredients.

Pharmaceutical manufacturing is shifting from the traditional batch process to continuous process,driven by advantages such as high process robustness, improved risk assessment, enhanced process control, and easier transfer from process development to commercial manufacturing[103]. However, when developing a continuous process, in addition to traditional powder processing issues, new problems emerge, potentially leading to product failure[104, 144]. For example, in continuous pharmaceutical manufacturing, gravimetric feeders are a key process component. A successful process requires feeder discharging material consistently and accurately because the mass flow rate directly influences the quality attributes of the intermediate and final product. Any negative results of inconsistent and variable feeding can propagate downstream and eventually lead to content uniformity problems [7, 145, 146]. Numerous works in the literature attempted to investigate the effect of feeder critical process parameters on powder feeding stability[6, 105]. A considerable amount of work has also been devoted to examine the correlation between feeder performance and powder flow properties[56, 106]. In comparison to the growing body of investigation in process development, far too little attention has been paid to the agglomeration of cohesive material in the continuous pharmaceutical process, even though, several papers have reported the adverse effect of API agglomeration in the continuous process[51, 147-149]. Because they involve different processing mechanisms than batch processes, a investigation should be conducted for continuous manufacturing with respect to API agglomeration. While in this study powder agglomeration tendency is investigated

during powder feeding and continuous process, the methodology and conclusions regarding agglomeration tendency are approporiate also for batch and semi-continuous processes.

The objectives of this study are to: (1) quantifiy powder agglomeration tendency. And (2) correlate agglomeration with powder properties. To that end, a methodology has been first developed, applying image analysis, to measure agglomerates size when a pure ingredient is passing through a screw feeder. Four indexes are further defined to represent powder agglomerate size distribution.

When a powder passes through a screw feeder, it has potential to be densified into the pocket created by screw flights; then, agglomerates form when it is discharged. It has also been found that the formation of the agglomerates highly depends on the type and volume of screw pitch but correlates more weakly with the feeding speed. In this study, 22 pharmaceutical powders were examined by using a new proposed method.

According to its agglomerates size, it is suggested that powders can be classified into five groups. However, it is noted that some of the captured agglomerates are unenduring and can be easily eliminated in the downstream process. Thus, a conical-mill study was implemented to examine the endurance of agglomerates generated in the feeder. In this portion of study, a conical mill is placed after the feeder and agglomerates are measured after the conical mill. According to the endurance of agglomerates after the conical mill, powders are further classified as unenduring-agglomerating and enduring-agglomerating. Furthermore, we attempt to reveal the correlation between powder agglomeration and powder properties, including particle size and flowability descriptors. It is proposed that powder agglomeration tendency (both size and endurance) can be explained in terms of the

particle size, compressibility and cohesion value from the shear cell test. In the last section, aiming to clarify the significance of agglomerates characterization, a case study is performed by applying a semi-continuous process to blend two APIs of different agglomeration tendency with other excipients. Then, content uniformity is measured and compared with their agglomeration measurement.

4.2 Materials and characterization methods

4.2.1 Material

Table 4-1 Materials and their suppliers for chapter 4

Materials	Suppliers
Maize Starch	Everest Starch, Gujarat, India
MgSt	Mallinckrodt Pharmaceuticals, St. Louis, MO
Micronized Ibuprofen	Air jet milled
Microcrystalline cellulose (Avicel 105)	FMC Biopolymer, Philadelphia, PA
Crospovidone	Ashland, Bridgewater, NJ
Milled Ibuprofen (S)	Air jet milled
Milled Acetaminophen (M)	Air jet milled
Semi-fine Acetaminophen	Mallinckrodt Pharmaceuticals, St. Louis, MO
Caffeine	CSPC Innovation Pharmaceutical, Shijiazhuang, China
Milled Ibuprofen (M)	Air jet milled
Powder Acetaminophen	Mallinckrodt Pharmaceuticals, St. Louis, MO
Croscarmellose Sodium	FMC Biopolymer, Philadelphia, PA
API1	Janssen Pharmaceutical Inc., Beerse, Belgium
API2	Janssen Pharmaceutical Inc., Beerse, Belgium
Sodium Starch Glycolate	Maruti Chemicals, Ahmedabad, India
Solka Floc	International Fiber Corporation, Urbana, OH
Lactose Monohydrate (Lactose310)	Foremost Farm, Baraboo, WI
Ibuprofen USP	RIA International LLC, East Hanover, NJ
Microcrystalline cellulose (Avicel 101)	FMC Biopolymer, Philadelphia, PA
Dense Acetaminophen	Mallinckrodt Pharmaceuticals, St. Louis, MO
Microcrystalline cellulose (Avicel 102)	FMC Biopolymer, Philadelphia, PA
Microcrystalline cellulose (Avicel 200)	FMC Biopolymer, Philadelphia, PA

As aforementioned, it was documented that materials of small particle and cohesive nature potentially formed agglomerates during the pharmaceutical process. According to this empirical observation, we decided to explore pharmaceutical powder ranging from 10μm

to 200 μm, from very cohesive regime to free-flowing regime. In total, 22 materials were selected, as listed in ***Table 4-1***. API1, API2 are active pharmaceutical ingredients supplied by Janssen Pharmaceutical Inc. There are 4 powders modified by micronizing commercially available APIs using air jet mill in our lab. They are named as Micronized Ibuprofen, Milled Ibuprofen (S), Milled Acetaminophen (M), Milled Ibuprofen (M), where the (S) and (M) represent the different grade of particle size.

4.2.2 Powder Characterization

Powder properties are characterized by using the FT4 powder rheometer (Freeman Technology Inc., Worcestershire, UK). The following tests were performed: compressibility test, shear cell test, dynamic flow test, and permeability test. Each test provides information that can be used to examine powder flowing behavior under different conditions. Particle size distribution was characterized using a laser diffraction analyzer. All the tests are detailed below. For each test, at least three replicates were performed.

4.2.2.1 Particle size distribution

Particle size distribution is determined using a multi-wavelength laser diffraction particle size analyzer (LS 13320) with a tornado dry module (Beckman Coulter, Indiana, USA). This instrument conducts Polarization Intensity Differential Scattering (PIDS) testing so that particle size ranging from 0.017μm to 2000μm can be measured. The dry module creates vacuum in system with the pressure of 1990.7Pa (8 inches of water) for all the samples. In this way, approximately 20 ml of sample is subject to analyzing and particle size is calculated using the Fraunhofer method. Particle size information of D10, D50, D90 are documented.

4.2.2.2 Shear cell test

Shear cell test is detailed in section 2.2.1. In this chapter, shear cell test is implemented under an initial consolidation stress of 6 kPa.

4.2.2.3 Compressibility test

Compressibility test is detailed in section 2.2.2.

4.2.2.4 Dynamic flow energy test

Dynamic flow energy test is detailed in section 2.2.3.

4.2.2.5 Permeability test

Permeability test is detailed in section 2.2.4.

4.3 Methodology for agglomerates measurement.

4.3.1 Sampling agglomerates

In order to assess ingredient agglomerate tendency, several challenges need to be addressed. The first challenge is how to sample agglomerates with minimal disturbance. Agglomerates should be collected gently to avoid breakage or any other external effect so that the measured agglomerate sizes represent the real agglomeration behavior. Secondly, defining the proper index to represent agglomerate tendency adequately is also a critical point. The defined index should be statistically meaningful and be based on the measurement of a suitable number of individual agglomerates. In this study, a novel methodology is developed, in which the agglomerates are collected under a controlled condition aiming to maximize its original state. Moreover, indexes quantifying the distribution were defined to statistically represent agglomerate size. It is worth noting that ingredients agglomeration is an issue both for the batch and the continuous process. Having a method to assess powder

agglomeration tendency is essential in process development. Although our methodology is presented during powder feeding and continuous process, its applicability is much broader than that. The method can be used generally to quantify the agglomeration of ingredients in any relevant situation.

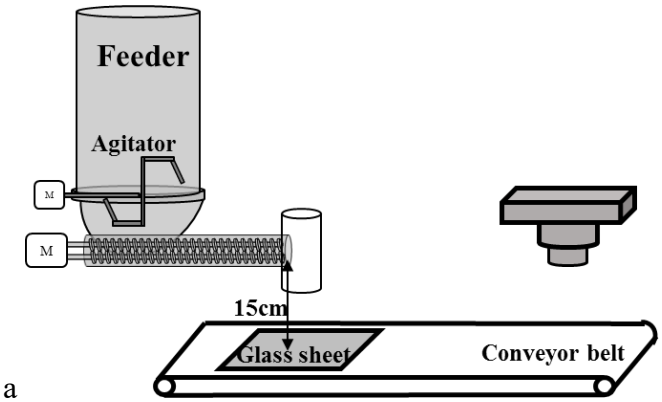

a

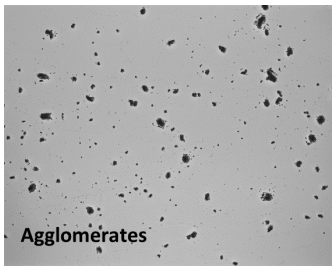

b i.

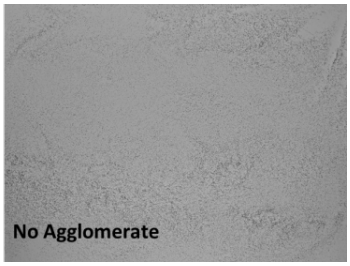

ii.

Figure 4-1 Sampling agglomerates. a) Experimental set-up. b) Sample images: i. Agglomerates, ii. No agglomerate.

According to previous observations, in continuous manufacturing, the formation of agglomerates occurs for some material when passing through a twin-screw feeder. The agglomerates possibly lead to blends inhomogeneity. In order to understand powder agglomeration further, a novel methodology was developed, based on image analysis, measuring agglomerates mean size and size distribution after a feeder. In this work, we used a commercially available twin screw loss-in-weight feeder, the K-Tron KT-20

(Coperion K-Tron Pitman, Inc. Sewell, NJ, USA.). Fine concave screws were utilized. The volumetric feeding mode was selected to maintain a constant screw speed. Two feeding speeds were used: 80% drive command (123rpm) and 20% drive command (DC) (31rpm). ***Figure 4-1a*** displays the experimental set-up. A conveyor belt carried one glass sheet to collect discharged powder agglomerates from the feeder at various speeds. The height between the glass sheet and the feeder is set at 15cm. Once the sample collection is completed, it was photographed using a digital camera (Nikon Coolpix B500). By repeating this sampling procedure, at least five replicates were taken. As shown in ***Figure 4-1b***, the method is able to distinguish materials with and without agglomeration tendency.

4.3.2 Image analysis and agglomerate size calculation.

As the next step, the photograph was analyzed using ImageJ. By applying a pre-defined threshold for all the images, this original picture was converted to a new picture of binary pixels, as shown in ***Figure 4-2***. In this binarized image, each "black spot" is equivalent to one agglomerate. By measuring the size of each "black spot", the agglomerate size was determined. ImageJ automatically measured the area of each "black spot". Then, the size of each agglomerate can be defined as the circular equivalent diameter (D):

$$D = \sqrt{\frac{4A}{\pi}} \tag{4-1}$$

where A is the area of the "black spot" in the image.

As mentioned before, the size of only one agglomerate is not sufficient to be an index representing powder agglomerate tendency. It is essential to measure enough agglomerates to obtain a statistically representative estimate. Fortunately, the cumulative distribution of

agglomerates size can be also obtained from the measurement, as ***Figure 4-3***. Similar to particle size distribution description, D50%, D75%, D90% were then defined, where D50% means the diameter at which 50% of agglomerates (by the area of the "black spot") are comprised of smaller size agglomerate. Likewise, the definition is also described for D75% and D90%. Note that, it is less meaningful to account for too many small agglomerate as D10%, because small agglomerate moderate the effects of agglomeration on mixing homogeneity. Additionally, the span of distribution was calculated to represent the width of the distribution, shown as:

$$Span = \frac{D90\% - D50\%}{D75\%} \tag{4-2}$$

Above all, D50%, D75%, D90%, and span are selected as indexes referring to ingredient agglomeration behavior in this study.

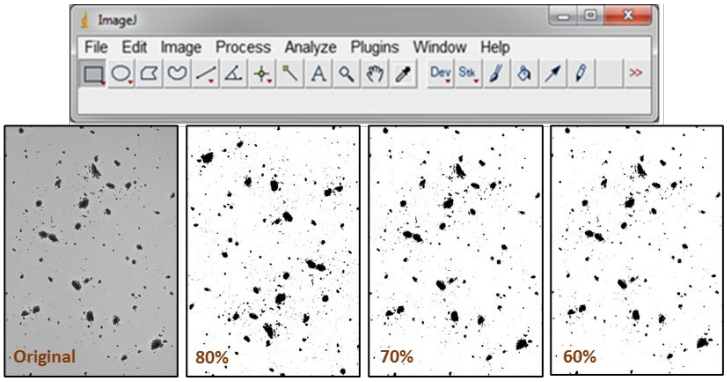

Figure 4-2 Converting images using ImageJ at different threshold.

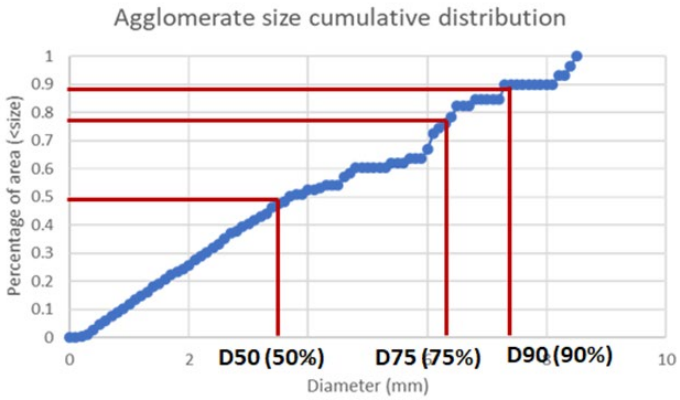

Figure 4-3 Defining agglomerate size distribution.

4.3.3 The effect of the belt moving speed on agglomeration measurement

In this measurement, the speed of the conveyor belt has to be adjustable according to the feeding speed. If the speed is too low, this results in the occurrence of more than one agglomerate overlapping at one spot. Conversely, if the speed is too high, too few agglomerates will be analyzed. In our case, the speed range of 1cm/s-4cm/s enables the successful sample collection for low speed feeding (20% DC). Hereby, method validation is required to clarify the possible effect of the belt moving speed on agglomerate measurement in this range. As the preliminary study, Avicel 105 and API1 were selected. Agglomerates were measured by implementing constant binarizing threshold and constant feeding speed of 20%DC. Three belt speeds were studied: 1.5cm/s, 2.4cm/s, 3.3cm/s. As shown in ***Figure 4-4***, it is evident that the variation of agglomerates size quantified at various belt speeds was insignificant, although, for Avicel 105, it seems that the lowest belt speed of 1.5cm/s yielded slightly larger agglomerate size. In the later investigation, we selected the belt speed of 2.4cm/s for the low feeding speed (20% DC). By using the same criteria, we used 6cm/s for the high feeding speed (80% DC).

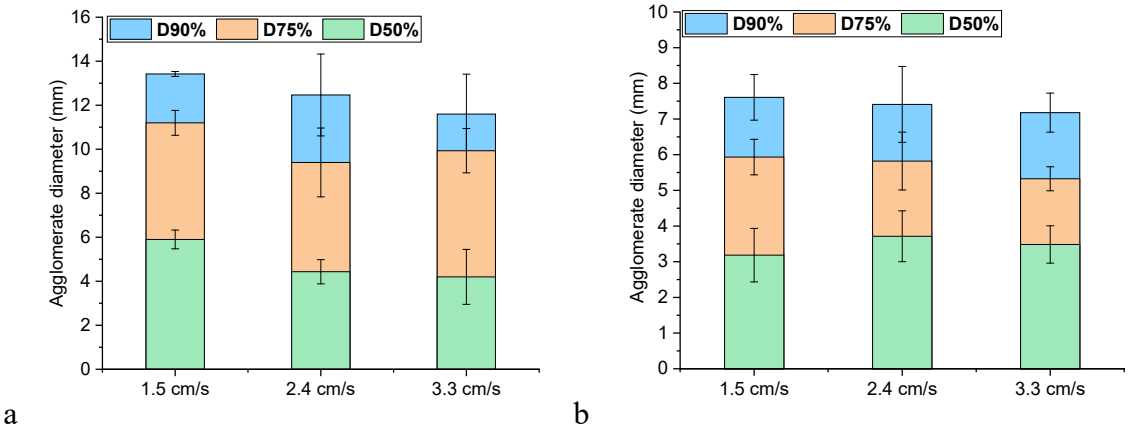

Figure 4-4 Agglomerate size characterized under different conveying speed: a) Avicel 105. b) API1.

4.3.4 The effect of threshold setting on agglomeration measurement

When binarizing the original picture, a threshold has to be defined. The ImageJ can be used to binarize picture by auto-thresholding which is based on a algorithm that differentiates the backgrough and foreground. In this section, we further explore the possible effect of threshold on agglomeration measurement in a range that covers the auto-thresholding algorithm. Three materials: Avicel 105, Ibuprofen USP, API1 were selected. Agglomerates size was calculated underlying three threshold levels: 60%, 70% and 80% of the maximum count (binarized images at these thesholds can be seen in ***Figure 4-2***). As shown in ***Figure 4-5a-c***, it is apparent that the results display no major variation underlying multiple thresholds. Although it is common sense that the higher threshold setting allows more pixels to be counted as agglomerates, which yields slightly larger agglomerate size, the effect of the threshold is insignificant in comparison to the variation of agglomerate size itself. In the later investigation, we determined to use the auto-thresholding given by ImageJ.

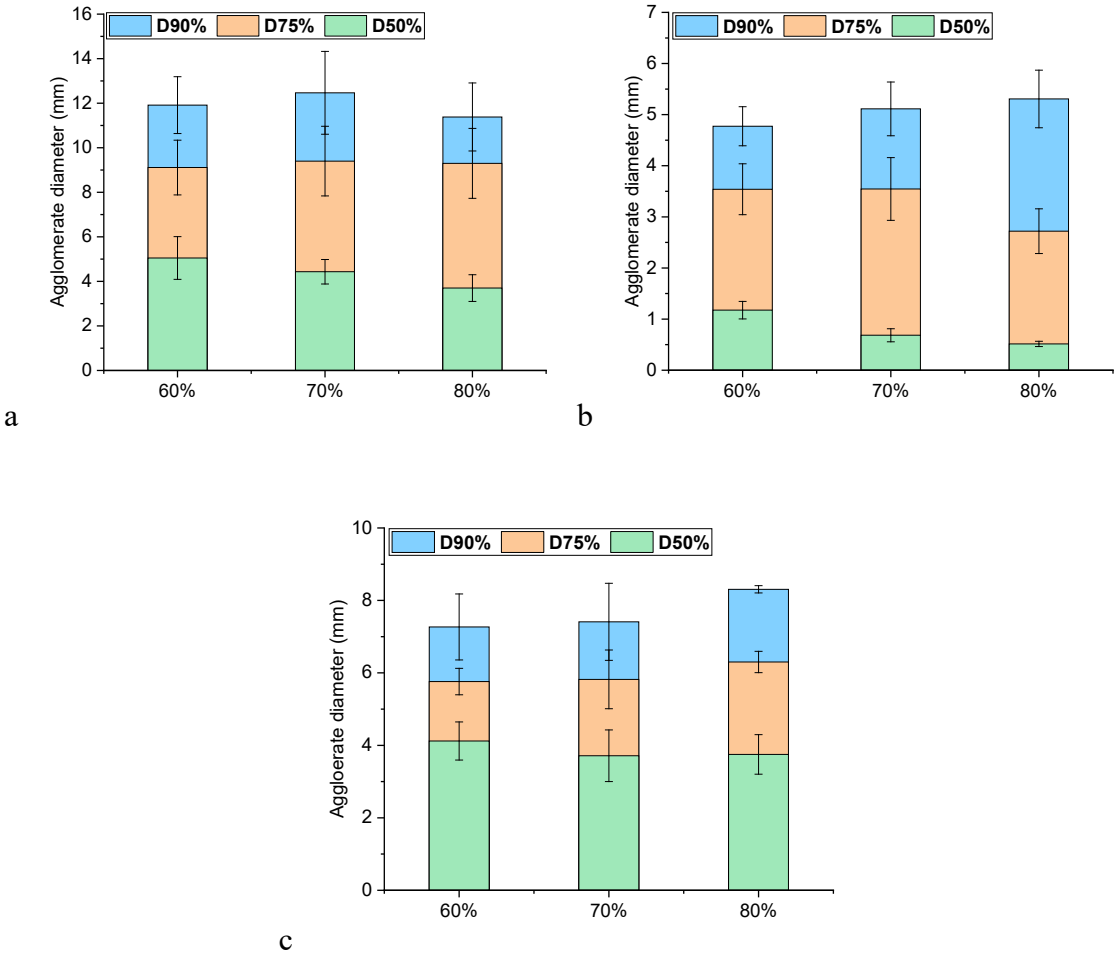

Figure 4-5 Agglomerate size calculated underlying various threshold: a) Avicel 105. b) Ibuprofen USP. c) API1.

4.4 Results and Discussion

4.4.1 The formation of powder agglomerates after feeder

Powder passing through the twin-screw feeder can be briefly described by the following steps. First, the powder in the hopper flows towards the screws at the bottom of the feeder stirred by the agitator. Then, the powder at the bottom of the feeder is consolidated within the pocket created by screw flights due to the normal stress applied by the paddles of the rotational agitator, the weight of the powder in the hopper, and the rotational screws.

Material forms a “densified powder bed” carried by the screw flights and moves forward within “feeding zone” dragged by the rotating screws. ***Figure 4-6a*** shows a top view of the hopper of a KT-20 feeder where the wall of the hopper, the agitator, and the feeding zone at the bottom are displayed. The material is conveyed to the end of the screws in such a consolidated state. At the end of the screws, and depending on the powder properties, as we will discuss later, the consolidated powder produces lumps that may remain formed, even after the stress is removed. Consequently, the powder may be discharged as compressed lumps. This is the qualitative description of the agglomeration process as we have been able to observe it. An example of the lumps formed at the exit of the screws is shown in ***Figure 4-6b***. In fact, lumps of materials (precursor of the agglomerates) coming out of a twin-screw feeder have been documented previously[56]. As mentioned, it also has been reported that powder consolidation is a common factor that leads to the formation of agglomerates in the batch process[133]. Likewise, during the continuous process, the twin-screw feeder provides a powder consolidation environment at the feeding zone and then introduces agglomerates to the downstream process.

a 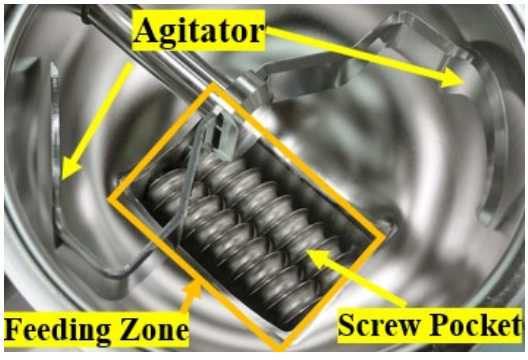

b 

Figure 4-6 a) Top view of the hopper of a KT-20 feeder. b) The formation of agglomerate at the exit of the feeding zone of the feeder.

4.4.2 Efect of screw configuration and feeding speed on agglomeration

In this work, we have first explored how the configuration of the screw and the feeding speed impact powder agglomeration by studying a problematic material (Semi-fine Acetaminophen). ***Figure 4-7*** presents the agglomerate size of Semi-fine Acetaminophen when comparing three screw configurations: fine concave screws, coarse concave screws and fine auger, and two feeding speeds: 80% DC and 20% DC. Firstly, this graph reveals that the agglomerate size depends on the volume per unit length of the screw pocket. The volume of powder being consolidated with screw pocket is determined by its volume per unit length. With small screw pocket, less amount of material is filled into the pocket, which results in smaller agglomerates size. The fine concave screw gives the smallest pocket volume of these three configurations. Thus, it generates the smallest agglomerates. Secondly, the size of agglomerates also depends on the shape of screws. For a K-Tron feeder, the concave screws are specifically shaped so that they have the function of "self-cleaning", where the flights of the paired screws interspersed each other tightly. The "self-cleaning" function may fragment powder lumps, which creates smaller agglomerates. The auger screws have no self-cleaning ability. Therefore, although the coarse concave screws yield slightly larger pocket volume than fine auger screws, it generates smaller agglomerates. To sum up, the agglomerates size follows the rank order of fine concave screws<coarse concave screws<fine auger screws. In contrast, when comparing the outcomes of different feeding speeds, there is no noticeable difference in the size of the agglomerates produced.

In order to further understand the role of feeding speed in powder agglomeration, the agglomerate size underlying feeding speed of 80%DC for 16 materials was also

documented and compared with the measurement underlying feeding speed of 20%DC. As ***Figure 4-8*** shows, the agglomerates size for 20%DC vs 80%DC located along with an x-y equivalent line, indicating that the size of the agglomerates does not depend on the feeding speed. This suggests that the formation of agglomerates is the result of powder being compressed within the screw pocket. The size of agglomerates is expected to be determined by the volume and shape of the screw no matter how fast it moved throughout the feeder.

In a later study, we specifically examine powder agglomeration tendency at the low speed feeding (20%DC) and using fine concave screws.

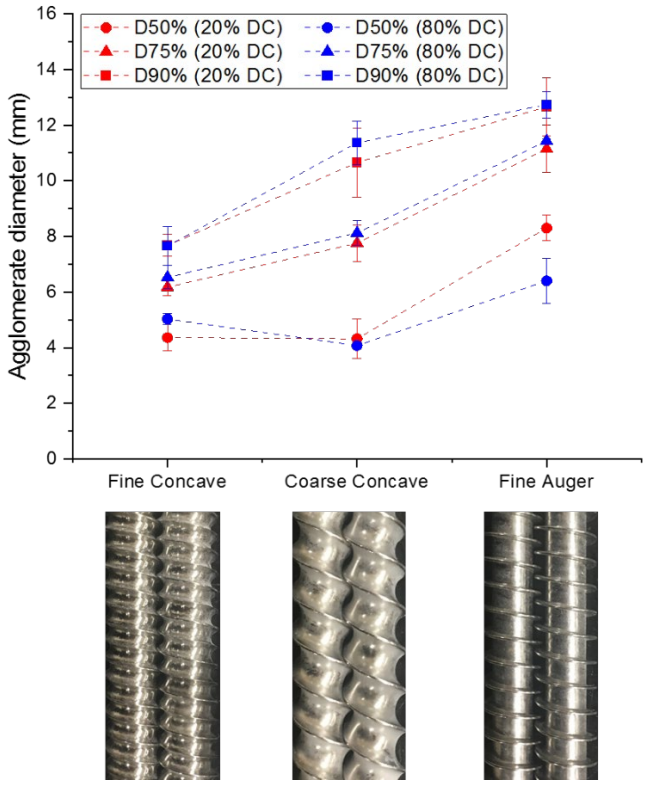

Figure 4-7 Screws configuration and dependence of agglomerate diameter on screw type and feeding speed.

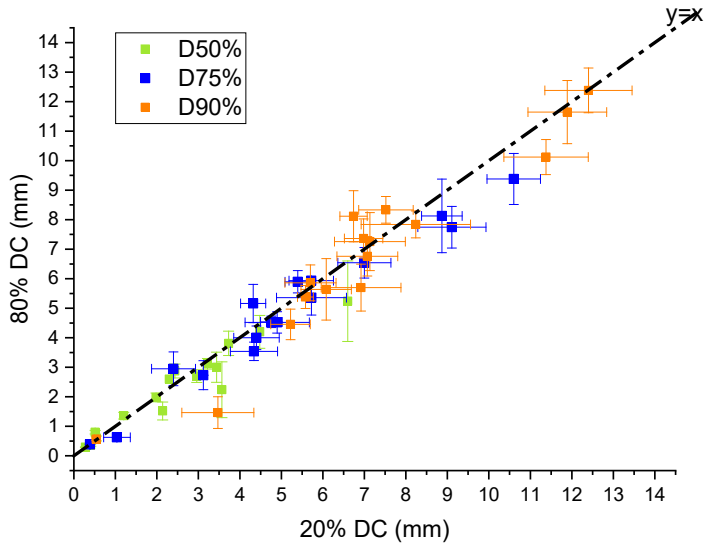

Figure 4-8 Agglomerates size at high-speed feeding and low-speed feeding.

4.4.3 The size of agglomerates

By utilizing the proposed methodology, agglomerate size is quantified and represented by D50%, D75%, and D90%. Fig.9 shows the agglomerates size of 22 selected powders and its cluster analysis according to D50%, D75% and D90%, at a feeding speed of 20%DC with fine concave screws. Cluster analysis were performed with The Unscrambler X 10.4 (Camo, Oslo, Norway), using the Ward hierarchical analysis method. This clustering method analyzes all the variance and evaluate the squared Euclidean distance between two clusters and attempts to minimize the sum of squares. ***Figure 4-9a*** on the left shows the dendrogram of the clustering. ***Figure 4-9a*** on the right shows the relative distance between clusters as a function of the number of clusters, which displays a large rate of distance decrease at four clusters. ***Figure 4-9b*** shows the measured agglomerates size of 22 powders.

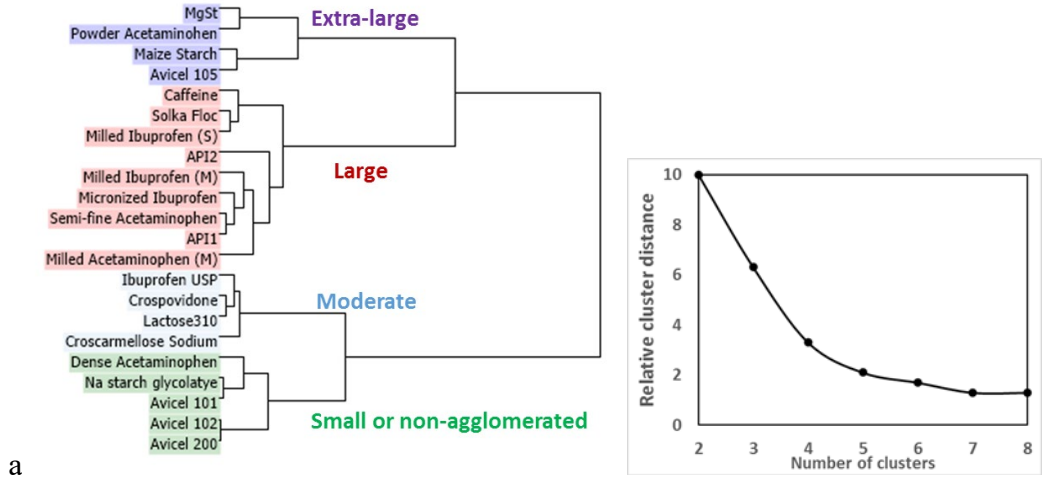

a

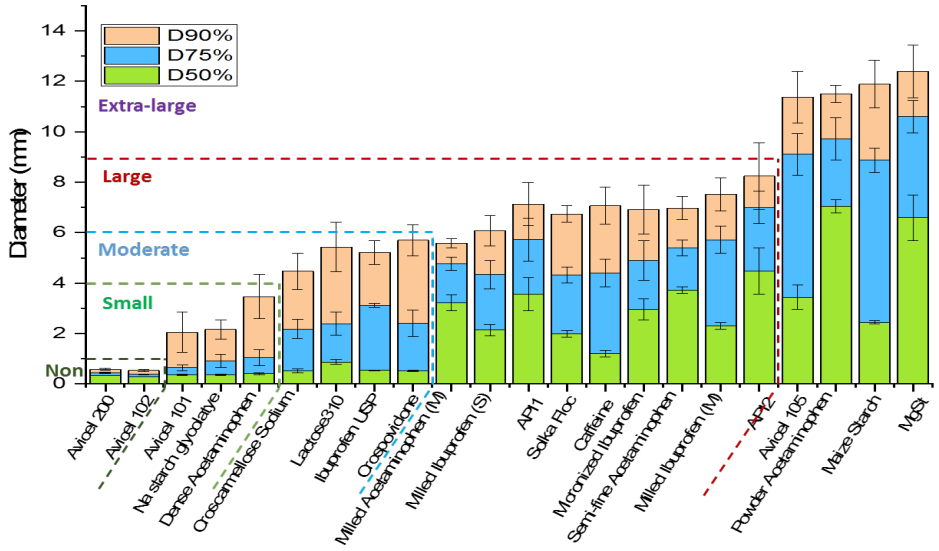

b

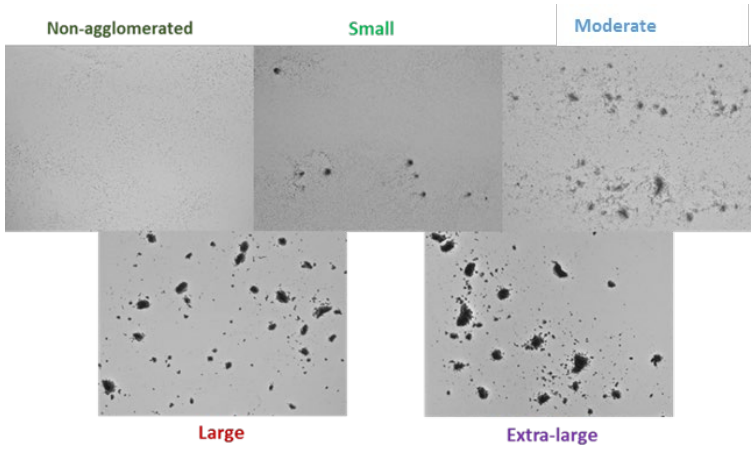

c

Figure 4-9 Cluster analysis of agglomerate size: a) Dendrogram (left) and cluster distance vs cluster number (right). b) Agglomerate size of 22 pharmaceutical powders. c) The representative picture of agglomerate in each group.

The 4 regions marked as “extra-large”, “large”, “medium” and “small” correspond to the four clusters shown in the dendogram. We further split the small agglomerate group into two, based on our qualitative observation that Avicel 200 and Avicel 102 don’t form any agglomerates at all (the representative pictures is shown at top left of ***Figure 4-9c***), while the others form some small agglomerates (top-center picture in ***Figure 4-9c***). The non-agglomerated material is the one that its maximum calculated agglomerate size (i.e D90%) is below 1mm. We can regard them as non-agglomerated materials due to that (1) this methodology is difficult to accurately discriminate agglomerate below 1mm; (2) The formation of agglomerates is powder being consolidated within a relatively large volume of screw pocket so it is less meanful to discriminate agglomerate below 1mm (comparing with extra-large agglomerates up to 12mm). In summary, five groups were defined according to its agglomerates size: non-agglomerates (1mm<D90%), small agglomerates (1mm>D90%>4mm, D75%<1mm), medium size agglomerates (4mm<D90%<6mm, 1mm<D75%<3mm), large agglomerates (6mm<D90%<9mm, 3mm<D75%<7mm) and extra-large agglomerates (D90%>9mm, D75%>8mm). As we will see later, the definition of these groups will also correlate with their possibility to be eliminated the agglomerates in downstream processes.

From ***Figure 4-9b***, Avicel 200 and Avicel 102 is regarded as non-agglomerated materials. The maximum agglomerate size is below 0.5mm. For Avicel 101, Na starch glycolate and Dense Acetaminophen (in ‘small’ group), only small agglomerates are ocassionally observed, showing the relatively large D90% but minimal D75% and D50%. Next, for the materials in the “moderate” group, a even larger D90% and D75% are captured but the D50% of them are still minimal. Large agglomerates can be observed frequently,

accompanied with large numbers of miniscule agglomerates whose diameter is below 1mm. In contrast, for the group of “large” and “extra-large”, most of the powder is observed in the form of agglomerates without seeing many primary or miniscule agglomerates (<1mm). These results are evidence that these powders remain in a consolidated state when they are discharged from the feeder.

Figure 4-10 shows that D75% and D90% have a strong linear correlation, which suggests that they can be used to equivalently represent agglomerates size. In this study, we consider that D90% represents the possibly maximum agglomerate size and the D75% indicates the mean agglomerates size since the distribution of agglomerates is close to a lognomal distribution with longer left-tail. Note that D50% and D90% have a non-linear relation, where two groups can be observed (D50%<2mm and D50%>2mm). This means that the width of the agglomerate distribution (i.e. span) is different for the two different groups of materials, as discussed in the next section.

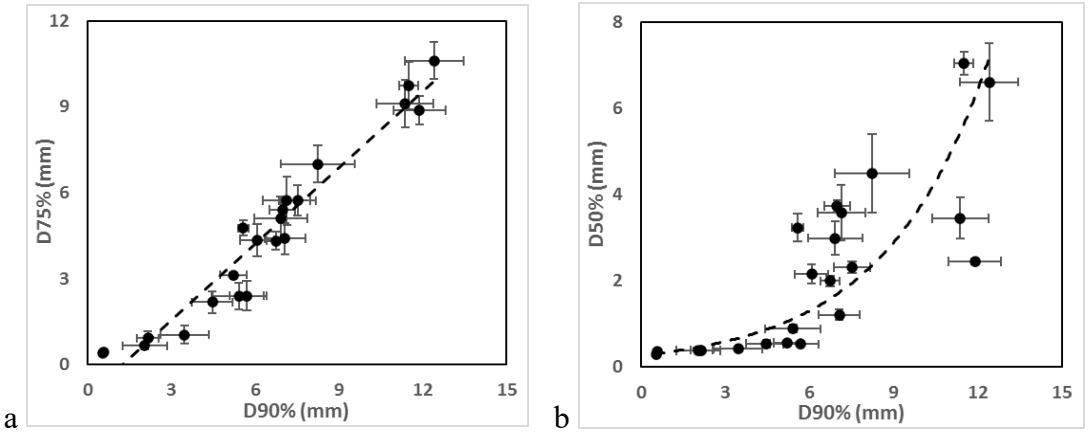

Figure 4-10 Correlation between D50%, D75% and D90% a) D75% vs. D90%. b) D50% vs. D90%.

4.4.4 The qualitative evaluation of agglomerates endurance

In the last section, we have seen how materials can be classified according to the size of the agglomerates they produce when fed by a twin screw feeder. However, a more important question is whether agglomerates observed after a feeder are strong enough to survive the subsequent mechanical processes, which may further impact the final product. In analogy to previous definition[127], agglomerates can be classified as “unenduring” when they can be readily eliminated and dispersed as primary particles when mechanical stress is applied as part of the manufacturing process. In contrast, if the agglomerates remain present even under mechanical stress through the process, the agglomerates are classified as “enduring”. In order to assess the endurance of agglomerates, a conical mill that imparts a strong shearing stress on the material after the feeders was used.

Conical mills are prevalently used to reduce the ingredient agglomeration and provide micro-mixing for pharmaceutical formulations[150-152]. It has been reported that using this unit can significantly improve product content uniformity[51]. the conical mill is equipped with an impeller rotating at high speed that eject material towards a screen, imparting a high shear environment to the powder. When a coarse screen is used, the powder residence time in this unit is very short. When agglomerates pass through a conical mill, a high-speed rotating impeller generates tremendous shear stress and centrifugal forces, which propel powder outward and toward the impeller tip and a conical screen, where agglomerates may be broken because of both particle-particle and particle-screen collisions. As the unenduring agglomerates are the ones that are not present after the mill, they are eliminated as primary particles, and powder will not form agglomerates any further. However, for enduring agglomerates, although the large agglomerates are fractured and

particles are rearranged, smaller agglomerates are still present after the mill. This is associated with the following possible mechanisms. In the first place, large agglomerates generated in the feeder are fractured as several smaller agglomerates. Additionally, these sub-agglomerates are tapped and then consolidated in the gap between the impeller and the screen, where high normal stress is also applied to the powder. The size of agglomerates after the mill is expected to correspond with the size of the holes in the screen.

In a setup similar to the one described before, a conical mill (Glatt, Ramsey, NJ) is added between the feeder and the conveyor belt. The agglomerate size after the conical mill is measured by using the same methodology as described before. A screen with holes 2mm in size was used, and the impeller speed was set to 1000rpm. As discussed above, five groups were defined when measuring agglomeration after the feeder. In this conical-mill study, except for the non-agglomerated group, several materials were selected from each group, as listed in ***Table 4-2***. In total, 12 powders were studied.

Table 4-2 Materials selected for conical-mill study

Group	Small	Moderate	Large	Extra-large
Materials	Dense Acetaminophen	Ibuprofen USP Lactose 310 Crospovidone	API1 Solka Floc Caffeine Milled Ibuprofen (M) Semi-fine Acetaminophen API2	Avicel 105 Maize Starch

Figure 4-11 shows the agglomerate size after the conical mill. As explained before, agglomerates of D90% below 1mm are regarded as non-agglomerated materials. Thus, these post-mill agglomerates with D90% below 1mm are considered unenduring agglomerates as they can be eliminated readily in the manufacturing process by applying a

mechanical stress. In contrast, the post-feeder agglomerates can be defined as enduring agglomerates when D75% of post-mill agglomerates is above 1mm, and the D90% is comparable to the screen hole size of the conical mill. For these materials, a large fraction of the material is still agglomerated form even after conical mill. The classification showed in this figure is determined previously according to the agglomerate size after feeder. It is apparent that the small and moderate agglomerates after the feeders are all unenduring and the extra-large are enduring. Materials in the large group can be either unenduring or enduring. Caffeine, API1 and Solka Floc (classified as large agglomerates after feeder), are partially eliminated (for Caffeine) and completely eliminated (for Solka Floc and API1) after the conical mill, so they produced unenduring agglomerates after being fed. Milled Ibuprofen(M), semi-fine APAP and API2 (also large agglomerates) produce enduring agglomerates. As a result, a classification based only on the size D90% or D75% of the agglomerates produced after the feeders is not enough to fully describe the behavior of materials during processing conditions. The classification needs to include the agglomerate size after the feeder-conical mill system.

We mentioned before that the span of the agglomerates divided them into two groups. We are going to show here that the span of agglomerate size after feeder correlates with the "endurance" of the agglomerates after the conical mill. ***Figure 4-12*** shows the span versus D90% of post-feeder agglomerates and adds the classification of the agglomerates into unenduring and enduring according to their performance through the conical mill. The graph shows, very clearly, how the span of the agglomerates produced after the feeder correlates well with their endurance: agglomerates presenting a large span are not present further downstream, while the ones than the ones showing a smaller span are. A possible

explanation for this is that the unenduring agglomerates are potentially spread and fractured as sub-agglomerates when they get in contact with the glass. Therefore, it leads to a wider distribution of agglomerates showing a larger span value. In contrast, enduring agglomerates result in a small span, which presents narrower distribution.

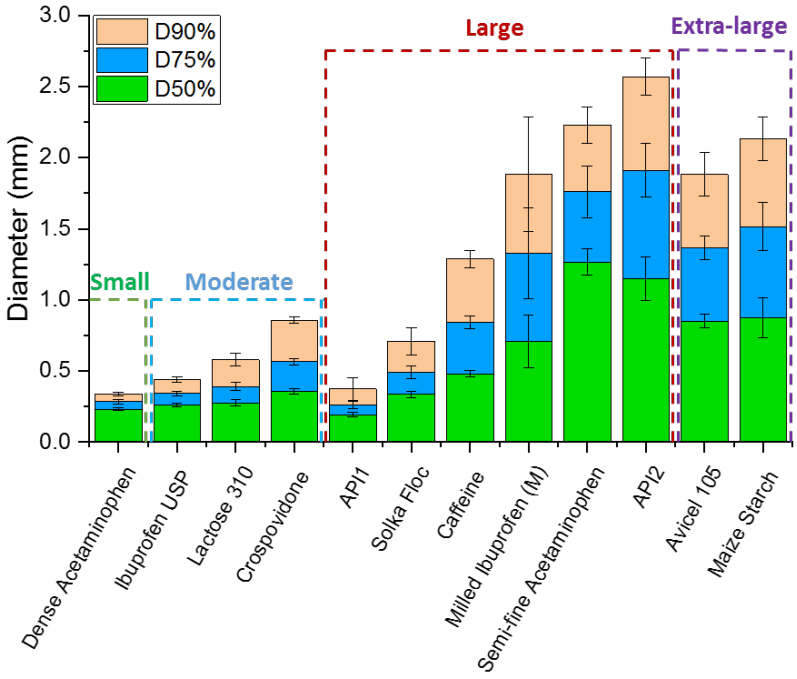

Figure 4-11 Agglomerate size after conical mill.

API1 seems to be an outlier, which has large size value and small span, but it forms unenduring agglomerates. For this reason, when ImageJ processing the original image, a large volume of primary particles on the glass sheet weren't detected clearly and are thus regarded as background, which results in only large agglomerates to be considered. However, this agglomeration behavior can be well explained when examining the post-mills agglomeration. Also, it can be well explained when coupling with its raw properties, which will be discussed in next two sections.

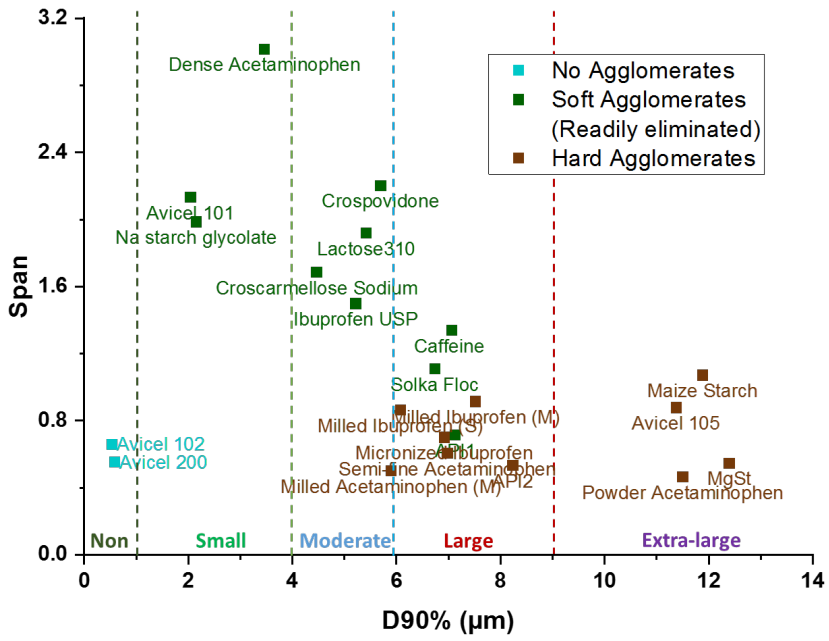

Figure 4-12 Classification of agglomeration considering agglomerates endurance.

4.4.5 Correlation of powder agglomerates size with material properties

In this section, we explore the correlation between powder agglomeration tendency and its properties characterized by flow performance tests. Referring to previous empirical conclusions, cohesive or micronized powder forms agglomerates during manufacturing. This study aims to demonstrate that we are able to evaluate powder agglomeration tendency by using specific techniques and indexes.

Powder flow properties were characterized by multiple techniques described in section 4.2.2, which cover the static (shear cell), quasi-static (compressibility and permeability) and dynamic (flow energy test) conditions. These four flow testing methodologies together with the particle size distribution characterization technique give more than fifteen indexes (material descriptors). To screen through the most significant and less-dependent properties, a multivariate statistical approach, partial least squares regression (PLS), is used

based on the statistical software The Unscrambler X 10.4 (Camo, Oslo, Norway). Simply put, PLS models both X-matrix (variables) and Y-matrix (response) simultaneously to find the latent X-variables that can be best linked to the latent Y-variables either positively or negatively. In this way, it can be used to find the fundamental correlations between these two matrices (variables and responses) by maximizing the covariance between X-variables and Y-variables. In our case, agglomerate size indexes (D50%, D75% and D90%) are the responses (Y-variables) and raw material properties (all the parameters from flow measurement and particle size) are the input variables (X-matrix). Two 2-D correlation loadings plots displaying four factors of the PLS: factor 1 vs. factor 2, factor 3 vs. factor 4, are presented in ***Figure 4-13***. Apparently, The plot of factor 1 vs. factor 2 represents the largest variations in the X-data that can explain the largest variation in the Y-data. These two factors explain 69% of Y-variation and 60% of X-variation. In contrast, the plot of factor 3 vs. factor 4 only explains 6% Y-variation and the responses are located in the center, which suggests that both factors are insignicant and negligible in explaining powder agglomeration. Therefore, the plot of factor 1 vs. factor 2 reveals the correlation between material properties and agglomeration. Parameters that are clustered together (permeability and the three PSD descriptors) or aligned (FFC and cohesion value) make equivalent contribution to the responses. The ones that are perpendicular (PSD descriptors and BFE) make highly independent contribution to the responses. Especially, factor1 is considered as the most critical factor which explains 60% of Y-variation. In this factor, the parameters that have large loading weight (between the inner ellipse and outer eclipse) are particle size descriptors, permeability, compressibility, FFC, UYS and cohesion value. It means these parameters are highly correlated with agglomerate size. In contrast, for other parameters,

it seems they contribute moderately or marginally to interpret the formation of agglomerates. As aforementioned, particle size descriptors and permeability are highly correlated. Also, UYS linearly correlate with cohesion value and FFC reciprocally correlate with cohesion value[67]. Therefore, in later study, we specifically discuss the correlation between agglomerate size and particle size descriptors, compressibility and cohesion value.

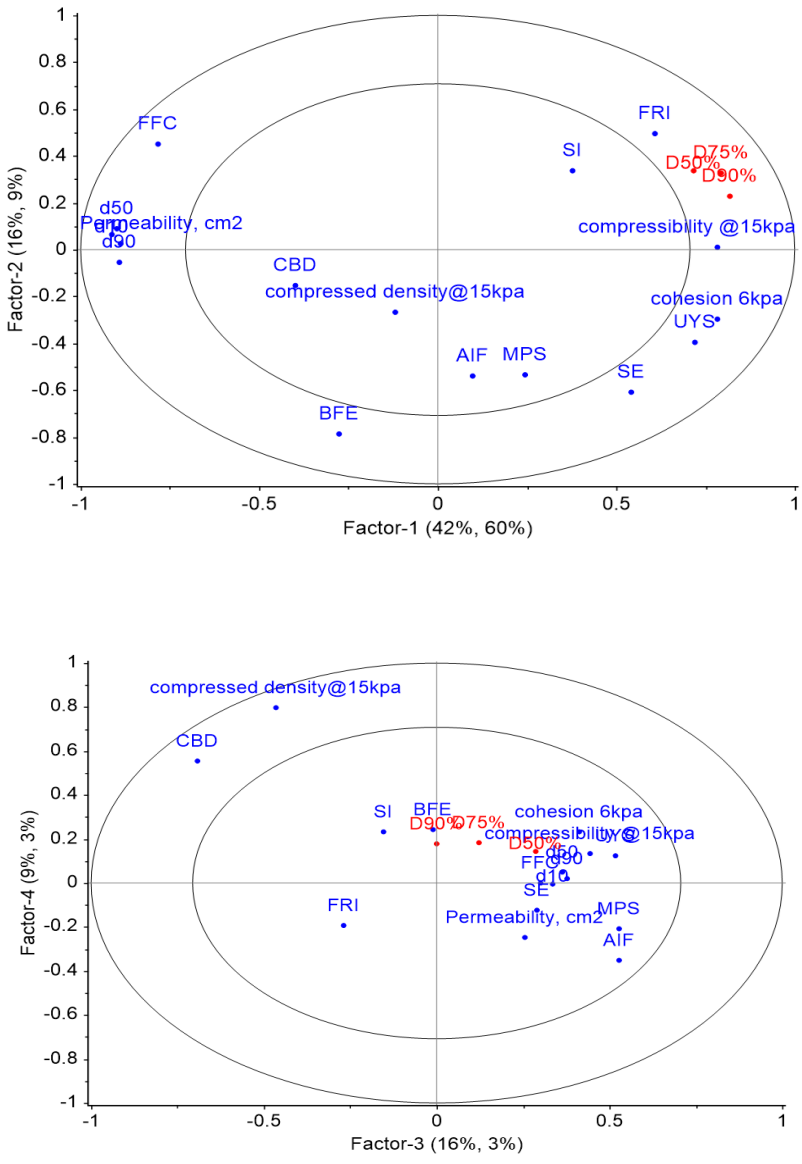

Figure 4-13 PLS correlation loading plot to correlation powder agglomerate size after feeder with its properties.

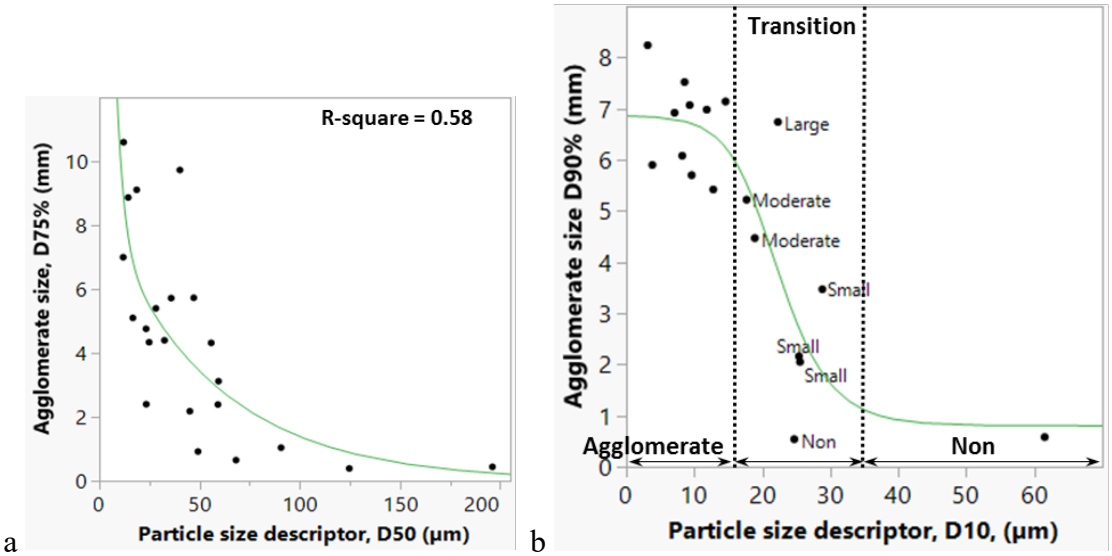

Figure 4-14 Agglomerate size versus particle size descriptor a) D75% vs D50. b) D90% vs D10.

The PLS regression shows a strong correlation between particle size descriptor and agglomeration, however the relation is nonlinear as shown in ***Figure 4-14a***, where the fitting yield a small R-square. While the decrease of the agglomerate size with the size of the original particles is evident, a large dispersion in the data is also seen: i.e., for values of D50 in the range of 50µm, there are materials that present large, medium and small agglomerates. The reason for this dispersion is partially attributed to the fact that other parameters are also important to describe the agglomeration phenomenon as we will discuss next. ***Figure 4-14b*** also shows that the maximum size of agglomerates (D90%) can be explained by a step-like function with respect to D10. When D10 is above 35µm, powder doesn't form any lumps during feeding, while all of powders is fed as lumps as long as its D10 is below 15µm. In fact, D10 represent the size of the fine portion of the powder. This portion generally determines the possibility of forming lumps. When this portion is larger than a certain level, the powder doesn't form lumps at all. In contrast, the powder definitely

forms lumps if this portion is smaller than a certain level, 15 µm. In the transitional range (15µm to 35µm, powder may form large, moderate, small and zero agglomerates. Therefore, D10 first enable us to assess the possibility of agglomeration.

Next, for the transitional range, agglomeration behavior can be explained by examining powder particle size D50 and compressibility, as shown in ***Figure 4-15***. In this graph, the bubble size represents the value of agglomerate size (D90%) and the label shows its classification according to the clustering analysis described in ***Figure 4-9***. Powders form larger agglomerates with the decrease of particle size and the increase of compressibility.

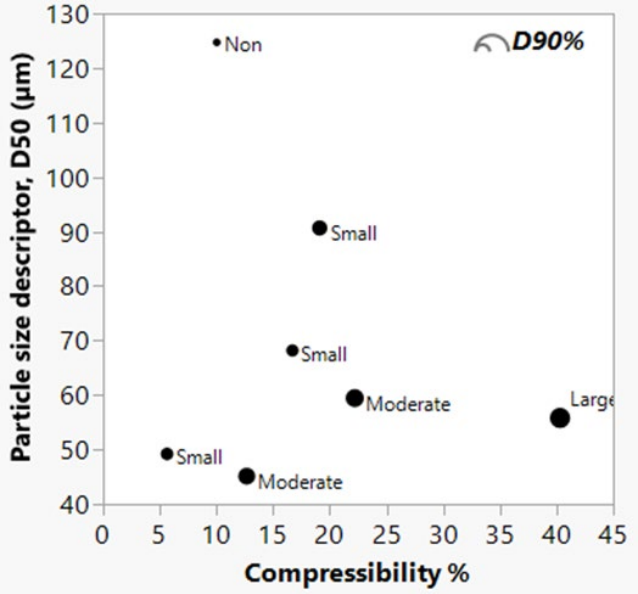

Figure 4-15 Seven materials in transitional range are explained by particle size (D50) and compressibility.

Then, we also plotted mean agglomerate size (from D75%) with particle size descriptor (D50) and compressibility, for all the materials in the extra-large, large, moderate, and small groups, as shown in ***Figure 4-16a.*** In this graphs, the value of D75% is represented by bubble size and the classification is described by color. The first observation arising

from the graph is that the large (and extra-large together), moderate and small agglomerate classification is discriminating. Powder tend to form larger agglomerates when having smaller particle size and larger compressibility. However, in some cases, it possibly appears that the particle size plus the compressibility of the powder explains agglomerate size with a degree of uncertainty although the explanation is still valid. For example, Caffeine, Avicel105 and Maize Starch are relatively less compressible powders (<25%), but they still form large and even extra-large agglomerates. Therefore, it is helpful to consider the contribution of another powder property descriptor, cohesion value (shear cell test), on agglomerates formation. ***Figure 4-16b*** displays the mapping of agglomerates size (D75%) with particle size vs. cohesion value. Likewise, the large (and extra-large together), moderate and small agglomerate classification is well demonstrated in this graph. Larger agglomerates are observed for powders with smaller particle size and larger cohesion value. Here, the formation of large and even extra-large agglomerates of Caffeine, Avicel105 and Maize Starch is associated with their high cohesion value. On the other hand, compressibility is also the supplement of cohesion value (shear cell test) as an explanantion for agglomeration. As a lubricant, MgSt shows relative low cohesion value in shear cell test, while its high compressibility enables the formation of extra-large lumps after the feeder. By using three material property discriptors together, we develop more certainty when assessing powder agglomeration. In summary, the size of agglomerates can be explained when incorporating particle size, compressibility and cohesion value. Powder yields larger agglomerates after passing through a twin-screw feeder when it shows smaller particle size and larger compressibility/or cohesion value.

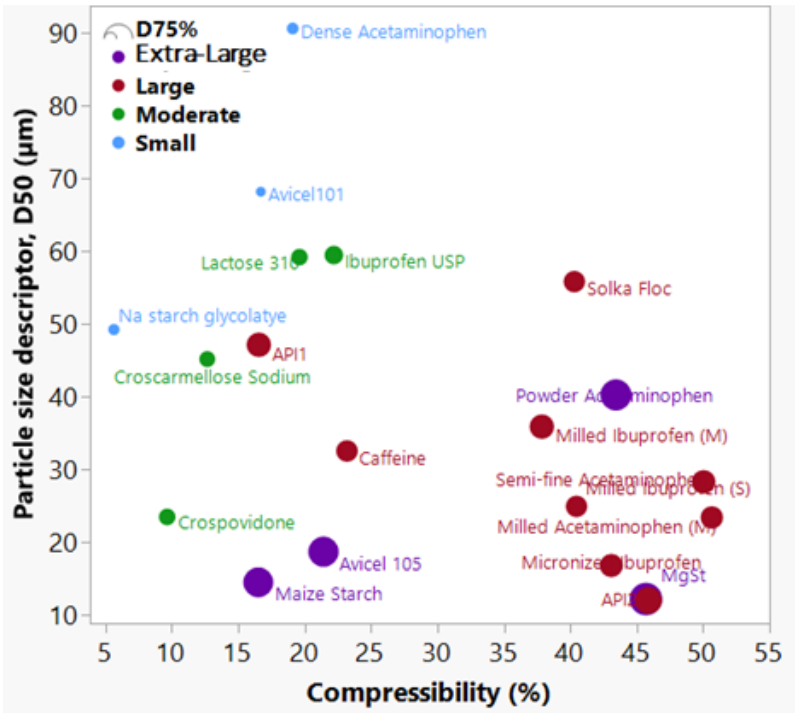

a

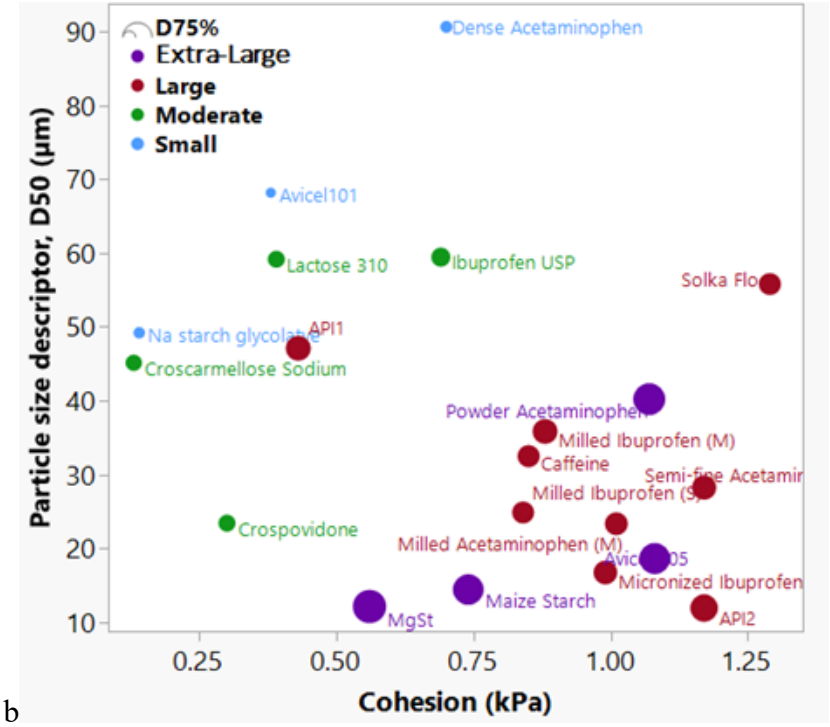

b

Figure 4-16 Correlating agglomerate size (D75%)with a) Particle size (D50) and compressibility. b) Particle size (D50) and cohesion value.

However, it seems that in both graphs we are not able to further differentiate the large and extra-large groups. The possible explanation is that powder can acquire large amount of electrostatic charges during feeding. The strong electrostatic repulsion within the matrix of an extra-large lump can cause it to fracture into several relatively smaller agglomerates, such as Semi-fine Acetaminophen, Micronized Ibuprofen, Milled Ibuprofen (S), Milled Acetaminophen (M) etc. We have documented this phenomenon in chapter 3. On the other hand, the large and not-fractured agglomerates may spread slightly when drop on the glass sheet which yield a further larger agglomerate to be detected. In fact, both large and extra-large agglomerates introduce difficulty in blending process. The more critical question is whether these agglomerates are easily eliminated, which can be answered by knowing their endurance.

Again, the only outlier of the above discussion is API1. As aforementioned, it is attributed to the error of measurement, which can be well explained in later discussion of agglomeration endurance.

4.4.6 Correlation of agglomerates endurance with material properties

According to our previous discussion, a large post-mill agglomerate size indicates a enduring agglomerate. In this section, we seek further understanding of agglomerates endurance by correlating post-mill agglomerates size with raw material properties. PLS analysis was also performed for visualizing the correlation between material properties and post-mill agglomerate size. The particle size descriptors, permeability, indexes from compressibility test and shear cell test are selected as the X-matrix. Post-mill agglomerate size indexes are selected as the Y-matrix. The correlation loading plot including factor1 and factor2 is shown in ***Figure 4-17***. Remarkably, the first factor explains 78% of Y-

variance, indicating a well-defined correlation between agglomerates size and high loading variables in factor1. Again, the structure of loading plot emphasizes that particle size, compressibility and cohesion value contribute to agglomeration significantly.

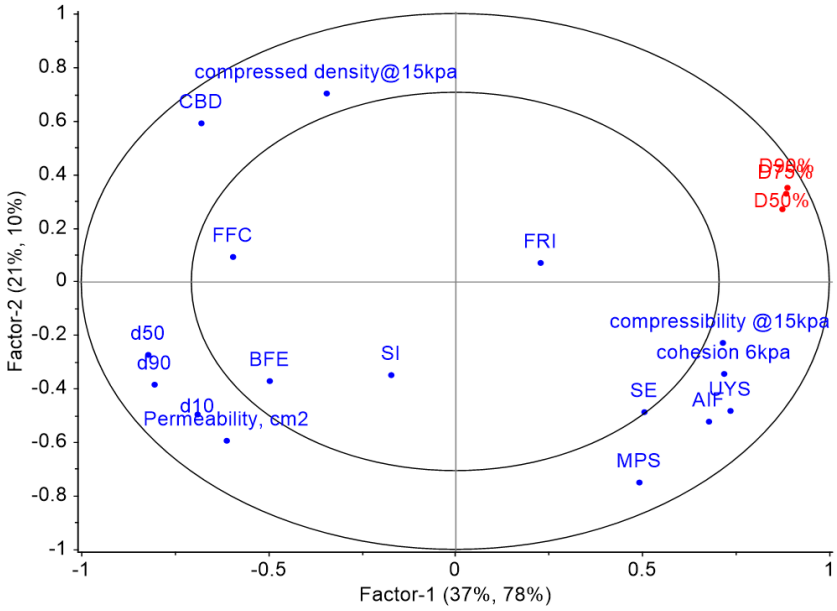

Figure 4-17 PLS correlation loading plot to correlation agglomerate size after conical mill with its properties.

Figure 4-18 further maps post-mill agglomerate size (D75%, represented by color gradient and bubble size) with particle size, compressibility, and cohesion value. The agglomerates smaller than 1mm can be considered as unenduring agglomerates, which are sufficiently de-agglomerated in the conical mill. It is quite revealing that the endurance of agglomerates is also highly correlated with particle size, compressibility, and cohesion value. Agglomerates increase endurance with the decrease of particle size, and the increase of compressibility and cohesion value.

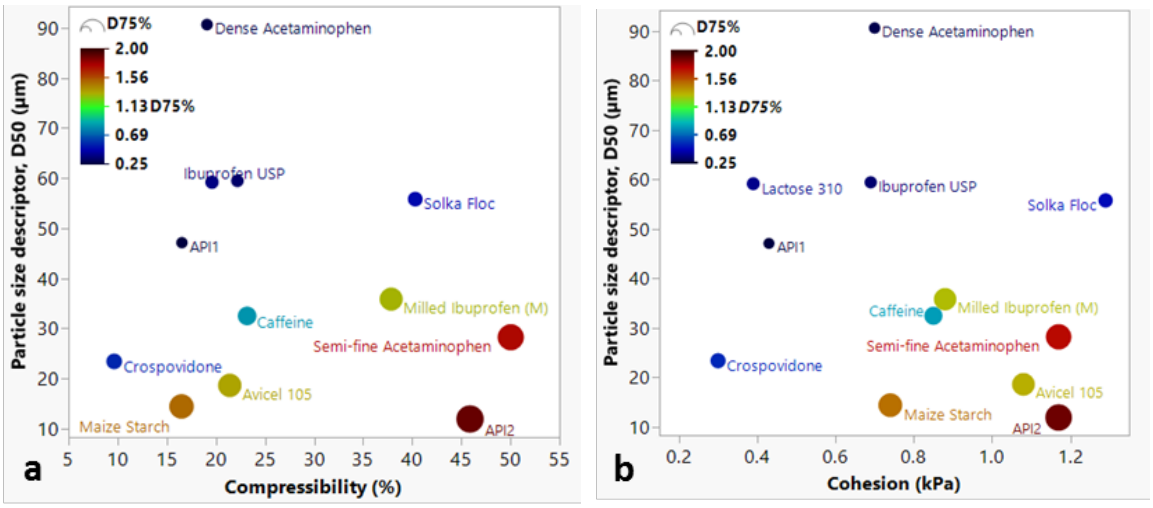

Figure 4-18 Correlating size (D75%) of post-mill agglomerates with a) Particle size (D50) and compressibility. b) Particle size (D50) and cohesion value.

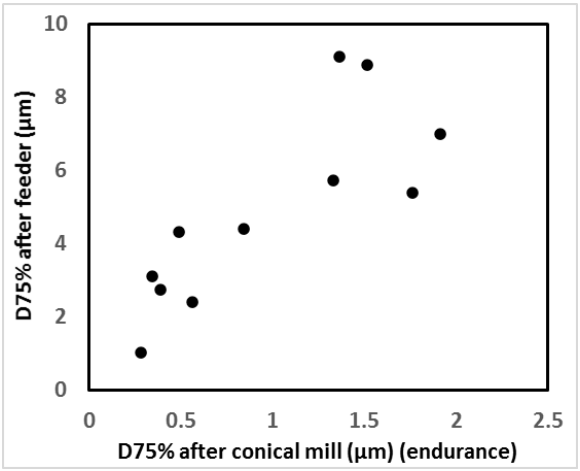

Figure 4-19 Agglomerate size after feeder (D75%) versus its endurance (D75% after conical mill).

As the trend for agglomerate size is similar to their endurance (shown in ***Figure 4-19***), it happens that small and moderate size agglomerates are also the ones readily eliminated (post mill D75%<1mm) due to large particle size, or small compressibility, or small cohesion value, as shown in ***Figure 4-18***. Previously, caffeine and Solka Floc forms large

agglomerates after the feeder. However, these agglomerates are unenduring agglomerates which can be adequately destroyed (D75%<1mm) in the conical mill. It can be interpreted as that Solka Floc has relatively large particle size and caffeine is a less compressible powder. Again, cohesion value (shear cell test) and compressibility are supplementary to each other. For instance, although Maize Starch and Avicel105 show relatively low compressibility (<25%), they still yield enduring agglomerates. This is the result of their small particle size and large cohesion value. Notably, API1 and Semi-fine Acetaminophen show highest compressibility and cohesion value. Meantime, both of them have small particle size (D50<30μm). This is the reason that they generate the most enduring agglomerates, which causes the particles remaining in relatively large agglomerates even after conical mill. *Error! Reference source not found.* also clearly described the agglomeration of API1. This material gives lows compressibility and cohesion value, which lead to the formation of unenduring agglomerates.

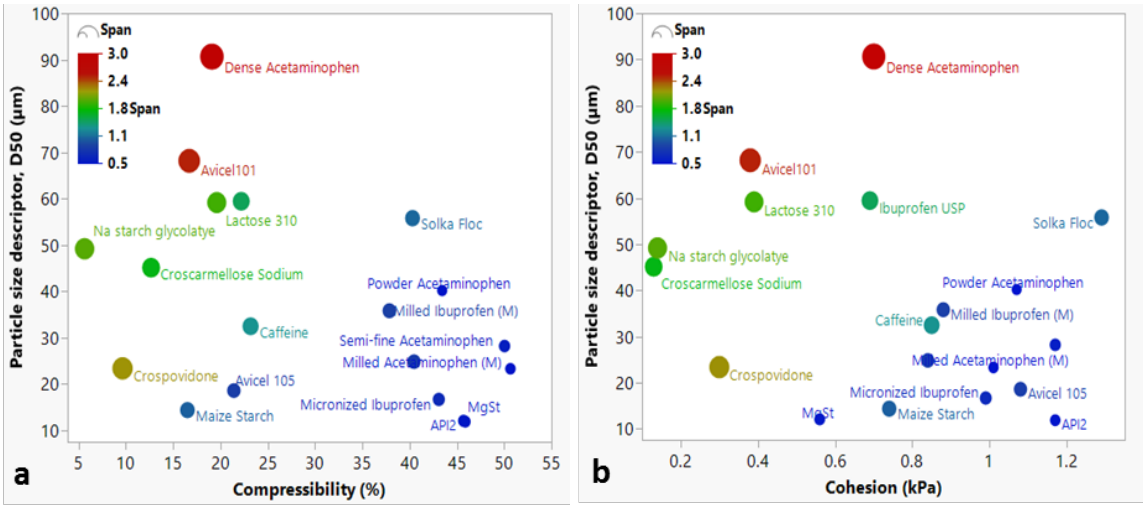

Figure 4-20 Correlating span of post-feeder agglomerates with a) Particle size (D50) and compressibility. b) Particle size (D50) and cohesion value.

Similarly, the span of agglomerates size distribution after feeder explains in part the endurance of agglomerates. A large span value corresponds to unenduring agglomerates. *Error! Reference source not found.* shows the mapping of span with particle size, compressibility, and cohesion value. Both the color gradient and bubble size describe span vale. A well-defined trend can also be observed; small particle size, large compressibility and high cohesion value contribute to the formation of enduring agglomerates.

4.4.7 The general discussion of relationship between agglomeration and material properties

As a summary of the previous two sections, powder agglomeration tendency (both size and persistance) highly correlates with particle size, and compressibility or cohesion value. First, as long as particle size D10 is above 35μm, the powder can be defined as non-agglomerating powder. When particle size D10 is smaller than 15μm, powder will be fed as lumps. Furthermore, as long as mean particle size (D50) is larger than 50μm, or compressibility is smaller than 20% (at 15kPa normal stress), or/and cohesion value is below 0.5kPa (at 6kPa shear cell test), a powder would form unenduring and small to medium size agglomerates (2 to 6mm) due to a consolidation stress applied to the powder bed during feeding. However, these unenduring agglomerates can be readily eliminated by shear when the powder exit the feeder. Remarkably, a high degree of agglomeration should be expected when powder has mean particle size smaller than 30μm, and compressibility is larger than 35% (at 15kPa normal stress), or/and cohesion is above 0.8kPa (at 6kPa shear cell test). These powders not only are fed as large lumps but also possibly remains as agglomerates even after a shearing process.

In fact, the total surface area of powder increases significantly when particle size decreases. When powder is densified and particles are forced to be packed more closely, the bonding force between particles is proportional to the surface area and increases with a decrease in particle size. Compressibility indicates whether a powder bed packing is susceptible when it is subjected to a normal stress. In general, a less susceptible powder bed (low compressibility) is not too far away from its initial packing status when the normal stress is applied. Likewise, when the normal stress is removed, a less susceptible powder bed would readily restore its initial packing. With respect to agglomeration tendency, powder with large compressibility is readily densified and form lumps when it is subjected to normal stress. The cohesion value suggests particle-particle cohesiveness, including Van der Waals force, capillary force, electrostatic force, particles interlock, etc. It refers to the yield point of a consolidated powder bed or lumps at zero normal stress. In order to have particle movement occurs, the yield point has to be overcome. Powder of large cohesion value indicates the powder lumps are difficult to be completely destroyed. The adequate shear stress is required to overcome the particle-particle cohesiveness so that agglomerates can be eliminated. Therefore, it is logical to correlate the agglomeration tendency with particle size, compressibility, and cohesion value.

4.4.8 Effect of material agglomerates on product content uniformity

So far, this chapter has focused on the powder agglomeration tendency when it passes through a twin-screw feeder and a conical mill, revealing that agglomerates are possibly generated in the feeder that might be difficult to eliminate. In this section, we examined the effect of powder agglomerates on tablet content uniformity. It is aimed to demonstrate that the formation of agglomerates in powder feeding possibly leads to a poor product. A

simplified continuous direct compaction process was established as shown in ***Figure 4-21***. The formulation was 94% of Avicel 102, 1% of MgSt and 5% of API by weight. To minimize the number of feeders, Avicel 102 and MgSt were preblended using a 7.6-liter capacity V-blender (Patterson-Kelley, Pennsylvania, USA), at 15rpm for 15mins (i.e., 225 revolutions). Then, the API and preblended excipient were loaded in the K-Tron loss-in-weight feeder respectively, using fine concave screws for API feeder and coarse concave screws for the excipients feeder. Following the two feeders, a Gericke GCM 250 continuous tubular blender (Gericke USA, Somerset NJ) was used to blend all the ingredients. Blends were collected and tablets were made offline using a Presster^{TM} compaction simulator (Measurement Control Corporation, East Hanover, NJ). In this case study, two APIs were selected: Dense Acetaminophen and Semi-fine Acetaminophen. As discussed earlier, Dense Acetaminophen forms small and unenduring agglomerates after the feeder, which are very easy to eliminate in the blender. Semi-fine Acetaminophen forms large and enduring agglomerates, which may generate difficulty to achieve a uniform mixture. The process parameters for both APIs are listed in ***Table 4-3***.

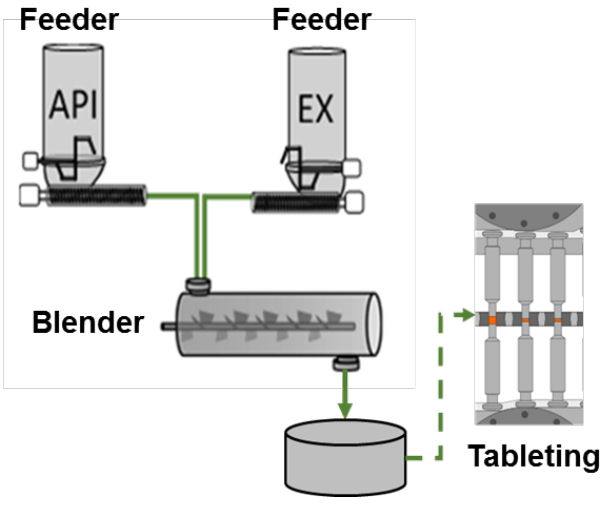

Figure 4-21 Simplified continuous direct compaction process.

Table 4-3 Process parameters to make tablets for two APIs.

	Semifine Acetaminophen	Dense Acetaminophen
Feeder screw type	Fine concave	Fine concave
Flow rate	1kg/h	1kg/h
Blender speed	150rpm	150rpm
# of blade pass	90.9	83.1
Compaction force	20 kN	20 kN
Tablet Mass	700mg	700mg

Content uniformity was analyzed by performing ultraviolet (UV) spectroscopic tests and presented as API content relative standard deviation (RSD= Standard deviation/Mean). First, one tablet was dissolved in 100ml pH5.8 Phosphate buffer, then a 4ml solution was precisely withdrawn and diluted to a 250ml solution. Then, a 1ml sample was taken to measure UV absorbance at the wavelength of 243nm. Ten tablets were treated in the same way to be ten samples. The RSD of the API content of ten samples was calculated and documented. The content uniformity of both APIs can be seen in ***Table 4-4***. It is evident that Semi-fine Acetaminophen tablets show very poor content uniformity. Note that, the calculated RSD of feeder flow rate is only 1.6%, which is much smaller than the RSD of the final product. Therefore, the failure of tablet homogeneity suggests the inverse correlation between agglomeration tendency with tablet uniformity. In other words, the agglomerates generated in feeder indeed result in product inhomogeneity. On the other hand, as a material of low agglomeration tendency, agglomerates of Dense Acetaminophen are eliminated in the blender. Tablets show acceptable content uniformity. The remarkable difference in content uniformity of these two APIs is associated with their agglomeration behavior.

Table 4-4 Content uniformity of tablets.

API	Content Uniformity (RSD)
Semi-fine Acetaminophen	16.6%
Dense Acetaminophen	1.8%

Our results also indicate that the high content variance in the final product is not only caused by the variance of feeder flow rate. The ingredient agglomeration is also a significant factor in explaining the non-uniform product in the continuous process.

4.5 Conclusion

The present study has provided an exciting opportunity to advance our understanding of powder agglomeration tendency during the process. We have developed a novel methodology, applying image analysis, to quantify powder agglomerates size when it passes through a screw feeder and a conical mill. Four indexes (i.e. D50%, D75%, D90%, and span) are defined to represent the distribution of agglomerates size.

We have observed when passing through a screw feeder, the powder possibly forms agglomerates due to the densification of powder in the pocket created by pitches of screws. It is shown that agglomerate size has a strong correlation with the type of screws. Coarse screws generate larger agglomerates than fine screws because of their larger screw pocket. The concave screws result in smaller agglomerates than auger screws, which may be attributed to its “self-cleaning”, while the feeding speed shows no effect on powder agglomeration. Hence, the characterization of agglomeration tendency can be done at a low feeding speed, which allows more reproducible and robust agglomerates sampling.

In this study, the agglomeration tendency of twenty-two pharmaceutical powders is examined when passing through a twin-screw feeder. According to the size of agglomerates,

they are classified as non-agglomerated, small, moderate, large and extra-large. In fact, the more critical question is whether the agglomerates survive in the next mechanical process (i.e. conical mill or blender), which can be answered by investigating the endurance of agglomerates. Thus, the conical mill study is performed later for 12 selected powders by adding a conical mill after the feeder. In such a way, unenduring agglomerates are eliminated and become dicrete particles, whereas enduring agglomerates can only be fractured, and agglomerates can also be observed after the conical mill. Results show the small and moderate agglomerates are eliminated immediately in conical mill but large and extra-large agglomerates still survive. Alternatively, the span of agglomerates distribution can also be used to represent agglomerate endurance.

This work also reveals that powder agglomeration tendency (both the size and endurance) can be explained by incorporating its particle size, compressibility and cohesion value. Materials of smaller particle size, larger compressibility, and larger cohesion value, tended to form larger agglomerates. In perticular, as long as particle size D10 is above 35μm, the powders in this study displayed no tendency to form any agglomerates. In contrast, the formation of agglomerates can be certainly observed when the particle size D10 is smaller than 15μm. Furthermore, as long as mean particle size (D50) is above 50μm, or compressibility (at 15kPa normal stress) is smaller than 20%, and/or cohesion value (at 6kPa shear cell test) is smaller than 0.5kPa, powder possibly forms unenduring agglomerates which can be eliminated immediate when exposed to a shearing environment. This is because that the powder is less compressibile. Even through the powder might be densified by a normal stress, the small particle-particle cohesive force results in agglomerates that can be completely destroyed effortlessly. Remarkably, when the mean

particle size is smaller than 30μm, or compressibility (at 15kPa normal stress) is larger than 35%, or/and cohesion value (at 6kPa shear cell test) is above 0.8kPa, the powder exhibits a high potential to form large and enduring agglomerates which are difficult to be eliminated completely in the downstream process.

Agglomerates may exist in the final product. In order to diminish agglomeration during manufacturing, an adequate shearing is required to overcome the cohesiveness within agglomerate matrix.

It is important to note that, although this study explores agglomeration tendency during powder feeding and continuous manufacturing, the methodology and conclusions of agglomeration tendency is approporiate to be referred not only in the continuous process but also in batch and semi-continuous process. This study is attempted to discuss powder agglomeration generally.

5 Chapter 5 Agglomeration Reduction of Cohesive Powder in Continuous Powder Mixing Process

5.1 Introduction

The manufacturing of solid dosage forms involves powder mixing as one of the most critical steps. The mixing performance of pharmaceutical active ingredients (APIs) with other functional excipients directly influences the homogeneity of blends which further impacts the quality of the final product[13, 51, 124, 147, 153, 154]. As discussed in the previous chapter, a major aspect that introduces inhomogeneity in blends is ingredient agglomeration. A powder agglomerate is a group of particles that assembles due to surface cohesive interaction. In traditional pharmaceutical manufacturing, the issue of agglomeration has received considerable attention[155-157]. The existence of API agglomerates possibly leads to large content variability, higher drug concentration and even super-potency in the finished product[51, 158-160]. Especially for a low drug loading formulation, successful blending requires a small amount of API particles to be distributed uniformly into a matrix with a large volume of excipients[161]. The formation of large API agglomerates significantly increases the variability of API concentration in each unit dose. Secondly, if the API is in agglomeration form, it may delay drug release rate which further reduces product bioavailability[162]. Especially in powders with a hydrophobic surface, agglomerates can cause a liquid to take longer to fully immerse every particle[163, 164]. Moreover, the formation of agglomerates may induce blend segregation due to the extensive size difference between excipient particles and API agglomerates[165].

As discussed in chapter 4, agglomeration is the result of strong cohesive particle-particle interactions that enable discrete particles to group together. The powder cohesive interactions include Van der Waals force, electrostatic force, capillary force and particle mechanical interlocking[132, 166-169]. Additionally, agglomeration occurs when powder is compressed at local areas under high consolidation stress[170]. Fine and cohesive powders often develop agglomerates during processing, for the reason that the total particle surface area and, correspondingly, all the cohesive components are a function of particle size[171-173]. For example, as particle size decreases, both the importance of Van der Waals force and electrostatic force increases significantly[123, 172, 174, 175]. On the other hand, for some solid dosage forms, particularly for poorly soluble drugs, the API is generally micronized to increase its surface area so that more surface is available to be immersed in liquid[176, 177]. Therefore, accomplishing sufficient de-agglomeration for micronized and cohesive API becomes a primary concern.

When processing a powder of high agglomeration tendency, it is possible to reduce or even eliminate agglomerates by applying external mechanical stress to overcome cohesive interactions between particles[46]. It has been demonstrated that API agglomeration can be significantly reduced by providing a sufficient shearing environment with a large velocity gradient between particles. In fact, shear mixing is the only mixing mechanism that generates adequate stress for deagglomeration[178]. Later studies further suggest that the mechanisms of deagglomeration in both convective and tumbling blender are abrasion rather than the deformation and fracture of agglomerate[140, 179]. In the batch blending process (V-blender, Tote blender, Double-cone blender and ribbon blender etc.), applying extra shear is the main strategy to improve homogeneity of blends, such as assembling

intensifier bar in v-blender[155, 157], using an internal impeller[155, 180], increasing tumbling body speed and total blending time[157, 181, 182], adjusting powder fill level[157], designing proper ribbon blade and increasing its speed[183]. Moreover, the agglomeration can be effectively diminished when passing the pre-blended mixture through a conical mill, which provides a high shear environment given by high-speed impeller, and then blending again[53, 155]. Since all these blending processes are operated in different patterns and scales, the dependence of shear rate and total applied shear are poorly understood. Thus, Llusa *et al.* explored the deagglomeration of three grades of Acetaminophen in a controlled shear environment, known as a modified Couette system[156]. They systematically investigated the role of shear rate and shear strain on API deagglomeration and concluded that increasing shear strain is effective for reducing agglomerates but the effects of shear rate is not well understood. However, there is an empiricalunderstanding that a certain minimal amount of shear rate is required to implement deagglomeration[147].

In the modern pharmaceutical industry, the manufacturing of drug products is shifting from traditional batch process to continuous process due to its high robustness, improved risk assessment, and easier transfer from process development to commercial manufacturing. With respect to API agglomeration, it is still an issue that needs to be considered during process development[51, 161, 184]. Due to the different processing dynamics compared to the batch process, it is necessary to invest new insight in continuous manufacturing for API deagglomeration. ***Figure 1-3*** depicts the schematic of three representative continuous solid dose manufacturing systems: a continuous direct compaction line, a continuous wet granulation line, and a continuous dry granulation line[50]. It is apparent that blending is

the second unit operation (after feeding) in all three manufacturing strategies. Therefore, it is critical to ensure that the API agglomerates are sufficiently diminished after blending to enable successful downstream processes and prevent poor product. The shearing environment within a continuous tubular blender and its effect on product properties have previously been considerably investigated experimentally[13, 147, 154, 185, 186], and the mixer performance as the function of critical process parameters, such as flow rate, impeller speed and impeller configuration, are represented in computational simulations[187, 188]. However, far too little attention has been paid to the ingredient agglomeration behavior during continuous blending. In chapter 4, it has been demonstrated that large lumps of cohesive ingredients are generated when passing through a twin-screw feeder because of powder being consolidated within the screw pocket. The tendency of powder agglomeration can be assessed by knowing the particle size, compressibility, and cohesion value. There is a high possibility that agglomerates will still survive in the blender if the blending process is improperly designed. Although a number of attempts have been made to determine the effects of blending parameters (flow rate, impeller speed and impeller configuration) on the homogeneity of blends[51, 154, 161, 184, 189], the systematic investigation of deagglomeration in continuous powder blending is still missing.

In this study, we aim to fully understand the efficiency of deagglomeration provided by continuous powder blending, at different process settings, with and without using a conical mill. To that end, a case study was performed to investigate the API agglomeration in a simple binary formulation (a cohesive API + a free-flowing excipient) of relatively low drug loading. Multiple blending processes were implemented involving different impeller rotational speed of the blender, different powder holdup in the blender, with/without using

a conical mill for delumping, and also varying impeller speed of conical mill and hole size of the mill screen. Three methodologies are applied to quantify API agglomerates in blends: Near-infrared spectroscopic technique, powder sieving, and chemical imaging. In the later section, we further examine the effects of API agglomerates on tablets content uniformity and dissolution profile.

5.2 Materials and methods

5.2.1 Materials

Table 5-1 Materials and composition for chapter 5

Material	D10 (µm)	D50 (µm)	D90 (µm)	Composition (w/w)
Fast-Flo Lactose	64.23	136.1	214.7	95%
Semi-fine Acetaminophen	11.83	28.22	52.28	5%

A binary formulation consisting of Monohydrate Lactose (NF Fast Flo Lactose, Foremost Farms USA) and a pharmaceutical active ingredient(API): Acetaminophen (Acetaminophen Semi-fine powder, Mallinckrodt Pharmaceuticals) was chosen. The quantitative composition (%w/w) of the formulation was determined as 95% of Fast-Flo Lactose and 5% Semi-fine Acetaminophen. Among them, Semi-fine Acetaminophen is a cohesive powder with high agglomeration tendency during process. Fast-Flo Lactose is a free-flowing powder with negligible agglomeration tendency. When making the tablets, Magnesium Stearate (MgSt, Mallinckrodt Pharmaceuticals) was used to lubricate dies and punches directly. Information about these materials is listed in ***Table 5-1***. The particle size distribution of Lactose and Acetaminophen was measured using a laser diffraction analyzer with a Tornado Dry Powder System (LS 13320, Beckmann Coulter) and is presented in terms of D10, D50, D90.

5.2.2 Continuous powder blending process

5.2.2.1 Continuous Tubular blender

In our study, a Gericke GCM250 (Gericke USA, Inc. Somerset, NJ) continuous tubular blender is used. The shearing environment is provided by an impeller rotating along its axis, which consists of 12 triangular shaped blades, as shown in ***Figure 5-1***. This blender is equipped with a weir, located at the exit of the blender. It is used to control the amount of powder hold-up in the blender (M_{holdup}) by rotating to change the fill level of powder in the mixer. Additionally, by knowing the mass flow rate of system ($m_{flow\ rate}$), the space time ($\tau_{mean-residence}$) of the system at steady state can be determined, which indicates the amount of time that the powder spends in the blender.

$$\tau_{mean-residence} = \frac{M_{holdup}}{m_{flow\ rate}} \tag{5-1}$$

Then, the total number of blade passes (NOB) experienced by a blend through its trajectory along the blender's axis can be calculated by knowing the impeller's angular speed (ω, RPM).

$$NOB = \omega \times \tau_{mean-residence} \tag{5-2}$$

For a given continuous tubular blender, the impeller rotational rate determines the shear rate, since the energy needed for generating a velocity gradient between particles is provided by the impeller rotation. The mean residence time indicates the duration of material exposure to the shearing environment. Previous studies reported the correlation between the residence time and the level of mixing[190]. The total applied mechanical shear strain is proportional to the shear rate and the duration of the applied shear stress,

thus, the total shear level is correspondingly proportional to the NOB, which was also reported to greatly influence blend homogeneity and blend properties of shear sensitive formulation [13, 147, 165, 191].

In a continuous powder blending process, sufficient bulk mixing (or macro-mixing) is required to blend several initially unmixed ingredients and to diminish the variability of the mass flow rate. On the other hand, a high level of micro-mixing might be desired to de-lump ingredient agglomerates in order to accomplish satisfactory content uniformity[51]. Both adequate macro-mixing and micro-mixing constitute a successful powder blending process.

Figure 5-1 Impeller of continuous tubular blender.

5.2.2.2 Continuous powder mixing

A modified continuous powder feeding-blending system was established to prepare blends, as shown in ***Figure 5-2a***. Both ingredients were respectively loaded into two twin-screw loss-in-weight K-Tron20 feeders (Coperion K-Tron Pitman, Inc. Sewell, NJ). Fine concave screws were used for Semi-fine Acetaminophen feeding and course concave screws were used for Fast-Flo Lactose feeding. The flow rate of the system remained constant at 20kg/h. Following the feeders, the blender discussed above mixed the ingredients at multiple impeller speeds and weir angles. As shown in ***Figure 5-2b***, three different weir configurations were applied. Weir angle of 0º refers to no weir equipped, which gave the

lowest level of powder holdup in blender. Weir angle of 180º is defined when the bottom half of the exit was blocked. For the weir angle of 270º, the exit of the blender was only at the upper-left area. The highest level of powder holdup can be obtained at this configuration. When the blender reached steady state, blends were collected and subjected to further analysis. Also, the mass of powder holdup in the blender can be directly weighted after reaching steady state. ***Table 5-2*** lists the process parameters and the calculated number of blades passes (NOB) in the blender. The purpose of this experiment design is to investigate the effect of blender operation on API agglomerate reduction.

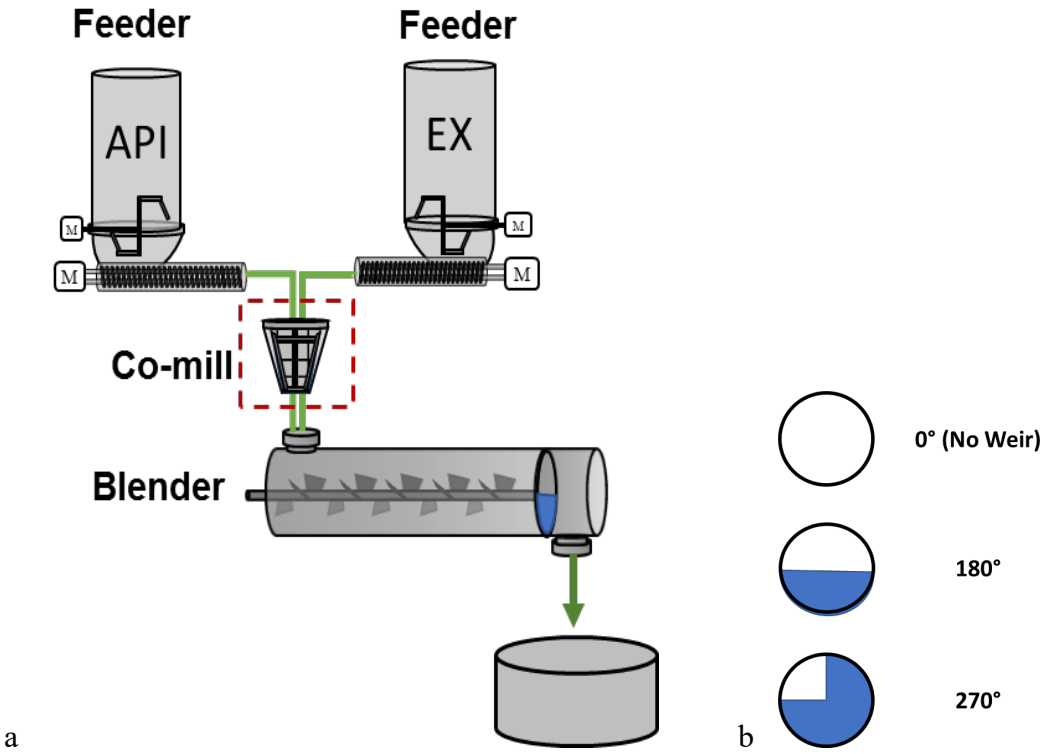

Figure 5-2 a) Configuration of feeding-blending system. b) Angle of the weir.

Table 5-2 Process parameters for continuous blending

	Name of the Blends	Conical mill screen size (mm)	Conical mill blade speed (rpm)	Blender blade speed (rpm)	Weir angle	NOB
Blender	B-50-0º	N	N	50	0º	58
	B-150-0º	N	N	150	0º	68

	B-250-0º	N	N	250	0º	55
	B-50-180º	N	N	50	180º	88
	B-150-180º	N	N	150	180º	91
	B-250-180º	N	N	250	180º	62
	B-50-270º	N	N	50	270º	148
	B-150-270º	N	N	150	270º	345
	B-250-270º	N	N	250	270º	125
	B-100-270º	N	N	100	270	275
	B-200-270º	N	N	200	270	211
Conical mill	C-2-500	2	500	N	N	N
	C-2-1000	2	1000	N	N	N
	C-5-500	5	500	N	N	N
	C-5-1000	5	1000	N	N	N
Conical mill + Blender	CB-150-0º	2	1000	150	0º	72
	CB-150-180º	2	1000	150	180º	91
	CB-150-270º	2	1000	150	270º	347

Additionally, in another set of studies, a conical mill supplied by Glatt (Glatt Air Techniques, Inc. Ramsey, NJ) was added between the feeders and the blender. As a high shear unit, it is equipped with an internal impeller with a rotational rate of up to 1000rpm. Below the impeller, a conical screen is installed with multiple hole sizes. The purpose of the conical mill is deagglomeration instead of particle size reduction. Thus, screens of relatively coarse mesh are selected. Blends were collected after the conical mill alone and after conical mill+blender. The process parameters are also listed in ***Table 5-2***.

5.2.3 Agglomerates measuring methods

5.2.3.1 Near-infrared (NIR) spectroscopic technique

Setup for NIR spectroscopy acquisition

Near-infrared spectroscopic technique(NIR) is used to monitor blends composition. Then, by capturing the fluctuation in composition, API agglomerates in blends can be monitored. The spectra acquisition was implemented offline, as shown in ***Figure 5-3a***. Approximately,

120g of powder was first loaded into a funnel, which equipped above a conveyor belt. The conveyor belt further carried blends moving towards an NIR sensor for spectra acquisition. The gap between the botton of the funnel and the conveyor belt was controlled, which maintained that the powder ribbon was 3mm in thickness and 12mm in width. The spectra were collected continuously when the powder ribbon moved through the NIR sensor. In total, 2500 spectra were collected. The distance between the NIR sensor and powder ribbon kept 3mm throughout the experiments. It is worthwhile to note that the speed of conveyor belt (i,e. sampling speed) was adjustable which referred to the sampling size during each spectrum acquisition. This is a critical parameter that need to be determined properly. More discussion of this parameter is performed in section 5.3.2. In the later study (section 5.4), the speed of the conveyor belt (i.e., sampling speed) remains constant at 0.13cm/s.

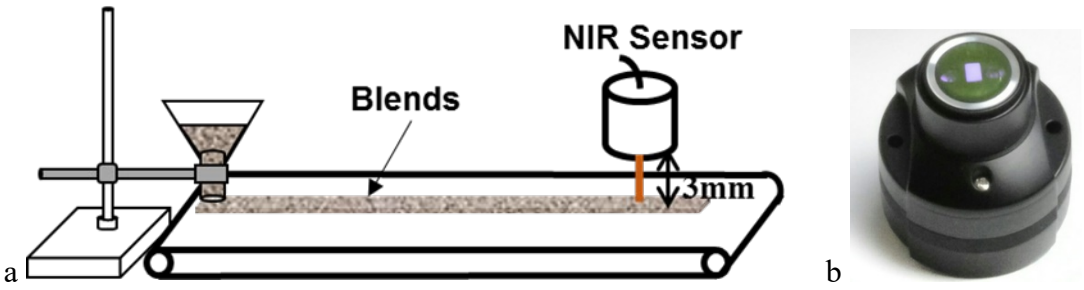

Figure 5-3 a) Set-up for NIR spectra acquisition. b) JDSU Micro NIR 1700.

NIR instrument and spectroscopy

A portable NIR spectrometer was used for spectra acquisition: JDSU MicroNIR 1700 (VIAVI Solution Inc, Santa Rosa, CA), in diffuse reflection mode, as shown in ***Figure 5-3b***. It is equipped with a 128-pixel uncooled InGaAs photodiode array detector. The active area for sampling is a 4×2mm rectangular. A pair of integrated vacuum tungsten lamps in the probe was used as the illumination source. The spectral range of MicroNIR

1700 were 908-1677nm with the wavelength resolution of 6nm. Spectra were collected every one second at the scan count (the number of scans averaged to represent a single spectrum) of 50 and the integration time (the time consuming for the detector to capture light) of one scan setting to 10.1ms. The dark current was scanned by facing detector to environment and the reference scans were performed by focusing on a 99% diffuse reflectance panel.

Calibration model and data analysis

The LabRAM Acoustic mixer was used to mix Semi-fine Acetaminophen and Fast-Flo Lactose as calibration blends with the mixing intensity of 50% for 2min. Since a high shear blending process was applied to prepare standard blends, they are expected to be highly uniform blends without any agglomerates in them. The calibration blends (i.e., standard blends) were prepared containing Semi-fine Acetaminophen of 0%, 5%, 9%, 13%. All of the spectra for calibration model were acquired using the setup described in section 5.3.1.1 with the speed of conveyor belt setting to 0.13cm/s. In total, 100 spectra were collected. Among them, 67 spectra were used to build prediction model and 33 spectra were used for model validation.

Quantitative data analysis was completed using the Unscrambler X 10.4 (CAMO. Oslo, Norway). By comparing the spectra of Fast-Flo Lactose and Semi-fine Acetaminophen, it was demonstrated that the spectra in the range of 1093-1676 nm discriminated these two ingredients adequately, which can be used further for model development. A multivariate calibration model was then developed by performing partial least squares (PLS) regression with non-linear partial least square (NIPALS) algorithms, defining the percentage of Semi-fine Acetaminophen as Y-variable and the ranged spectra as X-variable. After careful

selecting spectrum pretreatment (SNV+1st derivative) and number of PLS factors (3 factors), this model was able to robustly and accurately predict blends composition, giving the root mean square error of cross-validation (RMSECV) of 0.14 and the root mean square error of prediction (RMSEP) of 0.13.

In the section 5.3, the proof-of-concept for using NIR to monitor API agglomeration is demonstrated. The application of NIR techniques in mornitoring API agglomerates in blends is based on capturing the fluctuation of composition caused by API agglomerates. In order to distinguish the effect of insufficient bulk mixing and ingredient agglomeration on composition fluctuation, two different patterns of fluctuation are defined. The "spike-type" fluctuation is used to represent ingredient agglomeration and the "wave-type" fluctuation specifiy insufficient bulk mixing, as discussed in section 5.3.

5.2.3.2 Sieving

The sieving method was performed to measure the quantity of agglomerates in a specific size. A large volume of blends (~500g) were passed through the following sequence of US standard sieve mesh: NO.10 (2mm), NO.18 (1mm), NO.20 (850μm), NO.30 (600μm). As a free-flowing powder, Fast-Flo Lactose can pass through the mesh easily when a slight vibration is applied to sieves. Thus, only agglomerates of Semi-fine Acetaminophen remained on each sieve. The mass of agglomerates was weighed and the proportion of agglomerated API was calculated. Note that, it was difficult to analyze agglomerates below 600μm since a stronger vibration is required to enable blends to flow through mesh finer than NO.30. Agglomerates would be destroyed if a strong vibration was applied.

5.2.3.3 Raman Imaging

In order to quantify API micro-mixing with excipients in a unit dose, a chemometric Raman imaging system is used, the mPAT LAB^{TM} Raman image (H2Optx Inc. San Jose, CA). This instrument can achieve a spatial (XY plane) resolution of 10×10μm^2 with a depth(Z step) scan as low as 1μm. As a high-resolution instrument, it is able to identify each ingredient and map them on either 2D or 3D images. In our study, this system is used as a precise and relatively fast method to determine API micro-mixing status when one layer of a compacted tablet is scanned, and a 2D grey scale map is generated which only shows the distribution of one ingredient. The tableting parameter will be listed in next section. Each tablet was shaved manually to remove multiple layers, then two different layers of the entire tablets were analyzed. Five tablets of each blend were randomly selected. When the scanning was completed, a 4000×4000μm grey map was generated which visualized the distribution of Semi-fine Acetaminophen in the layer, as shown in ***Figure 5-4a***. In this grey map, all of the white pixels represented Semi-fine Acetaminophen. Therefore, the size of each white spot quantified the size of an agglomerate. Additionally, by performing the image analysis, the agglomerates size cumulative distribution can be calculated and presented as the percentage of area versus circular equivalent diameter. The indexes of agglomeration were further defined as the diameter that the percentage of area were comprised of smaller agglomerates, such as 30%(D30), 50%(D50), 70%(D70), 90%(D90), as shown in ***Figure 5-4b***.

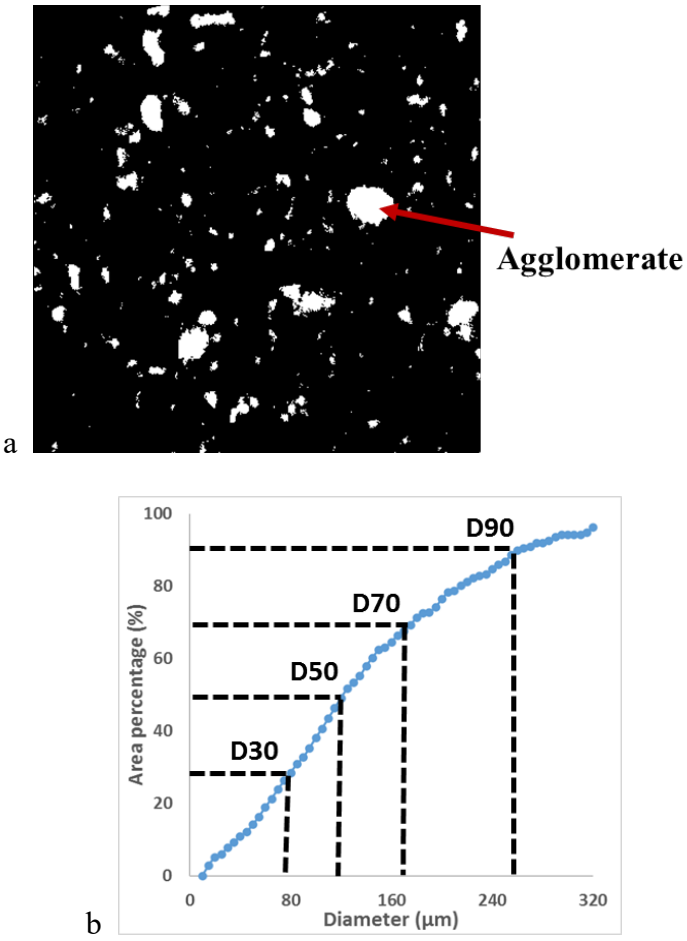

Figure 5-4 Raman imaging: a) Grey map of Raman imaging. b) Agglomerates size distribution.

5.2.4 Tableting, content uniformity and Dissolution study

Tablets were prepared offline using a Presster™ compaction simulator (Natoli Engineering Company, Inc., Saint Charles, MO). 185mg of blends were compressed at 10kN compaction force, resulting in tablets that were 7mm in diameter. Fifty-five tablets were made for each blend. Then, the amount of Semi-fine Acetaminophen in each tablet was measured by applying transmission NIR techniques. A bench-top Fourier transform near-infrared (FT-NIR) spectrometer, the Multipurpose Analyzer (MPA) (Bruker Optics, Billerica, MA) was used to collect spectra for each tablet. A calibration model for tablet

content prediction was also developed by applying PLS regression with NIPALS algorithms.

Tablet dissolution tests were performed by using a dissolution tester of USP apparatus II (paddle apparatus) (Agilent Technologies, Santa Clara, CA). The rotational speed of the paddle was 50rpm. Phosphate buffer at PH 5.8 was prepared as the dissolution medium. 500ml of the medium was added into each vessel and its temperature was maintained at 37.0 ± 0.5ºC. A peristaltic pump was used to withdraw 10ml of medium every 3min and pumped back to the vessel after measurement. The amount of released Acetaminophen was analyzed using a Cary 60 UV-Vis spectrophotometer (Agilent Technologies, Santa Clara, CA) at the wavelength of 243nm. The percentage of drug release as a function of time was plotted as the dissolution profile.

5.3 Proof-of-concept for NIR technique to monitor API agglomerates

5.3.1 Method for proof-of-concept

The main question addressed in this section is whether the NIR method is capable to capture the fluctuations in composition locally as a result of the agglomeration of API. Therefore, this is a sampling question rather than a question of chemometrics/spectroscopy.

A proof of concept is first performed by investigating a controlled situation, where 'knowing-in-size' agglomerates were presented in blends and evaluated by using the proposed setup. Pure Acetaminophen tablets were prepared to simulate the natural agglomerates in blends. Tablets were made using a benchtop tablet press: Gamlen (Gamlen Instrument, London, UK) with compaction force of 4KN. Two different size of tablets were prepared: 6mm and 2mm in diameter. Three standard blends containing 0%, 5%, and 15%

of semi-fine Acetaminophen (w/w) were also produced using LabRAM Acoustic mixer with mixing intensity of 50% for 2min. The other ingredient in these blends was Fast-Flo Lactose. Since a high shear blending process was applied to prepare standard blends, they are expected to be highly uniform blends without any agglomerates in them. As shown in ***Figure 5-5***, when standard blends were loaded on the conveyor belt as described in section 5.2.3.1, ten 6mm and ten 2mm 'agglomerates' were placed on the powder ribbon manually with distance of 3cm. The NIR sensor was aimed to monitor the composition fluctuation while the conveyor belt carried the powder containing 'known' agglomerates. The speed of the conveyor belt was controlled and five various speeds were implemented: 0.13cm/s, 0.23cm/s, 0.46cm/s, 0.92cm/s, and 1.83cm/s. For this proof-of-concept study, the length of being analyzed powder ribbon remained constant of 65cm. Namely, the total sample size was comparable. Different sampling speed resulted in various number of spectra being collected.

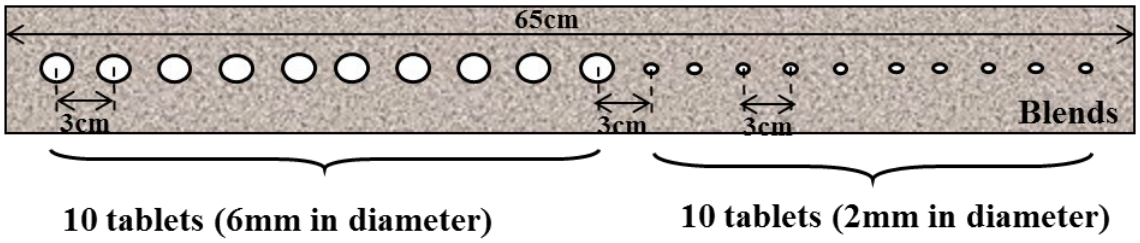

Figure 5-5 Proof of concept for monitoring 'known' agglomerates.

5.3.2 NIR technique to discern "known" agglomerates

As aforementioned, we propose using the NIR spectroscopic technique to discern API agglomerates by capturing the fluctuation of composition locally as the result of agglomerates. ***Figure 5-6*** shows the NIR-measured concentration of Semi-fine

Acetaminophen versus the spectra number at different sampling speed in the case of 0% API blends containing 20 pure Acetaminophen tablets. It is important to note that the spectra number correspond to the time point of spectrum acquisition which further refer to the location of NIR active spot on the blend ribbon.

The first observation arising from these graphs is that the agglomerates are represented as an increment in composition. Each composition increment refers to an agglomerate being detected, and each agglomerate is expressed as a "spike". When the NIR active spot has passed the agglomerate, the measured concentration declines to the target composition value of the standard blends, as highlighted using a red line. The fluctuation of composition only occurs locally at the position that contains the agglomerate. Moreover, the size of agglomerates can be illustrated in a way when examining the maximum composition reading. The smaller agglomerate gives a lower peak composition value. This is due to that the measured composition is the average of the entire NIR active area in each sampling duration. The smaller agglomerate results in that less volume of API is taken into account. However, it should be noted that the maximum composition reading may not accurately represents the real composition since the density of "know" agglomerates is much higher than the bulk blends, which is not considered in calibration. The different matrix of the system possibly leads to a prediction of relative low accuracy. Here, the NIR is used to capture the fluctuation of composition instead of precisely measuring the maximum possible composition.

Secondly, the different sampling speed results in different numbers of spectra being collected in a constant length. Results show that approximate 500 spectra are collected throughout the 65cm powder ribbon, at the sampling speed of 0.13cm/s, while only 35

spectra can be collected at the speed of 1.83cm/s. With the increasing of sampling speed, the total amount of collected spectra is gradually reduced, also, the number of composition readings on each "spike" correspondingly decreases. In general, less information is captured by using a smaller number of spectra. When the sampling speed is 0.13cm/s, it is apparent that all of 20 agglomerates are captured as 20 well-defined spikes. Although 20 agglomerates are also presented to the NIR sensor for the sampling speed of 0.92cm/s, each composition peak only consisted of one or two composition readings. This indicates that less information about agglomerates is captured by the NIR sensor. In contrast, several agglomerates are not captured when the sampling speed is 1.83cm/s, namely, API agglomeration information is not fully registered at the high sampling speed. Under this speed, only 11 out of 20 agglomerates are detected. Also, the maximum composition of each peak is relative smaller in comparison to the values measured at low sampling speed.

Figure 5-7 and ***Figure 5-8*** show the composition of the blends containing 5% API and 15% API with 20 "known" agglomerates at the sampling speeds of 0.13cm/s and 1.83cm/s, respectively. Similar observation can be made that all of the agglomerates are clearly defined as "spikes", under low rather than high sampling speed. These graphs also suggest that the NIR methodology to discern API agglomerates is independent of blend's composition, i.e., that is suitable for blends of any composition. Consequently, based on detecting the sudden and local concentration increment, it is possible to discern API agglomerates in blends using NIR techniques at relatively low sampling speed. In all subsequent studies reported here, the speed of the conveyor belt (i.e., sampling speed) remains constant at 0.13cm/s.

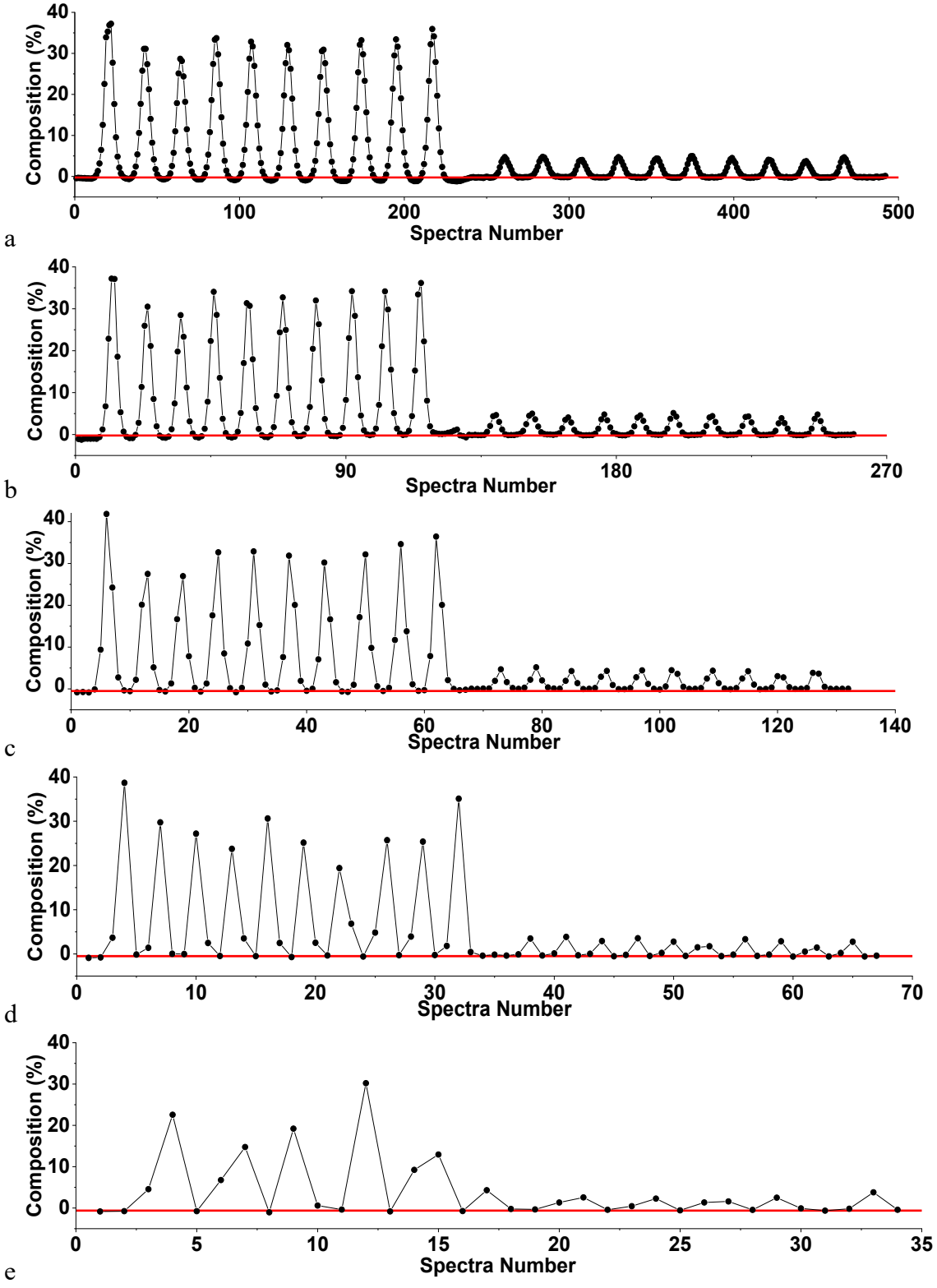

Figure 5-6 Composition fluctuation of 0% Acetaminophen blends caused by agglomerates at the sampling speed of a) 0.13cm/s. b) 0.23cm/s. c) 0.46cm/s. d) 0.92cm/s. e) 1.83cm/s.

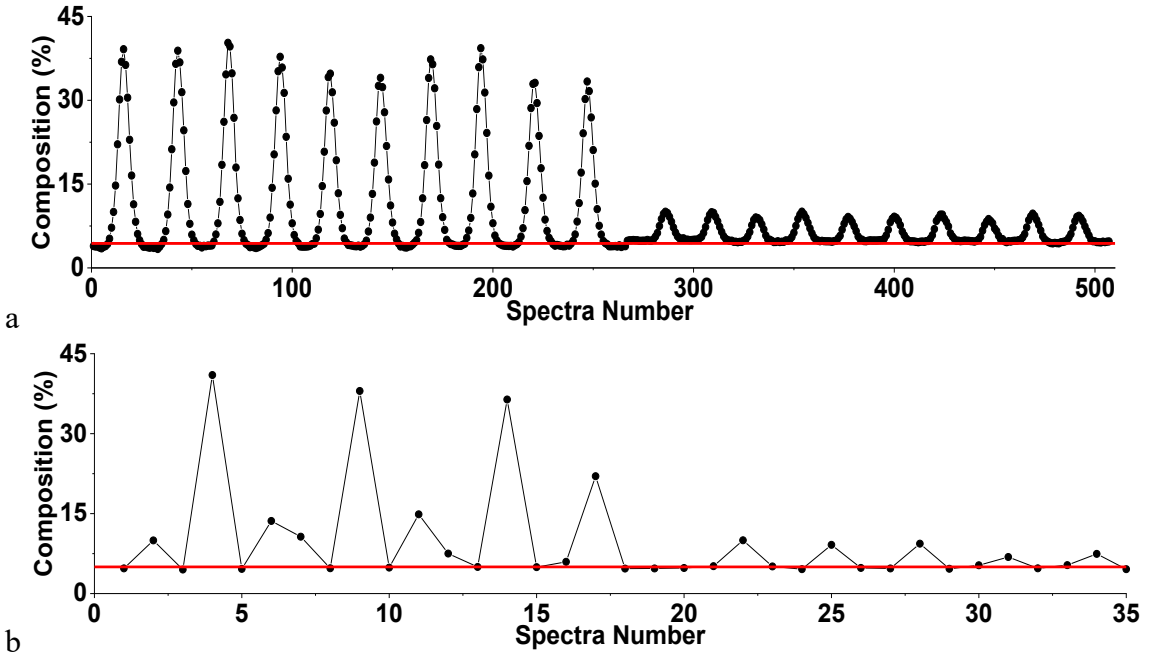

Figure 5-7 Composition fluctuation of 5% Acetaminophen caused by agglomerates at the sampling speed of a) 0.13cm/s. b) 1.83cm/s.

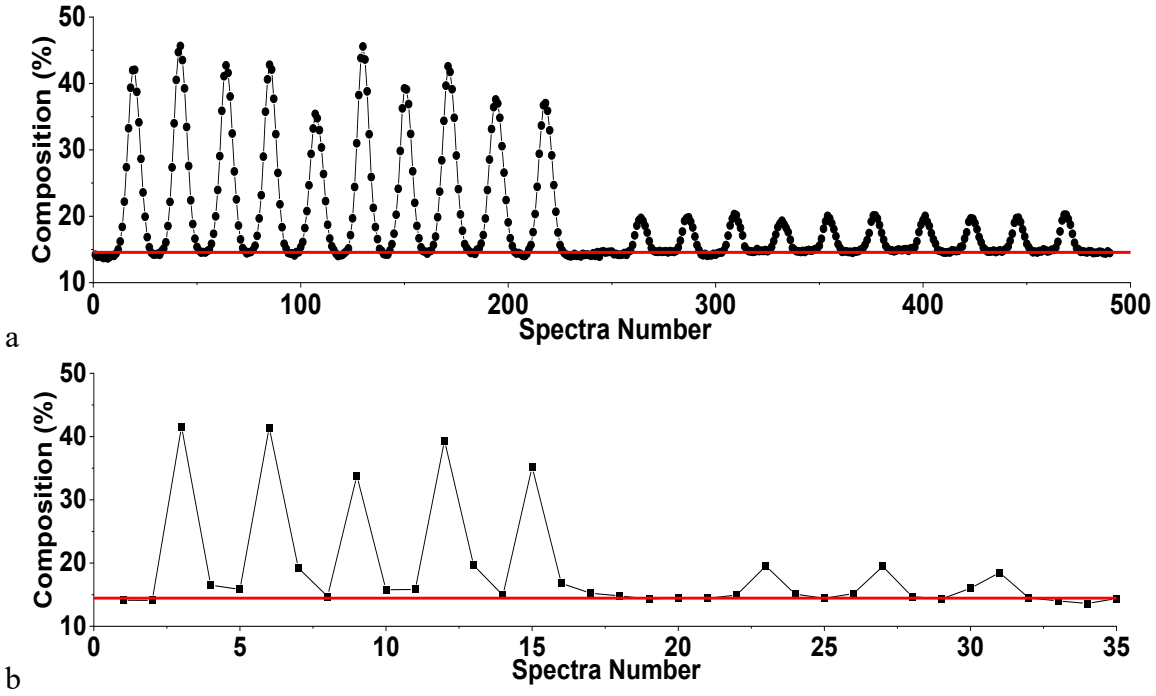

Figure 5-8 Composition fluctuation of 15% Acetaminophen caused by agglomerates at the sampling speed of a) 0.13cm/s, b) 1.83cm/s.

5.3.3 Composition reading of "good" blend and "bad" blend containing no agglomerates

In general, blend inhomogeneity can be attributed not only to the ingredients agglomeration but also to insufficient bulk blending (macro-mixing) or inconsistent powder feeding. For example, in continuous pharmaceutical processing, the perturbation of feeders possibly leads to inconsistent feeding, which further results in the variation of blends composition. In order to further validate the concept of NIR methodology measuring API agglomerates in blends, two specific cases were also investigated: a homogeneous blend without API agglomerates (good blend) and a non-homogeneous blend without API agglomerates (bad blend). The sampling speed of 0.13cm/s was used for both cases. The 5% Semi-fine acetaminophen standard blend was regarded as the good blend since the standard blend was made using a high shear blends process. Bad blend was prepared by gently mixing 0% and 15% Semi-fine acetaminophen standard blends. 30 grams of 0% and 15% blends was added in a container. Then, the powder was blended by shaking the container manually and gently for 10s. This powder can be regarded as the non-homogeneous blend without API agglomerates (bad blend) due to that standard blends doesn't contain agglomerates and the mixture of two standard blends is insufficiently blended. This section is aiming to discriminate the composition fluctuation caused by API agglomeration from insufficient bulk blending.

For each case, in total, 1600 NIR spectra were collected. As shown in ***Figure 5-9a***, for the good blend, the measured Semi-fine Acetaminophen composition is 5% with no fluctuation being discerned. It suggests that the composition of a homogeneous and non-agglomerated blend is perfectly consistent without any fluctuation throughout the entire blend. ***Figure***

5-9b shows the composition fluctuation caused by an insufficient bulk blending process. The red line suggests the theoretically mean composition of this blend. In comparison to the fluctuations caused by API agglomerates which are shown in ***Figure 5-6*** to ***Figure 5-8***, this composition variation occurs in a much broader range, and fluctuations appear as blunt waves. There is gradual increase or decrease in composition. However, for the case of containing ingredient agglomerates, a sudden change of composition is captured in a short range which is presented as a narrow and sharp spike. In order to distinguish the composition fluctuations caused by these two aspects of poor mixing, different terminology is used, where "wave-type" fluctuation is used to describe the variation caused by insufficient bulk blending and "spike-type" fluctuation is applied for API agglomeration. Thereby, by examining the different pattern of composition fluctuation, we are able to assess the performance of both macro-mixing and micro-mixing.

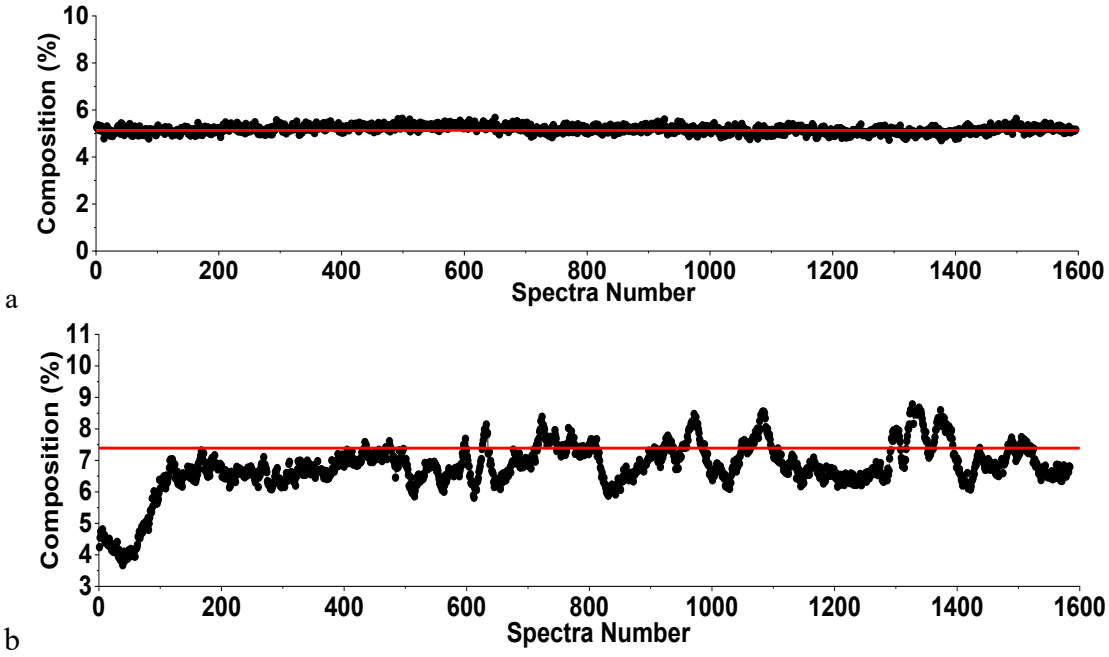

Figure 5-9 a) Measured composition of 5% Acetaminophen standard blend (good blend). b) Composition fluctuation caused by insufficient bulk blending (bad blend).

5.4 Results and discussion

Referring to the investigation in chapter 4, the K-Tron20 twin-screw feeder with fine concave screw assembled introduces Semi-fine Acetaminophen as consolidated powder lumps to the next unit operations. The diameter of the powder lumps, which are the precursor of the agglomerates, can be up to 7mm. In the following sections, it will be demonstrated how the lumps are diminished or even eliminated in the blender acting alone, in the conical mill only, and in the blender with a conical mill assembled.

5.4.1 API agglomeration after blender without using conical mill

By using NIR technique, the API agglomerates are detected as the fluctuation of composition. ***Figure 5-10*** shows the measured composition of Acetaminophen for the blends of B-150-0° and B-150-270°. In total, 2500 NIR spectra were collected throughout experiment for each blend, which is presented as 2500 composition readings. The dash line indicates the theoretical composition of blends. It is apparent that the "spike-type" fluctuation in composition is captured for the case of B-150-0°, which suggests that Acetaminophen agglomerates exist in this blend. When an agglomerate pass through the NIR active spot, there is a sudden increment of detected composition. This fluctuation of composition only occurs at the position that contains an agglomerate. Thus, each "spike" represents one agglomerate. In addition, the size of agglomerates can be described when examining the maximum composition reading. Each composition reading is the average value at the entire NIR active area in each sampling duration. Smaller agglomerates lead to a smaller amount of Acetaminophen considered in each acquisition. Note that it seems most composition readings of B-150-0º are very close to the theoretical value and no "wave-type" fluctuation is captured, indicating that the bulk blending (or macro-mixing) is

adequate. In contrast, for the case of B-150-270°, the fluctuations of composition are marginal. No agglomerate is detected. Under this blending condition, all of the agglomerates are possibly eliminated and the blend exhibits high-level uniformity. It is worth emphasizing that the number of "spikes" doesn't necessarily represent the total number of agglomerates in blends since only the agglomerates pasing by the NIR active area is considered. In fact, it reveals the frequency of agglomerates being detected.

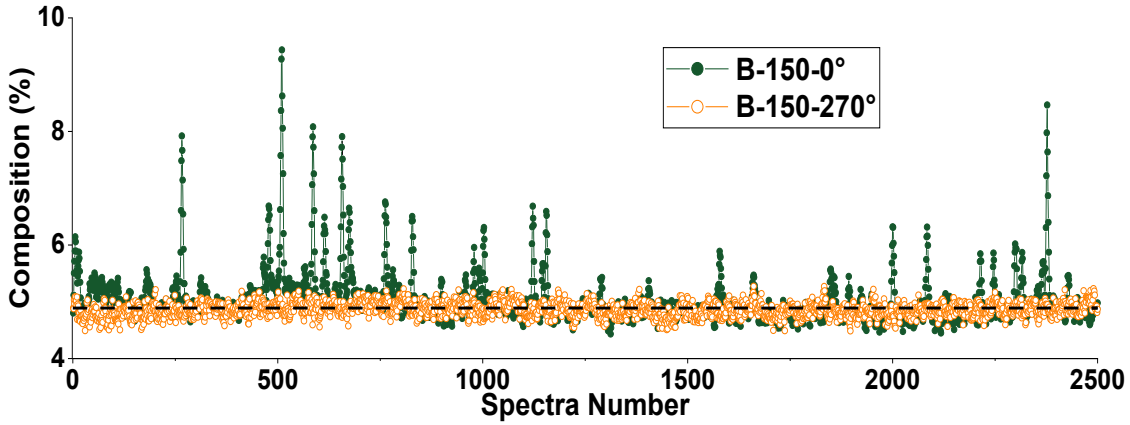

Figure 5-10 Composition fluctuation caused by API agglomerates.

In order to quantitatively compare API agglomeration at different blending conditions, several indexes are extracted from the NIR composition results, as summarized in ***Table 5-3***. First, the relative standard deviation (RSD) is defined as the ratio of standard deviation and mean composition value, which refers to the homogeneity of blends. It is important to note that both API agglomeration and insufficient mixing of bulk powder (or macro-mixing) contribute to a large RSD. Thus, it is necessary to define more indexes to specifically represent API agglomeration in blends. In this study, the amount of API agglomerates in different sizes is exhibited by counting the number of spikes whose maximum value is larger than 110%, 120%, 130% and 150% of the theoretical composition, respectively.

According to the data listed in ***Table 5-3***, the most immediate implication is that agglomerates infrequently appear in blends resulting in a relatively small number of "spikes" being detected in any case. At conditions of higher NOB (>150), even lower frequency of agglomerates is detected. Ultimately, no agglomerate is observed in B-150-270º which is the case showing the largest NOB value. On the other hand, as aforementioned, a wave-shape composition pattern indicates insufficient bulk powder mixing (i.e macro-mixing). Nevertheless, all of the blends exhibit a similar composition pattern to the B-150-0º (as shown in ***Figure 5-10***), in which most of the composition reading is very close to the theoretical value and no wave-shape pattern is observed. It represents that macro-mixing is complete for all of these cases.

Table 5-3 Summary of agglomeration information after blender by NIR technique

Name of Blends	NOB	RSD (%)	>110%	>120%	>130%	>150%
B-50-0º	58	12.9	34	25	16	10
B-150-0º	68	8.9	33	20	11	5
B-250-0º	55	8	22	13	8	5
B-50-180º	88	10.4	29	21	11	7
B-150-180º	91	8.5	23	12	7	4
B-250-180º	62	8	21	9	6	4
B-50-270º	150	2.4	1	0	0	0
B-150-270º	345	3.1	0	0	0	0
B-250-270º	125	6.9	16	12	5	3
B-100-270º	275	3.1	3	1	1	0
B-200-270º	211	3.1	6	2	0	0

Moreover, API agglomerates of different sizes can also be quantified by measuring the mass of agglomerates remaining on each sieve. In our case study, large Acetaminophen agglomerates (>2mm) possibly exist in blends when the blender is operated with insufficient shearing. ***Figure 5-11*** displays the morphology of agglomerates remaining on each sieve. Agglomerates appear in the spherical shape as "snowball". As mentioned, this is because shear-induced de-agglomeration in a convective blender is a process of particle-

particle abrasion rather than the deformation or the fracture of agglomerates[140]. ***Table 5-4*** lists the permillage (‰) of Semi-fine Acetaminophen in agglomerated forms at different size levels. There is a good agreement in the results from NIR technique and Sieving. Overall, these results suggest that both size and amount of API agglomerates are significantly reduced as blends passing through a larger number of blades (NOB). In the case of B-150-270º, where an extensive amount of shear is applied to powder, nearly zero agglomerates are captured by using the sieving method, indicating that we are able to adequately eliminate API agglomerates adequately without using a conical mill.

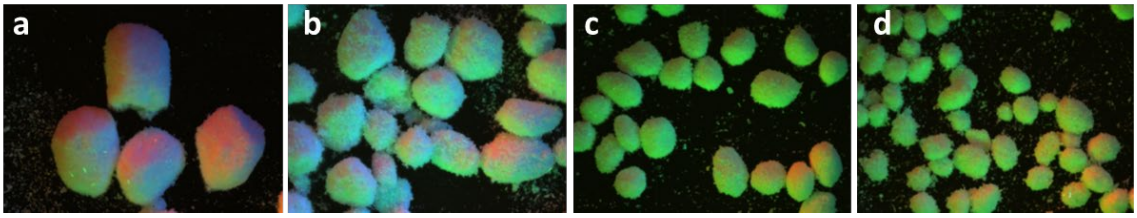

Figure 5-11 Agglomerates of different size for B-150-0º (showing at same magnification): a) >2mm. b) 1mm~2mm. c) 850µm~1mm. d) 600µm~850µm.

Table 5-4 Summary of agglomeration information after blender by sieving.

Name of Blends	NOB	>600µm (‰)	>850µm (‰)	>1mm (‰)	>2mm (‰)
B-50-0º	58	38.6	35.5	32.4	10.7
B-150-0º	68	22.4	19.5	16.7	4.4
B-250-0º	55	12.7	10.4	8.7	1.2
B-50-180º	88	10.7	9.7	8.8	2.1
B-150-180º	91	15.7	13.9	12.5	2.6
B-250-180º	62	8.8	7.2	5.5	1.3
B-50-270º	148	3.3	3.0	2.6	1.2
B-150-270º	345	0.1	0.0	0.0	0.0
B-250-270º	125	10.0	8.5	7.1	1.6
B-100-270º	275	0.7	0.5	0.4	0.0
B-200-270º	211	2.8	2.3	1.8	0.0

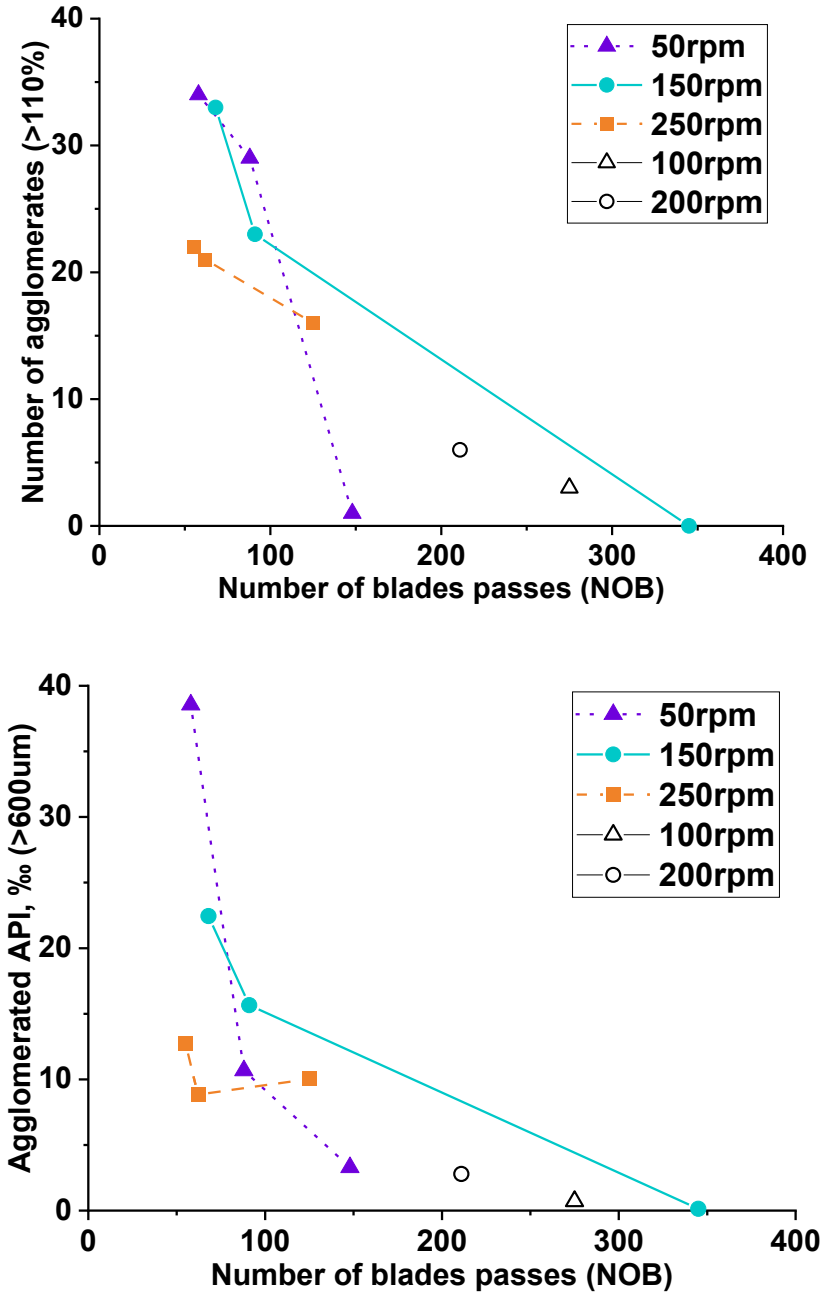

Figure 5-12 Acetaminophen agglomeration at different blending condition measured by a) NIR. b) Sieving.

In ***Figure 5-12***, aiming to illustrate the role of blender speed (i.e., shear rate) and NOB (i.e., shear strain) on API de-agglomeration, we further plot the number of "spikes", whose maximum reading is larger than 110% of target in NIR technique, and the mass fraction of

agglomerates, which is larger than 600μm in sieving method, versus NOB. The different patterns of curves represent the blender speed. It is quite revealing that the total amount of shear (i.e., shear strain) plays a critical role in API de-agglomeration. When blends are produced via a blending process of extensive NOB, ingredient agglomerates can be reduced significantly. In fact, the considerably de-agglomerated blends can be obtained exclusively when the NOB is extensive. Especially, in our case study, nearly no agglomerates were observed on all of the sieves when in-process material experienced more than 300 blade passes.

However, the effect of blender speed on de-agglomeration is ambiguous. First of all, as mentioned, a certain minimal shear rate is required to overcome the interparticle force within the agglomerate matrix of cohesive material. It is evident that the lowest blender speed in our case study (50 RPM) already reaches this limit and de-agglomeration indeed occurs under this blender speed. Moreover, the magnitude of mechanical stress within the blender chamber increases with shear rate (i.e., blender speed) because the flow pattern in the convective blender is either in the elastic-inertial regime or the inertial regime[42, 192], where the inertia, which is shear rate dependent, also contribute to overcoming interparticle force. This can interpret that fewer Acetaminophen agglomerates are obtained at higher blender speed when in-process materials experience a minimal NOB. On the other hand, the impeller speed significantly affects powder holdup in the blender. At a constant feed rate, the increase of impeller speed results in the decrease of holdup and mean residence time of the powder in the blender. It may lead to reduced NOB. Therefore, the in-process material usually experiences the maximum number of blades at an intermediate blender speed. Additionally, at a high impeller speed, powder can be fluidized, which causes a

significant reduction in powder bed solid fraction and creates more void region. Thus, unenduring or instantaneous particle-particle contact occurs at this condition. This further scales down the total shear strain applied to blends. Thus, at a high impeller speed, the increasing of NOB possibly shows less effect on API de-agglomeration. This explains that the B-250-270º yield similar API agglomeration in comparison with B-250-180º even though the former process doubles the NOB.

Consequently, in continuous powder blending, operating blender at a higher number of blade passes contributes to API de-agglomeration much more than at a higher rotational rate only. Restating, using a high blender speed is not recommended due to that (1) it usually yields a low NOB, (2) the severe powder fluidization actually inhibits API de-agglomeration. The agglomerates of API are possibly eliminated in blender when it is operated at an extensive number of blade passes.

5.4.2 API agglomeration after conical mill

For a given conical mill in continuous process, two critical process parameters are impeller speed and screen size. In this section, the role of both parameters on API de-agglomeration are discussed. Plain-hole screens of different mesh size are used: 2mm and 5mm. Two impeller speeds are implemented: 500rpm and 1000rpm. Blends were collected after conical mill and analyzed by both NIR technique and sieving method. ***Figure 5-13*** shows the normalized composition by the mean composition of 2500 collected spectra, using NIR techniques. The dash line indicates the mean composition of blends. In all the conditions, “wave-type” fluctuations are captured suggesting insufficient macro-mixing. In our study, the size of screens is much larger than the particle size of all the ingredients, which enables the powder to pass through the mill effortlessly even at a relatively low impeller speed (at

500rpm). Thus, there is nearly zero powder hold-up in the conical mill, and the residence time of powder is quite short. As a result, the macro-mixing in conical mill is moderate and incomplete. On the other hand, the high-speed impeller generates an environment of high shear stress. All of the powder has to pass through the high-shear environment before exiting the conical mill, in which API agglomerates are possibly destroyed. With the assembling of a screen, the size of agglomerates in blends after conical mill is expected to be smaller than the mesh size. With other excipients surrounding, it is difficult for de-agglomerated API particles to reform large lumps after conical mill. ***Figure 5-13*** also confirms this working principle of conical mill. Significantly reduced "spikes" are presented in the composition pattern when the screen size is 2mm, which suggests that smaller agglomerates are discerned. ***Figure 5-14*** depicts the mass fraction of agglomerates that are larger than 600μm from the sieve analysis. Apparently, by using a 2mm screen, the amount of API agglomerates is dramatically reduced, even at a relatively lower impeller speed (500rpm). In fact, with 2mm screen assembled, the mass of agglomerates is comparable when the conical mill is operated at both impeller speeds. Moreover, no agglomerates are observed on the NO.10 sieve mesh (2mm) for both C-2-500 and C-2-1000. Conversely, when a 5mm screen is used, large and numerous agglomerates still remain in the blends. With the coarser screen assembled, we also observe relatively greater agglomerate reduction at a higher impeller speed but it is not as effective as using the finer screen. In summary, a conical mill is able to de-agglomerate and improve micro-mixing significantly when a screen of fine mesh is used. The screen size has a more pronounced effect on de-agglomeration than impeller speed. In comparison with its high efficiency on

micro-mixing, the conical mill provides a modest macro-mixing. Further blending units are needed to complete the macro-mixing.

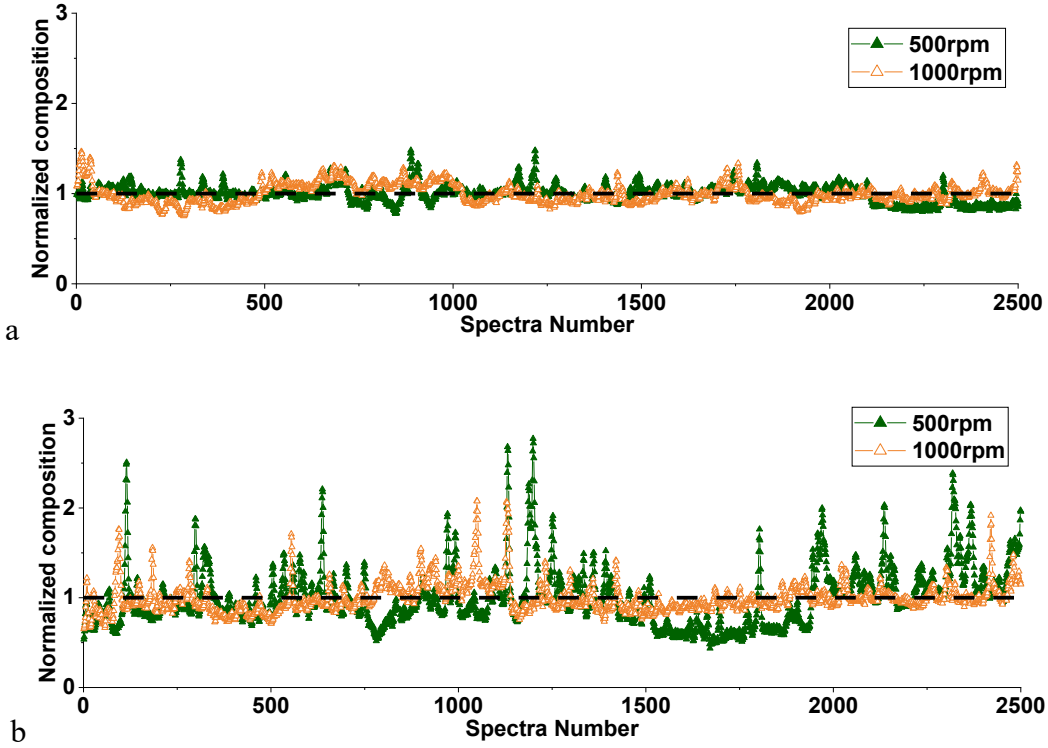

Figure 5-13 Normalized composition of blends after conical mill with screen size of a) 2mm. b) 5mm.

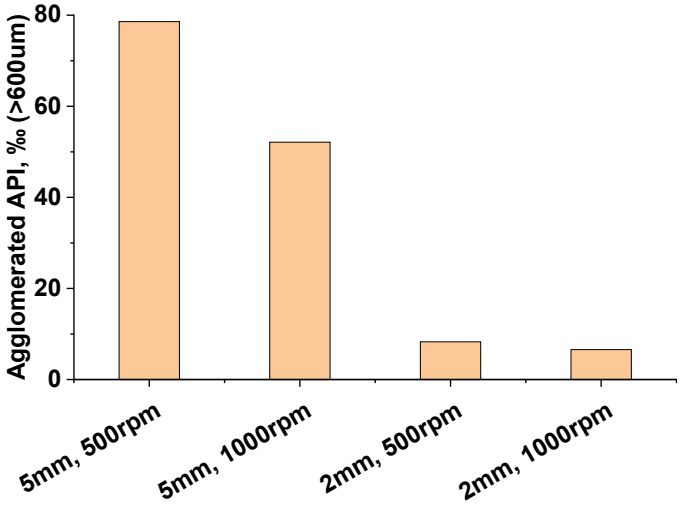

Figure 5-14 Mass fraction of Acetaminophen in agglomerates after conical mill at different process condition by sieving.

5.4.3 API agglomeration after conical mill + blender

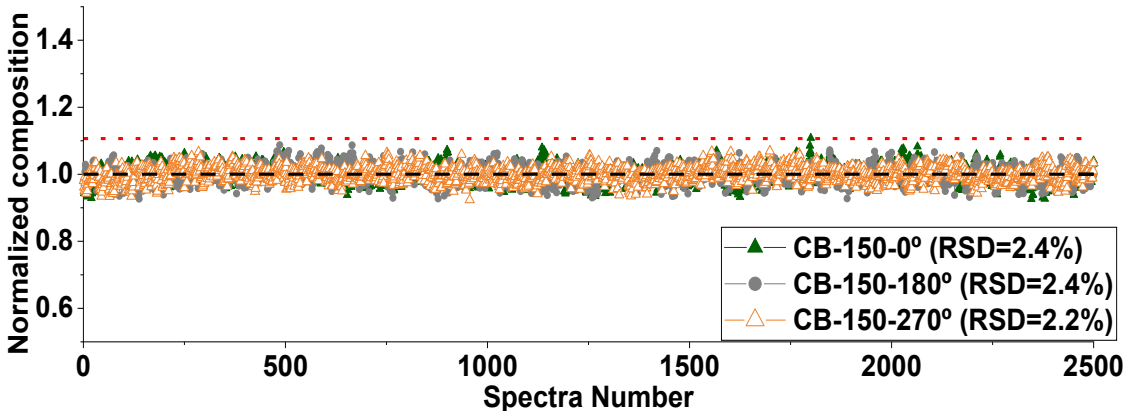

Figure 5-15 Normalized composition of blends after conical mill + blender by NIR technique.

In the previous two sections, we have investigated the effect of two individual units on powder mixing performance and API de-agglomeration. It has been concluded that the conical mill efficiently reduces ingredient agglomeration and mainly contributes to micro-mixing. The continuous tumbler blender provides macro-mixing and can also significantly mitigate agglomeration only at an extensive number of blade passes. In this section, processes combining both units (conical mill + blender) are examined. The impeller speed of the conical mill is maintained at 1000rpm and screen of 2mm is used. The impeller speed of the blender also remains constant at 150rpm, but the weir angle is varied as 0º, 180º, and 270º. Previously, we have shown that B-150-0º and B-150-180º contains large agglomerates. However, as shown in ***Figure 5-15,*** when the appropriate conical milling is involved before blending, the agglomerates are eliminated. It is apparent that all three blends are perfectly homogeneous, showing no spikes on composition pattern and a minimal RSD. The red dot line represents 110% of theoretical composition. There is no composition reading above this line, suggesting that no agglomerates are detected by the

NIR technique. In fact, by passing blends through sieves, only a scattering of agglomerates is observed remaining on NO.30 (600μm) mesh. As presented in ***Table 5-5***, only a trivial mass fraction of API is in agglomerate form even if a relatively gentle blending condition is performed.

Table 5-5 Acetaminophen agglomeration after conical mill + blender by sieving.

Name of Blends	NOB	>600μm (‰)
CB-150-0º	72	0.3
CB-150-180º	91	0.3
CB-150-270º	347	0.1

5.4.4 The micro-mixing of blends in tablets

It is worthwhile to note that both the NIR technique and the sieving method are not sufficiently sensitive to detect small agglomerates (<600μm). In the NIR technique, each composition reading is the average value of a certain volume of blends. Minuscule agglomerates result in a trivial fluctuation or even zero fluctuations. For the sieving method, we were not able to use a sieve finer than 600μm considering the possible damage to agglomerates due to vibration. Therefore, in this study, a Raman imaging technique is used to virtualize the distribution of API in the unit dose. It also enables us to measure the size distribution of minuscule agglomerates (10μm-600μm).

Conditions B-150-270º, CB-150-0º and CB-150-270º were selected for Raman imaging, which were previously demonstrated as blends containing nearly no agglomerates larger than 600μm. In addition, conditions B-250-270º and B-50-270º, which were found to have numerous agglomerates larger than 600μm, were also chosen. For these two blends, powder after the NO.30 sieve (600μm) passage was collected and subjected to Raman imaging. Thus, no large agglomerates exist in these samples. In this section, we specifically

focus on examining the minuscule agglomerates (<600μm) and API micro-mixing in unit dose.

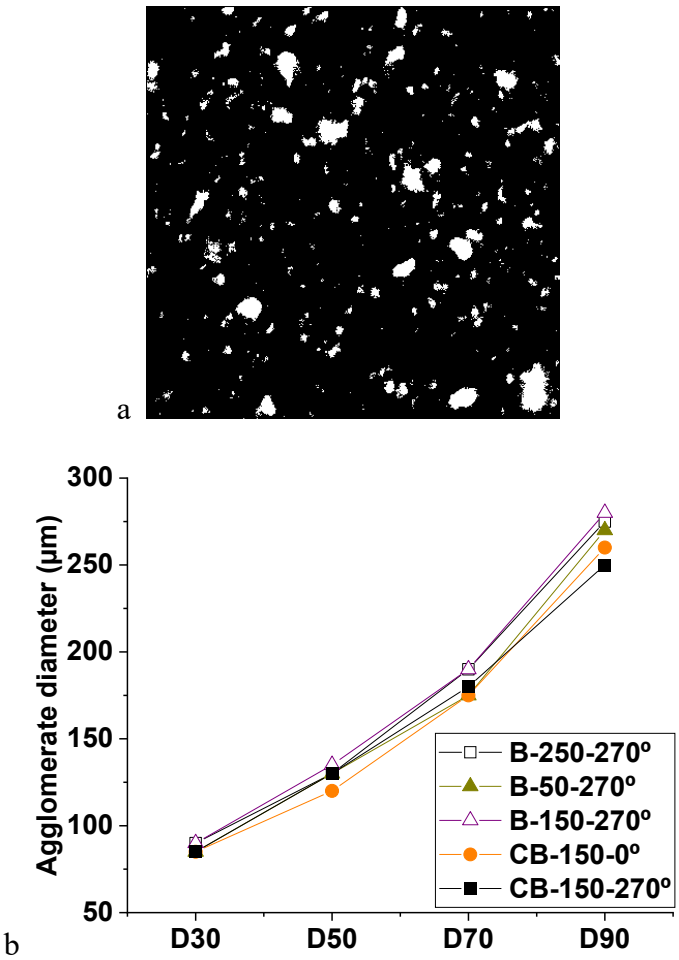

Figure 5-16 Agglomeration measured by Raman imaging a) The gray map showing micro-mixing of API (B-150-270°). b) Agglomerates size distribution.

Figure 5-16 shows the agglomerate size and distribution(D30, D50, D70, and D90) of the 5 blends. Interestingly, all of these blends show marginal differences with respect to agglomeration in the unit dose. The first implication is that the blending process (with or without using conical mill) is not able to destroy and disperse all the agglomerates as primary particles (D90=52μm) for Semi-fine Acetaminophen. The optimal de-

agglomeration that can be accomplished in our study is reducing the size of agglomerates to 300μm in D90. The API cannot be de-agglomerated further by only using a shearing process. The ultimate size of agglomerates is probably only determined by the intrinsic properties of API, such as particle size and particle-particle cohesiveness. In fact, these minuscule agglomerates lead to minimal blend inhomogeneity and content nonuniformity, which is also demonstrated in later sections. Therefore, we obtained a small RSD value throughout NIR composition readings for the cases of B-150-270º, CB-150-0º and CB-150-270º. It seems the goal of sufficient de-agglomeration can be achieved by eliminating the large agglomerates which were discerned previously.

Second, for B-250-270º and B-50-270º, when excluding agglomerates larger than 600μm, the rest of the blends present the same micro-mixing of API as the sufficiently deagglomerated cases: B-150-270°, CB-150-0°, and CB-150-270°. In addition, this result further confirms that the mechanism of shear induced de-agglomeration, as mentioned above, is abrasion. Due to the attrition between excipient particles and agglomerates, a layer of agglomerate matrix is removed, which results in a relatively smaller agglomerates and a few minuscule agglomerates. Therefore, for a low dose formulation, agglomerates infrequently exist in blends while the rest of the blends are homogenous.

5.4.5 Tablets content uniformity and dissolution

In this study, the drug content was assessed by only measuring tablet composition since the weight of each tablet was controlled. Fifty-five tablets were tested and the content uniformity was presented as the relative standard deviation (RSD) of composition. Additionally, the number of tablets with a drug content larger than 110%, 115% and 125% of theoretical content was counted. In this section, six blends are investigated, as shown in

Table 5-6. Among them, B-150-0º and B-150-180º have been demonstrated to contain large Acetaminophen agglomerates, while the other 4 blends are de-agglomerated adequately. The first observation from the results is that the minimal RSD is obtained when the blends are de-agglomerated sufficiently. Next, tablets of high-potency (>110%) and even super-potency (>125%) are possibly produced if large agglomerates exist. The tablet performance corresponds to API agglomeration in blends, confirming the need for measuring ingredient agglomerates in blends during product development.

Table 5-6 Tablets content uniformity (n=55)

Name of Blends	NOB	RSD	>100%	>115%	>125%
B-150-0º	68	7.6%	6	4	2
B-150-180º	91	5.7%	6	4	0
B-150-270º	345	2.1%	0	0	0
CB-150-0º	72	2.5%	0	0	0
CB-150-180º	91	2.4%	0	0	0
CB-150-270º	347	2.2%	0	0	0

In the tablet dissolution study, three replicates were performed for these cases: B-150-0°, B-150-270°, CB-150-270°, and 7% standard blend. With respect to B-150-0º, 2 different cases are defined. Three tablets with a composition close to 7% were selected which are regarded as B-150-0º containing large agglomerates. Another three tablets with a composition around 5% were chosen which are defined as B-150-0º containing no agglomerates. Both B-150-270º and CB-150-270º are considered as uniform products containing no agglomerates. In order to understand the effect of API agglomeration on dissolution under the same composition, the 7% standard blend is examined which is also considered to be uniform product. ***Figure 5-17*** displays the tablet dissolution profiles, showing the mass of released drug as function of time. It is apparent that all of the tablets containing 5% Acetaminophen without agglomerates show consistent dissolution behavior.

Due to containing a larger amount of Acetaminophen, the tablets of B-150-0º with agglomerates release more drug at the end of dissolution. However, at the early stage of dissolution, the mass of released drug equals to the non-agglomerated case. This result is consistent with the above conclusions that the layers of tablet containing no large agglomerates are equally uniform in all of these cases.

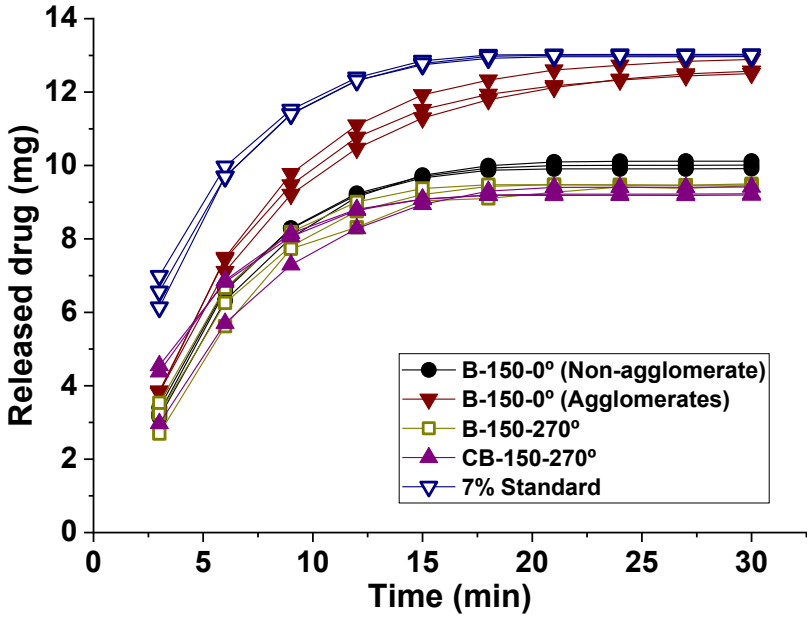

Figure 5-17 Dissolution profile of tablets containing API agglomerates and containing no agglomerates.

Markedly, in comparison to the 7% standard blend, the agglomerated B-150-0º releases a comparable amount of drug ultimately but its dissolution rate is slower. Firstly, the existence of agglomerates results in a non-uniform distribution of API in tablets. There is less API content in certain layers compared to uniform tablets. Thus, less drug is released from these layers. At the early stage of the dissolution, the agglomerated B-150-0° tablets (containing near 7% API) release similar amount of API to the non-agglomerated tablet (containing 5% API). Ultimately, this agglomerated B-150-0° tablets releases entire 7%

API. Secondly, the existence of API agglomerates reduces the area of particle's surface that is exposed to media, which further causes a delayed dissolution. It is important to note that Acetaminophen has good solubility and wettability. API agglomeration possibly delays dissolution much more for a poorly soluble drug.

5.5 Conclusion

In this study, we have proposed three methods to discern and quantify API agglomerates in a powder mixture, using NIR spectroscopic techniques, sieving blends, and a chemometric imaging (i.e., Raman imaging). Each method has both advantages and limitations that allow them to be appropriately used under certain conditions. Among them, the NIR spectroscopic technique has the capability to discern ingredient agglomerates in blends by capturing the composition fluctuation locally. The application of the NIR technique is independent to the formulation and material properties. It can also be widely used in other unit operations, such as wet granulation and roller compaction. However, it is necessary to note that the NIR technique provides the frequency rather than the total number of agglomerates in the blends because only the powder that passes through the NIR active area is subjected to analysis. A low frequency of agglomerates does not absolutely mean that there are no agglomerates in the blend. For sieving blends, although it can be used to directly measure the number of agglomerates by passing a large volume of blends through a sieve, the key limitation is that it can be used exclusively for a formulation which contains single cohesive API and other free-flowing ingredients. In this condition, only the agglomerates of the cohesive API remain on the sieve. As mentioned, for both the NIR technique and blend sieving, agglomerates below a certain size range are difficult to be discerned and quantified, which can possibly be measured by chemometric imaging.

However, the chemometric imaging system generally has a small sample size per measurement. Large but infrequent agglomerates are hardly sampled. Thus, it is a useful application for understanding the micro-structure of blends or unit dose.

By using all of three techniques, we sought to advance our understanding of agglomeration behavior and micro-mixing of cohesive (i.e., high agglomeration potential) ingredients in a continuous powder blending system. Ultimately, the combination of approaches enables us to suggest the appropriate process setting that can sufficiently and efficiently mitigate API agglomeration in blends. As a result, without using a conical mill, we observed that large agglomerates (>600μm) appear in blends when a low-shear blending process is applied. Both the size and number of agglomerates decrease with the increasing of total number of blades passed by a portion of powder. Notably, when blending is processed at an extensive number of blade passes, these large agglomerates can be sufficiently eliminated. In contrast, operating a blender at a high impeller rotational rate may not effectively de-agglomerate cohesive ingredients. The high impeller speed not only leads to a smaller number of blade passes but also promotes powder fluidization which further reduces the total shear strain. It is important to note that, in this study, the blender holdup is controlled by adjusting the weir angle, but the flow rate through the system remains constant. In fact, the controlling of holdup can also be accomplished by adjusting system flow rate for a continuous blender with a fixed weir design. For this type of blender, the conclusion drawn from this study is still applicable as long as the total number of blade passes (i.e., shear strain) is calculated.

Next, a conical mill is assembled between the feeder and blender. The study has shown that the de-agglomeration provided by the conical mill deeply relies upon the size of the

screen. The maximum agglomerate size after the conical mill is smaller than the size of the screen's holes. On the other hand, the impeller speed of the conical mill only shows a minor effect. Moreover, when the conical mill is implemented (1000rpm in impeller speed and 2mm in screen size), the agglomerates can be sufficiently eliminated even a low-shear blending process being assembly subsquently. Consequently, the conical mill provides micro-mixing efficiently while the blender enables macro-mixing efficiently.

Additionally, we have examined the quality attributes of the finished product: tablet content uniformity and dissolution. Although tables were made offline without involving a feed frame, which is another shearing process, the results still allow us to expand our knowledge on how ingredient agglomerates affect product uniformity and dissolution profile. In conclusion, the existence of large agglomerates can lead to a final product that displays high-potency and even super potency, while the sufficiently de-agglomerating process results in products that are highly uniform in drug content. Moreover, the existence of large agglomerates possibly causes a delayed dissolution due to less particle surface being exposed to dissolution media.

This study has systematically investigated how the continuous powder blending process mitigates and eliminates agglomeration for given cohesive ingredients. It would be interesting to further establish the understanding of ingredient agglomeration in downstream unit operations of continuous solid dose manufacturing until the final product, such as wet granulation, roller compaction, and powder mixing in feed frame.

6 Chapter 6 Melt-coating of APIs with Surfactants for Drug Dissolution Enhancement

6.1 Introduction

In the pharmaceutical industry, solid dosage forms, including tablets, capsules, granules, reconstitutable powders and chewable product etc., play a critical role in the dispensing of medicine[193-195]. In fact, they are the most convenient way to take medications[196]. For solid dosage forms, medicine is dispensed based on the dissolving of active pharmaceutical ingredients (APIs) in the luminal fluids of the gastro-intestinal tract. The significance of the dissolution rate of a drug on its clinical performance has been recognized for a long time. One of the most important quality attributes required for commercial release of a product is often the *in vitro* dissolution behavior[197, 198]. In past decades, the investigation on product dissolution behavior has considerably expanded, not only for the purpose of quality control, but also because it is a critical consideration of the drug solid state determination[194, 199, 200], dosage form design[194, 201] and formulation screening[202-204]. The Biopharmaceutics Classification system (BCS) considers three key factors that govern the bioavailability of solid oral dosage forms: *in vitro* dissolution rate, solubility and intestinal permeability. The BCS divides APIs into the following four groups with respect to solubility and permeability: Class I (High solubility and high permeability), Class II (low solubility and high permeability), Class III (high solubility, low permeability), and Class IV (low solubility and low permeability). Unfortunately, a significant number of FDA approved drugs and developmental drugs are hydrophobic and poorly soluble (BCS class II and IV drugs). It has been documented that approximately 40% of approved drugs and 90% of drugs under development are

categorized as low water-solubility and low bioavailability molecules[205]. Since discovering new alternative drugs is difficult, there is currently a considerable amount of effort devoted to enhancing the solubility of available drugs. In particular, the release of drugs from dosage forms is the only rate limiting step for the adsorption of BCS class II molecules. Thus, enhancing dissolution of these drug products directly converts to the increasing of drug bioavailability.

Improving dissolution of poorly soluble drug products is a key challenge in drug product development. A large and growing number of approaches has been developed to accomplish dissolution enhancement. For example, particle size reduction or micronization have been widely used to increase particle surface area, which allows greatly enhanced interaction between dissolution medium and drug particles, and further increases the kinetics of dissolution. However, the micronized API usually creates handling issues and generates difficulty in the manufacturing process. The intensive particle-particle cohesiveness also causes the formation of API agglomerates which results in poor content uniformity. Secondly, a few techniques have also been developed to ionize drug molecules. The common methods are adjusting pH by adding pH modifier in the formulation[206] or producing salt forms of a weak acid or weak basic drug[207]. Unfortunately, this strategy is only suitable for ionizable drugs. Furthermore, since disordered amorphous forms are more soluble than stable crystal forms, changing solid states has become a popular approach[208]. One technique to create amorphous forms is by solid dispersion, which has been extensively explored in the pharmaceutical industry[209-212]. The two most prevalent manufacturing processes for solid dispersion are hot-melt extrusion and spray drying. In hot-melt extrusion, eutectic mixtures of APIs and polymeric carriers are

processed at a high temperature, in which the drug is either in amorphous form or dispersed as individual molecules in a water-soluble polymer matrix[213, 214]. In the spray drying process, APIs and carriers are dissolved or suspended in an organic solvent or solvent mixture followed by atomization using a nozzle. Then, the solvent is evaporated quickly by introducing a stream of heated air and solid dispersion is formed as a dry powder[215, 216]. The main mechanisms of dissolution enhancement via solid dispersion are (1)conversion of API from crystalline to amorphous form, (2) molecular-level dispersion of API in carrier matrix and (3) retaining dissolved API as a solid solution. However, instability of amorphous forms, high energy consumption and low drug loading capacity limit the application of this technique in certain scenarios. Another newly developed technique for dissolution enhancement is “liquisolid” (i.e., Impregnation), in which the drug is first dissolved (or suspended) in a liquid vehicle, and then the liquid form is absorbed into a porous and particulate carrier incorporated with a fine coating material[217-219]. The major disadvantage of this technique is the requirement of large quantities of functional excipients, including liquid vehicle, carrier and coating materials. Thus, producing high drug loading product is difficult. In this study, we developed a novel technique that allows melt-coating of poorly soluble APIs with a small amount of surfactant ($\leq$ 10% w/w of API) by using a simple process of low temperature (at least 20°C below melting point of API). This melt-coating technique significantly enhances the dissolution of poorly soluble API product by overcoming many of these aforementioned limitations, which (1) enables the manufacturing of unit dose of very high drug loading, (2) maintains API original solid-states and prevents the degradation of chemical entities, and (3) acts as a low-energy and low-cost process.

The surface coating is widely applied in the pharmaceutical industry to enhance the properties or maximize the functions of either APIs or excipients. It is derived from the concept of ordered mixing that is initially defined by Hersey et al, which is a process following "disorder to order" mixing[220-222]. In this concept, a "guest" material covers the other "host" particles (as show in ***Figure 6-1***), driven by certain interactions, such as adoption, surface tension, surface fusion, electrostatic or any other adhesion form[223]. One of the most sophisticated application of surface coating is to adhered nanoparticles, such as TiO_2, Al_2O_3, and SiO_2[224], on the outer surface of micronized particles to improve its flowability during manufacturing. It has been substantially documented that the nanosized SiO_2 can coat evenly on the surface of micrometer size API by providing a high shear environment, such as V-blender with intensity bar, milling, and acoustic mixer, which alters API surface nano-roughness and reduces surface free energy[150, 225-227]. In this way, cohesive powder flowability is dramatically improved. The other prevalent application of surface coating is in dry powder inhaler (DPI) dosage forms, which requires API particles with diameter below 5μm. To prevent API agglomeration, achieve satisfying content uniformity and aerosol performance, high shear processing is usually applied which enables the micronized drug particles to attach on the surface of coarse excipients (carriers), such as Lactose, Mannitol, or sorbitol, as the formation of an "ordered unit"[228, 229]. Moreover, coating a lubricant on drug particles vis mechanofusion approach[230] or coating anti-adhesion excipients on drug particles vis spray drying[231, 232] have also been documented for improving aerosol performance. Additionally, the so-called over-lubrication phenomenon during solid dose manufacturing is also associated with surface coating, in which the hydrophobic lubricant (i.e. MgSt) smear and coat on the surface of

other coarse particles when the powder system is exposed to a high shear environment[233-235]. The surface coating with lubricant enlarges the lubrication effect and improves flowability of blends[234, 236, 237]. On the other hand, it results in less particle-particle bonding in tableting and decreases tablet strength[108, 234]. The coating of hydrophobic lubricant on the surface also decreases powder wettability and postpones product dissolution[107].

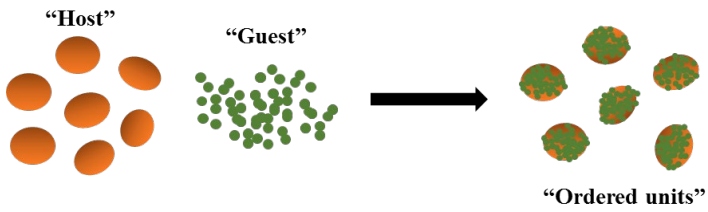

Figure 6-1 Schema of surface coating (or ordered mixing).

This study provides an additional approach to enhance dissolution of poorly soluble drugs by applying the concept of surface coating. A simple process, twin-screw extrusion at low process temperature, is used in a methodology that enables the melt-coating of API particles with a small amount of low-melting-point surfactant. In this paper, we list four case studies to prove the practicality of our methodology, which are denoted as case 1, case 2, case 3, and case 4. Our investigation has covered three BCS class II drugs and three surfactants, including both non-ionic and ionic surfactant. Specifically, in case 1, three grades of Ibuprofen by particle size are coated with Poloxamer407. In case 2, Fenofibrate is coated with Poloxamer407. In case 3, melt-coating is implemented for Carbamazepine with Cetylpyridinium Chloride. In case 4, an Ibuprofen is coated with Polyoxyethylene Stearate. Dissolution of both unformulated powder and finished product (tablets and

capsules) are inspected. The main conclusion is that the melt-coating technique significantly improves dissolution of poorly soluble drugs.

6.2 Materials

In this study, three poorly soluble APIs (BCS class II) were explored as examples: Ibuprofen, Carbamazepine, and Fenofibrate. In addition, there were three different batches of Ibuprofen which are labeled as Ibuprofen1, Ibuprofen2, and Ibuprofen3. Three low-melting-point (T_m<100°C) surfactants were selected: Poloxamer407, Polyoxyethylene Stearate, and Cetylpyridinium Chloride. The Poloxamer407 and Polyoxyethylene Stearate are non-ionic surfactant. Cetylpyridinium Chloride is a cationic surfactant. Information of APIs and surfactants is listed in ***Table 6-1***. The particle size was measured using a laser diffraction analyzer with Tornado Dry Powder System (LS13320, Beckmann Coulter). When preparing the finished drug product, other excipients were also used in formulation, as listed in ***Table 6-2***.

Table 6-1 Information of APIs and surfactants for chapter 6.

Materials	Particle size (D50, µm)	Melting point (T_m, ºC)	Manufacturer
Ibuprofen1	35.8	76ºC	Mille material of Ibuprofen2
Ibuprofen2	59.4	76ºC	RIA International LLC, NJ
Ibuprofen3	76.5	76ºC	Encore Scientific, OK
Carbamazepine	15.0	190ºC	BOC Sciences, NY
Fenofibrate	353.7	81ºC	LGM Pharma, FL
Poloxamer407	45.6	53-57ºC	BASF Corporation, NJ
Polyoxyethylene Stearate (n=55)	379.3	53ºC	TCI America, PA
Cetylpyridinium Chloride	103.0	84ºC	Spectrum Chemical, NJ

Table 6-2 Excipients list for chapter 6.

Materials	Manufacturer
Microcrystalline cellulose (Avicel 102)	FMC Biopolymer, PA
Lactose Monohydrate (Lactose 310)	Foremost Farm, WI
Crospovidone	Ashland, NJ
MgSt	Mallinckrodt Pharmaceuticals, MO

6.3 Experimental methods

6.3.1 Pre-blends preparation

Table 6-3 Pre-blending binary mixture of APIs and surfactants.

	Name of Trials	API	Surfactant	Mass ratio (API : Surfactant)
Case 1	**Case 1-1 (1)**	Ibuprofen1	Poloxamer407	10:1
	Case 1-1 (0.5)	Ibuprofen1	Poloxamer407	10:0.5
	Case 1-2 (1)	Ibuprofen2	Poloxamer407	10:1
	Case 1-2 (0.5)	Ibuprofen2	Poloxamer407	10:0.5
	Case 1-3 (1)	Ibuprofen3	Poloxamer407	10:1
	Case 1-3 (0.5)	Ibuprofen3	Poloxamer407	10:0.5
Case 2	**Case 2 (1)**	Fenofibrate	Poloxamer407	10:1
	Case 2 (0.5)	Fenofibrate	Poloxamer407	10:0.5
Case 3	**Case 3**	Carbamazepine	Cetylpyridinium Chloride	10:1
Case 4	**Case 4**	Ibuprofen2	Polyoxyethylene Stearate	10:1

A series of binary mixtures were produced containing API and surfactant of 10:1 or 10:0.5 in mass ratio. Only 5% or 10% surfactant:API w/w is applied to implement treatment. It was required that the selected surfactant at least partially melt at a temperature that was at least 20 ºC below the melting point of API, so that this API had negligible change in crystallinity. Therefore, the combinations of APIs and surfactants were determined as listed in ***Table 6-3***. Each trial is named according to the case study number and mass ratio of API

and surfactant. These binary mixtures were prepared using a V-blender (without intensifier bar). Each component was added into the blender following the specified mass ratio. Then, they were blended at 25 rpm for 15min.

6.3.2 Melt-coating by using a hot-melt extruder

A Thermo Scientific^{TM} Pharma 11Twin-screw Extruder (Thermo Fisher Scientific, Karlsruhe, Germany) was used to perform melt-coating. This instrument can be used in either hot-melt extrusion (HME) mode or twin-screw granulation(TSG) mode. The temperature of barrels is controllable in both modes up to 280°C. The parallel co-rotating twin screws are 11mm in diameter and enable the processing length to diameter (L/D) ratio up to 40:1. In our investigations, the TSG mode was selected. Two screw configurations were used as shown in ***Figure 6-2a***. They contained either 3 kneading blocks (3KBs) or 4 kneading blocks (4KBs) which were spaced along the screw. In both configurations, each kneading block consisted of three 0.25 L/D kneading elements (KEs) arranged in 60º staggering angle and forward direction. Between two kneading blocks, five standard (1 L/D) conveying elements (CEs) with helix pitch were assembled. At the entrance of the extruder, two long pitch conveying elements (lCEs) of 2 L/D were assembled. Also, close to the exit of extruder, a distributive feed screw (DFS) of 1 L/D was fitted. Therefore, the configuration of 3 kneading blocks can be abbreviated as 2lCEs-9CEs-3KEs-5CEs-3KEs-5CEs-3Kes-5CEs-1DFS-4CEs. The configuration of 4 kneading blocks can be abbreviated as 2lCEs-3CEs-3KEs-5CEs-3KEs-5CEs-3KEs-5CEs-3KEs-5CEs-1DFS-4CEs. Note that, each type of element was specifically designed for a certain functionality during the process, which will be discussed later in the results section.

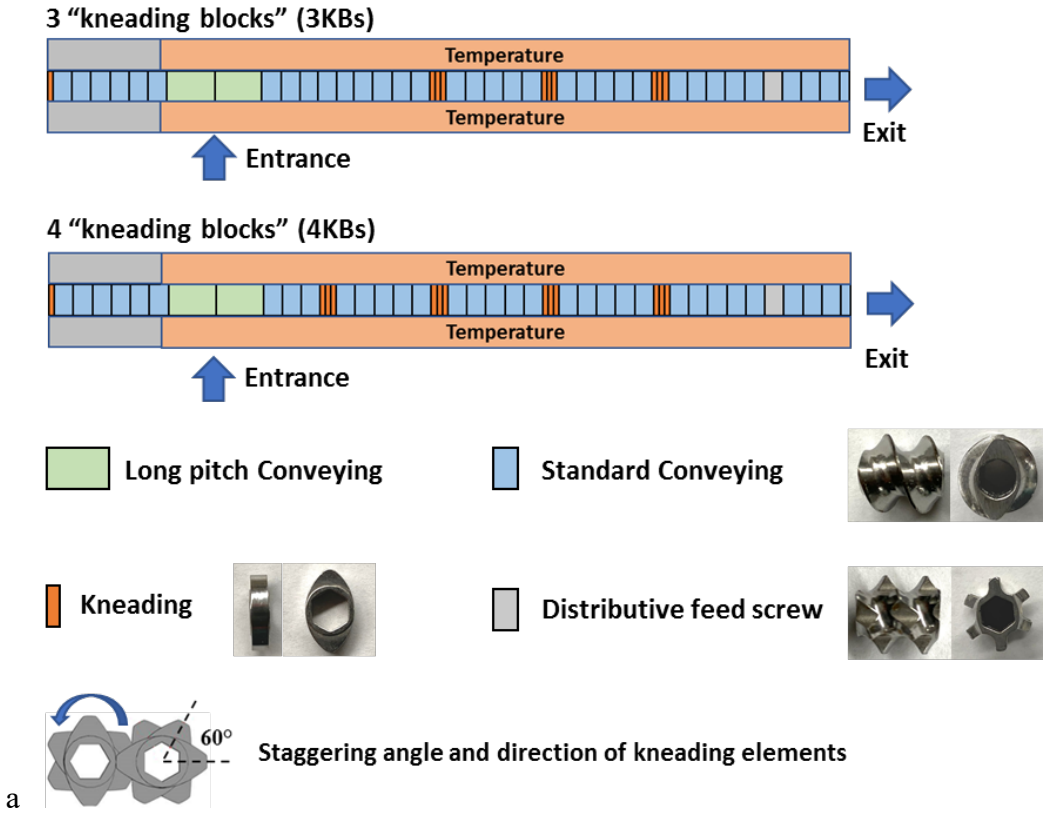

a

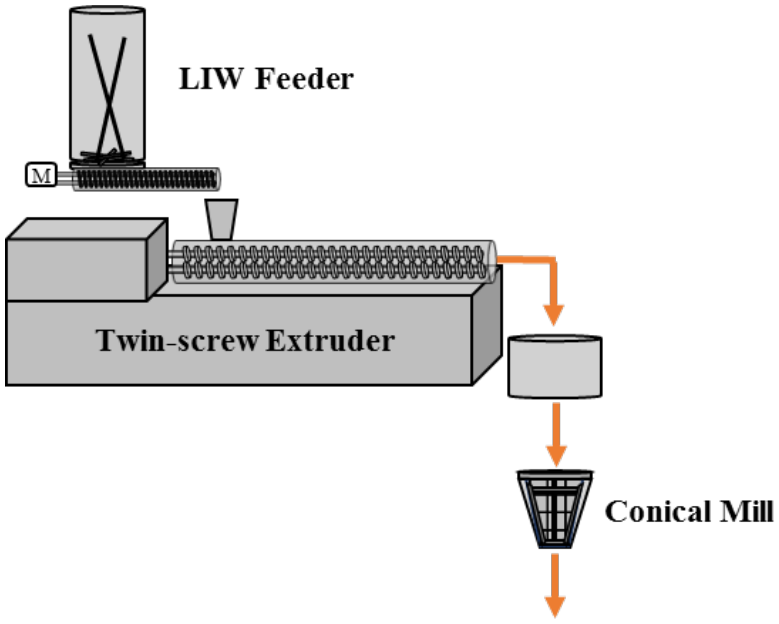

b

Figure 6-2 a) Schema of twin-screw extruder. b) Melt-coating process.

As shown in ***Figure 6-2b***, the preblended binary mixture was fed into the extruder by using a loss-in-weight feeder (MT12, Coperion K-Tron, Sewell, NJ) at a controlled flow rate. The melt-coated materials were then collected and then passed through a conical mill (Glatt, Ramsey, NJ) to destroy any unenduring and oversized agglomerates. The conical mill was operated at 1000rpm in blade speed and assembled with a coarse (2mm) round-hole screen. The flow rate, selection of screws configuration, and barrel temperature of extruder were specified in each case study, as detailed below:

Case 1: 3 KBs were configured for the trials containing high surfactant loading (10% w/w of API) and 4 KBs were utilized for the trials containing low surfactant loading (5% w/w of API). The temperature of the barrels was set to 35ºC. The screw rotational speed was maintained at 150rpm. The feeder flow rate was 0.2kg/h.

Case 2: 3 KBs were assembled for the trial of high surfactant loading (10% w/w of API) and 4 KBs were applied to the trial of low surfactant loading (5% w/w of API). The temperature of the barrels was set to 43ºC. The screw rotational speed was 150rpm. The flow rate was 0.5kg/h. Moreover, in this case study, we were also interested in exploring the effect of process parameters on the performance of coated product. Thus, three additional temperature settings were performed for the trial with low surfactant loading: 25ºC, 50ºC and 53ºC . Also, two additional flow rates of the system were implemented for the trial with high surfactant loading: 0.1kg/h and 0.3kg/h.

Case 3: 3 KBs were assembled in this case study. The temperature of the barrels was maintained at 83ºC. The screw rotational speed was 150rpm. The flow rate was 0.2kg/h.

Case 4: 4 KBs were assembled in this case study. The temperature of the barrels was set to 50ºC. The screw rotational speed was 150rpm. The flow rate was 0.2kg/h.

6.3.3 Producing finished drug product (tablets or capsules)

In the study of case 1, case 2 and case 3, formulated tablets or capsules were produced as the finished products. When preparing the finished products using treated API, the surfactant and the API were first pre-blended and then processed by the melt-coating methodology. The treated powder was further blended with other excipients. However, when preparing the product of physical mixture or without-surfactant mixture, all of the ingredients were directly blended following specified blending procedure. The formulation and preparation of drug product is detailed below.

Table 6-4 Formulation of tablets in case 1.

	Treated or Physical mix	Without Surfactant
Ibuprofen2	15.9 mg (9.1%)	15.9 mg (9.1%)
Poloxamer407	1.6 mg (0.9%)	-
Avicel102	49.0 mg (28%)	49.0 mg (28%)
Lactose310	98 mg (56%)	99.6 mg (56.9%)
Crospovidone	8.8 mg (5%)	8.8 mg (5%)
MgSt	1.7 mg (1%)	1.7 mg (1%)
Total	175.0 mg	175.0 mg

Case 1: Tablets of Ibuprofen2 were produced. The formulation of the tablets is shown in ***Table 6-4***, where surfactant is either excluded or the loading of surfactant is 10% w/w of API via melt-coating or physical mixing. The blends were produced using V-blender at 15 rpm for 15min followed by additional 2min after adding MgSt separately. Then, the blends were compacted at 12kN using a Presster^{TM} compaction simulator (Measurement Control

Corporation, East Hanover, NJ), resulting in cylindrical tablets with flat surfaces and are 8mm in diameter. The mass of each tablet is about 175mg.

Case 2: Tablets were produced in this case study. The formulation is shown in ***Table 6-5***, where surfactant is either excluded or the loading of surfactant is 10% w/w of API via melt-coating or physical mixing. Blends were produced using a LabRAM Acoustic Mixer (Resodyn Acoustic Mixers, Butte, MT) at 20% intensity for 40s followed by additional 20s after adding MgSt separately. Then, the blends were compressed into cylindrical tablets with flat surfaces and are 8mm in diameter at a compaction force of 7kN. The mass of each tablet is about 150mg.

Table 6-5 Formulation of tablets in case 2.

	Treated or Physical mix	**Without Surfactant**
Fenofibrate	60 mg (40%)	60 mg (40%)
Poloxamer407	6 mg (4%)	-
Avicel102	37.5 mg (25%)	37.5 mg (25%)
Lactose310	37.5 mg (25%)	43.5 mg (29%)
Crospovidone	7.5 mg (5%)	7.5 mg (5%)
MgSt	1.5 mg (1%)	1.5 mg (1%)
Total	150.0 mg	150 mg

Case 3: Capsules were produced in this case study. The formulation is shown in ***Table 6-6***, where surfactant is either excluded or the loading of surfactant is 10% w/w of API via melt-coating or physical mixing. Blends were produced using a LabRAM Acoustic Mixer (Resodyn Acoustic Mixers, Butte, MT) at 20% intensity for 40s followed by additional 20s after adding MgSt separately. Then, 70mg of blended powder was manually fed into each hard gelatin capsule.

Table 6-6 Formulation of capsules in case 3.

	Treated or Physical mix	Without Surfactant
Carbamazepine	50.9 mg (72.7%)	50.9 mg (72.7%)
Cetylpyridinium Chloride	5.1 mg (7.3%)	-
Avicel102	9.8 mg (14%)	14.9 mg (21.3%)
Crospovidone	3.5 mg (5%)	3.5 mg (5%)
MgSt	0.7 mg (1%)	0.7 mg (1%)
Total	70.0 mg	70.0 mg

6.3.4 In vitro dissolution test

The dissolution test was performed for both unformulated powders (treated powder and physically mixed preblends) and finished products (tablets and capsules) by using a dissolution tester of apparatus II (Paddle type) (Agilent Technologies, Santa Clara, CA). 900ml of the medium was added into each vessel and the temperature of the medium was maintained at 37.0 ± 0.5ºC throughout the dissolution test. The medium and the paddle speed were specified for each case study, as listed in ***Table 6-7***. At each pre-defined time point, 12ml of solution was withdrawn by using a peristaltic pump and then pumped back to the vessel after measurement. The amount of released drug was analyzed using a Cary 60 UV-Vis spectrophotometer (Agilent Technologies, Santa Clara, CA) at an API-specified wavelength (as shown in table 7). For dissolution of unformulated powder, a mass of API-equivalent powder (m_{API}) (as shown in table 7) was directly poured into each vessel at the starting point. When performing the dissolution test for capsules, each capsule was placed into a Japanese sinker. Three replicates were implemented for dissolution of unformulated powder and six replicates were performed for finished products. Then, the dissolution profile was plotted as the percentage of drug release versus time. The cumulative % of drug release at the beginning of the dissolution (e.g. at 5min (Q_{5min}) or

20min (Q_{20min})) and the time required to accomplish 80% drug release ($T_{80\%}$) were also documented. Moreover, a model independent approach was applied to compare dissolution profiles by calculating the mean dissolution time (MDT), which describes the mean time needed for the API molecule to be released from a solid dosage form, as expressed in equation 6-1[238, 239].

$$MDT = \frac{\sum_{i=1}^{n} \bar{t}_i \Delta M_i}{\sum_{i=1}^{n} \Delta M_i} \quad (6\text{-}1)$$

Where n represents the total number of time point, i is the sample point, $\overline{t_i}$ is the midpoint of ith time period (calculated with $(t_i + t_{i-1})/2$), ΔM_i represents the increased amount of drug release between t_i and t_{i-1}.

Table 6-7 The specified conditions of dissolution test.

	API	Medium	Paddle speed (rpm)	UV wavelength (nm)	m_{API} (mg)
Case 1	Ibuprofen	0.02M HCl buffer, pH1.8	75	220	12
Case 2	Fenofibrate	0.7% (w/v) SLS solution	100	287	50
Case 3	Carbamazepine	Deionized water	100	286	50
Case 4	Ibuprofen	0.02M HCl buffer, pH1.8	75	220	12

6.3.5 Scanning Electron Microscopy (SEM) and Energy Dispersive X-ray Spectroscopy (EDS)

The morphology of melt-coated API and physical mixture is visualized using a Zeiss Sigma field emission SEM (Carl Zeiss Microscopy, Jena, German). All of the powder samples were mounted on the aluminum pin stubs which was covered by carbon tape. Samples were pre-coated with conductive gold of 20nm thickness by using an EMS150T ES turbo-pumped sputter coater (Electron Microscopy Sciences, PA, USA) to prevent the

accumulation of static field. The secondary electrons (SE) were selected as signal detector. The bean energy was set to 5kV and the sample was photographed at 500X magnification.

In addition, this system was equipped with an energy dispersive X-ray spectrometer with Oxford X-Max EDS detector (Oxford Instruments, MA, USA). The EDS imaging and spectra acquisition were implemented to obtain the chemical information of the sample by the Aztec software using in-built TruMap algorithm. In our study, the powders of interest were compressed into tablets measuring 8mm in diameter at a low compression force (2kN). The samples were also pre-coated with gold measuring 20nm in thickness in the sputter coater. Then, the gold-coated tablets were mounted on the aluminum pin stubs covered by carbon tape so that the top surfaces were exposed for analysis. The bean energy was set to 10kV. Then, the EDS images were obtained at the pixel-dwell time of 2000us and the output count rate of 9500-12500cps.

6.3.6 Powder X-ray diffraction

Drug crystallinity was examined by performing powder X-ray diffractions (PXRD). A Philips X'PERT MPD diffractometer (PANalytical, Almelo, The Netherlands) was used to record PXRD patterns with Cu Kα radiation (1.5405Å) at the generator voltage of 45 kV and amperage of 40mA. The sample was scanned at the speed of 4s per step and the 2θ values ranging from 5° to 50° with a step size of 0.02°.

6.3.7 Tablet porosity and disintegration time

In case 2, tablet porosity and disintegration time were also evaluated. The tablet porosity (ε) can be calculated with equation 6-2

$$\varepsilon = 1 - \frac{m}{\rho V} \tag{6-2}$$

Where, m was the mass of the tablet; V was the volume of the tablets; ρ was the true density of the tablets, which was calculated according to the weight percentage of each ingredient and its true density.

Disintegration time was assessed using a USP standard disintegration tester with fluted disks placed: Agilent 100 Automated disintegration apparatus (Agilent Technologies, Santa Clara, CA). 1000ml 0.7% SLS solution was added in each beaker as immersion fluid and maintained at 37.0 ± 0.5ºC. Six tablets were placed into six tubes. The frequency of tubes raising and lowering in the immersion fluid was 30 cycles/min. The end of the disintegration was determined visually when no more tablet residue remained on the mesh of each tube. The time required for complete disintegration is documented as disintegration time.

6.3.8 Powder wettability

In case 2, powder wettability was measured using drop penetration techniques. The drop penetration methodology is detailed in section 2.4. We documented the cosine of contact angle as the index of wettability.

6.4 Results and discussions

6.4.1 Case 1: Melt-coating of Ibuprofens with poloxamer407

6.4.1.1 Process dynamics and output

As mentioned, for a twin-screw extruder, different types of screw elements are specially shaped for a specific functionality during the process. The CE is designed primarily for the function of transporting materials forward with low mechanical energy input. In contrast, the limited conveying capacity of KE results in a certain degree of powder holdup. The co-

rotating of KE enables extensive compressing and shearing of particles within the extruder barrel. Due to the high mechanical energy input, both high dispersive and distributive mixing occurs simultaneously. The use of DFS can promote distributive mixing by generating an intensive distributive flow. In our melt-coating process, the key steps for a pre-blended mixture within the intermeshing twin screws can be (1) powder handling by CEs, (2) surfactant melting, and (3) dispersive and distributive mixing at kneading blocks. It is worthwhile to note that there are three possible mechanisms of surfactant melting. Firstly, the powder gains the conductive heat from the extruder barrel at both CEs and kneading blocks. Secondly, the mechanical energy input can also convert to heat as particles repeatedly being compressed and sheared exclusively at kneading blocks. In particular, the compression and deformation of particles convert to thermal energy by plastic energy dissipation. The shearing of particles further leads to the friction between particles and between particle and barrel surface, which converts to thermal energy by frictional energy dissipation. Additionally, the possible viscous energy dissipation, when an unmelted particle is compacted with a melted one, can further induce the melting of surfactant. Therefore, the softening and melting, or at least the localized melting, of surfactant occurs at a temperature that is below its melting point (or glass-transition temperature). Furthermore, at the kneading blocks, the melted surfactant is smeared, then coats the outer surface of API particles, which enables the formation of surfactant layers on API surface. The dispersive mixing capacity of kneading blocks also allows a uniform coating.

Table 6-8 lists the residence time and temperature of post-extruder materials in case 1, in which the temperature of post-extruder material is measured immediately at the exit of

extruder. It reveals that the presented screw configurations resulted in processes of short residence time, because the kneading elements are arranged in the forward direction as rotating of the screw. In fact, at this arrangement of kneading elements (60° in staggering angle and forward direction), the powder moves through the extruder mainly in plug flow with low back mixing. Moreover, the short processing time plus low barrel temperature leads to the temperature of post-extruder powder being far below the melting point of API (Room temperature is 19 ºC). It further implies that the process has low risk of material degradation.

Table 6-8 Mean residence time and temperature of post-extruder powder.

	Barrel temperature	Flow rate	Number of kneading blocks	Screw speed	Mean residence time	Temperature of post-extruder powder
Case 1-1 (1)	35 ºC	0.2kg/h	3	150rpm	44.3s	25.2 ºC
Case 1-2 (1)	35 ºC	0.2kg/h	3	150rpm	31.2s	24.0 ºC
Case 1-3 (1)	35 ºC	0.2kg/h	3	150rpm	41.3s	23.9 ºC

Note that it was found that the size of primary particles was slightly reduced for Ibuprofen3 when passing through the extruder in both configurations, resulting in the D50 of post-extruder powder being 66.9μm (76.5 for as-received powder). Therefore, we further prepared new binary mixtures for Ibuprofen3 by physical blending of a post-extruder API with Poloxamer407 at the same process conditions and mass ratios, which is denoted as the physical mixture in the later discussion. That is to say, the primary particle size of API in the physical mixture and in the melt-coated powder for Ibuprofen3 are comparable. In such manner, the effect of particle size on dissolution performance is excluded. In contrast, the size of primary particles for Ibuprofen1 and Ibuprofen2 remains constant, as compared with as-received material.

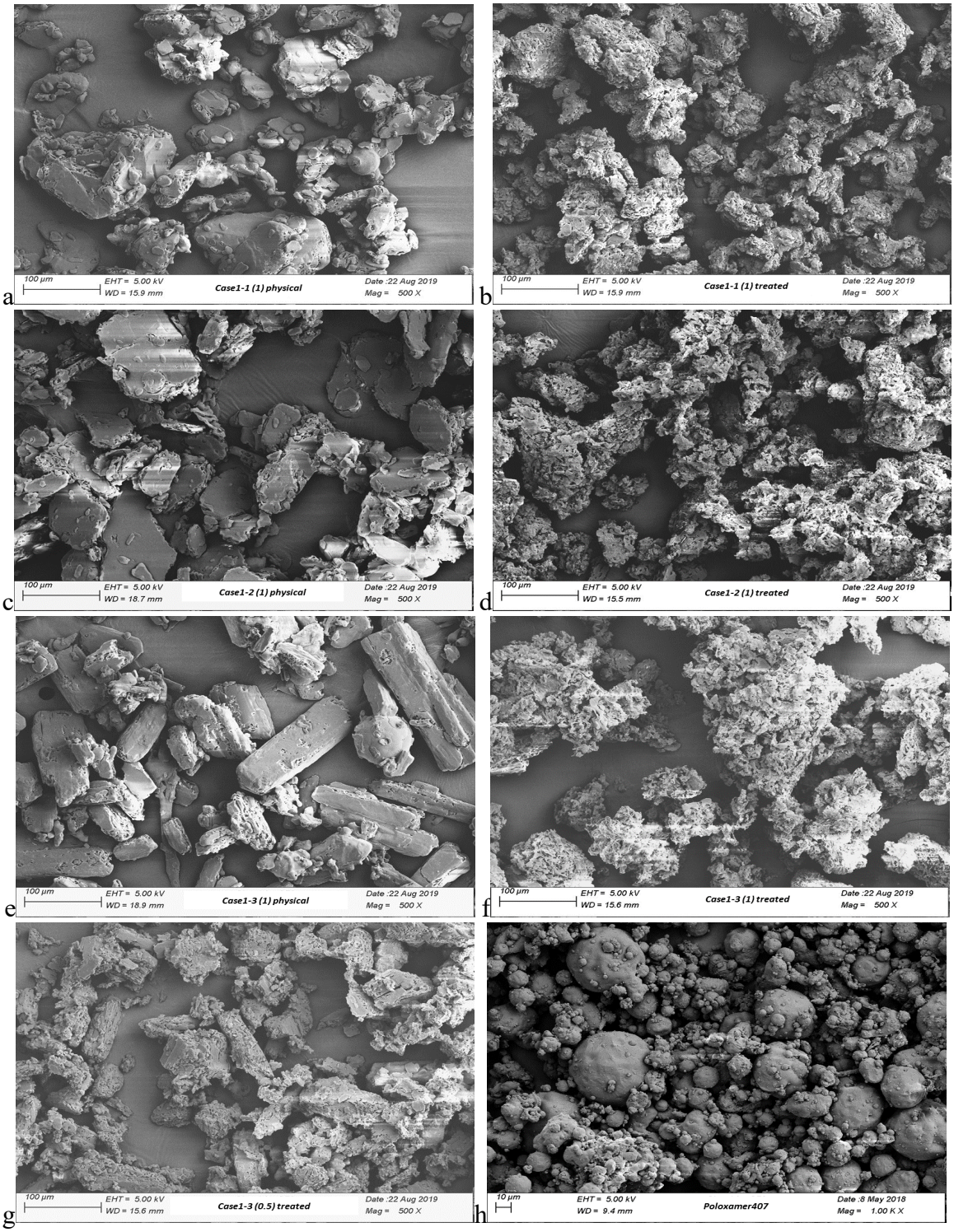

Figure 6-3 SEM images for case1.

a) Ibuprofen1:Poloxamer407=10:1 physical mixture. b) Ibuprofen1:Poloxamer407=10:1 melt-coating. c) Ibuprofen2:Poloxamer407=10:1 physical mixture. d) Ibuprofen2:Poloxamer407=10:1 melt-coating. e) Ibuprofen3:Poloxamer407=10:1 physical mixture. f) Ibuprofen3:Poloxamer407=10:1 melt-coating. g) Ibuprofen3:Poloxamer407=10:0.5 melt-coating. h) As-received Poloxamer407 (1000X magnification).

From SEM images in ***Figure 6-3***, a distinct morphology can be observed for physical mixtures and correspondingly treated APIs. Apparently, APIs in physical mixtures present a smooth surface initially. However, after treatment, new layers of coating appear on the previously smooth surface. When the mass ration of Ibuprofen and Poloxamer407 is 10:1, the entire Ibuprofen surface is coated, resulting in an entirely new lumpy surface. This phenomenon suggests that the APIs are completely coated by surfactant. In contrast, when the mass ratio of Ibuprofen and Poloxamer407 is 10:0.5, each particle seems to be only partially coated. Some area of surface still remains uncoated. As a result, the performance of coating highly depends on the mass fraction of surfactant in physical mixture. A lesser amount of surfactant leads to a lower degree of coating and possibly incomplete coating. Another observation rising from SEM images is that the treated powder is slightly agglomerated, in which the fine API particles adhere on the other particles and are bonded by the melted surfactant. However, the coating process should be distinguished from a granulation process since the product is not necessarily the large granules or pellets.

6.4.1.2 Dissolution of treated powder

The dissolution performance is first investigated for the unformulated powders. ***Figure 6-4*** shows the powder dissolution of treated API, physical mixture, and pure API for Ibuprofen1, Ibuprofen2, and Ibuprofen3. Note that, since an acidic buffer solution (pH 1.8) is used as the medium, a low dissolution rate of non-treated Ibuprofen is expected. Remarkably, at a relatively high surfactant loading (10% w/w of API), the treatment significantly enhanced the release rate for all of these Ibuprofens, while if the surfactant is just physically blended with the API, there is no effect on its dissolution in comparison to pure API. When the treatment is implemented for the trials containing a relatively low

surfactant loading (5% w/w of API), we also observed the noticeable improvement of dissolution for Ibuprofen2 but marginal effect for Ibuprofen1 and Ibuprofen3. The extracted information from the dissolution profile is listed in ***Table 6-9***. Results show that by melt-coating API with 10%w/w surfactant, it enables all three powders to release Ibuprofen molecules two to three-fold faster than the physical mixture, leading to 80% drug release in less than about one hour. Nevertheless, the physical mixtures spend more than two hours (for Ibuprofen1 and Ibuprofen3) or four hours (for Ibuprofen2) to release 80% of the drug. Additionally, in a short amount of time (20min), the treated powder dissolves two-fold (for Ibuprofen1) or three-fold (for Ibuprofen2 and Ibuprofen3) more than the physical mixture. In summary, the melt-coating of API with surfactant successfully enhances dissolution of Ibuprofen in an acidic medium. Also, higher enhancement is obtained when a larger mass of surfactant is coated. According to the SEM images (***Figure 6-3***), the 5% w/w surfactant in this case study results in an incomplete coating, which may explain the modest improvement of dissolution.

Table 6-9 Summary of drug release from powders in case1 (API : surfactant = 10:1).

	MDT (min)	**$T_{80\%}$ (min)**	**Q_{20min} (%)**
Case 1-1 (1) treated	27.9±3.7	64.2±10.2	59.8±5.0
Case 1-1 (1) physical	52.6±3.7	123.3±5.8	30.0±1.9
Case 1-2 (1) treated	26.1±3.5	51.7±10.4	63.3±5.3
Case 1-2 (1) physical	67.4±3.6	>240.0	19.6±1.1
Case 1-3 (1) treated	22.3±3.9	41.2±10.3	67.3±5.7
Case 1-3 (1) physical	56.2±3.3	127.0±10.4	26.1±1.7

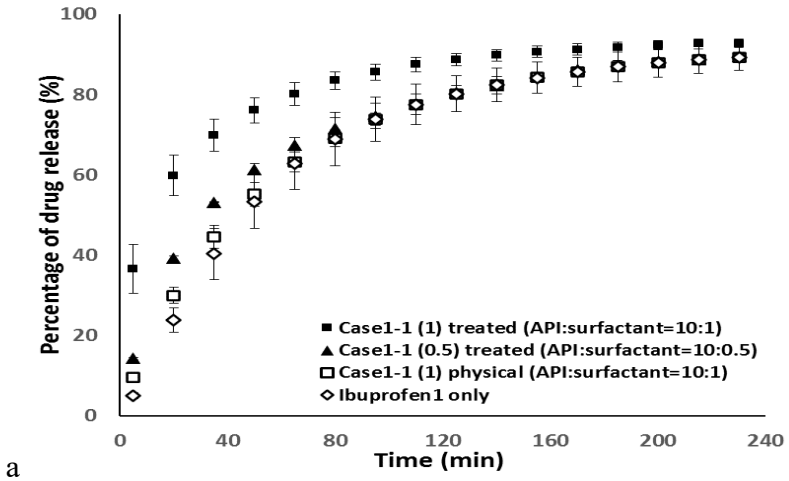

a

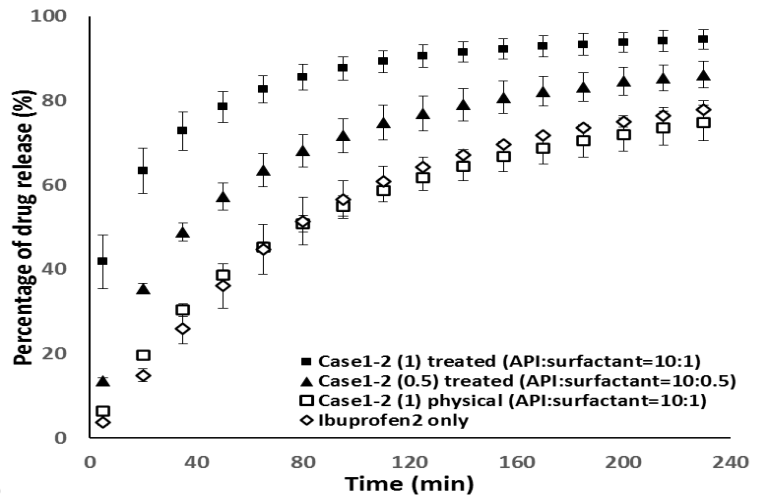

b

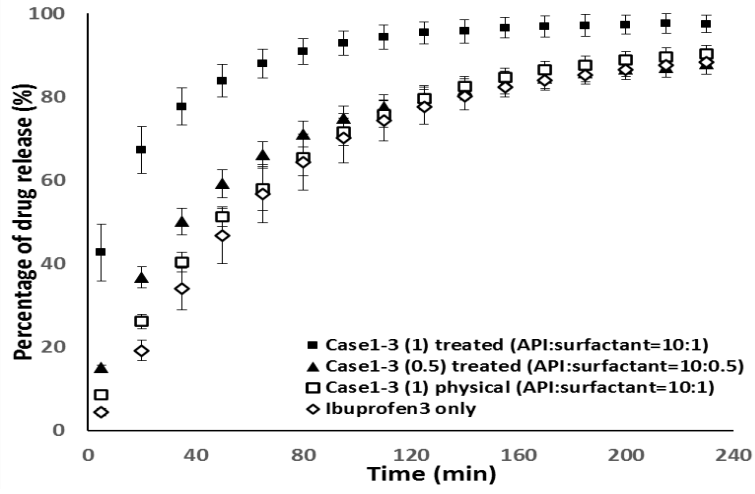

c

Figure 6-4 Dissolution of powder for the trials of a) Ibuprofen1 (Case 1-1). b) Ibuprofen2 (Case 1-2). c) Ibuprofen3 (Case1-3).

6.4.1.3 Powder X-ray diffraction

Figure 6-5 presents the PXRD crystallinity of as-received Ibuprofen2, physical mixture, and the melt-coating with 10% w/w Poloxamer407. The PXRD pattern of as-received Ibuprofen shows sharp distinct characteristic peaks indicating its high crystalline state. The physical mixture and treated sample also show numerous sharp distinct peaks, which suggests high crystallinity and no formation of amorphous states during melt-coating process. Additionally, the detected sharp peaks of treated API appear at a similar 2θ value to the original Ibuprofen and physical mixture, which further implies that the original crystalline structure remains unchanged in treated API, while the slight change in peak intensity may be attributed to the coating of surfactant on Ibuprofen surface.

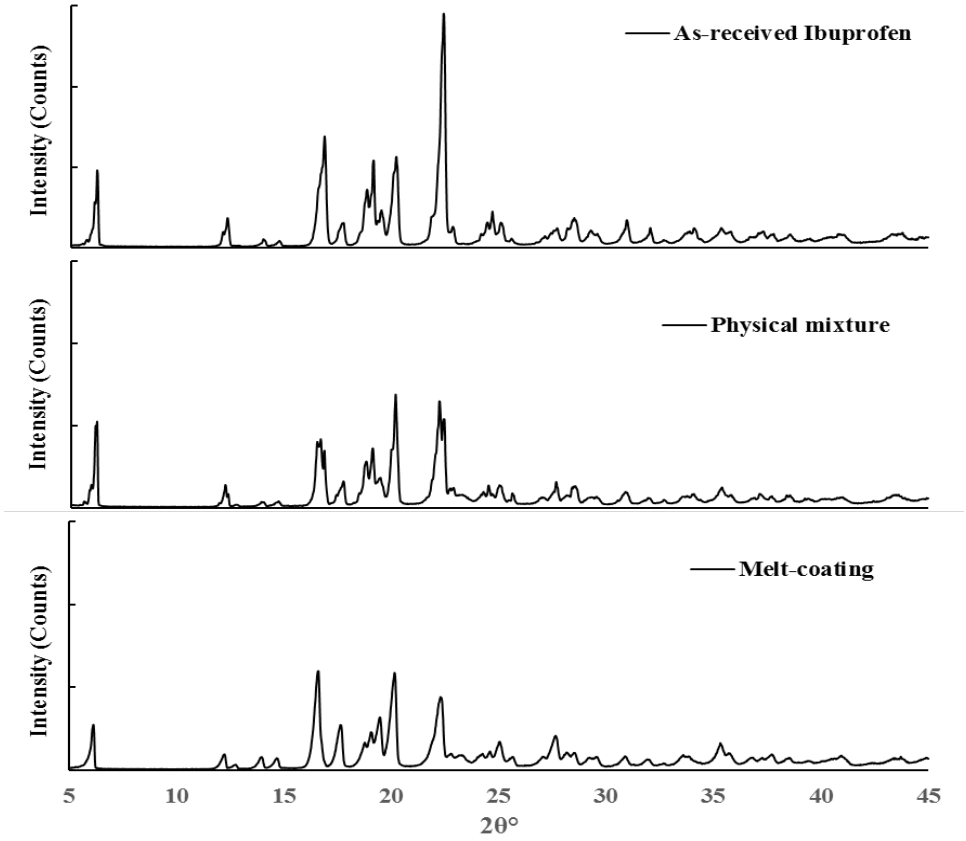

Figure 6-5 PXRD pattern of Ibuprofen2: As-received Ibuprofen, Physical mixture (API : Poloxamer407=10:1), and Melt-coating (API : Poloxamer407=10:1).

6.4.1.4 Dissolution of tablets (finished product)

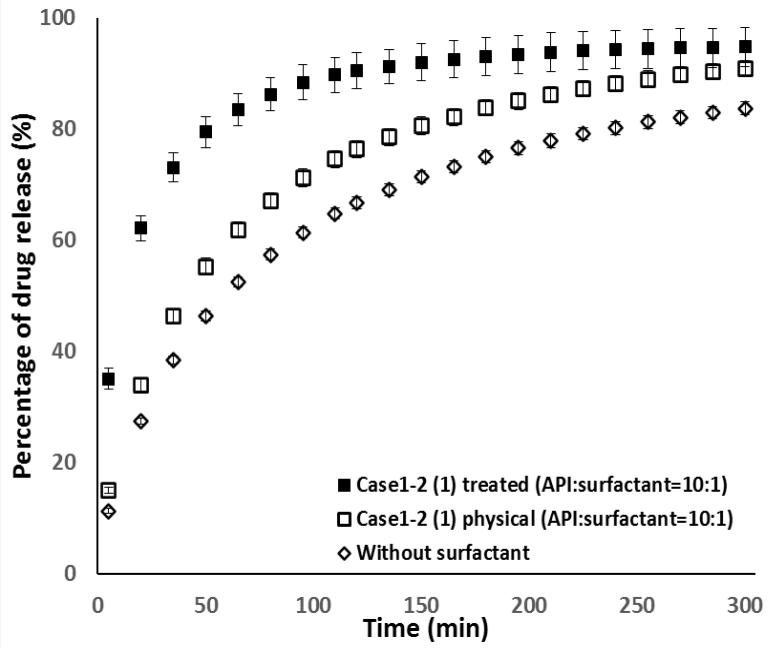

Figure 6-6 Dissolution of tablets in case 1.

Table 6-10 Summary of drug release from tablets in case 1 (API : surfactant = 10:1).

	MDT (min)	$T_{80\%}$ (min)	Q_{20min} (%)
Case1-2 (1) treated	26.9±1.4	54.0±8.9	62.1±2.2
Case1-2 (1) physical	59.1±1.1	150.0±13.4	33.8±1.1
Without surfactant	68.5±1.2	232.5±15.7	27.4±0.6

In this section, we further investigated the dissolution of the tablets containing a low dose of Ibuprofen2 (9% of the total mass). Poloxamer407 was either excluded (without surfactant) or included in formulation as 10% w/w of API via melt-coating (treated) or physical mixing (physical). ***Figure 6-6*** displays the dissolution profiles of tablets. Also, ***Table 6-10*** lists the mean dissolution time, time needed for 80% drug release, and the % of drug release at 20min. In all of three conditions (treated, physical, and without surfactant), tablets disintegrated immediately and simultaneously when dropped into the vessel. It is apparent that, with API treatment, the dissolution of Ibuprofen tablets in acidic

medium is significantly improved, which leads to the mean dissolution time of treated tablets being more than two-fold shorter than tablets of physical mixture. The tablets of melt-coated API achieve 80% of drug release three- and four-fold faster than the tablets of physical mixture and without surfactant. Again, in a short amount of time (20min), tablets of melt-coated API have doubled the amount of drug release compared to tablets of physical mixture and without surfactant. Admittedly, slight improvement of dissolution is observed in this case by adding surfactant in formulation physically, but the melt-coating shows much more enhancement.

6.4.2 Case 2: Melt-coating of Fenofibrate with Poloxamer407

6.4.2.1 Dissolution of treated powder

First, the temperature of post-extruder powder was measured immediately at the exit of the extruder as 36ºC for both screw configurations, which is far below the melting temperature of Fenofibrate (81 ºC), suggesting the low risk of API amorphization and degradation in coating process. It is noteworthy that the size of primary particles of Fenofibrate is significantly reduced when passing through the extruder, which is attributed to the milling of fragile particles at each kneading block. The mean particle size (D50) of post-extruder Fenofibrate, at both screw configurations was 94-96µm in comparison to 353.7µm for the as-received one. Due to the great change in particle size, the dissolution performance of post-extruder material would be different from pre-extruder material even if the API is not coated with surfactant. Therefore, in this case study, we also implemented trials of specific conditions: the physical mixtures of API and surfactant were passed through the extruder at the same process parameters as melt-coating but using a cooled barrel (maintained at 25ºC). The specific trials were expected to only have the particle size reduction without

melt-coating occurring as there is no thermo-treatment being conducted in the process. In our later discussion, they are denoted as “untreated” trials which should be discriminated from the physical mixture with no extruder passage.

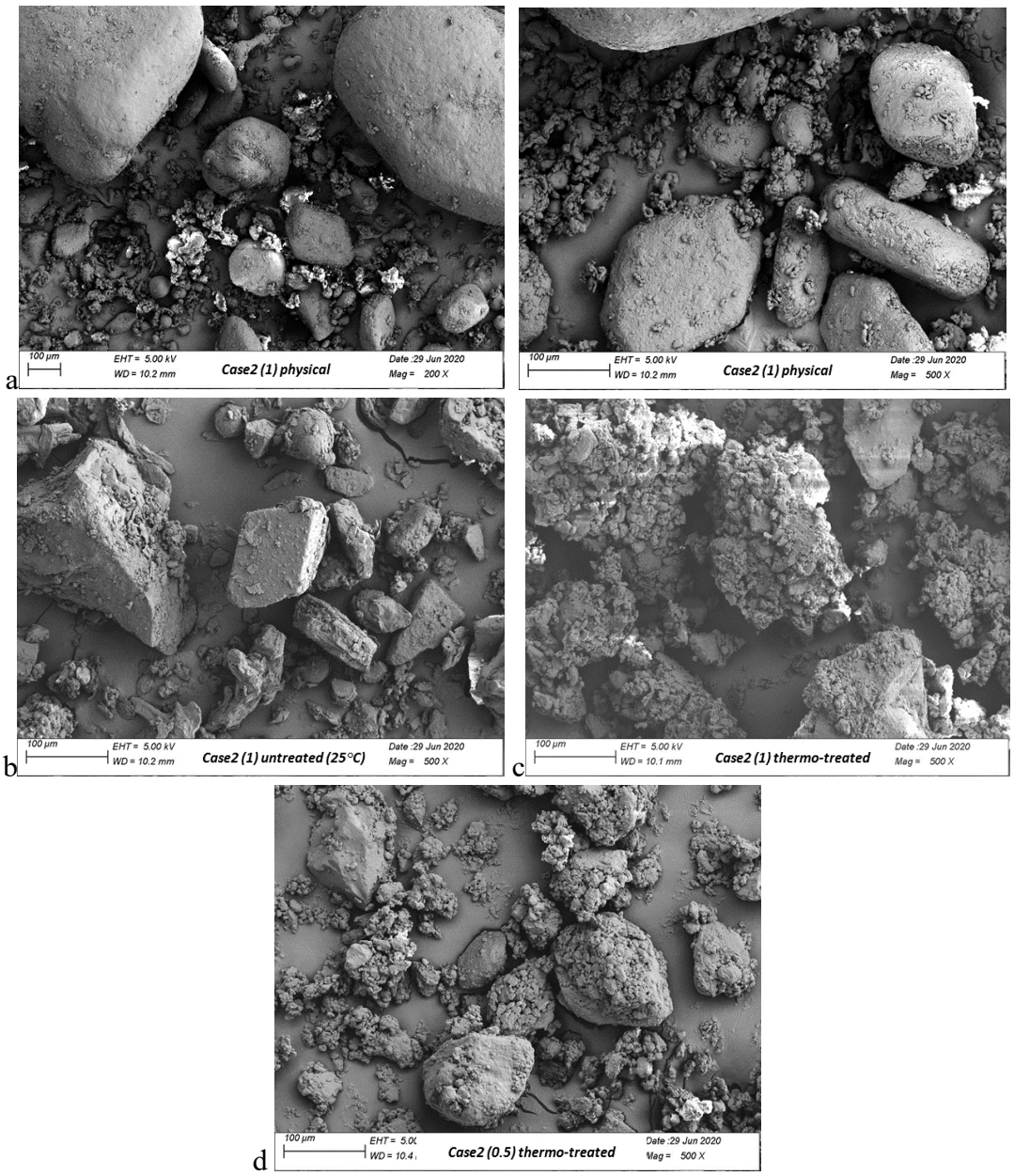

Figure 6-7 SEM images for case2:

a) Fenofibrate : Poloxamer407=10:1 physical mixture (left: 200X magnification, right: 500X magnification). b) Fenofibrate : Poloxamer407=10:1 untreated (25°C). c) Fenofibrate: Poloxamer407=10:1 thermo-treated. d) Fenofibrate : Poloxamer407=10:0.5 thermo-treated.

Figure 6-7 presents particle morphology by SEM for physical mixture, untreated mixture, and treated mixture at high (10% w/w) and low (5% w/w) surfactant loading. Apparently, in comparison to the physical mixture, the untreated mixture shows significant reduction in particle size, from spherical and rounded particles to angular and irregular particles. The smooth particle surface can be observed in both physical and untreated mixture. After the thermo-treatment, analogous to case1, the mixture with high surfactant loading (10% w/w) exhibits the distinct surface, displaying new layers of coating on its originally smooth surface. The relatively less coating is observed when mixture contains lower amount of surfactant (5% w/w). Particles seems only partially coated or still remains uncoated. As a result, the SEM images evidence that the degree of coating greatly relates to the mass fraction of surfactant. In addition, it supports that the extruder passage leads to the breaking of particles in this specific case, but the coating does not occur when the mixture is only processed at a very low temperature. The localized melt of surfactant is the prerequisite for coating.

Next, the dissolution of treated powder, untreated powder and physical mixture were examined, as shown in ***Figure 6-8***. Also, the extracted information from dissolution profiles is reported in ***Table 6-11***, including the mean dissolution time, time needed for 80% drug release, and the percentage of drug release at 20min. The most striking observation is that the treated powders (both high and low surfactant loading) displayed a substantially increased dissolution rate, as compared to the physical mixture. Note that, as mentioned, the primary crystal size of Fenofibrate is reduced as extruder passage. Both surface coating and reduction of API crystal size contribute to the enhancement. In contrast, for the untreated powders, the enhancement of dissolution is only attributed to crystal size

reduction. Thus, it is more meaningful to compare the dissolution of treated powder with untreated powder to evaluate the effectivity of melt-coating. The results further indicate that the melt-coating of Fenofibrate with 10%w/w Poloxamer407 significantly enhances the dissolution rate in comparison to untreated powder, resulting in at least a three-fold faster release of more than 80% drug. It also nearly doubles the amount of drug release at the beginning of dissolution (at 20min). It is also evident that the mean dissolution time of API-treated powder is greatly shorter than untreated one, which further shorter than physical mixture. On the other hand, when the Fenofibrate is coated with 5% w/w Poloxamer407, the enhancement is only marginal. Also, the variation of surfactant loading in untreated trials shows no effect on dissolution, which is attributed to that there is no interaction between surfactant and API, the untreated powder can be regarded as a physical mixture of milled-API with surfactant. In summary, the results confirm that the melt-coating of API with a certain amount of surfactant is able to considerably improve its dissolution.

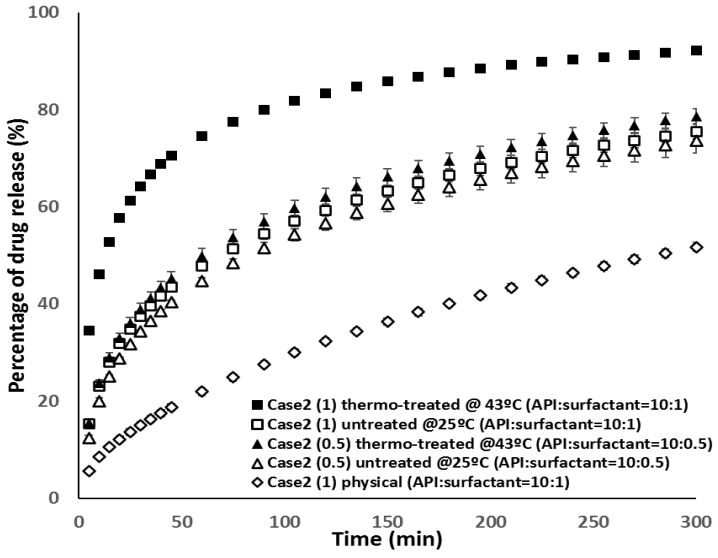

Figure 6-8 Dissolution of Fenofibrate powder

Table 6-11 Summary of drug release from powder in case2 (API : surfactant=10:1)..

	MDT (min)	$T_{80\%}$ (min)	Q_{20min} (%)
Case2 (1) thermo-treated	36.6±0.5	95±8.6	56.6±2.3
Case2 (1) untreated	66.2±0.6	>300	31.7±0.7
Case2 (1) physical	102.6±2.1	>300	12.1±0.6

6.4.2.2 Effect of screw-filling level on melt-coating

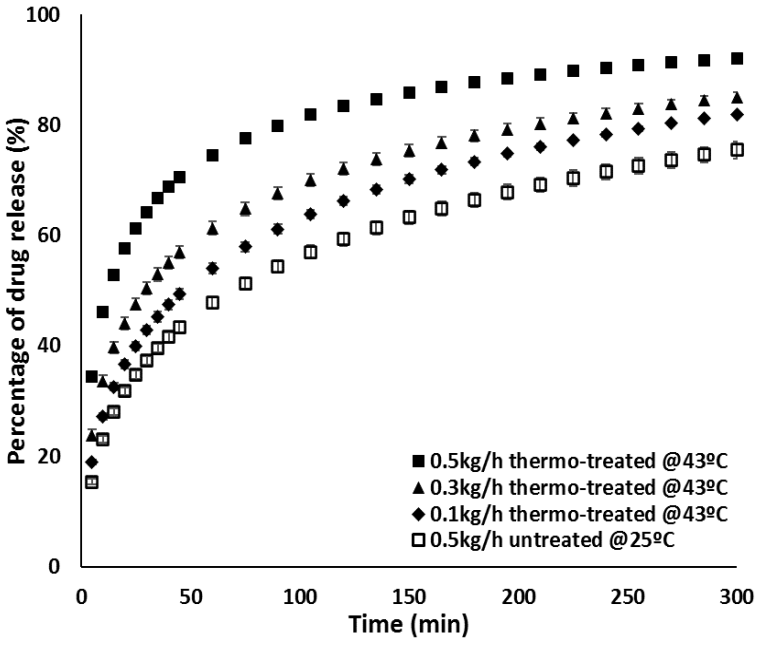

Figure 6-9 Melt-coating at different screw-filling level (API : surfactant = 10:1).

A series of experiments was implemented by varying the feed rate (0.1kg/h, 0.3kg/h and 0.5kg/h) while maintaining the constant screw speed (150rpm) and barrel temperature (43ºC) for coating Fenofibrate with 10% w/w Poloxamer407. In this manner, the feed rate corresponds to the level of screw-filling, which further determines the degree of mechanical stress within the extruder. ***Figure 6-9*** presents the dissolution of treated powder at different feed rates. For comparison, we also plotted the dissolution profile of the untreated powder. This graph indicate that all of the treated powders show improved

dissolution. The coating process of higher screw-filling yields a greater dissolution improvement. The possible explanation of this phenomenon is that the larger mass of powder in each kneading block leads to a higher degree of localized compression and more intensive shearing being applied to particles. Additionally, it also causes the increased friction between powder and screw or barrel wall. These enhanced mechanical energies result in a high degree of surfactant melting and dispersive mixing, which further converts to a high degree of coating.

4.2.3 Effect of temperature on melt-coating

In the previous discussion, we have shown that when the process is implemented in a cooled barrel (at 25ºC), the dissolution of Fenofibrate can be much slower than the process in a relatively high barrel temperature. In this section, we further reveal the possible effect of barrel temperature on melt-coating for trials containing 5% w/w Poloxamer407. Four temperature levels are discussed: 25ºC, 43°C, 50ºC, and 53°C, in which the highest temperature is at the melting point of Poloxamer407. As shown in ***Figure 6-10***, processes with relatively high barrel temperature (43ºC or 50°C) yield product with faster dissolution than the trial with low barrel temperature (25ºC), although the enhancement of dissolution is likely modest due to an insufficient mass of surfactant for a higher level of coating. Interestingly, the result also implies that increasing the barrel temperature to the melting point of surfactant doesn't yield the optimal dissolution. It even causes a slightly delayed dissolution in comparison to the untreated powder. Especially, at the beginning of the dissolution (<100min), a smaller amount of drug molecules is released at each sampling point. Such behavior can be interpreted as the formation of hard granules (or pellets) when the surfactant is completely melted. The formation of hard granules prevents dissolution

medium from penetrating into the matrix of granules, which reduces the total area of surface that is fully exposed to the dissolution medium.

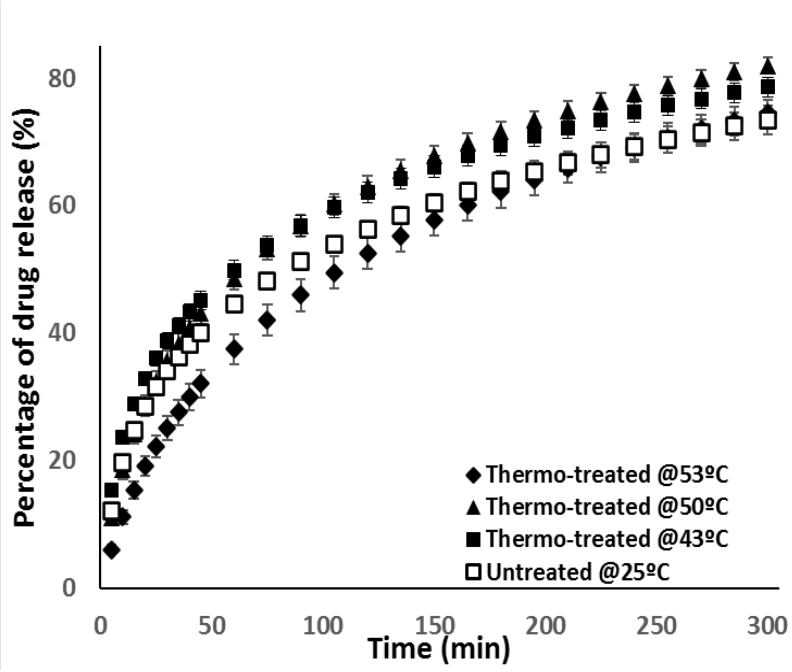

Figure 6-10 Melt-coating at different barrel temperature (API : surfactant = 10:0.5).

6.4.2.3 Wettability of powder

Water wettability of powder is assessed by calculating the cosine value of dynamic contact angle. In general, the larger cosine value represents higher wettability of powder. ***Figure 6-11*** presents the cosine of dynamic contact angle between water and treated, untreated and physical mixed powder. It is necessary to note that the pure Fenofibrate is the hydrophobic powder with water contact angle larger than 90° (the cosine of contact angle is negative). Apparently, the melt-coated Fenofibrate with 10% w/w surfactant presents the highest wettability and both treated powders (low and high surfactant loading) show improved wettability compared to untreated and physical mixed powder. In contrast, the wettability of untreated powder is comparable with physical mixture. This result suggests

that melt-coating is able to manipulate the wettability of hydrophobic API associated with the formation of the "hydrophilic" surface. Interestingly, when the API is coated with 5% w/w surfactant, although the improvement of dissolution is modest, the significant increase in wettability is observed. That is to say, the level of dissolution enhancement highly depends on the degree of coating (and reduces as formation of hard granules), however, the significant improvement of bulk powder wettability can be achieved even if the coating is insufficient.

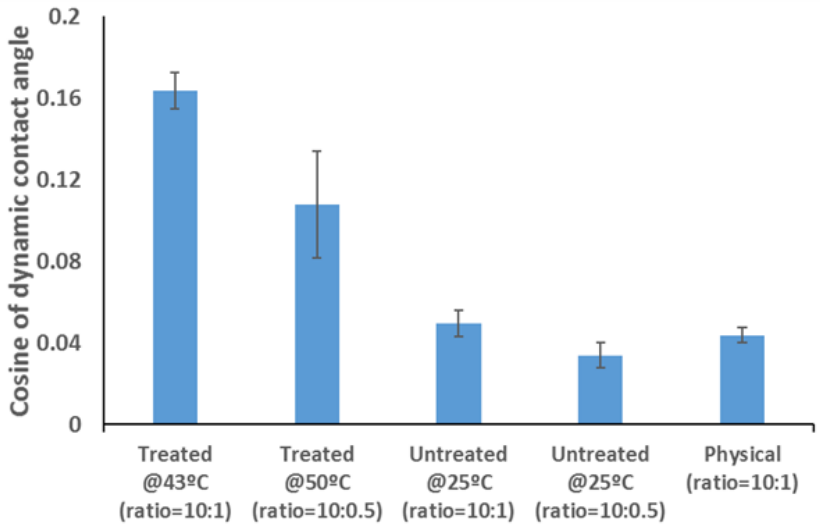

Figure 6-11 Wettability of treated, untreated and physically mixed powder.

6.4.2.4 Disintegration and dissolution of tablets (finished product)

In this section, the performance of formulated tablets is studied for these trials: 10% w/w Poloxamer407 treated, untreated, physically mixed Fenofibrate and the formulation without Poloxamer407. As each tablet containing a relatively large fraction of drug (40%w/w) in this case study, tablet porosity and disintegration time may be significantly influenced by API-surfactant interaction (treated, physical or without surfactant). Therefore, the investigation of tablets performance start from the measurement of porosity

and disintegration time. As shown in ***Figure 6-12a***, no significant difference is observed in tablet porosity. ***Figure 6-12b*** presents the disintegration time. This result shows that the tablets of both thermo-treated and untreated API yield a longer disintegration time than physical mixed ingredients, whereas the tablets without surfactant are able to disintegrate immediately. This trend is at least partially due to the fact that the crystal size of treated and untreated API are much smaller than the API without extruder passage, which creates more available surface for bonding. In addition, the Poloxamer407 in the formulation has binding capacity when it is compressed into a tablet[240]. The enhancement in tablets strength then results in moderately postponed disintegration. Even so, all of the tablets completely disintegrate in a short amount of time (within 2min), which indicates that the effect of disintegration on drug release throughout the dissolution is marginal.

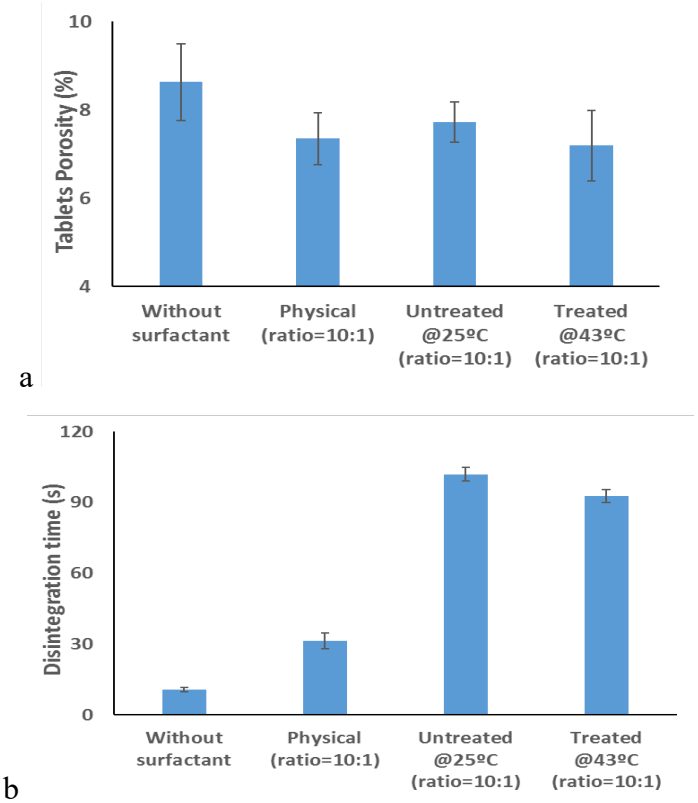

Figure 6-12 Case 2: a. Porosity of tablets. b. Disintegration time of tablets.

The dissolution profiles of the tablets are plotted in ***Figure 6-13***. It is evident that the melt-coating of API with surfactant also greatly improves the drug release of tablets in comparison to both untreated (extruder passage at low temperature) and physical mixed trials. It also shows that the physical addition of surfactant in formulation results in a comparable dissolution profile with no surfactant addition. As reported in ***Table 6-12***, tablets present much shorter mean dissolution time when the API is thermo-treated with surfactant, which is able to release more than 80% drug within two hours. However, it requires five hours for untreated and much more than five hours for physically mixed tablets to approach 80% drug release. Moreover, within a short time range (20min), the melt-coating allows the amount of drug release about two- and four-fold higher than untreated and physically mixed tablets.

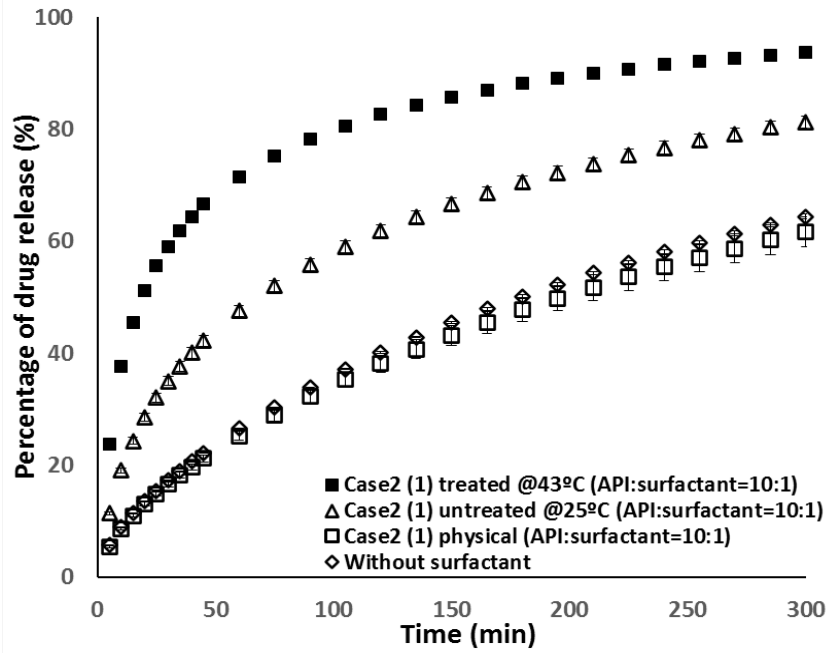

Figure 6-13 Dissolution of tablets in case 2.

Table 6-12 Summary of drug release from tablets in case 2 (API : surfactant=10:1)

	MDT (min)	$T_{80\%}$ (min)	Q_{20min} (%)
Case 2 (1) thermo-treated	44.4±0.8	105.0±0.0	51.2±0.2
Case 2 (1) untreated	73.8±1.1	282.5±11.3	28.5±0.7
Case 2 (1) physical	104.7±0.6	>300	13.0±0.3

6.4.3 Case 3: Melt-coating of Carbamazepine with Cetylpyridinium Chloride

6.4.3.1 Dissolution of treated and physically mixed powder

In this section, we seek to examine the effectiveness of melt-coating with a non-ionic and non-polymeric surfactant: Cetylpyridinium Chloride. Since the melting point of this surfactant is relatively high (84ºC), an API (Carbamazepine) of even higher melting temperature (190ºC) is selected. The mass ratio of API and surfactant is 10:1 for all of investigations in this case study.

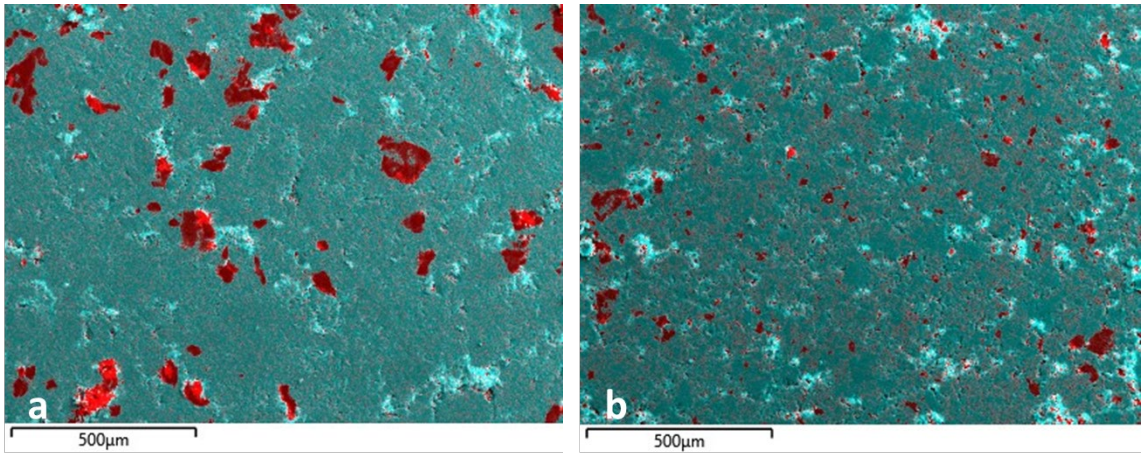

Figure 6-14 EDS maps of Carbamazepine (blue) with Cetylpyridinium Chloride (red): a) Physical mixture. b) Melt-coating.

First, we report the EDS images of treated and physical mixture in ***Figure 6-14*** with chemical information represented by different color: red and blue pixels stands for the detection of Chloride (characteristic element of Cetylpyridinium Chloride) and Oxygen

(characteristic element of Carbamazepine), respectively. These images viralize the distribution of surfactant in mixture. Apparently, the Cetylpyridinium Chloride in physical mixture is distributed in the matrix non-homogeneously in molecular level, showing as clusters. It indicates that Cetylpyridinium Chloride remains as large-size primary particles (particle size in the range of 100μm). In contrast, with melt-coating process, the Cetylpyridinium Chloride is distributed more homogenously throughout the sample rather than the high degree of clustering. According to previous discussion, the homogenous distribution is the result of surfactant melting and coating.

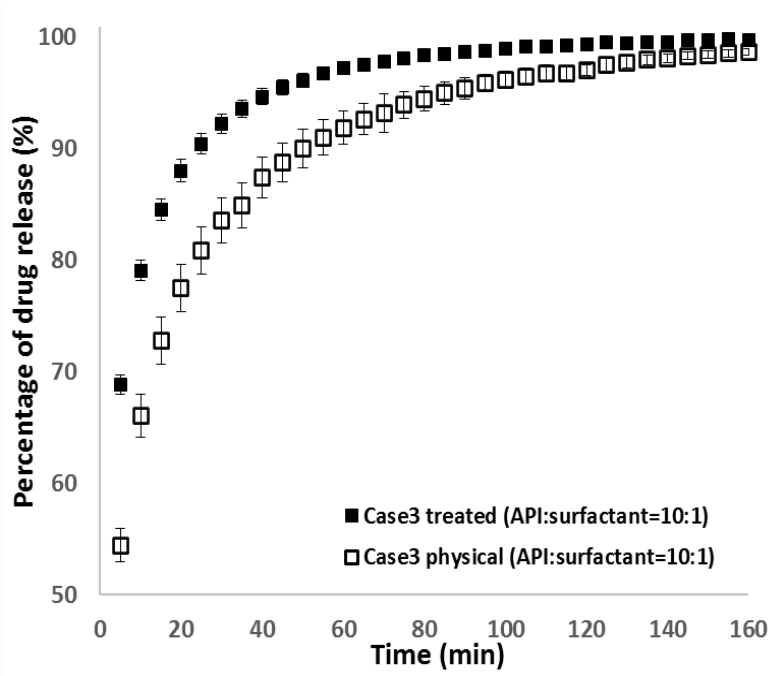

Figure 6-15 Dissolution of Carbamazepine powder.

Table 6-13 Summary of drug release from powder in case3.

	MDT (min)	$T_{80\%}$ (min)	Q_{5min} (%)
Case 3 treated	9.2±0.5	12.5±2.9	68.8±0.8
Case 3 physical	15.5±1.4	26.7±2.9	54.4±1.5

Figure 6-15 shows the dissolution profile of treated and physically mixed powder and ***Table 6-13*** summarizes the extracted dissolution information. It seems that the physical mixture already presents a relatively high dissolution rate, showing the mean dissolution time of about 15min and completing 80% drug release within 30min. This is probably because the primary particle size of as-received Carbamazepine is very small, which enables a large particle-liquid interface. Surprisingly, the melt-coating methodology further enhances the dissolution rate and shortens the mean dissolution time, allowing the required time for 80% drug release to be nearly two-fold shorter than physical mixture. Also, after 5min (Q_{5min}) of dissolution, an enlarged amount of API molecules is released from the melt-coated powder.

6.4.3.2 Dissolution of capsules (finished product)

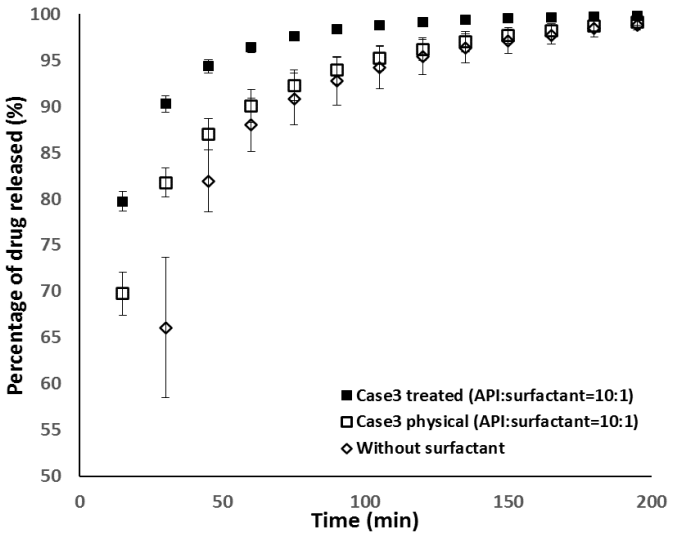

Figure 6-16 Dissolution of capsules in case 3.

Table 6-14 Summary of drug release from capsules in case 3.

	MDT (min)	$T_{80\%}$ (min)	Q_{15min} (%)
Case 3 treated	11.9±0.7	16.4±2.4	79.8±1.0
Case 3 physical	20.4±2.6	28.3±2.6	69.7±2.3
Without surfactant	28.1±3.8	41.2±4.8	41.4±3.5

The capsules of high drug loading (72.7% w/w) were prepared as finished product in this case study. All of the capsules disintegrated and released powder at approximately 2min, simultaneously. We report the dissolution of treated, physically mixed, and no-surfactant capsules in ***Figure 6-16*** and ***Table 6-14***. Once again, the melt-coated products exhibit enhanced dissolution. The mean rate of dissolution is significantly enlarged when the Carbamazepine is melt-coated with surfactant, showing a two-fold smaller MDT than physical mixed and no-surfactant products. A shorter time for 80% drug release and more drug release at 15min of dissolution can be also observed. Conclusively, these results support that the melt-coating of API with a non-ionic and non-polymeric surfactant is also able to enhance its dissolution.

6.4.4 Case 4: Melt-coating of Ibuprofen2 with Polyoxyethylene Stearate.

In this case study, the other non-ionic and polymeric surfactant: Polyoxyethylene Stearate is tested. The Ibuprofen2 is selected as model drug. The ratio of API and surfactant is 10:1. The dissolution of treated and physically mixed powder is reported in ***Figure 6-17*** and summarized in ***Table 6-15***. Results show that the melt-coating with this surfactant also successfully expedite Ibuprofen dissolution in acidic medium (Ph 1.8). The shorter mean dissolution time and time for 80% drug release are obtained. Also, the mass of drug release at 20min is almost doubled for treated Ibuprofen.

It is worthy to note that the enhancement of dissolution in this case study seems to be less than coating poloxamer407 in case 1 even if both of them have comparable melting temperature. One of the possible interpretations can be that the primary particles of Polyoxyethylene Stearate are oversized (D50=379.3μm), which generates difficulty during thermo-treatment resulting in nonuniform and incomplete surface coating. Firstly, the

oversized particles minimize the surface contact area between API and surfactant. Namely, the area of surfactant exposed to shearing at kneading blocks is minimal, which minimizes the amount of locally melted surfactant. On the other hand, the small surface contact area and low frequency of contacting between API and surfactant reduce dispersive mixing at kneading blocks, which causes less API surface being smeared and coated with melted surfactant, and nonuniform coating.

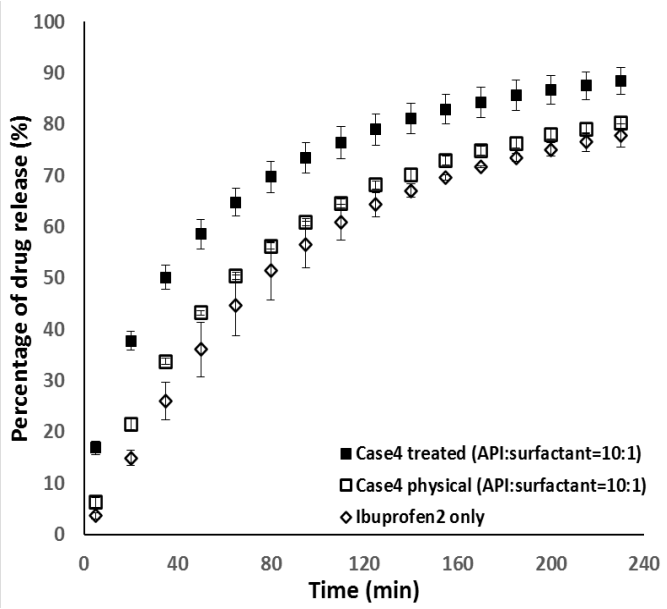

Figure 6-17 Dissolution of Ibuprofen powder in case 4.

Table 6-15 Summary of drug release form powder in case 4.

	MDT (min)	$T_{80\%}$ (min)	Q_{20min} (%)
Case4 treated	48.6±1.0	128.7±14.9	37.8±1.5
Case4 physical	64.4±1.2	228.3±10.4	21.5±1.0

6.5 Conclusion

In this study, we have innovated a methodology to enhance dissolution of poorly soluble drugs effectively and efficiently by coating API particles with a low melting point (at least

20°C lower than API) surfactant. In this methodology, the API and a small amount of surfactant (≤ 10%w/w of API) is first preblended using any blender. Then, this pre-mixture is processed in a twin-screw extruder, in which the combination of shear and heat is applied simultaneously. In this manner, the surfactant locally melts at a temperature below its melting point and coats on the outer surface of the API. The presence of the surfactant on the surface of the drug promotes wetting, and greatly reduces its dissolution time. There are three key advantages of this methodology: (1)A very simple process (extruder passage) is implemented at a low temperature, which prevents amorphization and degradation for the thermosensitive API. (2)The proposed technique relates to a continuous process, including continuously introducing a pre-mixture of API and surfactant into a processor, and continuously heating and shearing the preblended API and surfactant. Thus, it provides significant advantages over batch processing techniques. (3)Since a small amount of surfactant is utilized and it does not rely on dispersing the drug in a matrix of another ingredient, the proposed methodology is also suitable for very high drug loading of a unit dose.

In order to demonstrate the practicality of this methodology, we have performed four specific case studies, in which the combination of three different poorly soluble (BCS class II) APIs and three surfactants, including non-ionic and ionic, are examined. The dissolution of both unformulated powder and finished product (tablet and capsule) is investigated. Results support that the melt-coating of API with surfactant considerably improves APIs dissolution in both unformulated powder and finished product compared to physical mixture, resulting in a much shorter dissolution time and a significantly higher mass of drug released at the beginning of dissolution. Surprisingly, in most cases, the melt-coated

product released drug molecules at least two-fold faster than the physical mixture. It also at least doubles the mass of drug released at certain period.

Additionally, this study evidences that the critical process parameters of melt coating can be temperature and the filling-level of screws which is determined by flow rate and screw rotational speed. In fact, the effect of filling level on melt-coating is associated with the effect of shear. In other word, sufficient temperature and shear are required to obtain a high degree of coating. The degree of coating further determines the level of dissolution enhancement. Therefore, more investigations need to be done in the future to fully understand the role of these process parameters on the degree of coating.

Moreover, the current study just shows modest improvement of dissolution when 5% w/w surfactant is used. It would be interesting to explore in further research the possible processes that achieve similar dissolution enhancement but use less surfactant (<5% w/w of API). For example, the reversed staggering of kneading elements enables longer powder residence at the processor and more dispersive mixing, which possibly leads to a higher degree of coating even if the mixture contains a small amount of surfactant.

7 Chapter 7 Conclusions and Recommendations for Future Work

Each investigation presented in this dissertation is motivated by the demand for addressing a common process issue during manufacturing or improving the therapeutic efficiency of the drug product. The first part of this dissertation seeks to advance our understanding of how certain powder behavior in a process can be correlated with its raw material properties. The methodologies are selected or newly developed to characterize and quantify the potential process issue of interest. Then, based on the relationship between powder properties and its behavior in the process, we further enhance the capability to evaluate the manufacturability of a solid dosage form and assess the risk of process failure.

This dissertation also seeks to examine the correlations between process parameters and performance of output material or the final product, and to provide a basis for developing manufacturing protocols to overcome the process failure. Once again, the methodologies are selected (or developed) to capture and quantify the quality attributes of output material or final product. By knowing the process dynamics and the relationship between process parameter and output material, we are able to determine the optimal process for a similar ingredient rapidly.

Finally, the dissertation focuses on the enhancement of the drug release efficiency of the poorly soluble drug, in which a novel technique is developed that overcomes the limitations of traditional approaches. This dissertation has successfully evidenced the effectivity and practicality of this technique. This chapter summarizes the investigations and presents the

key conclusions of each technical chapter (chapter 3-chapter 6). Then, the intuitive recommendations for future work are outlined.

7.1 Conclusions

Chapter 3 demonstrated how powder flow behavior is altered when passing through a screw feeder. In this study, fourteen pharmaceutical powders are characterized before and immediately after the feeder in terms of their electrostatic charge accumulation and flowing behavior using multiple techniques. It has been observed that the charge-to-mass ratio tends to increase for every material, suggesting that particles acquire the electrostatic charges during the feeding process. For some materials, their flowing behavior changes compared to the pre-feeding powder, as characterized by a decrease of conditioned bulk density, an increase of compressibility, and a decrease of dynamic flow energy. Simply put, the powder becomes more cohesive. However, the indexes from the shear cell test, such as cohesion value, FFC, and UYS, do not change substantially. Moreover, the charge acquisition and changes in flowing behavior are independent of feeding mass flow rate. Remarkably, the phenomenon of flowing behavior change is highly associated with powder electrostatic properties and particle size. As long as a powder has a small particle size, generally less than 30μm, and exhibits a high electrostatic charging tendency, its flow behavior will be altered by feeder passage. Such change occurs because the electrostatic forces between such particles are much larger than the weight of particles. Therefore, the material behavior change can be easily captured by using low-stress characterization techniques, such as compressibility test and dynamic flow test, rather than the high-stress characterization techniques, for example, the shear cell test. These conclusions can also be generalized to how the electrostatic charging during any process affects powder flowing

behavior. Namely, powder of small particle size generally appears more cohesive when electrostatically charged. And this behavior should be examined using a low-stress characterization technique instead of a high-stress technique. Another observation arising from this chapter is that the powder builds up considerably and immediately on the feeder surface as long as a large amount of electrostatic charge is acquired (above 6nC/g in this study), which can affect drug content uniformity in the final product.

Chapter 4 advances our understanding of powder agglomeration tendency during the process. In continuous solid dose manufacturing, when powder passes through a screw feeder, it possibly forms agglomerates due to the densification of powder in the pockets between the screw flights. The agglomerates size highly depends on the volume capacity of the screws. A coarse screw generates larger agglomerates than a fine screw. In contrast, powder agglomeration is not associated with the feeding speed. Therefore, low-speed feeding can be implemented to understand powder agglomeration behavior. In a portion of the study, a conical mill is assembled after the feeder. The agglomeration behavior after the conical mill represents the endurance of agglomerates generated by the feeder. The agglomerates generated by a feeder can be defined as “unenduring” as long as the conical mill can completely eliminate it. Such agglomerates can be easily destroyed in the downstream shearing process. However, enduring agglomerates could persist in the final product, which undermines the content uniformity of drug products. Proper processing is required to diminish agglomeration. Furthermore, this chapter reveals that powder agglomeration tendency (both the size and endurance) can be correlated with particle size, compressibility, and cohesion value (from shear cell test). In particular, as long as mean particle size (D50) is above 50μm, or compressibility (at 15kPa normal stress) is smaller

than 20%, or/and cohesion value (at 6kPa shear cell test) is smaller than 0.5kPa, powder either has no agglomeration tendency or possibly forms only unenduring agglomerates. Such a drug product presents no agglomeration issue since the downstream shearing process can effortlessly and immediately eliminate the possibly formed but unenduring powder lumps. Remarkably, when the mean particle size is smaller than 30μm, or compressibility (at 15kPa normal stress) is larger than 35%, or/and cohesion value (at 6kPa shear cell test) is above 0.8kPa, the powder exhibits a high potential to form large and enduring agglomerates which are difficult to be eliminated in the downstream process.

Chapter 5 seeks to advance the understanding of agglomeration behavior and micro-mixing of cohesive (i.e., high agglomeration potential) ingredients in continuous powder blending system. The goal of this chapter is to increase our knowledge to suggest the appropriate process setting that can sufficiently and efficiently diminish the API agglomeration in blends. In chapter 4, it is shown that the feeder introduces enduring agglomerates to the next unit operation for a cohesive powder. Chapter 5 further demonstrates the approaches for eliminating them. As a result, the large agglomerates (>600μm) infrequently appear in blends when a low-shear blending process is applied. Both the size and the number of agglomerates decrease with the increase in the total number of blades passes (i.e., shear strain). The API agglomerates can be adequately diminished exclusively as long as the blending process is performed at an extensive number of blades passes. In contrast, operating the blender only at a high impeller speed cannot efficiently mitigate agglomeration. This is because (1) the high impeller speed reduces the residence time of powder in the blender, resulting in a relatively small number of blades passes. (2) the high-speed impeller creates powder fluidization, which significantly reduces powder

bed density. As a result, the mechanical interaction between particles correspondingly decreases. Furthermore, it is also evidenced in this chapter that the assembling of a conical mill between feeder and blender can effectively and efficiently eliminate API agglomerates, even if a low-shear blending process is performed to complete macro-mixing after conical mill. The efficiency of the conical mill in de-agglomeration highly depends on the hole size of the screen. In other words, the conical mill efficiently provides micro-mixing while the tubular blender enables macro-mixing efficiently. Additionally, it is exhibited that API agglomerate in the final product not only undermines content uniformity and creates super-potency but also possibly delays dissolution.

Chapter 6 presents a novel methodology to significantly enhance the dissolution of poorly soluble drugs (BCS class II). In this methodology, the API and a small amount of low melting point surfactant is initially preblended using any blender. Then, this mixture is introduced continuously into a twin-screw extruder, operating at a barrel temperature at least 20°C lower than API melting point, wherein the mechanical stress and heat are applied to powder simultaneously. This process allows that the surfactant locally melts at the temperature below its melting point and coats on the outer surface of the API particles. The presence of the surfactant on the API surface facilitates the wetting by dissolution medium and further significantly increases its dissolution rate. Compared to traditional approaches for dissolution enhancement, this methodology exhibits multiple advantages, such as implementing a very simple and low cost process (extruder passage at low barrel temperature), allowing the production of very high drug loading dosage form due to only a small amount of surfactant is used, and its advantage of continuous processing over batch processing techniques. The effectivity and efficiency of the methodology are demonstrated

by performing four case studies covering three different poorly soluble APIs and three surfactants. In each case study, the considerable enhancement in the dissolution rate is observed for the API coated with the surfactant over the physical mixture. Additionally, the finished drug product (tablet and capsule) is prepared by formulating the treaded or untreated API with other excipients. Remarkedly, the significant improvement of drug release from the product is obtained when the API is coated with a surfactant.

7.2 Recommendations for future work

Based on the investigations presented in this dissertation, it is interesting and worthy to further expand the work in several directions.

7.2.1 Advancing the characterization techniques and understanding of electrostatics in pharmaceutical manufacturing

Electrostatic charging plays a critical role in powder handling and powder processing. Many issues in pharmaceutical manufacturing, such as inconsistent flow, insufficient mixing, powder sticking on surfaces, and jamming, are attributed to electrostatic charging when electrically non-conductive particles contact, roll, and slide against each other or equipment surface. The appropriate characterization methodologies and fully understanding of powder electrostatics are essential to assess these risks rapidly. Unfortunately, electrostatic charging during a process is a complex phenomenon, which is the function of both material intrinsic properties and environmental conditions. Many material properties, including particle size, particle shape, conductivity, surface area, bulk powder density, crystal form, moisture content, surface chemistry, affect the electrostatic charging. Also, electrostatic behavior is dependent on environment humidity and external stress. Although a growing number of literature works attempted to reveal the fundamental

causing of this phenomenon, the complete theory of powder electrostatic charging and prediction of electrostatic behavior is missing. In chapter 3, it has been demonstrated that the change in bulk powder properties and material buildup in the feeder can be associated with powder charge-to-mass ratio. However, similar to powder flow characterization, charge-to-mass is more of a functional or performance test that may not be adequate to fully represent powder electrostatic-related behavior, considering that the charge-to-mass ratio only describes the acquisition of electrostatic charge under a certain set of process conditions rather than the universal behavior (or intrinsic property) of the material. In fact, this inconsistency has also been observed in the previous experiments for Avicel102. In chapter 3, it is shown that Avicel102 acquire a relatively small amount of charge after passing through a twin-screw feeder and there is no considerable amount of powder buildup being observed within a short time (shown in ***Figure 3-10a***). However, it has ever been observed the severe "bearding" at the exit of feeder after a long time feeding, as shown in ***Figure 7-1a***, which is also the result of electrostatic accumulation. Therefore, multiple characterization techniques are required to fully represent powder electrostatic behavior. The suggested characterization techniques include powder resistivity measurement, powder impedance measurement, charge-to-mass ratio, and powder dielectrophoresis measurement. The experimental methodology of these techniques is detailed in chapter 2.

Powder resistivity directly correlates with charge accumulation. As aforementioned, during a powder handling and processing, tribo-electrification occurs as particles rolling, slides, and rubbing. For a powder of high resistivity, the electrostatic charges accumulate in local areas easily and retain for a long time. In contrast, for the powder of low resistivity, the generated charges dissipate rapidly. The impedance of powder bed under an alternating-

current (AC) voltage is the response of this powder to an alternating electric field charging and discharging the powder bed as the function of frequency. The dielectric permittivity of material can further be calculated as the function of frequency, which implies how the powder is polarized when subjected to an electric field as occurring during contact charging. There is a number of literatures has reported the observed correlation between powder impedance and its electrostatic behavior in processes[69, 72, 241].

Note that, powder resistivity, AC impedance, and dielectric permittivity are intrinsic powder properties. They suggest the dynamic of charge acquisition, dissipation, and storage. However, they are less direct measurements of powder electrostatic behavior during handling. The extrinsic electrostatic measurements, i.e., performance measurements, that are necessary to be highlighted, are the charge-to-mass ratio and dielectrophoresis measurement. Both measurements directly quantify the powder electrostatic behavior during a controlled process.

Dielectrophoresis refers to the tendency for an insulative material to develop a dipolar moment and to be attracted at a non-uniform electrical field. Powder dielectrophoresis measurement quantifies the mass of powder sticking on a metallic surface at a controlled electric field. In many pharmaceutical unit operations, such as feeding, blending, powder transferring in a chute, powder unloading from a hopper, the strong and non-uniform electric field is created due to the tribo-electrostatic charging and charge accumulation at local areas. When powder is subjected to such an electric field, it is polarized and experiences net dielectrophoresis forces in the direction of the converging field, which further results in powder building up at equipment surface or jamming in pipeline, as shown in ***Figure 7-1a***. Therefore, such behavior can be correlated with the result of powder

dielectrophoresis measurement. As an example, Avicel102 exhibits a severe dielectrophoresis phenomenon during the dielectrophoresis measurement, as shown in ***Figure 7-1b***, which can be used to interpret the "bearding" at the exit of feeder for a long time feeding.

a 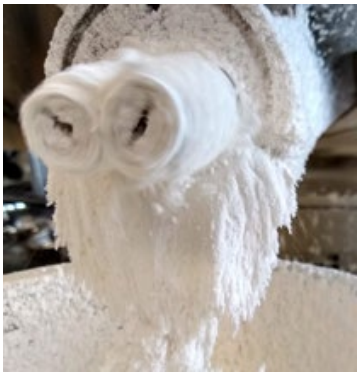 b 

Figure 7-1 Electrostatic behavior of Avicel 102: a) Powder buildup at the exit of feeder after a long time running. b) Powder sticking on metal surface in dielectrophoresis measurement.

The charge-to-mass ratio has been discussed substantially in both chapter 2 and chapter 3. This is the measurement that quantifies the amount of the net charge generated during a process. Powder presenting a larger charge-to-mass ratio is easy to develop a strong electric field in certain areas during processes. The large electrostatic force between particles acts as the cohesive component, which causes the aforementioned handling problems, such as inconsistent flow, jamming, building up, agglomeration, etc.

Additionally, other powder properties can also be correlated with powder electrostatic behavior, such as particle size distribution, particle shape, bulk density, moisture content, surface energy etc. To address the multi-dimensional data set and comprehensively understanding powder electrostatic behavior, the multivariate statistic approaches can be

used to build the data-library for powder electrostatic properties. One of the most prevalent statistical approaches is principal component analysis (PCA). The PCA reveals the hidden structure within the data set by modeling a data set in a reduced dimension (latent variable plane). The input variables can be resistivity, impedance at multiple frequencies, dielectric permittivity at multiple frequencies, charge-to-mass ratio at different processes, the mass of powder sticking in dielectrophoresis measurement, moisture content, particle size descriptors, particle shape descriptor, bulk density, surface energy, etc. Once the PCA model is established, it is possible to define what are the most relevant characterization techniques and indexes to a response of powder behavior in the process. Then, it enables us to select the optimal characterization techniques to assess the risk of such process failure in later study. In addition, the PCA model can be used to define the similarity and dissimilarity of two powders to facilitate the understanding of new material based on previous knowledge.

7.2.2 Investigating powder agglomeration in downstream continuous process

In chapter 4 and chapter 5, it has been demonstrated that the screw feeder introduces agglomerates to the next unit for a cohesive ingredient due to powder consolidation at screw pockets. The agglomerates generate difficulty for micro-mixing of API with excipients, and API even remains as agglomerated form after blending, which significantly detriments product uniformity. As shown in ***Figure 1-3***, in a typical continuous process, the next unit operation after blending can be wet granulation, roll compaction, or feed frame. The existence of agglomerates would generate more secondary problems in these unit operations. On the other hand, applying mechanical stress during these unit operations would also contribute to the de-agglomeration, which would diminish the potential content

non-uniformity. Therefore, in the future, it is interesting to investigate further how API agglomeration affects the quality attributes of output material of these unit operations, and how these unit operations diminish API agglomeration or insufficient mixing coming from the upstream blender.

In wet granulation process, for the formulation of both high and low drug loading, the nonuniform pre-mixture would lead to nonuniformly nucleate, especially, when the wettability of API is significantly lower than excipient. In such a nonuniform premixture, the wettability of each portion material is inconsistent. The fluid drop takes a longer time to penetrate into the API agglomerate matrix and results in ungranulated or weakly granulated material. The low strength granules would destroy as finer granules during the drying stage. Thus, the output granules show a broad size distribution. In addition, it leads to non-uniformity in drug content. The fine granules would be super-potent due to insufficient nucleating of poorly wettable API agglomerate, but the coarse granules would be sub-potent. The further segregation of fine and coarse granules enlarges the inconsistency of product content.

Similarly, in the roller compaction process, the nonuniform pre-mixture would lead to inconsistency in ribbon hardness. Less bonding is created within the API agglomerate matrix when it is subjected to the compaction. Thus, the ribbon would show lower strength at the spot that contains API agglomerates. At the milling stage, the fragile portion of the ribbon destroys easily as much finer granules, which results in broad size distribution and potential segregation risk in later manufacturing.

For a direct compaction solid dose manufacturing, the next unit operation after blending is feed frame and tableting. It has been substantially documented that the rotating of paddles

in the feed frame can also apply a high degree of shear to blend[242-244] due to the long residence time of powder in the feed frame chamber. The micro-mixing of ingredients still occurs within the feed frame. Therefore, it is also worthwhile to devote effort in examining how the feed frame eliminates API agglomeration and diminishes the poor micro-mixing coming from the blender. Such investigation would also contribute to the development of control strategy for continuous manufacturing that when and how to adjust paddle speeds, turret speed, and filling level of feed frame chamber to diminish insufficient micro-mixing generated by the blender.

7.2.3 Optimization of melt-coating process to enhance coating efficiency

Chapter 6 presented an innovative technique that improves the product dissolution of poorly soluble drugs by melt-coating the API with a small amount of surfactant. Results show that, by coating API with 10% w/w surfactant, the dissolution of both powder and the finished product is remarkably enhanced. Additionally, this study evidences that the critical process parameters of melt coating can be temperature and the filling-level of screws which is determined by flow rate and screw rotational speed. In fact, the effect of filling level on melt-coating is associated with the effect of mechanical stress. In other words, sufficient temperature and shearing are required to obtain a high degree of coating. On the other hand, it seems the degree of coating is also a function of surfactant particle size. The small particle size of the surfactant facilitates the localized contact between API and surfactant, which further promotes dispersive mixing between them. Also, the heat transfer is accelerated for smaller surfactant particles, which engender a higher extent of melting at a relatively low barrel temperature and short residence time. The degree of coating further determines the level of dissolution enhancement. Therefore, more

investigations need to be done in the future to fully understand the role of these process parameters and material attributes on the degree of coating. Ideally, an appropriate design of experiment (DOE) is necessary to involve the variation of screw speed, flow rate, barrel temperature, the number of kneading elements, the staggering angle and direction of kneading elements, and surfactant particle size. The response of interest can be particle size of output material, Hausner ratio (flowing behavior), tablet strength, and dissolution. In such a manner, the process dynamics of melt-coating and its design space can be well understood.

Moreover, the current study just shows the modest improvement of dissolution when 5% w/w surfactant is used. The major reason is that, under the current process setting, the melt-coating of API is insufficient when 5%w/w surfactant is used. It would be interesting to explore in further research the possible processes that achieve similar dissolution enhancement but use less surfactant (<5% w/w of API). The less input of surfactant renders the production of further higher drug-loading dose. Ultimately, it is possible to make the products that are almost entirely comprised of drug substance and contain only a minimal amount of excipient. As discussed above, one of the approaches to increasing the degree of coating is applying a higher level of mechanical energy. The staggering direction plays a key role in mechanical energy input. In chapter 6, the forward staggering is implemented which facilitates the moving of powder through the extruder, resulting in short residence time. In contrast, the reversed staggering of kneading elements obstructs certain passage for material to move forward, which prolongs powder residence at the processor and enables more dispersive mixing. Such screw configurations possibly lead to a higher degree of coating even if the mixture contains a small amount of surfactant. Further work can

devote more effort to such screw configurations. Another way to enhance mechanical energy is by changing the staggering angle of the kneading elements. The staggering angle dictates the volume of the gap between the tips of each pair of kneading elements. The smaller staggering angle provides a larger gap volume which allows powder to pass through kneading blocks more easily and subjects the material to less frequent kneading interactions. Therefore, the kneading discs staggered as 90° neutral angle applies a larger amount of total mechanical stain to material, which possibly enlarges the degree of coating.

7.2.4 Coating of API with a hydrophobic additive to mitigate its hygroscopic behavior

The hygroscopicity refers to the capacity of a solid material to readily take up moisture from the surrounding atmosphere either by absorption or adsorption. The hygroscopic behavior is a non-structured way, which means the moisture is only absorbed on the solid surface or in its pores instead of structured within the crystal lattice. Thus, such moisture up-take is reversible. In the pharmaceutical industry, the physical and chemical stability of hygroscopic material or so-called moisture-sensitive pharmaceutical substance is greatly influenced by the humidity of the surrounding environment. For example, some drugs potentially undergo hydrolysis when absorbing moisture from the atmosphere. Also, the flow behavior during handling and the formation of bonding during compaction depends on the level of moisture content. At a relatively high humidity level, the hygroscopic powder behaves cohesively, which further generates the issues, such as caking, agglomeration, inconsistent flow, avalanche etc. The high moisture content also causes deterioration of the tableting process, such as powder sticking on the punch, tablet capping, and laminating. Therefore, the hygroscopicity of pharmaceutical material is one of the

criteria when determining dosage form, selecting drug crystal form, and selecting excipients.

In chapter6, a novel methodology to implement surface coating is introduced, and the using of such methodology to enhance drug dissolution by coating API with surfactant is demonstrated. On the contrary, coating hygroscopic API with hydrophobic material likely prevents the up-take of moisture at a high humidity environment due to the formation of a hydrophobic layer on the outer surface of API particles. Likewise, a small amount of low melting point but hydrophobic material is pre-blended with API. Then, the mixture is introduced into the twin-screw extruder continuously and the melt-coating is implemented under a temperature slightly below the melting point of the hydrophobic additive. The potential candidates of the hydrophobic additives can be Magnesium Stearate, fatty acid, and fatty alcohol, such as Lauric acid, Stearic acid, Stearyl alcohol, etc. The hygroscopicity of output material can be characterized by measuring the behavior of water up-take by using the Dynamic Vapor Sorption (DVS) technique. The saturated moisture content under a controlled environment humidity can be measured by using the loss-on-dying method. The dynamic of moisture up-take can be quantified by measuring the moisture content of material that is stored in an environment of high humidity after 1h, 2h, 6h, 12h, 24h… It is important to note that the dissolution of output material and the mechanical strength of tablets should also be investigated due to the hydrophobic coating possibly deteriorate both product quality attributes.

Besides, the coating of these low melting point materials on the outer surface of host particles may also be implemented by using the batch-wise high shear mixers, with or without assembling a heat jacket, such as high shear granulator, V-blender with intensifier

bar, conical mill, and LabRAM acoustic mixer with high intensity. The efficiency and effectivity of coating and the properties of output material are interesting to be evaluated in the future.

8 Reference

1. Lekhal, A., et al., *Characterization of granular flow of wet solids in a bladed mixer.* AIChE journal, 2006. **52**(8): p. 2757-2766.
2. Muzzio, F., et al., *Solids mixing.* Handbook of industrial mixing, 2004: p. 887-985.
3. van Ommen, J.R., J.M. Valverde, and R. Pfeffer, *Fluidization of nanopowders: a review.* Journal of nanoparticle research, 2012. **14**(3): p. 737.
4. Shenoy, P., et al., *Effect of powder densities, particle size and shape on mixture quality of binary food powder mixtures.* Powder technology, 2015. **272**: p. 165-172.
5. Bridgwater, J., *The dynamics of granular materials–towards grasping the fundamentals.* Granular Matter, 2003. **4**(4): p. 175-181.
6. Engisch, W.E. and F.J. Muzzio, *Method for characterization of loss-in-weight feeder equipment.* Powder technology, 2012. **228**: p. 395-403.
7. Gao, Y., F. Muzzio, and M. Ierapetritou, *Characterization of feeder effects on continuous solid mixing using fourier series analysis.* AIChE Journal, 2011. **57**(5): p. 1144-1153.
8. Engisch, W.E. and F.J. Muzzio, *Feedrate deviations caused by hopper refill of loss-in-weight feeders.* Powder Technology, 2015. **283**: p. 389-400.
9. Chau, C.-F., Y.-T. Wang, and Y.-L. Wen, *Different micronization methods significantly improve the functionality of carrot insoluble fibre.* Food Chemistry, 2007. **100**(4): p. 1402-1408.
10. Chaumeil, J., *Micronization: a method of improving the bioavailability of poorly soluble drugs.* Methods and findings in experimental and clinical pharmacology, 1998. **20**(3): p. 211-216.
11. Iveson, S.M., et al., *Nucleation, growth and breakage phenomena in agitated wet granulation processes: a review.* Powder technology, 2001. **117**(1-2): p. 3-39.
12. Parikh, D.M., *Handbook of pharmaceutical granulation technology*. 2016: CRC Press.
13. Moghtadernejad, S., et al., *Mixing Cell: a Device to Mimic Extent of Lubrication and Shear in Continuous Tubular Blenders.* AAPS PharmSciTech, 2019. **20**(7): p. 262.
14. Çelik, M., *Pharmaceutical powder compaction technology*. 2016: CRC Press.
15. Muzzio, F.J., T. Shinbrot, and B.J. Glasser, *Powder technology in the pharmaceutical industry: the need to catch up fast*. 2002, Elsevier.
16. Gohel, M. and P.D. Jogani, *A review of co-processed directly compressible excipients.* J Pharm Pharm Sci, 2005. **8**(1): p. 76-93.
17. Pifferi, G. and P. Restani, *The safety of pharmaceutical excipients.* Il Farmaco, 2003. **58**(8): p. 541-550.
18. Rowe, R.C., P. Sheskey, and M. Quinn, *Handbook of pharmaceutical excipients*. 2009: Libros Digitales-Pharmaceutical Press.
19. Strickley, R.G., *Solubilizing excipients in oral and injectable formulations.* Pharmaceutical research, 2004. **21**(2): p. 201-230.
20. Gad, S.C., *Pharmaceutical manufacturing handbook: production and processes*. Vol. 5. 2008: John Wiley & Sons.
21. Huang, Y. and W.-G. Dai, *Fundamental aspects of solid dispersion technology for poorly soluble drugs.* Acta Pharmaceutica Sinica B, 2014. **4**(1): p. 18-25.

22. Kumar, S.K., M. Sushma, and P.Y. Raju, *Dissolution enhancement of poorly soluble drugs by using complexation technique-A review.* Journal of Pharmaceutical Sciences and Research, 2013. **5**(5): p. 120.
23. Lee, S.L., et al., *Modernizing pharmaceutical manufacturing: from batch to continuous production.* Journal of Pharmaceutical Innovation, 2015. **10**(3): p. 191-199.
24. Moghtadernejad, S., et al., *A training on: continuous manufacturing (direct compaction) of solid dose pharmaceutical products.* Journal of Pharmaceutical Innovation, 2018. **13**(2): p. 155-187.
25. Badman, C., et al., *Why We Need Continuous Pharmaceutical Manufacturing and How to Make It Happen.* Journal of pharmaceutical sciences, 2019. **108**(11): p. 3521-3523.
26. Lawrence, X.Y., et al., *Understanding pharmaceutical quality by design.* The AAPS journal, 2014. **16**(4): p. 771-783.
27. Lawrence, X.Y., *Pharmaceutical quality by design: product and process development, understanding, and control.* Pharmaceutical research, 2008. **25**(4): p. 781-791.
28. Drennen, J.K., *Quality by Design—What Does it Really Mean?* Journal of Pharmaceutical Innovation, 2007. **2**(3): p. 65-66.
29. Matero, S., et al., *Towards better process understanding: chemometrics and multivariate measurements in manufacturing of solid dosage forms.* Journal of pharmaceutical sciences, 2013. **102**(5): p. 1385-1403.
30. Rietema, K., *Powders, what are they.* Powder Technology, 1984. **37**(5).
31. Rios, M., *Developments in powder flow testing.* Pharmaceutical technology, 2006. **30**(2).
32. Leturia, M., et al., *Characterization of flow properties of cohesive powders: A comparative study of traditional and new testing methods.* Powder Technology, 2014. **253**: p. 406-423.
33. Kapelle, R. and D. Schott, *Calibration and Verification experiments for Discrete Element Modelling of cohesive materials.* Delft University of Technology, 2015.
34. El-Kassem, B., et al., *A multivariate regression parametric study on DEM input parameters of free-flowing and cohesive powders with experimental data-based validation.* Computational Particle Mechanics, 2020: p. 1-25.
35. Thakur, S.C., et al., *Micromechanical analysis of cohesive granular materials using the discrete element method with an adhesive elasto-plastic contact model.* Granular Matter, 2014. **16**(3): p. 383-400.
36. Wu, C.-Y., *DEM simulations of die filling during pharmaceutical tabletting.* Particuology, 2008. **6**(6): p. 412-418.
37. Sheng, Y., et al., *Numerical studies of uniaxial powder compaction process by 3D DEM.* Engineering Computations, 2004.
38. Hassanpour, A., et al., *Analysis of particle motion in a paddle mixer using Discrete Element Method (DEM).* Powder Technology, 2011. **206**(1-2): p. 189-194.
39. Hou, Q., K. Dong, and A. Yu, *DEM study of the flow of cohesive particles in a screw feeder.* Powder Technology, 2014. **256**: p. 529-539.

40. Jackson, R., *Some mathematical and physical aspects of continuum models for the motion of granular materials*, in *Theory of dispersed multiphase flow*. 1983, Elsevier. p. 291-337.
41. Campbell, C.S., *Rapid granular flows.* Annual Review of Fluid Mechanics, 1990. **22**(1): p. 57-90.
42. Campbell, C.S., *Granular shear flows at the elastic limit.* Journal of fluid mechanics, 2002. **465**: p. 261-291.
43. Campbell, C.S., *Granular material flows–an overview.* Powder Technology, 2006. **162**(3): p. 208-229.
44. Campbell, C.S., *Stress-controlled elastic granular shear flows.* Journal of Fluid Mechanics, 2005. **539**: p. 273-297.
45. Campbell, C.S., *Elastic granular flows.* International Journal of Chemical Reactor Engineering, 2004. **2**(1).
46. Muzzio, F.J., et al., *Solids mixing.* Handbook of Industrial Mixing, 2004: p. 887-985.
47. Vervaet, C. and J.P. Remon, *Continuous granulation in the pharmaceutical industry.* Chemical Engineering Science, 2005. **60**(14): p. 3949-3957.
48. Leuenberger, H., *New trends in the production of pharmaceutical granules: batch versus continuous processing.* European journal of pharmaceutics and biopharmaceutics, 2001. **52**(3): p. 289-296.
49. Teżyk, M., et al., *Recent progress in continuous and semi-continuous processing of solid oral dosage forms: a review.* Drug development and industrial pharmacy, 2015.
50. Rogers, A.J., A. Hashemi, and M.G. Ierapetritou, *Modeling of particulate processes for the continuous manufacture of solid-based pharmaceutical dosage forms.* Processes, 2013. **1**(2): p. 67-127.
51. Vanarase, A.U., J.G. Osorio, and F.J. Muzzio, *Effects of powder flow properties and shear environment on the performance of continuous mixing of pharmaceutical powders.* Powder technology, 2013. **246**: p. 63-72.
52. Razavi, S.M., et al., *Prediction of tablet weight variability in continuous manufacturing.* International Journal of Pharmaceutics, 2020. **575**: p. 118727.
53. Hoffmann, M., et al., *Investigation into process-induced de-aggregation of cohesive micronised API particles.* International journal of pharmaceutics, 2015. **493**(1-2): p. 341-346.
54. Huang, Z., et al., *Improving blend content uniformity via dry particle coating of micronized drug powders.* European Journal of Pharmaceutical Sciences, 2017. **104**: p. 344-355.
55. Schiano, S., L. Chen, and C.-Y. Wu, *The effect of dry granulation on flow behaviour of pharmaceutical powders during die filling.* Powder Technology, 2018. **337**: p. 78-83.
56. Escotet-Espinoza, M.S., et al., *Using a material property library to find surrogate materials for pharmaceutical process development.* Powder technology, 2018. **339**: p. 659-676.
57. Llusa, M., et al., *Shear-induced APAP de-agglomeration.* Drug development and industrial pharmacy, 2009. **35**(12): p. 1487-1495.

58. Fassihi, A. and I. Kanfer, *Effect of compressibility and powder flow properties on tablet weight variation.* Drug Development and Industrial Pharmacy, 1986. **12**(11-13): p. 1947-1966.
59. Lumay, G., et al., *Measuring the flowing properties of powders and grains.* Powder Technology, 2012. **224**: p. 19-27.
60. Wang, Y., et al., *Predicting feeder performance based on material flow properties.* Powder technology, 2017. **308**: p. 135-148.
61. Freeman, R., *Measuring the flow properties of consolidated, conditioned and aerated powders—a comparative study using a powder rheometer and a rotational shear cell.* Powder Technology, 2007. **174**(1-2): p. 25-33.
62. Taylor, M.K., et al., *Composite method to quantify powder flow as a screening method in early tablet or capsule formulation development.* AAPS PharmSciTech, 2000. **1**(3): p. 20-30.
63. Krantz, M., H. Zhang, and J. Zhu, *Characterization of powder flow: Static and dynamic testing.* Powder Technology, 2009. **194**(3): p. 239-245.
64. Van Snick, B., et al., *A multivariate raw material property database to facilitate drug product development and enable in-silico design of pharmaceutical dry powder processes.* International journal of pharmaceutics, 2018. **549**(1-2): p. 415-435.
65. Jenike, A.W., *Storage and flow of solids.* Bulletin No. 123, Utah State University, 1964.
66. Ferreira, A.P., J.C. Menezes, and M. Tobyn, *Multivariate analysis in the pharmaceutical industry*. 2018: Academic Press.
67. Wang, Y., et al., *A method to analyze shear cell data of powders measured under different initial consolidation stresses.* Powder Technology, 2016. **294**: p. 105-112.
68. Vasilenko, A., B.J. Glasser, and F.J. Muzzio, *Shear and flow behavior of pharmaceutical blends—Method comparison study.* Powder Technology, 2011. **208**(3): p. 628-636.
69. Pingali, K.C., et al., *An observed correlation between flow and electrical properties of pharmaceutical blends.* Powder Technology, 2009. **192**(2): p. 157-165.
70. Choi, K., M. Taghavivand, and L. Zhang, *Experimental studies on the effect of moisture content and volume resistivity on electrostatic behaviour of pharmaceutical powders.* International journal of pharmaceutics, 2017. **519**(1-2): p. 98-103.
71. Murtomaa, M., J. Peltonen, and J. Salonen, *One-step measurements of powder resistivity as a function of relative humidity and its effect on charging.* Journal of Electrostatics, 2015. **76**: p. 78-82.
72. Pingali, K.C., M.S. Tomassone, and F.J. Muzzio, *Effects of shear and electrical properties on flow characteristics of pharmaceutical blends.* AIChE journal, 2010. **56**(3): p. 570-583.
73. LaMarche, K.R., et al., *Granular flow and dielectrophoresis: The effect of electrostatic forces on adhesion and flow of dielectric granular materials.* 2010. **199**(2): p. 180-188.
74. Mehrotra, A., F.J. Muzzio, and T.J.P.r.l. Shinbrot, *Spontaneous separation of charged grains.* 2007. **99**(5): p. 058001.

75. Zisman, W.A., *Relation of the Equilibrium Contact Angle to Liquid and Solid Constitution*, in *Contact Angle, Wettability, and Adhesion*. 1964, AMERICAN CHEMICAL SOCIETY. p. 1-51.
76. Llusa, M., et al., *Measuring the hydrophobicity of lubricated blends of pharmaceutical excipients.* Powder technology, 2010. **198**(1): p. 101-107.
77. Liu, Z., et al., *Capillary drop penetration method to characterize the liquid wetting of powders.* Langmuir, 2016. **33**(1): p. 56-65.
78. Thielmann, F., et al., *The effect of primary particle surface energy on agglomeration rate in fluidised bed wet granulation.* Powder Technology, 2008. **181**(2): p. 160-168.
79. Ho, R., et al., *Role of surface chemistry and energetics in high shear wet granulation.* Industrial & engineering chemistry research, 2011. **50**(16): p. 9642-9649.
80. Das, S.C., et al., *Use of surface energy distributions by inverse gas chromatography to understand mechanofusion processing and functionality of lactose coated with magnesium stearate.* European Journal of Pharmaceutical Sciences, 2011. **43**(4): p. 325-333.
81. Shah, U.V., et al., *Decoupling the contribution of surface energy and surface area on the cohesion of pharmaceutical powders.* Pharmaceutical research, 2015. **32**(1): p. 248-259.
82. Jallo, L.J., et al., *Prediction of inter-particle adhesion force from surface energy and surface roughness.* Journal of Adhesion Science and Technology, 2011. **25**(4-5): p. 367-384.
83. Rowe, R., *Interaction of lubricants with microcrystalline cellulose and anhydrous lactose—a solubility parameter approach.* International Journal of Pharmaceutics, 1988. **41**(3): p. 223-226.
84. Gamble, J.F., et al., *Investigating the applicability of inverse gas chromatography to binary powdered systems: An application of surface heterogeneity profiles to understanding preferential probe-surface interactions.* International journal of pharmaceutics, 2013. **445**(1-2): p. 39-46.
85. Fichtner, F., et al., *Effect of surface energy on powder compactibility.* 2008. **25**(12): p. 2750-2759.
86. Young, S.A. and G. Buckton, *Particle growth in aqueous suspensions: the influence of surface energy and polarity.* International journal of pharmaceutics, 1990. **60**(3): p. 235-241.
87. Buckton, G. and H. Gill, *The importance of surface energetics of powders for drug delivery and the establishment of inverse gas chromatography.* Advanced drug delivery reviews, 2007. **59**(14): p. 1474-1479.
88. Khan, H., J.T. Fell, and G.S. Macleod, *The influence of additives on the spreading coefficient and adhesion of a film coating formulation to a model tablet surface.* International Journal of Pharmaceutics, 2001. **227**(1-2): p. 113-119.
89. Ticehurst, M., R. Rowe, and P. York, *Determination of the surface properties of two batches of salbutamol sulphate by inverse gas chromatography.* International Journal of Pharmaceutics, 1994. **111**(3): p. 241-249.

90. Ticehurst, M., et al., *Characterisation of the surface properties of α-lactose monohydrate with inverse gas chromatography, used to detect batch variation.* International Journal of Pharmaceutics, 1996. **141**(1-2): p. 93-99.
91. York, P., et al., *Characterisation of the surface energetics of milled dl-propranolol hydrochloride using inverse gas chromatography and molecular modelling.* International journal of pharmaceutics, 1998. **174**(1-2): p. 179-186.
92. Jallo, L.J. and R.N. Dave, *Explaining electrostatic charging and flow of surface-modified acetaminophen powders as a function of relative humidity through surface energetics.* Journal of pharmaceutical sciences, 2015. **104**(7): p. 2225-2232.
93. Ahfat, N.M., et al., *An exploration of inter-relationships between contact angle, inverse phase gas chromatography and triboelectric charging data.* European journal of pharmaceutical sciences, 2000. **9**(3): p. 271-276.
94. Storey, R., *The nucleation, growth and solid state properties of particulate pharmaceuticals*. 1997, University of Bradford, UK.
95. Swaminathan, V., J. Cobb, and I. Saracovan, *Measurement of the surface energy of lubricated pharmaceutical powders by inverse gas chromatography.* International journal of pharmaceutics, 2006. **312**(1-2): p. 158-165.
96. Newell, H.E., et al., *The use of inverse phase gas chromatography to study the change of surface energy of amorphous lactose as a function of relative humidity and the processes of collapse and crystallisation.* International journal of pharmaceutics, 2001. **217**(1-2): p. 45-56.
97. Newell, H.E., et al., *The use of inverse phase gas chromatography to measure the surface energy of crystalline, amorphous, and recently milled lactose.* Pharmaceutical research, 2001. **18**(5): p. 662-666.
98. Steele, D.F., et al., *Surface energy of microcrystalline cellulose determined by capillary intrusion and inverse gas chromatography.* The AAPS journal, 2008. **10**(3): p. 494-503.
99. Dove, J., G. Buckton, and C. Doherty, *A comparison of two contact angle measurement methods and inverse gas chromatography to assess the surface energies of theophylline and caffeine.* International journal of pharmaceutics, 1996. **138**(2): p. 199-206.
100. Van Oss, C.J., *Interfacial forces in aqueous media*. 2006: CRC press.
101. Gutmann, V., *Donor-acceptor approach to molecular interactions*. 1978: Plenum Press.
102. Drago, R.S., G.C. Vogel, and T.E. Needham, *Four-parameter equation for predicting enthalpies of adduct formation.* Journal of the American Chemical Society, 1971. **93**(23): p. 6014-6026.
103. Plumb, K., *Continuous processing in the pharmaceutical industry: changing the mind set.* Chemical Engineering Research and Design, 2005. **83**(6): p. 730-738.
104. Oka, S., et al., *Design of an integrated continuous manufacturing system.* Jukka Rantanen, 2017. **4**.
105. Blackshields, C.A. and A.M. Crean, *Continuous powder feeding for pharmaceutical solid dosage form manufacture: a short review.* Pharmaceutical development and technology, 2018. **23**(6): p. 554-560.

106. Imole, O.I., et al., *Experiments and discrete element simulation of the dosing of cohesive powders in a simplified geometry.* Powder technology, 2016. **287**: p. 108-120.
107. Wang, Y., et al., *A drop penetration method to measure powder blend wettability.* International journal of pharmaceutics, 2018. **538**(1-2): p. 112-118.
108. Pawar, P., et al., *The effect of mechanical strain on properties of lubricated tablets compacted at different pressures.* Powder Technology, 2016. **301**: p. 657-664.
109. Teunou, E. and J. Fitzpatrick, *Effect of relative humidity and temperature on food powder flowability.* Journal of Food Engineering, 1999. **42**(2): p. 109-116.
110. Visser, J., *Van der Waals and other cohesive forces affecting powder fluidization.* Powder Technology, 1989. **58**(1): p. 1-10.
111. Lachiver, E.D., et al., *Insights into the role of electrostatic forces on the behavior of dry pharmaceutical particulate systems.* Pharmaceutical research, 2006. **23**(5): p. 997-1007.
112. Hou, M., et al., *Electric field controlled dilute–dense flow transition in granular flow through a vertical pipe.* Powder technology, 2003. **135**: p. 105-111.
113. Zhu, K., et al., *Influence of particle wall adhesion on particle electrification in mixers.* International journal of pharmaceutics, 2007. **328**(1): p. 22-34.
114. Glor, M., *Hazards due to electrostatic charging of powders.* Journal of electrostatics, 1985. **16**(2-3): p. 175-191.
115. Bailey, A.J.J.o.E., *Charging of solids and powders.* 1993. **30**: p. 167-180.
116. Guardiola, J., V. Rojo, and G. Ramos, *Influence of particle size, fluidization velocity and relative humidity on fluidized bed electrostatics.* Journal of Electrostatics, 1996. **37**(1-2): p. 1-20.
117. Peart, J., *Powder electrostatics: theory, techniques and applications.* KONA Powder and Particle Journal, 2001. **19**: p. 34-45.
118. Naik, S., R. Mukherjee, and B. Chaudhuri, *Triboelectrification: A review of experimental and mechanistic modeling approaches with a special focus on pharmaceutical powders.* International journal of pharmaceutics, 2016. **510**(1): p. 375-385.
119. Ireland, P.M., *Triboelectrification of particulate flows on surfaces: Part I—Experiments.* Powder Technology, 2010. **198**(2): p. 189-198.
120. Ireland, P.M., *Triboelectrification of particulate flows on surfaces: Part II—Mechanisms and models.* Powder Technology, 2010. **198**(2): p. 199-210.
121. Naik, S., et al., *A combined experimental and numerical approach to explore tribocharging of pharmaceutical excipients in a hopper chute assembly.* International journal of pharmaceutics, 2015. **491**(1-2): p. 58-68.
122. Capece, M., et al., *Prediction of powder flow performance using a multi-component granular Bond number.* Powder technology, 2015. **286**: p. 561-571.
123. Castellanos, A., *The relationship between attractive interparticle forces and bulk behaviour in dry and uncharged fine powders.* Advances in physics, 2005. **54**(4): p. 263-376.
124. Liew, C., A. Karande, and P. Heng, *In-line quantification of drug and excipients in cohesive powder blends by near infrared spectroscopy.* International journal of pharmaceutics, 2010. **386**(1-2): p. 138-148.

125. Venables, H.J. and J. Wells, *Powder mixing.* Drug Development and Industrial Pharmacy, 2001. **27**(7): p. 599-612.
126. Flament, M.-P., P. Leterme, and A. Gayot, *The influence of carrier roughness on adhesion, content uniformity and the in vitro deposition of terbutaline sulphate from dry powder inhalers.* International journal of pharmaceutics, 2004. **275**(1-2): p. 201-209.
127. Nichols, G., et al., *A review of the terms agglomerate and aggregate with a recommendation for nomenclature used in powder and particle characterization.* Journal of pharmaceutical sciences, 2002. **91**(10): p. 2103-2109.
128. Lachiver, E.D., et al., *Agglomeration tendency in dry pharmaceutical granular systems.* European journal of pharmaceutics, 2006. **64**(2): p. 193-199.
129. Staniforth, J. and J. Rees, *Electrostatic charge interactions in ordered powder mixes.* Journal of Pharmacy and Pharmacology, 1982. **34**(2): p. 69-76.
130. Nienow, A.W., M.F. EDWARDS, and N. Harnby, *Mixing in the process industries*. 1997: Butterworth-Heinemann.
131. Podczeck, F., J.M. Newton, and M.B. James, *Influence of relative humidity of storage air on the adhesion and autoadhesion of micronized particles to particulate and compacted powder surfaces.* Journal of colloid and interface science, 1997. **187**(2): p. 484-491.
132. Galvin, J.E. and S. Benyahia, *The effect of cohesive forces on the fluidization of aeratable powders.* AIChE Journal, 2014. **60**(2): p. 473-484.
133. Orr, N. and E. Sallam, *Content uniformity of potent drugs in tablets.* Journal of Pharmacy and Pharmacology, 1978. **30**(1): p. 741-747.
134. Saunders, R., *The effect of particle agglomeration in pharmaceutical preparations.* The Statistician, 1991: p. 77-86.
135. Thiel, W., L. Nguyen, and F. Sberna, *Content uniformity of microdose tablets (dosage 1 μg-10 mg) produced by fluid bed granulation of interactive mixtures.* Journal of pharmacy and pharmacology, 1986. **38**(5): p. 335-343.
136. de Villiers, M.M., *Influence of agglomeration of cohesive particles on the dissolution behaviour of furosemide powder.* International journal of pharmaceutics, 1996. **136**(1-2): p. 175-179.
137. Stewart, P.J. and F.-Y. Zhao, *Understanding agglomeration of indomethacin during the dissolution of micronised indomethacin mixtures through dissolution and de-agglomeration modeling approaches.* European Journal of pharmaceutics and Biopharmaceutics, 2005. **59**(2): p. 315-323.
138. De Villiers, M. and J. Van der Watt, *Dissolution rate a measurement of the deaggregation of furosemide agglomerates during an interactive mixing process.* Drug Development and Industrial Pharmacy, 1990. **16**(8): p. 1391-1397.
139. de Villiers, M.M. and J.G. Van der Watt, *The measurement of mixture homogeneity and dissolution to predict the degree of drug agglomerate breakdown achieved through powder mixing.* Pharmaceutical research, 1994. **11**(11): p. 1557-1561.
140. Willemsz, T.A., et al., *Blending of agglomerates into powders 1: quantification of abrasion rate.* International journal of pharmaceutics, 2010. **387**(1-2): p. 87-92.
141. De Villiers, M.M., *Description of the kinetics of the deagglomeration of drug particle agglomerates during powder mixing.* International Journal of Pharmaceutics, 1997. **151**(1): p. 1-6.

142. Li, W., et al., *Measurement of drug agglomerates in powder blending simulation samples by near infrared chemical imaging.* International journal of pharmaceutics, 2008. **350**(1-2): p. 369-373.
143. Jérez Rozo, J.I., et al., *Complementary near-infrared and raman chemical imaging of pharmaceutical thin films.* Journal of pharmaceutical sciences, 2011. **100**(11): p. 4888-4895.
144. Moghtadernejad, S., et al., *A training on: continuous manufacturing (direct compaction) of solid dose pharmaceutical products.* Journal of Pharmaceutical Innovation, 2018. **13**(2): p. 155-187.
145. Pernenkil, L. and C.L. Cooney, *A review on the continuous blending of powders.* Chemical Engineering Science, 2006. **61**(2): p. 720-742.
146. Engisch, W.E. and F.J. Muzzio, *Loss-in-weight feeding trials case study: pharmaceutical formulation.* Journal of Pharmaceutical Innovation, 2015. **10**(1): p. 56-75.
147. Vanarase, A.U. and F.J. Muzzio, *Effect of operating conditions and design parameters in a continuous powder mixer.* Powder Technology, 2011. **208**(1): p. 26-36.
148. Gao, Y., F.J. Muzzio, and M.G. Ierapetritou, *Scale-up strategy for continuous powder blending process.* Powder technology, 2013. **235**: p. 55-69.
149. Sarkar, A. and C. Wassgren, *Continuous blending of cohesive granular material.* Chemical Engineering Science, 2010. **65**(21): p. 5687-5698.
150. Mullarney, M.P., et al., *Applying dry powder coatings to pharmaceutical powders using a comil for improving powder flow and bulk density.* Powder technology, 2011. **212**(3): p. 397-402.
151. Huang, Z., et al., *Flow and bulk density enhancements of pharmaceutical powders using a conical screen mill: a continuous dry coating device.* Chemical Engineering Science, 2015. **125**: p. 209-224.
152. Shi, W., E. Galella, and O. Sprockel, *Macro-and micro-mixing of a cohesive pharmaceutical powder during scale up.* Powder technology, 2015. **274**: p. 319-323.
153. Chaudhuri, B., et al., *Cohesive effects in powder mixing in a tumbling blender.* 2006. **165**(2): p. 105-114.
154. Palmer, J., et al., *Mapping key process parameters to the performance of a continuous dry powder blender in a continuous direct compression system.* Powder Technology, 2020. **362**: p. 659-670.
155. Llusa, M., et al., *Effect of high shear blending protocols and blender parameters on the degree of API agglomeration in solid formulations.* Industrial engineering chemistry research, 2009. **48**(1): p. 93-101.
156. Llusa, M., et al., *Shear-induced APAP de-agglomeration.* Drug development industrial pharmacy, 2009. **35**(12): p. 1487-1495.
157. Sudah, O.S., et al., *Mixing of cohesive pharmaceutical formulations in tote (bin) blenders.* Drug development industrial pharmacy, 2002. **28**(8): p. 905-918.
158. Le, V., E. Robins, and M. Flament, *Agglomerate behaviour of fluticasone propionate within dry powder inhaler formulations.* European Journal of Pharmaceutics Biopharmaceutics, 2012. **80**(3): p. 596-603.

159. Oka, S., et al., *The effects of improper mixing and preferential wetting of active and excipient ingredients on content uniformity in high shear wet granulation.* Powder Technology, 2015. **278**: p. 266-277.
160. Scherholz, M.L., B. Wan, and G. McGeorge, *A Rational Analysis of Uniformity Risk for Agglomerated Drug Substance Using NIR Chemical Imaging.* Aaps Pharmscitech, 2017. **18**(2): p. 432-440.
161. Van Snick, B., et al., *Development of a continuous direct compression platform for low-dose drug products.* International Journal of Pharmaceutics, 2017. **529**(1-2): p. 329-346.
162. Stewart, P.J. and F.-Y. Zhao, *Understanding agglomeration of indomethacin during the dissolution of micronised indomethacin mixtures through dissolution and de-agglomeration modeling approaches.* European Journal of pharmaceutics Biopharmaceutics, 2005. **59**(2): p. 315-323.
163. Kale, K., K. Hapgood, and P. Stewart, *Drug agglomeration and dissolution–what is the influence of powder mixing?* European journal of pharmaceutics biopharmaceutics, 2009. **72**(1): p. 156-164.
164. Liu, Z., et al., *Capillary drop penetration method to characterize the liquid wetting of powders.* Langmuir, 2017. **33**(1): p. 56-65.
165. Oka, S., et al., *Diminished segregation in continuous powder mixing.* Powder Technology, 2017. **309**: p. 79-88.
166. Staniforth, J., J.J.J.o.P. Rees, and Pharmacology, *Electrostatic charge interactions in ordered powder mixes.* Journal of Pharmacy Pharmacology, 1982. **34**(2): p. 69-76.
167. Lachiver, E.D., et al., *Agglomeration tendency in dry pharmaceutical granular systems.* European journal of pharmaceutics biopharmaceutics, 2006. **64**(2): p. 193-199.
168. Podczeck, F., J.M. Newton, and M.B. James, *Influence of relative humidity of storage air on the adhesion and autoadhesion of micronized particles to particulate and compacted powder surfaces.* Journal of colloid interface science, 1997. **187**(2): p. 484-491.
169. Zeng, X.M., G.P. Martin, and C. Marriott, *Particulate Interactions in Dry Powder Formulation for Inhalation*. 2000: CRC Press.
170. Orr, N., E.J.J.o.P. Sallam, and Pharmacology, *Content uniformity of potent drugs in tablets.* 1978. **30**(1): p. 741-747.
171. Feng, J.Q. and D.A. Hays, *Relative importance of electrostatic forces on powder particles.* Powder Technology, 2003. **135**: p. 65-75.
172. Yu, A., et al., *On the relationship between porosity and interparticle forces.* Powder Technology, 2003. **130**(1-3): p. 70-76.
173. Chen, L., et al., *Surface engineered excipients: I. improved functional properties of fine grade microcrystalline cellulose.* International journal of pharmaceutics, 2018. **536**(1): p. 127-137.
174. Jallo, L.J., et al., *Prediction of inter-particle adhesion force from surface energy and surface roughness.* Journal of Adhesion Science Technology, 2011. **25**(4-5): p. 367-384.
175. Rowley, G., *Quantifying electrostatic interactions in pharmaceutical solid systems.* International Journal of Pharmaceutics, 2001. **227**(1-2): p. 47-55.

176. Rasenack, N. and B.W. Müller, *Dissolution rate enhancement by in situ micronization of poorly water-soluble drugs.* Pharmaceutical research, 2002. **19**(12): p. 1894-1900.
177. Da Costa, M.A., et al., *Efavirenz dissolution enhancement I: co-micronization.* Pharmaceutics, 2013. **5**(1): p. 1-22.
178. Llusa, M. and F.J. Muzzio, *The effect of shear mixing on the blending of cohesive lubricants and drugs.* Pharmaceutical technology, 2005(7).
179. Nguyen, T., et al., *Numerical study of agglomerate abrasion in a tumbling mixer.* Chemical Engineering Science, 2014. **114**: p. 21-29.
180. Bridson, R., et al., *The effects of high shear blending on α-lactose monohydrate.* International journal of pharmaceutics, 2007. **339**(1-2): p. 84-90.
181. Brone, D. and F. Muzzio, *Enhanced mixing in double-cone blenders.* Powder Technology, 2000. **110**(3): p. 179-189.
182. Sudah, O.S., D. Coffin-Beach, and F.J. Muzzio, *Effects of blender rotational speed and discharge on the homogeneity of cohesive and free-flowing mixtures.* International Journal of Pharmaceutics, 2002. **247**(1-2): p. 57-68.
183. Muzzio, F.J., et al., *Evaluating the mixing performance of a ribbon blender.* Powder technology, 2008. **186**(3): p. 247-254.
184. Ervasti, T., et al., *The Comparison of Two Challenging Low Dose APIs in a Continuous Direct Compression Process.* Pharmaceutics, 2020. **12**(3): p. 279.
185. Razavi, S.M., et al., *Toward predicting tensile strength of pharmaceutical tablets by ultrasound measurement in continuous manufacturing.* International journal of pharmaceutics, 2016. **507**(1-2): p. 83-89.
186. Portillo, P.M., et al., *Investigation of the effect of impeller rotation rate, powder flow rate, and cohesion on powder flow behavior in a continuous blender using PEPT.* Chemical Engineering Science, 2010. **65**(21): p. 5658-5668.
187. Dubey, A., et al., *Computational approaches for studying the granular dynamics of continuous blending processes, 1–DEM based methods.* Macromolecular Materials and Engineering, 2011. **296**(3-4): p. 290-307.
188. Dubey, A., A.U. Vanarase, and F.J. Muzzio, *Impact of process parameters on critical performance attributes of a continuous blender—A DEM-based study.* AIChE journal, 2012. **58**(12): p. 3676-3684.
189. Marikh, K., et al., *Influence of stirrer type on mixture homogeneity in continuous powder mixing: a model case and a pharmaceutical case.* Chemical Engineering Research, 2008. **86**(9): p. 1027-1037.
190. Gao, Y., et al., *Characterizing continuous powder mixing using residence time distribution.* Chemical Engineering Science, 2011. **66**(3): p. 417-425.
191. Oka, S., et al., *Lubrication in continuous tubular powder blenders.* Pharmaceutical Technology Europe, 2016. **28**(11): p. 36-37.
192. Aarons, L. and S. Sundaresan, *Shear flow of assemblies of cohesive and non-cohesive granular materials.* Powder Technology, 2006. **169**(1): p. 10-21.
193. Muzzio, F.J., T. Shinbrot, and B.J. Glasser, *Powder technology in the pharmaceutical industry: the need to catch up fast.* Powder Technology, 2002. **124**(1): p. 1-7.
194. Qiu, Y., et al., *Developing solid oral dosage forms: pharmaceutical theory and practice*. 2016: Academic press.

195. Augsburger, L.L. and S.W. Hoag, *Pharmaceutical dosage forms-tablets*. 2016: CRC press.
196. Shaikh, R., et al., *The development of a pharmaceutical oral solid dosage forms*, in *Computer Aided Chemical Engineering*. 2018, Elsevier. p. 27-65.
197. Dressman, J.B. and J. Krämer, *Pharmaceutical dissolution testing*. 2005: Taylor & Francis Boca Raton, FL:.
198. Brown, C.K., et al., *Dissolution testing of poorly soluble compounds.* Pharm. Tech, 2004. **28**: p. 56-43.
199. Lenz, E., et al., *Solid-state properties and dissolution behaviour of tablets containing co-amorphous indomethacin–arginine.* European Journal of Pharmaceutics and Biopharmaceutics, 2015. **96**: p. 44-52.
200. Baghel, S., H. Cathcart, and N.J. O'Reilly, *Investigation into the solid-state properties and dissolution profile of spray-dried ternary amorphous solid dispersions: a rational step toward the design and development of a multicomponent amorphous system.* Molecular pharmaceutics, 2018. **15**(9): p. 3796-3812.
201. Singhal, D. and W. Curatolo, *Drug polymorphism and dosage form design: a practical perspective.* Advanced drug delivery reviews, 2004. **56**(3): p. 335-347.
202. Gohel, M., et al., *Formulation design and optimization of mouth dissolve tablets of nimesulide using vacuum drying technique.* AAPs PharmSciTech, 2004. **5**(3): p. 10-15.
203. Costa, F., A. Pais, and J. Sousa, *Analysis of formulation effects in the dissolution of ibuprofen pellets.* International journal of pharmaceutics, 2004. **270**(1-2): p. 9-19.
204. van der Merwe, J., et al., *The Role of Functional Excipients in Solid Oral Dosage Forms to Overcome Poor Drug Dissolution and Bioavailability.* Pharmaceutics, 2020. **12**(5): p. 393.
205. Kalepu, S. and V. Nekkanti, *Insoluble drug delivery strategies: review of recent advances and business prospects.* Acta Pharmaceutica Sinica B, 2015. **5**(5): p. 442-453.
206. Taniguchi, C., et al., *Microenvironmental pH-modification to improve dissolution behavior and oral absorption for drugs with pH-dependent solubility.* Expert opinion on drug delivery, 2014. **11**(4): p. 505-516.
207. Serajuddin, A.T., *Salt formation to improve drug solubility.* Advanced drug delivery reviews, 2007. **59**(7): p. 603-616.
208. Alonzo, D.E., et al., *Understanding the behavior of amorphous pharmaceutical systems during dissolution.* Pharmaceutical research, 2010. **27**(4): p. 608-618.
209. Mogal, S., et al., *Solid dispersion technique for improving solubility of some poorly soluble drugs.* Der Pharmacia Lettre, 2012. **4**(5): p. 1574-1586.
210. Sinha, S., et al., *Solid dispersion as an approach for bioavailability enhancement of poorly water-soluble drug ritonavir.* Aaps Pharmscitech, 2010. **11**(2): p. 518-527.
211. Jermain, S.V., C. Brough, and R.O. Williams III, *Amorphous solid dispersions and nanocrystal technologies for poorly water-soluble drug delivery–an update.* International journal of pharmaceutics, 2018. **535**(1-2): p. 379-392.

212. Sharma, D., *Solubility enhancement strategies for poorly water-soluble drugs in solid dispersions: A review.* Asian Journal of Pharmaceutics : Free full text articles from Asian J Pharm, 2016. **1**(1).
213. Repka, M.A., et al., *Melt extrusion with poorly soluble drugs–An integrated review.* International journal of pharmaceutics, 2018. **535**(1-2): p. 68-85.
214. Lee, J.-Y., et al., *Soluplus®/TPGS-based solid dispersions prepared by hot-melt extrusion equipped with twin-screw systems for enhancing oral bioavailability of valsartan.* Drug design, development, 2015. **9**: p. 2745.
215. Davis, M. and G. Walker, *Recent strategies in spray drying for the enhanced bioavailability of poorly water-soluble drugs.* Journal of Controlled Release, 2018. **269**: p. 110-127.
216. Singh, A. and G. Van den Mooter, *Spray drying formulation of amorphous solid dispersions.* Advanced drug delivery reviews, 2016. **100**: p. 27-50.
217. Lu, M., et al., *Liquisolid technique and its applications in pharmaceutics.* asian journal of pharmaceutical sciences, 2017. **12**(2): p. 115-123.
218. Khames, A., *Investigation of the effect of solubility increase at the main absorption site on bioavailability of BCS class II drug (risperidone) using liquisolid technique.* Drug delivery, 2017. **24**(1): p. 328-338.
219. Javadzadeh, Y., et al., *Liquisolid technique as a tool for enhancement of poorly water-soluble drugs and evaluation of their physicochemical properties.* Acta pharmaceutica, 2007. **57**(1): p. 99-109.
220. Yeung, C.C. and J.A. Hersey, *Ordered powder mixing of coarse and fine particulate systems.* Powder Technology, 1979. **22**(1): p. 127-131.
221. Hersey, J.A., *Ordered mixing: a new concept in powder mixing practice.* Powder Technology, 1975. **11**(1): p. 41-44.
222. Yip, C.W. and J.A. Hersey, *Ordered powder mixing.* Nature, 1976. **262**(5565): p. 202-203.
223. Saharan, V.A., et al., *Ordered mixing: mechanism, process and applications in pharmaceutical formulations.* Asian J. Pharm. Sci, 2008. **3**(6): p. 240-59.
224. Jiang, Y., et al., *Evaluation of flowability of composite particles and powder mixtures by a vibrating capillary method.* Journal of chemical engineering of Japan, 2006. **39**(1): p. 14-21.
225. Yang, J., et al., *Dry particle coating for improving the flowability of cohesive powders.* Powder technology, 2005. **158**(1-3): p. 21-33.
226. Jallo, L.J., et al., *Prediction of inter-particle adhesion force from surface energy and surface roughness.* Journal of Adhesion Science and Technology, 2011. **25**(4-5): p. 367-384.
227. Chen, L., et al., *Surface engineered excipients: II. Simultaneous milling and dry coating for preparation of fine-grade microcrystalline cellulose with enhanced properties.* International journal of pharmaceutics, 2018. **546**(1-2): p. 125-136.
228. Tee, S., et al., *The use of different sugars as fine and coarse carriers for aerosolised salbutamol sulphate.* International journal of pharmaceutics, 2000. **208**(1-2): p. 111-123.
229. El-Sabawi, D., et al., *Continued investigation into the influence of loaded dose on the performance of dry powder inhalers: surface smoothing effects.* Drug development and industrial pharmacy, 2006. **32**(10): p. 1135-1138.

230. Zhou, Q.T., et al., *Effect of surface coating with magnesium stearate via mechanical dry powder coating approach on the aerosol performance of micronized drug powders from dry powder inhalers.* AAPS PharmSciTech, 2013. **14**(1): p. 38-44.
231. Raula, J., A. Lähde, and E.I. Kauppinen, *A novel gas phase method for the combined synthesis and coating of pharmaceutical particles.* Pharmaceutical research, 2008. **25**(1): p. 242-245.
232. Pilcer, G., T. Sebti, and K. Amighi, *Formulation and characterization of lipid-coated tobramycin particles for dry powder inhalation.* Pharmaceutical research, 2006. **23**(5): p. 931-940.
233. Zhou, Q., et al., *Improving powder flow properties of a cohesive lactose monohydrate powder by intensive mechanical dry coating.* Journal of pharmaceutical sciences, 2010. **99**(2): p. 969-981.
234. Mehrotra, A., et al., *Influence of shear intensity and total shear on properties of blends and tablets of lactose and cellulose lubricated with magnesium stearate.* International journal of pharmaceutics, 2007. **336**(2): p. 284-291.
235. Qu, L., et al., *Investigation of the potential for direct compaction of a fine ibuprofen powder dry-coated with magnesium stearate.* Drug development and industrial pharmacy, 2015. **41**(5): p. 825-837.
236. Morin, G. and L. Briens, *The effect of lubricants on powder flowability for pharmaceutical application.* Aaps Pharmscitech, 2013. **14**(3): p. 1158-1168.
237. Kikuta, J.-I. and N. Kitamori, *Effect of mixing time on the lubricating properties of magnesium stearate and the final characteristics of the compressed tablets.* Drug development and industrial pharmacy, 1994. **20**(3): p. 343-355.
238. Rinaki, E., A. Dokoumetzidis, and P. Macheras, *The mean dissolution time depends on the dose/solubility ratio.* Pharmaceutical research, 2003. **20**(3): p. 406-408.
239. Costa, P. and J.M.S. Lobo, *Modeling and comparison of dissolution profiles.* European journal of pharmaceutical sciences, 2001. **13**(2): p. 123-133.
240. Desai, D., H. Zia, and A. Quadir, *Evaluation of selected micronized poloxamers as tablet lubricants.* Drug delivery, 2007. **14**(7): p. 413-426.
241. Pingali, K.C., et al., *Practical methods for improving flow properties of active pharmaceutical ingredients.* Drug development and industrial pharmacy, 2009. **35**(12): p. 1460-1469.
242. Mendez, R., F. Muzzio, and C. Velazquez, *Study of the effects of feed frames on powder blend properties during the filling of tablet press dies.* Powder Technology, 2010. **200**(3): p. 105-116.
243. Mateo-Ortiz, D. and R. Méndez, *Relationship between residence time distribution and forces applied by paddles on powder attrition during the die filling process.* Powder technology, 2015. **278**: p. 111-117.
244. Mendez, R., C. Velazquez, and F.J. Muzzio, *Effect of feed frame design and operating parameters on powder attrition, particle breakage, and powder properties.* Powder technology, 2012. **229**: p. 253-260.